VOLUME 124 NUMBER 2

THE ASTROPHYSICAL JOURNAL

AN INTERNATIONAL REVIEW OF SPECTROSCOPY AND ASTRONOMICAL PHYSICS

SEPTEMBER 1956

RADIAL-VELOCITY MEASURES OF 55 CYGNI AT MINIMUM LIGHT *Alfred H. Joy* 317
THE VELOCITY-CURVE OF 15 CANIS MAJORIS *C. R. Lynds, J. Sahade, and O. Struve* 321
SIMULTANEOUS SPECTROGRAPHIC AND PHOTOMETRIC OBSERVATIONS OF THE SHORT-PERIOD VARIABLES SX PHOENICIS AND CC ANDROMEDAE *O. C. Wilson and Merle F. Walker* 325
THE INFRARED SPECTRAL CLASSIFICATION OF M-TYPE STARS *Stewart Sharpless* 342
SPECTRAL CLASSIFICATION OF RED VARIABLES ALONG THE GALACTIC EQUATOR *Donald Cameron and J. J. Nassau* 346
THE LAW OF INTERSTELLAR REDDENING AND ABSORPTION *W. A. Hiltner and H. L. Johnson* 367
THREE-COLOR PHOTOMETRY IN THE GLOBULAR CLUSTER M3 *H. L. Johnson and A. R. Sandage* 379
EXCITATION IN NEBULAE: CHARGE TRANSFER AND THE CASSIOPEIA RADIO SOURCE *Joseph W. Chamberlain* 390
ROTATIONAL TEMPERATURE AND PHASE VARIATION OF THE CARBON DIOXIDE BANDS OF VENUS *Joseph W. Chamberlain and Gerard P. Kuiper* 399
THE SOURCE FUNCTION FOR AN EQUILIBRIUM GRAY ATMOSPHERE *Jean I. F. King* 406
ON CLUSTER-TYPE VARIABLES AND MAGNETIC FIELDS *G. R. Burbidge* 412
ON SYNCHROTRON RADIATION FROM MESSIER 87 *G. R. Burbidge* 416
TWISTED MAGNETIC FIELDS *P. H. Roberts* 430
ON AZIMUTHAL SOLAR MAGNETIC FIELDS *V. C. A. Ferraro and P. C. Kendall* 443
A STUDY OF MAGNETIC MAPS OF THE SUN *Marion B. Wood* 447
THE TEMPERATURE AND EQUILIBRIUM OF HYDROGEN IN SOLAR PROMINENCES *Harold Zirin* 451
SHOCK WAVES IN STEADY RADIAL MOTION UNDER GRAVITY *W. H. McCrea* 461
PRODUCTION OF THE SUN'S NON-THERMAL RADIO EMISSION BY CERENKOV RADIATION *L. Marshall* 469

NOTES

PHOTOMETRIC ANALYSIS OF A SPECTROGRAM OF A PERSEID METEOR *Allan F. Cook and Peter M. Millman* 476
A NEW COLOR-MAGNITUDE DIAGRAM FOR THE HYADES CLUSTER *O. Heckmann and H. L. Johnson* 477
OBSERVATIONS OF THE INTENSITY OF SOLAR LYMAN-ALPHA EMISSION *E. T. Byram, T. A. Chubb, H. Friedman, and J. E. Kupperian, Jr.* 480
A POSSIBLE CAUSE OF THE EJECTION OF MATERIAL BY LATE-TYPE GIANTS *F. Hoyle* 482
ACCRETION HEATING IN THE HERBIG-HARO OBJECTS *F. Hoyle* 484
THE ENERGY OF INTERACTION OF He^+ AND H^- *John Ross and Edward A. Mason* 485

ABSTRACTS OF ASTROPHYSICAL JOURNAL SUPPLEMENT SERIES

CATALOGUES OF Hα-EMISSION STARS AND NEBULAE IN THE MAGELLANIC CLOUDS *Karl G. Henize* 488
A PHOTOMETRIC CATALOGUE OF EMISSION NEBULOSITIES IN THE LARGE MAGELLANIC CLOUD *Lowell Doherty, Karl G. Henize, and Lawrence Aller* 488

THE UNIVERSITY OF CHICAGO PRESS
CHICAGO, ILLINOIS, U.S.A.

September 1956 Vol. 124, No. 2

THE ASTROPHYSICAL JOURNAL

AN INTERNATIONAL REVIEW OF SPECTROSCOPY AND ASTRONOMICAL PHYSICS

Founded in 1895 by George E. Hale and James E. Keeler

Published in Collaboration with the American Astronomical Society

S. CHANDRASEKHAR
Managing Editor

A. BLAAUW
Associate Editor

Yerkes Observatory of the University of Chicago

EDITORIAL BOARD

HAROLD F. WEAVER (1956-60)
Berkeley Astronomical Department
University of California

MARTIN SCHWARZSCHILD (1954-58)
Princeton University Observatory

LEO GOLDBERG (1955-59)
The Observatory of the University of Michigan

HORACE W. BABCOCK (1953-57)
Mount Wilson Observatory of the Carnegie Institution of Washington

O. HERZBERG (1951-56)
National Research Council, Ottawa

The Astrophysical Journal is published bimonthly by the University of Chicago at the University of Chicago Press, 5750 Ellis Avenue, Chicago 37, Illinois, during January, March, May, July, September, and November. ¶Two volumes are published per year, one beginning with the January issue and the other beginning with the July issue. On all orders from the United States and its possessions the subscription price is $7.50 per volume or $15.00 per year; the price of single copies is $3.50. ¶On all orders from Canada the subscription price is $8.00 per volume or $16.00 per year; the price of single copies is $3.65. On all orders from all other countries the subscription price is $8.25 per volume or $16.50 per year; the price of single copies is $3.75. (Orders for service of less than a volume will be charged at the single-copy rate.) ¶Subscriptions are payable in advance. Please make all remittances payable to The University of Chicago Press, in United States currency or its equivalent by postal or express money orders or bank drafts. (Exception: members of The American Astronomical Society must send their subscriptions and remittances to the Treasurer of the Society.)

The following is an authorized agent:

For the British Commonwealth, except North America and Australasia: The Cambridge University Press, Bentley House, 200 Euston Road, London, N.W. 1, England. Prices of yearly subscriptions and of single copies may be had on application.

Claims for missing numbers should be made within the month following the regular month of publication. The publishers expect to supply missing numbers free only when losses have been sustained in transit, and when the reserve stock will permit.

Business correspondence should be addressed to The University of Chicago Press, Chicago 37, Illinois.

Communications for the editors and manuscripts should be addressed to: S. Chandrasekhar, Editor of THE ASTROPHYSICAL JOURNAL, Yerkes Observatory, Williams Bay, Wisconsin.

Line drawings and photographs should be made by the author, and all marginal notes such as co-ordinates, wave lengths, etc., should be included in the cuts. It will not be possible to set up such material in type.

One copy of the corrected galley proof should be returned as soon as possible to the editor, Yerkes Observatory, Williams Bay, Wisconsin. Authors should take notice that the manuscript will not be sent to them with the proof.

The cable address is "Observatory, Williamsbay, Wisconsin."

The articles in this journal are indexed in the *International Index to Periodicals*, New York, N.Y.

Applications for permission to quote from this journal should be addressed to The University of Chicago Press, and will be freely granted.

Microfilms of complete journal volumes are available to regular subscribers only and may be obtained at the end of the year. Orders and inquiries should be addressed to University Microfilms, 313 North First Street, Ann Arbor, Michigan.

Notice to subscribers: If you change your address, please notify us and your local postmaster immediately.

Entered as second-class matter, July 31, 1940, at the Post-Office at Chicago, Ill., under the Act of March 3, 1879.
Acceptance for mailing at special rate of postage provided for in United States Postal Act of October 3, 1917, Section 1103, amended February 28, 1925.
Copyright 1956 by the University of Chicago.

[PRINTED IN U.S.A.]

THE ASTROPHYSICAL JOURNAL

AN INTERNATIONAL REVIEW OF SPECTROSCOPY AND ASTRONOMICAL PHYSICS

VOLUME 124 SEPTEMBER 1956 NUMBER 2

RADIAL-VELOCITY MEASURES OF SS CYGNI AT MINIMUM LIGHT

ALFRED H. JOY
Mount Wilson and Palomar Observatories
Carnegie Institution of Washington, California Institute of Technology
Received May 21, 1956

ABSTRACT

Spectrographic observations of SS Cygni at minimum show variations of velocity similar to those found for AE Aquarii. The absorption lines of the dG5 component are narrow and faint. Emission lines of the sd Be component are strong, with widths >20 A. The period is 0.276244 day, and the masses are nearly equal ($m \sin^3 i = 0.2 \odot$, $a \sin i = 450000$ km). Since no eclipses have been observed, the inclination of the orbit must be small.

The remarkable outbursts of the variable star SS Cygni, amounting to about 4 mag., have been persistently followed, especially by the American Association of Variable Star Observers, since its discovery at Harvard sixty years ago, but precise observations during minimum light are strangely lacking. The period averages about 50 days, with large deviations from the mean. In the interval of several weeks between outbursts, the average magnitude is about 11.9, with frequent irregularities which are usually not greater than 0.5 mag.

Spectroscopic results have been few and somewhat confused because of its peculiar variable spectrum and the faintness of the star except at times of maximum. In addition to objective-prism observations recorded in the Harvard catalogues, a few slit-spectrographic observations have been reported by Adams and Joy (1922), Elvey and Babcock (1940, 1943), Joy (1940), and Hinderer (1949).

At the peak of the nova-like outbursts, extremely wide, shallow absorption lines of hydrogen and Ca II appear, with a continuous spectrum corresponding to about A0 or earlier. At this phase, emission at λ 4686 (He II) was seen by Elvey and Babcock and by Hinderer.

Methods similar to those used for AE Aquarii (Joy 1954) have been attempted in a spectroscopic study of SS Cyg. At minimum light, when the hot continuous spectrum is comparatively weak, strong emission lines, 20 A or more in width with winged edges, are prominent. Fainter bright lines of He I and Ca II having the same width as the hydrogen lines are also present. The variation in intensity of the emission lines of SS Cyg at minimum is small on our plates, in strong contrast to the large variations found in AE Aqr.

A very faint, evanescent absorption spectrum of type about dG5 with fairly narrow

lines can usually be detected at this phase. The lines of this spectrum vary considerably in visibility and seem quite fuzzy on some of the plates. This effect may be due in part to rotation of the star, which causes a total width of 330 km/sec for the orbital period of 0.276 day, and to velocity changes during the exposure. The faint absorption lines are quickly veiled by any increase in the intensity of the continuous background. Some plates show a sharp emission in the K line of Ca II superposed on the wide emission line but yielding the same velocity as the absorption lines of the G-type star, as was noted in AE Aqr.

TABLE 1

VELOCITY OBSERVATIONS OF SS CYGNI

PLATE	JD 2430000+	PHASE (DAYS)	VELOCITY	
			Absorption (km/sec)	Emission (km/sec)
E 276	0267.770	0.000	+ 52	−106
1156	1309.944	.181	+ 52	− 76
1160	1310.774	.182	+ 40	− 52
1773	2098.661	.221	+110	−104
1774	2098.724	.008	+ 72	− 75
1775	2098.778	.062	− 93	+ 73
1776	2098.839	.123	−132	+ 95
1780	2110.719	.124	−106	+ 69
1781	2110.795	.201	+ 77	− 89
1785	2111.837	.137	− 16	+ 5
γ 33313	5028.644	.084	−111	+108
33316	5028.770	.210	+ 45	− 81
33317	5028.837	.001	+ 82	−100
33320	5029.626	.238	+113	−168
33321	5029.668	.003	+ 89	−148
33322	5029.708	.043	− 44	+ 36
33323	5029.774	.110	−114	+ 87
33324	5029.804	.139	− 92	+ 79
33325	5029.833	.168	− 18	+ 20
33326	5029.864	.199	+ 67	− 74
33329	5030.639	.145	− 63	+ 68
33330	5030.705	.211	+ 91	−127
33331	5030.755	.261	+130	−152
33333	5030.840	.071	− 84	+104
Xf 233	5316.769	.087	−110	+118
224	5316.810	.128	− 70	+ 70
225	5316.848	.166	+ 10	− 23
226	5316.881	.198	+ 88	−125
227	5316.915	.233	+ 83	−114
228	5316.958	.276	+102	− 54
229	5316.996	0.038	− 12	+ 32

The radial velocities from thirty-one Mount Wilson spectrograms (dispersion 70 or 110 A/mm at Hγ) which show measurable absorption lines are in Table 1. These observations were made at minimum light in 5 different years from 1941 to 1955. Exposures longer than 2 hours (0.08 day) have not been included.

The velocity measures of both dark and bright lines are exceedingly difficult and are subject to large errors. The visible absorption lines are few in number and extremely faint. The bright lines are much too wide for accurate measurement. Estimates of their displacements have been made with low magnification by setting on the mid-point of greatest intensity and also on the edges of these lines.

The determination of the period of the velocity variation was rendered much more certain by the fact that, on five nights, runs of several plates in succession were made. By cut-and-try methods, a period of 0.276244 day was derived. The phases of Table 1 are based on the epoch of the first plate (JD 2430267.7708). These results were assembled in nine normal places of three or four observations each and plotted in Figure 1. The average deviation of the velocities in these normals is 19 km/sec for the dark lines and 24 km/sec for bright lines. The accuracy of the observations hardly justifies a formal solu-

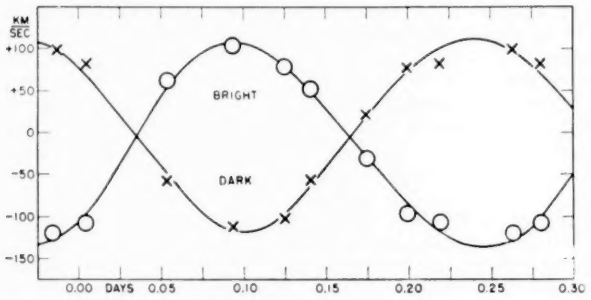

FIG. 1.—Velocity-curves of SS Cygni drawn through normal points, each representing three or four observations.

tion, but approximate values of the elements of the system considered as a spectroscopic binary can be estimated. From velocity-curves drawn through the normal places we find

$P = 0.276244$ day, $a_1 \sin i = 437000$ km,

$\gamma = -9$ km/sec, $a_2 \sin i = 463000$ km,

$e =$ small, $m_1 \sin^3 i = 0.20\ \odot$,

$K_1 = 115$ km/sec (narrow absorption lines), $m_2 \sin^3 i = 0.18\ \odot$.

$K_2 = 122$ km/sec (wide emission lines),

For the dG5 star, taking $T_1 = 5500°$ and $R_1 = 0.90\ \odot$,

$$M_1 = \frac{29500}{T_1} - 5 \log R_1 - 0.08 = +5.5.$$

This value of the absolute magnitude is only slightly fainter than that of G5 stars of the main sequence.

Because the strong continuum, which apparently originates in the same star as the wide emission lines, is of the same order of intensity at λ 5000 as that of the G-type star, we may assume that the hot component has the same absolute magnitude, +5.5. Then, using the same formula and $T_2 = 20000°$, as indicated by the intensity of the shortward continuum, a value of $R_2 = 0.150\ \odot = 105000$ km is found for the radius of the small hot star. If $i = 90°$, the distance between the surfaces of the two stars would be 168000 km.

Using 12.6 and +5.5 for the apparent and absolute magnitudes, respectively, of the G-type star, the corresponding parallax is 0".004. At this distance the well-determined proper motion of 0".115 would yield a tangential velocity of 135 km/sec.

The mean trigonometric parallax derived in the Yale Catalogue is 0".008, corresponding to $M = +7.1$ for each component. It is based on two discordant determinations—Mount Wilson (60-inch) −0".012 (van Maanen 1938) and Yerkes +0".032, $M = +10.1$ (Strand 1948). Strand's carefully determined parallax would put the two components of SS Cyg among the white dwarfs, but no stars of this class are known to have spectra resembling those of SS Cyg.

It seems unlikely that sufficient adjustments of the temperature or size of the G-type star can be made to bring the photometric into agreement with the trigonometric parallax, nor would a correction of several magnitudes on account of interstellar absorption be plausible in this region of the sky. In spite of the trigonometric parallax found by Strand, it is difficult to avoid the conviction that the G-type component belongs on or near the main sequence and that the hot component is a small subdwarf of nearly the same mass and luminosity, surrounded by an expanding gaseous envelope or by infalling turbulent matter as suggested by Crawford and Kraft (1956) for AE Aqr.

The stars are close together, and eclipses would occur unless the inclination of the orbit to the tangential plane is small. Gordon Grant (1955) made photoelectric observations of the star in 1955. Although his measures show rapid variations in brightness at minimum, amounting to as much as 0.3 mag. in yellow light, no certain evidence of eclipse was presented. If these dimensions are correct, the eclipse is total if $i > 60°$; only if $i < 50°$, which is well below the most probable statistical value, are eclipses entirely avoided. If $i = 50°$; $a_1 = 560000$ km, $a_2 = 600000$ km, $m_1 = 0.42\ \odot$, $m_2 = 0.40\ \odot$, and the distance between surfaces is 427000 km. At this distance heating and reflection must confuse the intrinsic radiation of the atmosphere of the G-type star to some extent.

The peculiar distortion of the velocity-curve found in AE Aqr is much less pronounced in the smoothed curve of SS Cyg. If present at all, it is lost in the uncertainty of the observations. These stars are so close together that the radiation of the small star can fall upon less than half the hemisphere of the larger star facing it. On the other hand, the effect of the radiation as well as gravitational attraction would be greatly enhanced as compared with AE Aqr on account of the much smaller distance between the surfaces, but, because of the higher temperature of the G-type star, the differential effect might be less evident in the total radiation.

Unless the inclination is near zero, photoelectric observations should show changes in light during the orbital period due to reflection and radiation effects on one side of the cool star. Changes in the spectrum might also be expected, but they have not been detected.

REFERENCES

Adams, W. S., and Joy, A. H. 1922, *Pop. Astr.*, **30**, 103.
Crawford, J. A., and Kraft, R. P. 1956, *Ap. J.*, **123**, 44.
Elvey, C. T., and Babcock, H. W. 1940, *Pub. A.A.S.*, **10**, 51.
———. 1943, *Ap. J.*, **97**, 412.
Grant, G. 1955, *Ap. J.*, **122**, 566.
Hinderer, F. 1949, *A.N.*, **277**, 193.
Joy, A. H. 1940, *Pub. A.S.P.*, **52**, 324.
———. 1954, *Ap. J.*, **120**, 377.
Maanen, A. van. 1938, *Ap. J.*, **87**, 424; *Mt. W. Contr.*, No. 590.
Strand, K. A. 1948, *Ap. J.*, **107**, 106.

THE VELOCITY-CURVE OF 15 CANIS MAJORIS*

C. R. LYNDS, J. SAHADE,† AND O. STRUVE
Berkeley Astronomical Department, University of California
Received May 11, 1956

ABSTRACT

Spectroscopic observations made in the interval from November, 1955, to January, 1956, confirm the classification by F. Henroteau of 15 Canis Majoris as a β Canis Majoris star. The period of the radial-velocity variation is found to be approximately 0.185 day, and the range of the mean velocity-curve is 7 km/sec. The observations also lend support to Henroteau's suspicion that the mean velocity is not constant. There is some indication that the velocity range undergoes variation.

15 Canis Majoris[1] was first found to have a variable radial velocity by W. W. Campbell (1911). However, this discovery was later withdrawn (Moore 1936). Henroteau (1922, 1924) listed the star as a possible member of the β Canis Majoris class of variables. He suggested a period in the neighborhood of 0.15 day. The observations available also suggested that a variation in the center-of-mass velocity was not unlikely. The light-variation of 15 Canis Majoris has been studied by Walker (1956). His observations indicate a light-range of approximately 0.01 mag. and a period of about 4 hours. His suggested ephemeris is

TABLE 1

LIST OF STAR LINES

Wave Length	Element	Wave Length	Element	Wave Length	Element
3964.73	He I	4143.76	He I	4471.48	He I
3973.26	O II	4340.47	Hγ	4481.23	Mg II
4026.19	He I	4345.56	O II	4552.65	Si III
4072.16	O II	4347.42	O II	4567.87	Si III
4075.87	O II	4349.43	O II	4574.78	Si III
4101.74	H δ	4387.93	He I	4590.97	O II
4119.22	O II	4414.91	O II	4596.17	O II
4120.81	He I	4416.98	O II		

$$\text{Maximum} = \text{Hel. JD } 2435411.973 + 0^d1565\ E\ (\pm 0^d0005\ E).$$

The observational material on which the present investigation is based consists of 86 spectrograms obtained with the coudé spectrograph of the 100-inch telescope of the Mount Wilson Observatory, on nine nights in the interval from November 23, 1955, to January 30, 1956. The linear dispersion of the spectrograms was 10 A/mm. The star lines which were measured are listed in Table 1, and the radial velocities are given in Table 2.

It was found impossible to make a reasonable representation of the periodicity of the observations on the basis of a period as short as those suggested by Henroteau and

* The spectrograms used in this work were obtained by O. Struve and J. Sahade as guest investigators at the Mount Wilson Observatory.

† John Simon Guggenheim Fellow.

[1] 15 Canis Majoris = HD 50707; $\alpha = 6^h51^m4$, $\delta = -20°09'.7$ (1950).

Walker. In fact, the observations of November 24, December 28, and January 30 suggest a period longer than 0.17 day. A period analysis of the observations yielded a value of 0.184558 ± 0.000005 day. We can set normal maximum at JD 2435502.882. The phases given in Table 2 are based upon these values and have been computed by means of the formula

$$\text{Phase in days} = T - (\text{JD } 2435502.882 + 0^d184558\ E).$$

The observations have been formed into normal velocities, and these are listed in Table 3. Figure 1 gives a plot of the individual observations, and Figure 2 gives a plot of the

TABLE 2

RADIAL VELOCITIES

JD 2435+	Radial Velocity (km/sec)	Phase (Fraction of Day)	JD 2435+	Radial Velocity (km/sec)	Phase (Fraction of Day)	JD 2435+	Radial Velocity (km/sec)	Phase (Fraction of Day)
434.972	+28.6	0.006	469.801	+27.7	0.140	500.794	+18.0	0.126
.985	28.2	.020	.817	30.0	.155	.813	22.5	.146
.999	24.3	.033	.831	32.5	.170	.848	30.5	.181
435.014	19.1	.049	.846	34.2	.000	.874	29.9	.206
.029	22.5	.064	.862	32.8	.016	.890	29.2	.223
.046	23.8	.081	.876	28.5	.030	.907	28.5	.240
.060	23.2	.095	.892	25.6	.046	501.781	27.9	.006
.894	32.1	.007	.907	24.5	.061	.799	26.0	.024
.910	29.2	.023	.922	22.8	.076	.810	26.5	.035
.925	25.4	.038	.938	24.4	.091	.856	26.1	.081
.940	23.5	.052	.952	26.8	.106	.871	26.0	.096
.954	24.3	.067	.967	22.0	.121	.886	24.1	.111
.969	24.6	.082	470.718	21.5	.134	.901	23.8	.126
.984	23.4	.097	.733	23.2	.149	502.688	31.1	.175
436.004	22.3	.116	.749	24.7	.164	.706	30.9	.008
.019	25.1	.131	.763	28.3	.179	.718	27.6	.021
.033	27.3	.146	.850	23.8	.081	.735	25.0	.037
.050	28.4	.163	.865	24.1	.096	.749	21.8	.052
.065	31.3	.178	472.708	24.2	.094	.763	21.6	.066
.892	23.1	.082	.723	23.5	.108	.777	23.3	.080
.908	19.3	.097	.738	25.4	.123	.792	25.3	.094
.920	20.3	.110	.752	25.7	.138	.806	25.6	.108
.937	19.6	.127	.767	27.2	.152	.820	26.4	.123
.951	23.4	.141	.781	26.9	.167	.839	27.0	.142
.966	25.7	.156	.796	29.1	.181	.854	28.0	.156
.981	31.3	.170	.810	26.0	.011	.868	29.2	.171
.998	28.9	.003	.826	22.6	.027	.882	31.2	.184
437.022	27.8	.027	.841	21.4	.042	.897	29.1	0.015
469.786	24.2	0.124	.856	22.4	0.057			

TABLE 3

NORMAL VELOCITIES

Phase (Fraction of Day)	Radial Velocity (km/sec)	Phase (Fraction of Day)	Radial Velocity (km/sec)	Phase (Fraction of Day)	Radial Velocity (km/sec)	Phase (Fraction of Day)	Radial Velocity (km/sec)
0.001	+30.31	0.044	+23.88	0.095	+23.64	0.140	+25.01
.015	+29.21	.063	+23.80	.111	+23.51	.156	+26.74
0.028	+26.41	0.082	+24.16	0.125	+23.21	0.172	+30.09

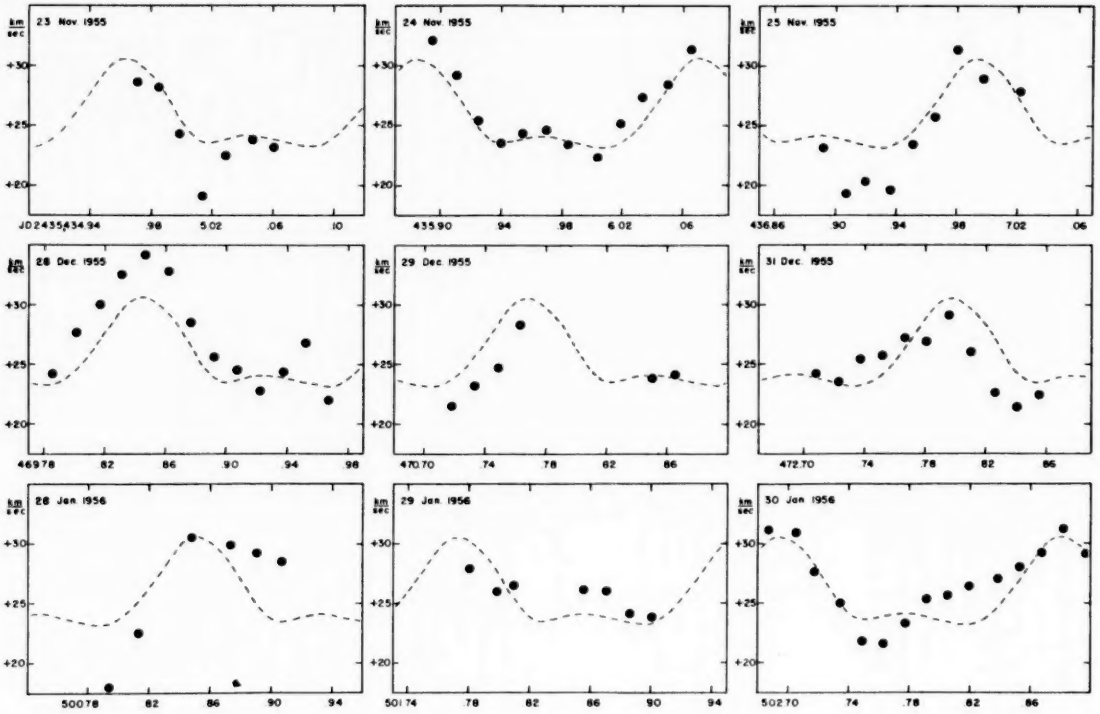

FIG. 1.—Plot of individual radial velocities of 15 Canis Majoris

normals. The dashed curves which appear in Figure 1 are representations of the normal points.

An inspection of the velocity-curves in Figure 1 leads to the conclusion that the velocity-curve does not repeat itself exactly from cycle to cycle. Many examples of differences in shape are readily apparent. For instance, the velocity-curve for November 24 is certainly quite different from that for January 30. There is also evidence that the maximum velocity undergoes variation from cycle to cycle. The velocity at maximum was 5 km/sec greater on December 28 than on December 31. Likewise, there seems to be considerable scatter in the minimum velocities attained in individual cycles. Finally, the present observational material does not contradict Henroteau's suggestion that the center-of-mass velocity changes. In short, it is fairly certain that we are dealing with interfering modes of periodic variation similar to those found in other members of the β Canis Majoris class.

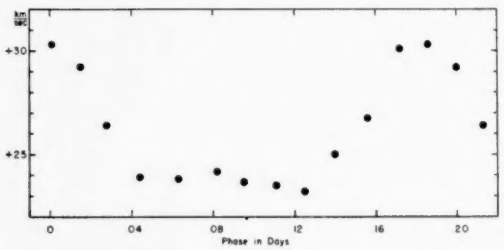

FIG. 2.—Plot of normal radial velocities of 15 Canis Majoris

In view of the fact that the observed velocity variation is probably the result of interfering modes, our determination of the period is somewhat uncertain. The uniqueness of the period determined and the value of the expected uncertainty are based upon velocity maxima of similarly shaped velocity-curves. It may be said with some confidence that the principal period of velocity variation of 15 Canis Majoris is near 0.185 day.

The present material contains no definite evidence that the spectrum of 15 Canis Majoris varies with phase. This is not surprising in view of the small velocity amplitude of the star. In appearance the spectrum closely resembles that of BW Vulpeculae. An estimate of the spectral type is B1–B2 III.

REFERENCES

Campbell, W. W. 1911, *Lick Obs. Bull.*, **6**, 140.
Henroteau, F. 1922, *Pub. Dom. Obs. Ottawa*, **5**, 333.
———. 1924, *ibid.*, **9**, 47.
Moore, J. H. 1936, *Lick Obs. Bull.*, **18**, 1.
Walker, M. F. 1956, *Pub. A.S.P.*, in press.

SIMULTANEOUS SPECTROGRAPHIC AND PHOTOMETRIC OBSERVATIONS OF THE SHORT-PERIOD VARIABLES SX PHOENICIS AND CC ANDROMEDAE

O. C. Wilson and Merle F. Walker*
Mount Wilson and Palomar Observatories
Carnegie Institution of Washington, California Institute of Technology
Received March 15, 1956

ABSTRACT

Radial velocity-curves and light-curves in three colors are derived from simultaneous spectrographic and photoelectric observations made at Palomar in 1953 and 1954. For both SX Phoenicis and CC Andromedae maximum brightness lags behind maximum size, as deduced from the radial velocities, by a quarter-period, as is true of the cepheid variables. The light-amplitude of SX Phoenicis is widely variable, but corresponding variations in the velocity-amplitude cannot be established with certainty. On the other hand, there is an obvious relationship between the light- and velocity-amplitudes of CC Andromedae, which seems to be the same as that for δ Scuti. It is probable that these two stars, together with DQ Cephei, belong to the same class of variable and that they may be considerably brighter than main-sequence stars of the same spectral type.

INTRODUCTION

The variability of SX Phoenicis (HD 223065) was discovered by (Eggen 1952*a*), who established that the period was 80 minutes. This very short period—the shortest known for any variable star—led one of the authors (O.C.W.) to make some experimental spectrographic observations in 1953 to test the feasibility of determining velocity-curves. Exposure times for such objects should be as short as possible and, in any event, should not exceed about 10 per cent of the period. This restriction to exposure times of the order of 8 minutes or less, together with the declination of the star (−42°) and the necessity for as large a dispersion as possible, severely limited the choice of equipment to be used. In fact, it was clear that the 200-inch telescope and the 8-inch camera of the coudé spectrograph offered the only possibility, and it was with this arrangement that the exposures were made.

In the meantime, Eggen had informed us privately of the variability of BD+41°119 (since designated CC Andromedae), and similar experimental observations of this star were made in October, 1953. Although CC Andromedae is fainter than SX Phoenicis, its more favorable position and longer period of about 3 hours (Lindblad and Eggen 1953) permitted the use of higher dispersion. It was found that, with the 18-inch camera of the Palomar coudé, good plates could be obtained under average conditions in exposure times of the order of 20 minutes.

The results of the earlier 1953 observations indicated that reliable velocity-curves could indeed be obtained for both stars, and the authors therefore planned a joint operation of simultaneous magnitude, color, and spectrographic observation for these objects. These observations were begun in November, 1953, for CC Andromedae and continued in the late summer of 1954 for both stars. Baked IIa-O plates were used throughout.

SPECTROGRAPHIC OBSERVATIONS AND RESULTS

Data concerning the spectrograms of SX Phoenicis and CC Andromedae and the measured radial velocities are in Table 1 and 2. The large reduction factor from slit to plate for the 8-inch camera required trailing over a slit length of 10 mm; the resulting

* Carnegie Fellow; now at the Warner and Swasey Observatory, Case Institute of Technology.

TABLE 1

SX PHOENICIS RADIAL VELOCITIES

Plate	Date 1953	P. S. T.	Heliac J. D. 2,430,000.	No. Lines	Vel. ± P. E. km/sec	Exp. Time Min:sec
Pe 1032a	July 4	14:47:20	4,563.9523	16	-9.8 ± 3.2	4:40
b	"	14:53:15	.9565	15	-13.8 ± 3.0	4:30
c	"	14:59:13	.9607	13	-31.8 ± 3.8	4:55
d	"	15:05:10	.9612	10	-42.0 ± 4.3	4:50
e	"	15:10:55	.9687	No Arc		
Pe 1033a	"	15:26:28	4,563.9808	25	-44.7 ± 2.8	4:55
b	"	15:34:45	.9852	21	-45.8 ± 2.6	4:20
c	"	15:40:20	.9891	31	-25.7 ± 2.0	4:40
d	"	15:46:08	.9932	27	-18.0 ± 2.2	4:45
e	"	15:52:13	.9974	35	-9.1 ± 1.6	5:05
Pe 1036a	July 5	14:28:10	4,564.9390	16	-30.6 ± 2.7	6:20
b	"	14:35:13	.9440	20	-14.5 ± 1.8	5:55
c	"	14:42:12	.9487	14	-33.3 ± 2.8	6:05
d	"	14:49:22	.9538	4	-59.5 ± 4.4	6:05
e	"	14:56:35	.9588	9	-50.8 ± 2.4	6:10
Pe 1037a	"	15:05:30	4,564.9649	9	-50.2 ± 3.6	6:20
b	"	15:12:25	.9698	24	-45.7 ± 2.2	6:20
c	"	15:19:17	.9745	23	-41.1 ± 2.1	5:45
d	"	15:26:25	.9794	26	-26.7 ± 1.8	6:30
e	"	15:33:00	.9840	25	-19.5 ± 1.4	6:00
Pe 1038a	"	15:42:07	4,564.9904	17	-9.6 ± 1.9	5:45
b	"	15:49:07	.9953	17	-19.9 ± 2.8	6:05
Pe 1108a	Aug. 25	11:24:10	4,615.8131	24	-39.5 ± 2.4	7:20
b	"	11:32:50	.8191	35	-29.9 ± 1.6	7:40
c	"	11:41:40	.8252	44	-23.3 ± 2.7	7:40
d	"	11:50:28	.8313	49	-5.9 ± 1.5	7:15
e	"	11:59:25	.8375	31	+3.4 ± 1.5	8:30
Pe 1109a	"	12:09:37	4,615.8447	20	-10.4 ± 1.8	6:35
b	"	12:17:18	.8499	8	-37.2 ± 2.2	6:35
c	"	12:25:07	.8554	9	-53.9 ± 3.8	7:05
d	"	12:32:55	.8608	11	-52.8 ± 3.5	6:40
e	"	12:40:37	.8661	29	-41.2 ± 2.4	6:35
Pe 1110a	"	13:25:45	4,615.8974	22	-15.8 ± 2.3	6:40
b	"	13:35:20	.9041	18	-38.1 ± 2.6	6:40
c	"	13:42:58	.9095	25	-47.6 ± 2.6	6:55
d	"	13:50:50	.9149	16	-41.6 ± 2.5	6:40
e	"	13:58:32	.9203	24	-41.2 ± 2.2	6:45
	1954					
Pe 1631a	Aug. 11	12: 7:47	4,966.8431	20	-19.2 ± 2.5	10:06
b	"	12:19:57	.8516	19	-47.4 ± 1.9	7:57
c	"	12:29:39	.8584	22	-56.8 ± 2.8	8:11
d	"	12:40:27	.8658	25	-50.1 ± 2.0	7:58
e	"	12:50:13	.8726	38	-39.6 ± 1.8	8:15
Pe 1632a	Aug. 11	13:02:36	4,966.8812	32	-23.1 ± 1.3	6:48
b	"	13:11:17	.8872	41	-23.6 ± 1.8	7:00
c	"	13:22:33	.8951	31	-21.0 ± 1.6	7:12
d	"	13:32:48	.9022	33	-31.7 ± 1.8	7:08
e	"	13:41:47	.9084	31	-35.3 ± 1.5	5:54
Pe 1633a	"	13:51:45	4,966.9153	22	-41.0 ± 2.0	5:49
b	"	14:00:06	.9212	34	-52.3 ± 1.7	6:05
c	"	14:08:42	.9271	31	-50.7 ± 1.6	5:48
d	"	14:17:31	.9233	40	-37.8 ± 1.6	6:54
e	"	14:26:45	.9396	35	-24.2 ± 1.3	6:46
Pe 1634a	"	14:37:07	4,966.9469	37	-17.6 ± 1.8	6:47
b	"	14:46:02	.9530	35	-27.3 ± 2.2	6:03
c	"	14:54:37	.9590	41	-24.2 ± 1.7	5:55
d	"	15:02:58	.9648	31	-42.1 ± 1.6	5:43
e	"	15:10:17	.9699	19	-49.8 ± 1.9	5:00
Pe 1635a	"	15:17:36	4,966.9749	21	-54.7 ± 2.7	4:50
b	"	15:26:28	.9810	28	-52.1 ± 2.0	7:26
c	"	15:37:00	.9884	47	-38.0 ± 1.8	9:21
d	"	15:48:52	.9967	42	-22.9 ± 1.5	9:57
e	"	16:01:01	4,967.0051	39	- 4.1 ± 1.5	9:26
Pe 1636a	Aug. 12	12:08:42	4,967.8439	21	-47.3 ± 2.2	7:08
b	"	12:19:08	.8511	25	-47.4 ± 1.9	8:11
c	"	12:30:10	.8588	31	-49.0 ± 2.0	7:56
d	"	12:41:18	.8665	33	-40.6 ± 2.2	9:48
e	"	12:52:51	.8745	36	-23.4 ± 1.6	7:52
Pe 1637a	"	13:03:05	4,967.8817	30	-16.1 ± 1.3	6:10
b	"	13:11:48	.8877	27	-19.7 ± 1.8	6:13
c	"	13:20:22	.8937	33	-34.1 ± 2.1	6:10
d	"	13:29:26	.8999	25	-56.1 ± 1.6	6:09
e	"	13:37:32	.9056	26	-51.4 ± 2.3	5:49
Pe 1638a	"	13:46:52	4,967.9120	27	-47.2 ± 2.0	6:58
b	"	13:56:29	.9187	27	-44.2 ± 2.0	7:42
c	"	14:07:19	.9262	37	-31.3 ± 1.0	9:35
d	"	14:19:17	.9346	33	-14.2 ± 1.8	9:37
e	"	14:29:42	.9418	36	-14.4 ± 2.0	6:40
Pe 1639a	"	14:42:01	4,967.9503	28	-28.7 ± 2.0	9:33
b	"	14:51:39	.9571	23	-59.4 ± 3.5	5:58
c	"	14:59:33	.9626	25	-46.8 ± 2.6	5:35
d	"	15:08:41	.9689	30	-57.9 ± 2.1	8:12
e	"	15:20:11	.9768	30	-35.4 ± 1.8	11:01
Pe 1640a	"	15:34:27	4,967.9867	39	-14.6 ± 2.0	11:13
b	"	15:47:43	.9960	36	-12.2 ± 1.3	11:09
c	"	15:59:57	4,968.0045	17	-45.2 ± 2.7	8:25
d	"	16:10:24	.0117	22	-43.0 ± 2.9	8:22

TABLE 2

CC ANDROMEDAE RADIAL VELOCITIES

Plate	Date 1953	P. S. T.	Heliac J. D. 2,430,000.	No. Lines	Vel. ± P. E. km/sec	Exp. Time Min
Pd 1187a	Oct. 24	6:40	4,675.6156	15	-0.1 ± 1.1	16
b	"	6:58	.6281	16	-4.7 ± 1.4	17
c	"	7:18	.6420	15	-15.1 ± 0.9	21
d	"	7:38	.6559	15	-17.6 ± 2.3	16
e	"	7:56	.6684	14	-15.1 ± 0.9	16
Pd 1188a	"	8:14	.6809	16	-11.6 ± 1.1	17
b	"	8:32	.6934	16	-9.4 ± 0.9	16
c	"	8:50	.7059	13	-1.2 ± 1.3	16
d	"	9:06	.7170	13	+1.6 ± 1.3	12
e	"	9:18	.7253	7	+1.6 ± 1.8	11
Pd 1189a	"	9:34	.7365	14	+3.2 ± 1.7	16
b	"	9:51	.7482	15	-3.2 ± 1.5	16
c	"	10:08	.7601	No Arc		15
d	"	10:24	.7712	15	-15.1 ± 1.6	15
e	"	10:42	.7837	14	-16.7 ± 0.9	15
Pd 1190a	"	10:58	.7948	12	-13.6 ± 1.1	15
b	"	11:16	.8072	14	-11.3 ± 1.6	15
Pd 1195a	Oct. 26	6:55	4,677.6260	7	+0.7 ± 2.4	20
b	"	7:16	.6406	13	-12.3 ± 1.1	19
c	"	7:37	.6552	13	-15.8 ± 1.1	19
d	"	7:57	.6691	14	-17.2 ± 1.2	18
e	"	8:18	.6837	14	-14.1 ± 1.6	21
Pd 1196a	"	8:43	4,677.7010	13	-3.0 ± 1.1	20
b	"	9:04	.7156	14	-5.4 ± 1.4	20
c	"	9:26	.7309	14	-4.6 ± 0.9	20
d	"	9:46	.7448	11	-3.3 ± 1.7	19
e	"	10:07	.7594	13	-5.0 ± 2.2	20
Pd 1197a	"	10:30	4,677.7752	14	-9.8 ± 0.9	21
b	"	10:51	.7899	13	-16.3 ± 1.8	21
c	"	11:14	.8059	13	-11.5 ± 0.7	22
d	"	11:36	.8212	15	-10.7 ± 1.3	20
e	"	11:56	.8350	14	+0.5 ± 1.1	18
Pd 1230a	Nov. 21	7:58	4,703.6693	10	-1.1 ± 1.2	26
b	"	8:24	.6874	15	-5.5 ± 0.8	20
c	"	8:44	.7012	14	-0.9 ± 0.7	18
d	"	9:05	.7158	16	-5.4 ± 1.0	21
e	"	9:26	.7304	10	-5.7 ± 0.7	18
Pd 1231a	"	9:47	4,703.7450	15	-5.0 ± 0.9	20
b	"	10:09	.7603	14	-17.9 ± 0.9	22
c	"	10:31	.7755	15	-18.1 ± 2.2	19
d	"	10:51	.7894	13	-15.2 ± 0.7	19
e	"	11:10	.8026	14	-6.5 ± 1.5	18
Pd 1233a	Nov. 22	6:30	4,704.6082			21
b	"	6:52	.6234			19
c	"	Clouds				
d	"	8:39	.6978	21	-9.8 ± 1.0	19
e	"	8:59	.7117	14	+1.3 ± 2.0	20
Pd 1234a	Nov. 22	9:22	4,704.7276	10	-2.4 ± 3.2	19
b	"	9:44	.7249	14	-11.6 ± 1.1	20
c	"	10:07	.7589	16	-12.8 ± 1.4	21
d	"	10:28	.7735	15	-14.4 ± 1.0	20
e	"	10:48	.7873	14	-8.2 ± 1.4	18
Pd 1235a	"	11:10	4,704.8026	14	-6.8 ± 2.1	22
b	"	11:31	.8172	13	+2.2 ± 1.5	18
c	"	11:50	.8304	13	-0.2 ± 1.7	18
	1954					
Pd 1725a	Sep. 17	12:38	5,003.8637	40	-5.7 ± 0.4	24
b	"	13:04	.8818	39	-11.0 ± 0.4	24
c	"	13:32	.9012	39	-13.5 ± 0.6	28
d	"	14:00	.9207	41	-16.1 ± 0.5	23
e	"	14:27	.9394	41	-13.2 ± 0.5	28
Pd 1726a	"	15:01	.9630	52	-6.1 ± 0.3	35
b	"	15:36	.9873	38	-3.5 ± 0.4	30
c	"	16:08	5,004.0096	44	-8.6 ± 0.4	30
Pd 1729a	Sep. 18	11:00	5,004.7957	41	-17.3 ± 0.5	32
b	"	11:30	.8165	35	-18.4 ± 0.6	23
c	"	11:55	.8338	39	-14.4 ± 0.6	22
d	"	12:17	.8491	34	-10.1 ± 0.9	19
e	"	12:37	.8630	40	-6.7 ± 0.5	20
Pd 1730a	"	13:00	5,004.8790	46	-8.9 ± 0.3	20
b	"	13:23	.8950	36	-20.7 ± 0.5	20
c	"	13:44	.9096	43	-21.1 ± 0.5	18
d	"	14:05	.9241	46	-22.7 ± 0.5	19
e	"	14:26	.9387	44	-14.3 ± 0.4	19
Pd 1731a	"	14:47	.9533	60	-9.7 ± 0.7	20
b	"	15:09	.9686	54	-4.9 ± 0.8	20
c	"	15:31	.9838	56	-2.9 ± 0.9	20
d	"	15:53	.9991	55	-4.5 ± 1.2	20
Pd 1734a	Sep. 19	10:28	5,005.7735	54	-17.0 ± 0.5	20
b	"	10:50	.7887	46	-24.9 ± 0.6	20
c	"	11:12	.8040	45	-22.4 ± 0.4	20
d	"	11:34	.8193	49	-17.4 ± 0.4	20
e	"	11:56	.8345	51	-11.4 ± 0.4	21
Pd 1735a	"	12:20	.8512	50	-4.6 ± 0.3	20
b	"	12:42	.8665	30	-1.8 ± 0.5	20
c	"	13:05	.8825	38	-4.3 ± 0.6	20
d	"	13:28	.8984	35	-16.2 ± 0.6	20
e	"	13:51	.9144	36	-25.8 ± 0.6	20
Pd 1736a	"	14:14	.9304	51	-17.7 ± 0.4	21
b	"	14:37	.9464	48	-14.5 ± 0.4	20
c	"	14:59	.9577	53	-7.9 ± 0.3	20
d	"	15:21	.9769	47	-4.1 ± 0.5	20
e	"	15:43	.9922	53	+0.2 ± 0.4	20
Pd 1737a	"	16:05	5,006.0075	54	-2.5 ± 0.5	20

spectra were about 0.25 mm wide on the plate. On the 1953 spectrograms of SX Phoenicis all possible lines were measured and the mean velocities derived. A list of possible contributors to each measured line was then drawn up, and, on the basis of a study of the residuals for the individual lines from the mean velocities, revised wave lengths were obtained. Lines appearing on only a few scattered spectrograms were eliminated at the start as being too uncertain for use. Fifty lines appeared in the final working list, although the entire number was not measurable on any single spectrogram. These revised wave lengths were used in the reduction of the 1954 observations, but it was not considered worth the effort to re-reduce the 1953 spectrograms with them. The 8-inch camera, which gives a dispersion of 38 A/mm, provides a somewhat limited range of wavelength coverage; all the spectrograms used in this investigation extended from about 4450 to 3800 A. By adjusting exposure times to correspond to the brightness of the star and the varying seeing, it was possible to keep the density of the exposures reasonably uniform.

For CC Andromedae, only twelve to fifteen lines were measured on the 1953 spectrograms, but these were adequate to give fairly reliable velocities. The 1954 plates were, however, measured much more completely, and the improvement in the probable errors is evident from Table 2. With the higher dispersion of the 18-inch camera (20 A/mm), it did not seem necessary to make an exhaustive study of residuals and corrected wave lengths. Instead, the few obviously discordant lines were simply eliminated at once and excluded from the means. The plates of CC Andromedae were measured, in general, between 4005 and 4415 A, although these limits were occasionally exceeded somewhat. Again, as with SX Phoenicis, the exposure times were adjusted to fit prevailing conditions and resulted in spectrograms of reasonably constant density. For both stars it was necessary in a few instances to exceed the arbitrary exposure time limit of $0.1P$, though not, it is believed, to a degree which will seriously affect the results.

PHOTOELECTRIC OBSERVATIONS

Both stars were observed photoelectrically in three colors. The photometer employed an EMI 6094 eleven-stage, end-on multiplier tube and the following filters: yellow, 1.7-mm of Schott GG11; blue, 1-mm of Scott BG12 plus 2-mm of Schott GG13; ultraviolet, 2.6-mm of Corning 9863. The output of the multiplier tube was amplified and used to drive a Brown recorder having a chart speed of 12 inches per hour.

SX Phoenicis

The large southern declination of SX Phoenicis placed it out of reach of the 20-inch reflector at Palomar. Consequently, the photoelectric observations were obtained by mounting the photometer from the 20-inch in the coudé observing room of the 200-inch reflector. A piece of clear plate glass, mounted in the coudé beam ahead of the slit of the spectrograph, reflected a few per cent of the light of the star into the photometer. In this way, the seeing fluctuations were integrated over the entire 200-inch mirror so that, in spite of the large zenith distance (which ranged between sec $Z = 3.9$ and 6.5 during the observations), the amount of seeing noise in the deflections on the star was fairly small. The photoelectric observations were then made while the star was being observed spectroscopically. Atmospheric dispersion made it impossible to adjust the photometer so that the displacement of the star as it was trailed along the slit of the spectrograph could be contained within the field of the Fabry lens of the photometer for all three colors. It was, however, possible to arrange for the maximum deflection in each color to be attained at some point along the trail. Thus the variable was observed in each color during successive excursions along the slit of the spectrograph, and the peak of each deflection was used in the reduction of the observations. Sky readings were taken about every 5–7 minutes while plates were being changed in the spectrograph.

The rapidity of the light-variation and the necessity for using the 200-inch for both photoelectric and spectrographic observations made it impossible to measure a comparison star during the simultaneous runs on SX Phoenicis without introducing undesirably large gaps in our record of the variable. Instead, photoelectric observations of a red and a blue extinction star were obtained earlier in the night, covering the same range in sec Z over which the variable would be observed later. These extinction measures were thus necessarily made in a different part of the sky and at a different time than the measures of the variable. Because of these differences, as well as the very large zenith distances involved and the possibility of error due to the trailing of the variable during the observations, no attempt has been made to put the measures of SX Phoenicis on any standard photometric system. The observations have been corrected only for differential extinction during the run, using the extinction coefficients inferred from the two extinction stars on the basis of their known colors and the color of SX Phoenicis given by Eggen (1952*b*). Variations in the sensitivity of the photometer during the runs were corrected by means of comparisons with a radium source.

Although four nights had been allotted to this investigation, satisfactory photometric results were obtained only on August 13. During the run of August 12 there appears to have been a progressive change in transparency which cannot be eliminated from the observations because of the lack of simultaneous extinction measures. Hence only the yellow curve has been plotted for this night (Fig. 1) to show the phase and amplitude relationships of the light- and velocity-curves. Although the photometry of August 13 appears to be fairly satisfactory, we cannot give a quantitative measure of reliability, and the lack of certainty about the finer points of our results must be kept in mind in any discussion based upon them. The observations of August 13 are given in Table 3 and are plotted with the simultaneous velocities in Figure 2. All tabulated and plotted magnitudes are on the instrumental system and have arbitrary zero points.

The observed times of maximum light are given in Table 5, where only the yellow maxima have been listed for August 12. For August 13 the observed maxima are given for each color, and no systematic phase differences depending upon the color are indicated.

CC Andromedae

For this variable, the photometer was mounted in the usual way on the 20-inch reflector. No suitable comparison star was sufficiently close to the variable to be reached without unclamping and resetting the telescope. Since the period of this star is only 3 hours, adequate coverage of the light-curve is therefore difficult by the usual procedure of alternate observations on the variable and a comparison star. Hence, on nights of good photometric quality, less frequent observations of reference stars were made, and, since resetting the telescope was necessary for the observation of any reference star, the variable was compared directly to stars from Johnson and Morgan's (1953) list of stars on the U, B, V system. On one night when the photometric quality of the sky was poor, observations were made only in yellow light, and the variable was compared only to a relatively nearby star. This star was subsequently tied to the U, B, V system, and the observations of the variable converted to V magnitudes. The observations of the variable on the U, B, V system are given in Table 4 and are shown with the radial velocities in Figures 3–7. The internal accuracy of the observations during any given run is quite good, as can be seen from the light-curves. The uncertainty of the tie-in to the U, B, V system is, however, somewhat greater and is probably of the order of 0.01 or 0.02 mag.

The observed light-maxima of CC Andromedae are listed in Table 6, where the first six maxima are repeated from the paper by Lindblad and Eggen (1953). The present three-color observations give no evidence of a systematic difference in the time of maximum light with wave length. Consequently, the times of maximum light listed are the averages of the observed times for each color. Using the present three-color observations, it

is now possible to determine the period of this variable. The elements of the light-variation are:

$$\text{Max.} = \text{Hel. JD } 2434604.958 + 0^d1249078E.$$

Both the present observations and those of Lindblad and Eggen show that the amplitude of the light-variation is variable, but the observations are insufficient to determine the period of this variation, if one exists. However, from the fact that the amplitudes of successive cycles on the same night do not change appreciably and from the behavior of the amplitudes on successive nights, the beat period is probably of the order of a few days.

DISCUSSION

For both stars the plots of the radial velocities and magnitudes show the usual quarter-period phase lag of maximum brightness behind maximum size which is encountered in the cepheid variables. Also, both exhibit a sizable range in the amplitude of light-variation. For SX Phoenicis this effect has been analyzed carefully by Walraven (1953–1955),

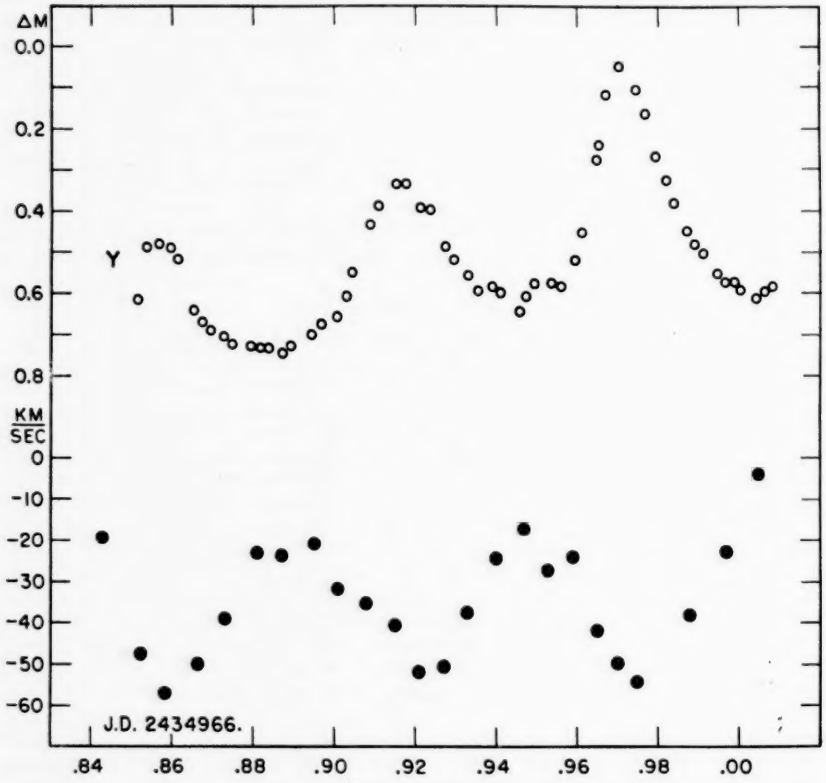

FIG. 1.—Radial velocities and magnitude variations (yellow only) of SX Phoenicis on Aug. 12, 1954

TABLE 3

PHOTOELECTRIC OBSERVATIONS OF SX PHOENICIS

YELLOW

Heliоc JD 2434000+	Δ Mag
967.8347	+0.424
.8425	0.262
.8444	0.240
.8468	0.217
.8507	0.256
.8530	0.300
.8571	0.382
.8591	0.403
.8613	0.416
.8651	0.515
.8674	0.541
.8693	0.562
.8735	0.581
.8755	0.595
.8776	0.610
.8818	0.628
.8842	0.640
.8880	0.629
.8939	0.553
.8962	0.508
.9003	0.381
.9026	0.319
.9060	0.279
.9080	0.284
.9121	0.333
.9142	0.386
.9178	0.449
.9198	0.492
.9218	0.524
.9253	0.585
.9274	0.590
.9295	0.612
.9330	0.651
.9350	0.645
.9366	0.664
.9385	0.668
.9420	0.662
.9440	0.642
.9489	0.568
.9508	0.479
.9528	0.348
.9542	0.210
.9564	0.060
.9578	0.019
.9594	0.017
.9622	0.091
.9642	0.161
.9676	0.301
.9693	0.364
.9713	0.425
.9746	0.495
.9766	0.543

YELLOW

Heliоc JD 2434000+	Δ Mag
967.9786	+0.558
.9805	0.584
.9846	0.616
.9867	0.634
.9885	0.637
.9905	0.630
.9938	0.631
.9956	0.603
.9977	0.567
.9996	0.523
968.0033	0.367
.0053	0.212
.0073	0.068
.0112	0.017
.0130	0.067
968.0150	0.101

BLUE

Heliоc JD 2434000+	Δ Mag
967.8364	0.527
.8430	0.297
.8454	0.281
.8494	0.302
.8514	0.343
.8535	0.380
.8577	0.477
.8598	0.497
.8620	0.521
.8657	0.607
.8678	0.660
.8699	0.685
.8743	0.719
.8761	0.705
.8804	0.745
.8827	0.757
.8865	0.759
.8886	0.753
.8926	0.692
.8947	0.647
.8988	0.514
.9010	0.427
.9045	0.340
.9066	0.317
.9108	0.354
.9128	0.422
.9148	0.456
.9184	0.575
.9203	0.594
.9241	0.650
.9260	0.690
.9281	0.728
.9301	0.741

BLUE

Heliоc JD 2434000+	Δ Mag
967.9337	+0.784
.9354	0.776
.9371	0.794
.9405	0.779
.9425	0.784
.9446	0.750
.9495	0.625
.9515	0.524
.9534	0.348
.9560	0.051
.9580	0.008
.9597	0.018
.9627	0.105
.9646	0.200
.9680	0.367
.9700	0.446
.9719	0.516
.9750	0.614
.9771	0.634
.9791	0.683
.9810	0.693
.9851	0.733
.9871	0.754
.9892	0.757
.9910	0.754
.9943	0.733
.9963	0.697
.9982	0.647
968.0003	0.580
.0039	0.394
.0060	0.195
.0081	0.092
.0097	0.010
.0118	0.029
.0135	0.078
968.0153	0.144

ULTRAVIOLET

Heliоc JD 2434000+	Δ Mag
967.8379	+0.550
.8436	0.316
.8458	0.299
.8499	0.326
.8522	0.396
.8543	0.431
.8583	0.518
.8605	0.587
.8643	0.616
.8664	0.646
.8685	0.716
.8727	0.722
.8748	0.737

ULTRAVIOLET

Heliоc JD 2434000+	Δ Mag
967.8768	+0.742
.8810	0.785
.8833	0.808
.8871	0.788
.8893	0.831
.8930	0.721
.8954	0.654
.8993	0.556
.9017	0.485
.9052	0.405
.9073	0.399
.9112	0.454
.9134	0.515
.9170	0.592
.9190	0.634
.9210	0.675
.9247	0.727
.9267	0.748
.9287	0.789
.9322	0.801
.9342	0.814
.9359	0.821
.9378	0.822
.9412	0.812
.9430	0.803
.9480	0.720
.9498	0.647
.9521	0.547
.9539	0.362
.9566	0.111
.9588	0.082
.9614	0.127
.9632	0.209
.9667	0.362
.9686	0.439
.9706	0.519
.9739	0.609
.9757	0.649
.9776	0.666
.9797	0.694
.9838	0.749
.9858	0.744
.9878	0.753
.9896	0.756
.9930	0.735
.9949	0.710
.9969	0.666
.9988	0.613
968.0025	0.466
.0046	0.356
.0065	0.123
.0078	0.042
.0103	0.004
.0122	0.032
968.0143	0.074

who finds that the light-variations can be reproduced by means of a curve which is the sum of two sine-curves, modified by distortions in both the time and the magnitude co-ordinates. In this respect SX Phoenicis resembles AI Velorum which has been discussed even more extensively by Walraven (1955). Moreover, Gratton (1953) has shown that the radial velocity-curves for AI Velorum also vary widely in amplitude and can be represented as the sum of two sine terms with the same periods as those deduced from the light-curves, together with a time- but no amplitude-distortion. SX Phoenicis, on the other hand, does not exhibit much, if any, variation in the amplitude of the velocity-curves. In Figures 1 and 2 there are five maxima and six minima of radial velocity. The

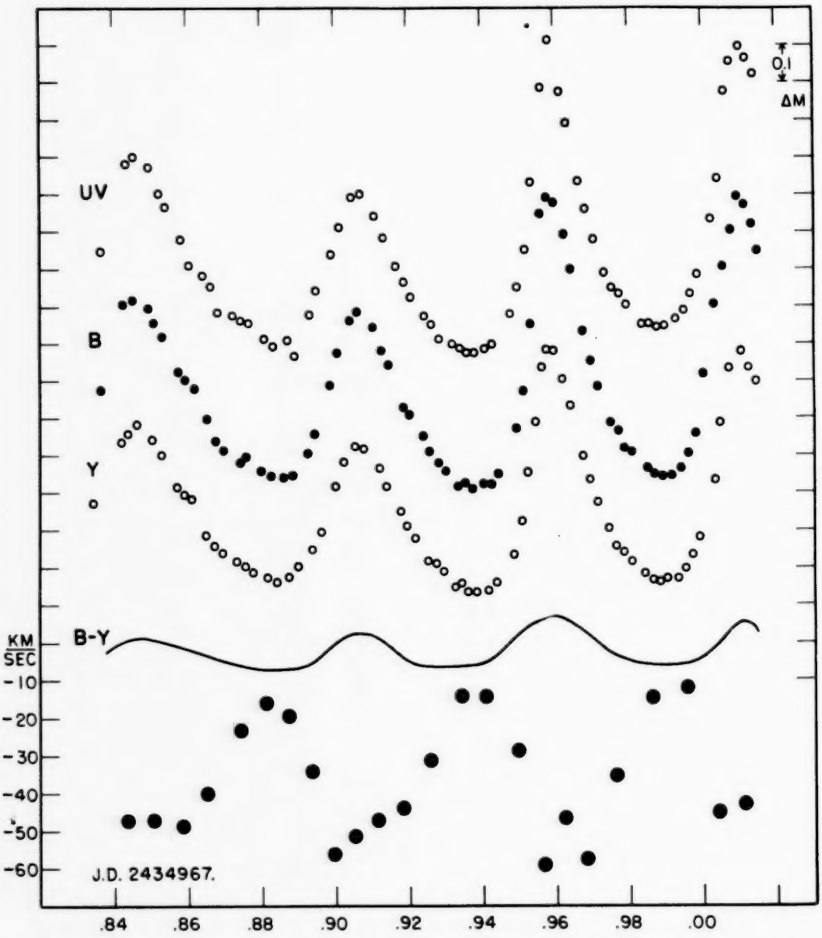

FIG. 2.—Radial velocities and magnitude variations in three colors of SX Phoenicis on Aug. 13, 1954. Color-curve ($B - V$) has been obtained by drawing smooth curves through B and V points and subtracting.

TABLE 4

PHOTOELECTRIC OBSERVATIONS OF CC ANDROMEDAE

Helioc JD 2434000+	V Mag
703.599	9.407
.605	9.372
.610	9.345
.619	9.270
.625	9.244
.629	9.220
.634	9.221
.639	9.236
.644	9.239
.663	9.357
.668	9.368
.673	9.369
.679	9.374
.692	9.408
.696	9.397
.702	9.396
.712	9.406
.718	9.389
.732	9.355
.737	9.335
.744	9.305
.757	9.241
.764	9.250
.771	9.259
.785	9.310
.790	9.336
.797	9.361
.806	9.379
.823	9.419
.830	9.421
.837	9.439
704.687	9.400
.689	9.396
.694	9.394
.698	9.416
.700	9.413
.702	9.412
.706	9.388
.712	9.394
.714	9.373
.717	9.371
.723	9.345
.729	9.327
.750	9.316
.754	9.302
.759	9.287
.762	9.299
.764	9.318
.778	9.356
.781	9.366
.785	9.369
.809	9.394
.813	9.414
.816	9.390
.820	9.390
.824	9.395
.828	9.383
.832	9.377
.836	9.366
.839	9.359
.843	9.355
.846	9.353
.851	9.339
.854	9.344
.859	9.338
.863	9.322
.867	9.312
.871	9.307
.875	9.300
.879	9.304
.883	9.307
.887	9.310
704.891	9.300

Helioc JD 2435000+	V Mag
003.869	9.360
.877	9.338
.883	9.315
.890	9.304
.896	9.294
.903	9.279
.910	9.276
.916	9.276
.923	9.286
.929	9.286
.935	9.324
.949	9.389
.955	9.407
.969	9.419
.975	9.428
.981	9.412
.987	9.403
.994	9.390
004.000	9.346
.007	9.328
.013	9.305
.807	9.315
.815	9.346
.822	9.359
.829	9.372
.837	9.402
.844	9.423
.850	9.426
.857	9.417
.862	9.443
.880	9.350
.886	9.288
.892	9.262
.898	9.240
.903	9.229
.909	9.221
.914	9.241
.920	9.246
.926	9.280
.932	9.311
.937	9.334
.942	9.365
.946	9.372
.952	9.401
.957	9.415
.963	9.422
.968	9.434
.973	9.458
.991	9.424
.996	9.398
005.002	9.358
.007	9.320
.012	9.288
.019	9.251
.789	9.202
.796	9.224
.801	9.244
.807	9.273
.815	9.307
.823	9.340
.828	9.362
.836	9.393
.842	9.430
.848	9.432
.864	9.455
.870	9.428
.876	9.408
.882	9.388
.887	9.360
.892	9.299
.896	9.256
.900	9.235
005.903	9.207

Helioc JD 2435000+	V Mag
005.907	9.187
.911	9.185
.914	9.204
.920	9.204
.925	9.235
.928	9.246
.932	9.270
.936	9.299
.940	9.316
.944	9.320
.949	9.345
.953	9.364
.957	9.392
.967	9.413
.977	9.428
.980	9.438
.984	9.445
.989	9.438
.993	9.438
.997	9.429
006.002	9.424
.007	9.402
.012	9.371

Helioc JD 2434000+	B Mag
703.602	9.756
.607	9.722
.611	9.691
.621	9.596
.626	9.550
.631	9.537
.635	9.545
.640	9.550
.645	9.572
.664	9.704
.669	9.717
.676	9.732
.681	9.744
.693	9.757
.698	9.758
.704	9.768
.714	9.773
.720	9.761
.733	9.701
.739	9.676
.745	9.625
.759	9.565
.766	9.561
.772	9.577
.787	9.653
.793	9.677
.799	9.708
.808	9.731
.826	9.758
.832	9.765
.840	9.789

2435000+

Helioc JD	V Mag
003.871	9.678
.879	9.636
.886	9.634
.892	9.599
.898	9.589
.905	9.581
.912	9.590
.919	9.587
.924	9.604
.930	9.628
.937	9.665
003.951	9.711

Helioc JD 2435000+	B Mag
003.957	9.745
.971	9.765
.977	9.770
.982	9.748
.989	9.735
.996	9.702
004.003	9.671
.009	9.636
.014	9.602
.810	9.631
.817	9.679
.824	9.703
.832	9.743
.839	9.766
.846	9.786
.852	9.790
.859	9.791
.864	9.772
.881	9.678
.888	9.607
.899	9.522
.905	9.514
.911	9.518
.916	9.546
.922	9.578
.928	9.605
.933	9.637
.938	9.665
.943	9.697
.948	9.727
.954	9.751
.960	9.776
.965	9.786
.970	9.799
.975	9.797
.992	9.770
.998	9.718
005.003	9.678
.009	9.638
.014	9.602
.021	9.563
.791	9.492
.797	9.511
.803	9.541
.809	9.591
.817	9.631
.825	9.677
.831	9.712
.837	9.757
.844	9.774
.850	9.802
.866	9.800
.870	9.797
.878	9.747
.883	9.717
.889	9.669
.894	9.609
.897	9.571
.901	9.532
.904	9.496
.908	9.475
.912	9.463
.915	9.474
.923	9.492
.926	9.520
.928	9.535
.933	9.575
.937	9.595
.942	9.637
.945	9.661
.950	9.681
.953	9.710
005.958	9.737

Helioc JD 2435000+	B Mag
005.968	9.760
.978	9.788
.981	9.796
.985	9.799
.990	9.795
.994	9.792
.998	9.792
006.003	9.772
.007	9.745
.014	9.686

Helioc JD 2434000+	U Mag
703.603	9.851
.608	9.800
.613	9.766
.623	9.691
.628	9.668
.632	9.649
.637	9.666
.642	9.678
.647	9.728
.666	9.832
.671	9.837
.677	9.849
.683	9.854
.695	9.869
.700	9.872
.706	9.884
.715	9.866
.722	9.836
.735	9.811
.742	9.754
.747	9.737
.761	9.674
.768	9.687
.774	9.715
.788	9.776
.794	9.803
.801	9.828
.811	9.848
.828	9.837
.835	9.877
.842	9.848

2435000+

Helioc JD	U Mag
003.874	9.725
.881	9.725
.888	9.701
.894	9.679
.901	9.669
.907	9.646
.908	9.654
.914	9.652
.921	9.679
.927	9.713
.933	9.712
.939	9.724
.953	9.786
.960	9.821
.973	9.842
.979	9.813
.985	9.822
.992	9.775
.998	9.755
004.005	9.706
.011	9.676
.016	9.677
.812	9.772
.820	9.723
004.826	9.827

Helioc JD 2435000+	U Mag
004.834	9.830
.842	9.868
.848	9.841
.854	9.834
.860	9.855
.866	9.835
.883	9.745
.890	9.666
.896	9.616
.901	9.580
.906	9.582
.912	9.623
.918	9.620
.923	9.668
.930	9.711
.935	9.722
.939	9.758
.945	9.763
.950	9.824
.956	9.831
.961	9.819
.966	9.843
.971	9.856
.977	9.873
.994	9.819
005.000	9.764
.005	9.708
.011	9.709
.017	9.675
.023	9.643
.794	9.579
.799	9.609
.805	9.637
.812	9.671
.820	9.714
.826	9.769
.833	9.783
.839	9.832
.845	9.837
.852	9.877
.868	9.899
.874	9.835
.880	9.802
.885	9.783
.890	9.700
.894	9.682
.898	9.653
.901	9.595
.905	9.553
.909	9.550
.912	9.562
.917	9.566
.923	9.582
.926	9.603
.930	9.647
.934	9.666
.938	9.688
.942	9.727
.947	9.750
.950	9.777
.960	9.833
.969	9.809
.978	9.897
.982	9.882
.987	9.849
.991	9.891
.995	9.881
.999	9.878
006.005	9.818
.010	9.808
.016	9.762

TABLE 5

OBSERVED MAXIMA OF SX PHOENICIS

Helioc. JD 2434000+	Color	Helioc. JD 2434000+	Color	Helioc. JD 2434000+	Color
966.8569	*Y*	967.8463	*UV*	967.9069	*B*
966.9160	*Y*	967.8468	*Y*	967.9584	*UV*
966.9705	*Y*	967.9059	*Y*	967.9585	*B*
967.8452	*B*	967.9063	*UV*	967.9588	*Y*

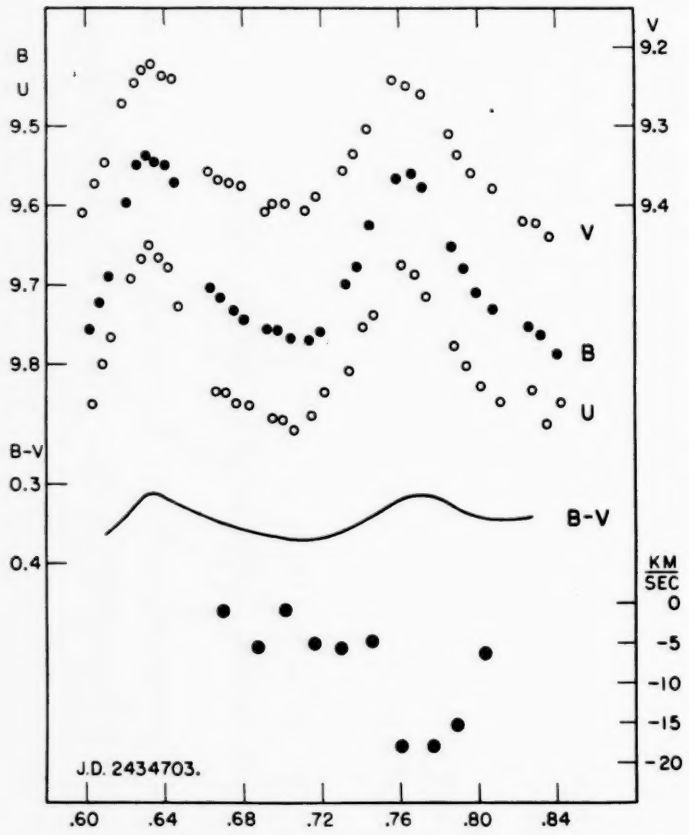

FIG. 3.—Magnitude, color, and radial-velocity observations of CC Andromedae

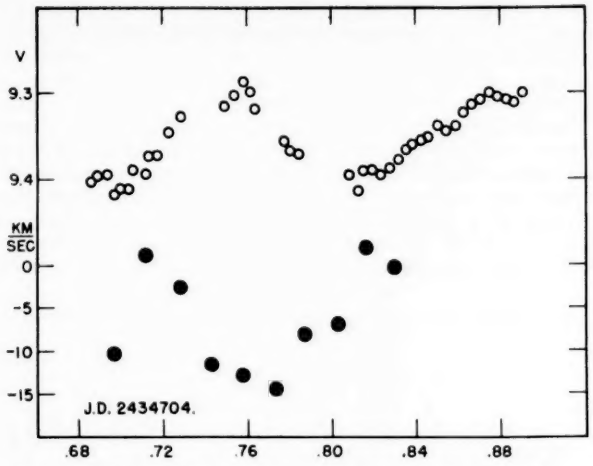

FIG. 4.—Magnitude (V only) and radial-velocity observations of CC Andromedae

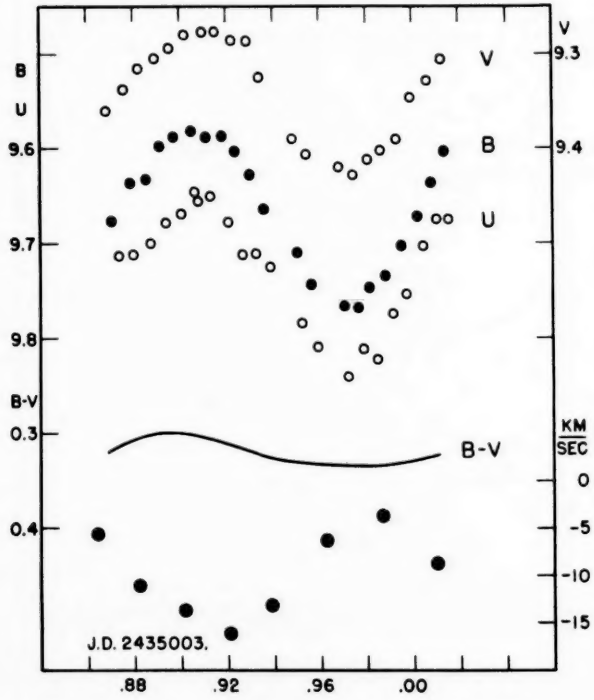

FIG. 5.—Magnitude, color, and radial-velocity observations of CC Andromedae

maxima and minima all lie within the respective ranges of -10 to -20 km/sec and -50 to -60 km/sec. If, as seems likely, the uncertainty in the determination of a maximum or minimum is of the order of ± 5 km/sec, there is no real evidence for lack of constancy in the velocity amplitude. The maxima and minima observed in 1953 (Fig. 8), when there were no corresponding photometric measures, also lie within the limits stated here, with the exception of the maximum of JD 2434615, which is perhaps unusually high. Probably the best statement which may be made from the existing material is this: The values of both the maxima and the minima of the radial velocity-curves of SX Phoenicis may have some real variation of a few kilometers per second, but the influence of a beat period, if any, is very much less than for AI Velorum.

This difference between SX Phoenicis and AI Velorum may be connected with the difference in the intrinsic luminosities of the two stars. SX Phoenicis is a subdwarf of

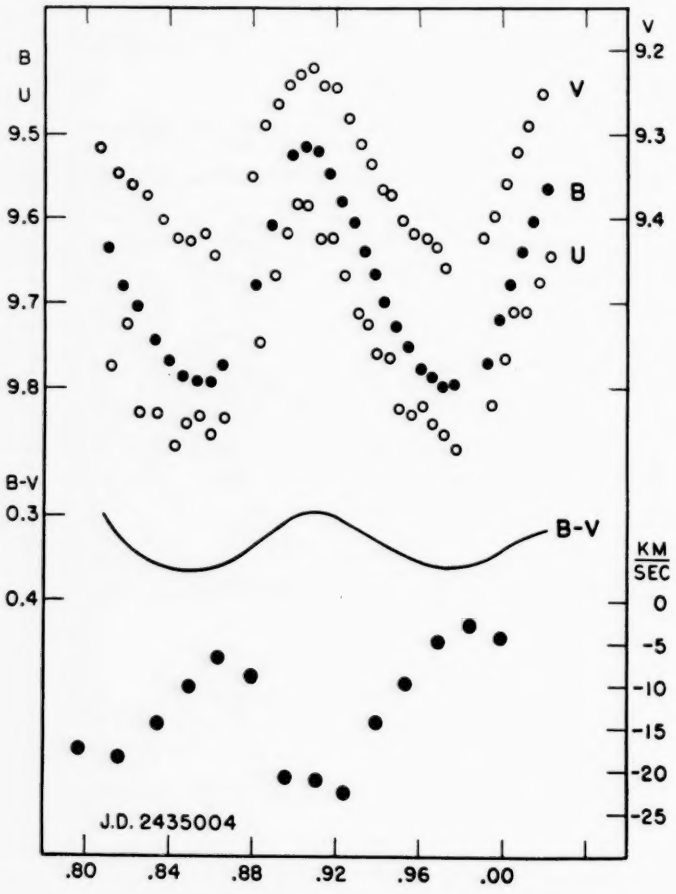

FIG. 6.—Magnitude, color, and radial-velocity observations of CC Andromedae

about absolute magnitude +4 (Joy 1947; Eggen 1952*a*), while AI Velorum has the small annual proper motion of 0".034 and is presumably a much brighter object.

Unlike SX Phoenicis also, the light- and velocity-amplitudes of CC Andromedae show an obvious correlation in Figures 3–7. The relationship between the amplitudes is given in Table 7 and suggests comparison with that found by Fath (1937) for the similar variable δ Scuti. Fath's photoelectric observations, made in integrated light, are probably most nearly like our *B* measurements, which have an effective wave length of 0.431 μ. Figure 9 compares Fath's results on δ Scuti with our observations of CC Andromedae

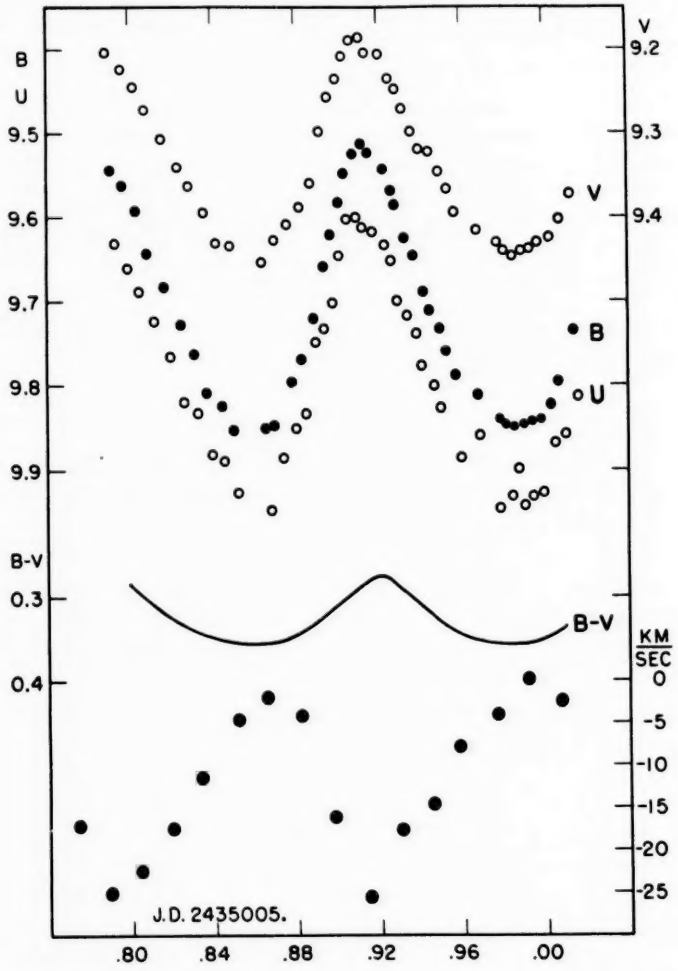

FIG. 7.—Magnitude, color, and radial-velocity observations of CC Andromedae

and indicates that both stars probably follow the same relationship between the light- and velocity-amplitudes. Hence the suggestion that CC Andromedae is a variable of the same class as δ Scuti (Lindblad and Eggen 1953) receives support. For completeness, the 1953 radial velocities are shown in Figure 10.

By means of small-scale spectrograms of a few standard stars and of CC Andromedae, we have estimated the latter to be F0–F2 II–III. Our material is inadequate to give a closer determination than this, but we feel that the star probably lies well above the main sequence in luminosity. This classification agrees with that of Herbig (Eggen 1953); however, Bidelman (private communication) from the same spectrogram used by Herbig gives the type as F3 IV–V. The colors of CC Andromedae at mean light are $B - V = +0.33$ mag., $U - B = +0.08$ mag., and these may be compared with corresponding

TABLE 6

OBSERVED MAXIMA OF CC ANDROMEDAE

Helioc. JD 2434000+	O−C* (day)	Helioc. JD 2434000+	O−C* (day)	Helioc. JD 2435000+	O−C* (day)
604.958.....	0.000	638.929.....	−0.004	003.910.....	−0.003
628.813.....	− .002	703.634.....	− .001	004.905.....	− .008
628.935.....	− .005	703.762.....	+ .002	005.912.....	0.000
635.826.....	+ .016	704.749:†....	−0.010		
638.809.....	+0.001				

* $P = 0^d.1249078$.

†: = Uncertain; shape of light-curve distorted.

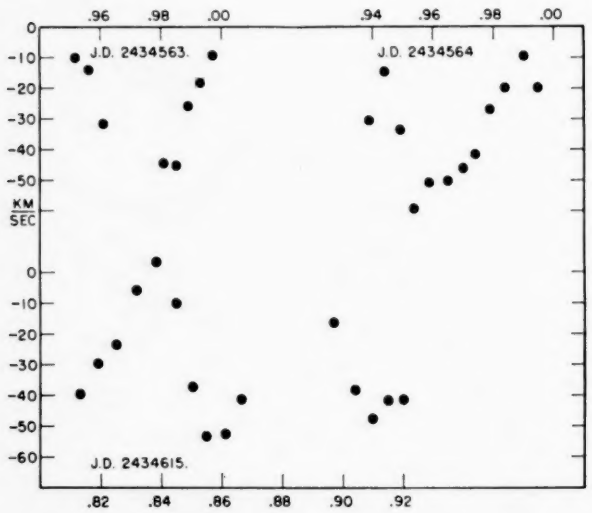

FIG. 8.—Radial-velocity observations of SX Phoenicis in 1953. There are no corresponding photometric measures.

TABLE 7

RELATIONSHIP BETWEEN AMPLITUDES OF LIGHT- AND VELOCITY-CURVES FOR CC ANDROMEDAE

DATE U.T.	LIGHT-RANGE (MAG.)			$2K$ (km/sec)
	V	*B*	*UV*	
1953:				
Nov. 22.....	0.162	0.215	0.210	13
Nov. 23.....	.112	(.148)*	.....	15
1954:				
Sept. 18.....	.152	.188	.191	12
19.....	.205	.282	.278	16
20.....	0.263	0.340	0.340	24

* Derived from *V* amplitude by multiplication by mean factor $B/V = 1.32$. This value has low weight.

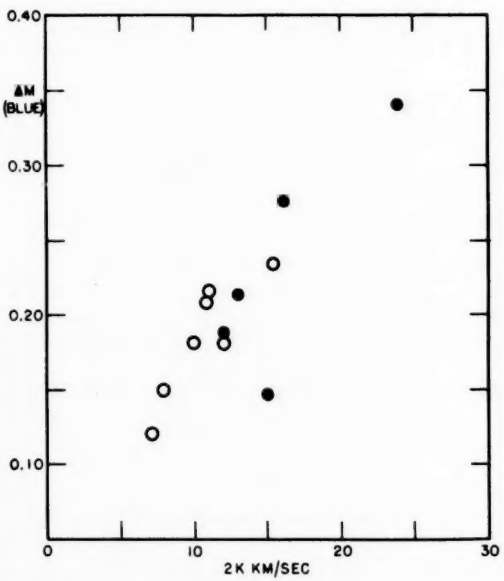

FIG. 9.—Relationship between light- and velocity-amplitudes for δ Scuti (*open circles*) and CC Andromedae (*filled circles*).

data taken from Johnson and Morgan's (1953) list of standard stars which is summarized in Table 8, where the numbers in parentheses are the numbers of stars included in the means. Comparison of the mean colors of CC Andromedae with the entries in Table 8 gives support to our conclusion that this object is considerably brighter than a main-sequence star of the same spectral type.

The only similar data on δ Scuti of which we are aware are the estimates by Adams, Joy, Humason, and Brayton (1935), who give the type and absolute magnitude as F4 and $M_v = +1.4$, respectively, thus also placing this star well above the main sequence.

A third object which may belong to the same group as δ Scuti and CC Andromedae is DQ Cephei (HD 199908), discovered by Walker (1952) and classified by him as F2 II, which was also classified by Herbig as F2 III (Eggen 1953). In a recent paper by Sahade,

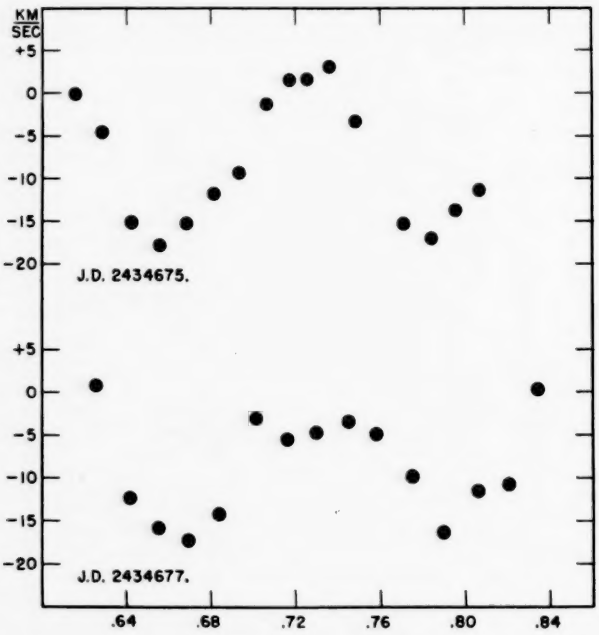

FIG. 10.—Radial-velocity observations of CC Andromedae in 1953. There are no corresponding photometric measures.

TABLE 8

MEAN COLORS FROM JOHNSON AND MORGAN

Type and Class	$B-V$ (Mag.)	$U-B$ (Mag.)	Type and Class	$B-V$ (Mag.)	$U-B$ (Mag.)	Type and Class	$B-V$ (Mag.)	$U-B$ (Mag.)
F2 III (1)....	+0.34	+0.06	F0 V (2).....	+0.32	−0.04	F3 V (1)....	+0.38	0.00
F0–F2 IV (4).	+0.31	+0.06	F2 V (2).....	+0.38	−0.02	F5 V (3)....	+0.44	0.00

Struve, Wilson, and Zebergs (1956) the classification is revised to F1 IV–V, and this object may be only slightly above the main sequence. In this connection it is perhaps significant that, with a dispersion of 18 A/mm, all the lines of DQ Cephei are noticeably wider than those of CC Andromedae, although otherwise the spectra are quite similar.

The evidence thus far, therefore, indicates that the variables of the δ Scuti group may be brighter than main-sequence stars of the same spectral types, though by how much is uncertain, as is also the range of luminosity occupied by these objects.

Spectral changes during the light-variation of CC Andromedae and SX Phoenicis are in the expected sense with respect to color variation. For the latter star the spectra show differences only in the immediate neighborhood of light-maximum, at which time all the metallic lines, including K of Ca II, weaken and the cores of the hydrogen lines become sharper. At this time also the ratio 4077 Sr II/4045 Fe I increases, although not by a large amount. No attempt has been made to estimate spectral types, since we do not have a set of standard spectra taken with the same equipment. Judging by the appearance of the spectra, a plot of spectral type against time would resemble the color-curve shown in Figure 2.

In CC Andromedae the changes in spectrum during a cycle are quite small, with a slight tendency toward earlier type near light-maximum. The total range in spectral type probably does not exceed one or two tenths of a spectral class, but again lack of a series of standard spectra prevents greater precision.

We had hoped to be able to calculate the dimensions of SX Pheonicis and of CC Andromedae by making use of Wesselink's (1946) method. However, the color-curves plotted in the various figures are so nearly in phase with the light-variations that we have been unable to find points of equal color at which the luminosities differ enough to enable the method to be applied with any hope of significant results. This part of the project has therefore been given up.

We wish to express our thanks to Mrs. M. F. Coffeen, who did most of the measuring on the spectrograms of SX Phoenicis, and to Miss A. L. Lowen, who was responsible for nearly all the radial-velocity work on CC Andromedae. Mrs. Coffeen also assisted ably in the photometric reductions.

REFERENCES

Adams, W. S., Joy, A. H., Humason, M. L., and Brayton, A. M. 1935, *Ap. J.*, **81**, 57.
Eggen, O. J., 1952*a*, *Pub. A.S.P.*, **64**, 31.
———. 1952*b*, *ibid.*, p. 305.
———. 1953, *Proc. N.S.F. Astronomical Photoelectric Conference* (Lowell Observatory).
Fath, E. A. 1937, *Lick Obs. Bull.*, **18**, 77.
Gratton, L. 1953, *B.A.N.*, **12**, 31.
Johnson, H. L., and Morgan, W. W. 1953, *Ap. J.*, **117**, 313.
Joy, A. H. 1947, *Ap. J.*, **105**, 96.
Lindblad, P. O., and Eggen, O. J. 1953, *Pub. A.S.P.*, **65**, 291.
Sahade, J., Struve, O., Wilson, O. C., and Zebergs, V. 1956, *Ap. J.*, **123**, 399.
Walker, M. F. 1952, *Pub. A.S.P.*, **64**, 192.
Walraven, T. 1953, *B.A.N.*, **12**, 57.
———. 1955, *ibid.*, p. 223.
Wesselink. A.J. 1946, *B.A.N.*, **10**, 91.

THE INFRARED SPECTRAL CLASSIFICATION OF M-TYPE STARS

STEWART SHARPLESS
U.S. Naval Observatory
Received May 10, 1956

ABSTRACT

Low-dispersion slit spectrograms of a number of M-type standard stars were obtained in the near infrared (λλ 7500–8900). Temperature and luminosity criteria applicable to this dispersion and wave-length range are discussed.

INTRODUCTION

Recently a number of faint red stars at low galactic latitudes have been discovered and catalogued at the Warner and Swasey Observatory (Nassau *et al.* 1954; Nassau and Blanco 1954). Since many of them have high luminosity, spectroscopic parallaxes of these stars will be of considerable interest in galactic research. The intrinsic redness of these stars, combined with the decrease of interstellar extinction with longer wave length, results in an appreciable increase in efficiency if they are observed in the infrared. In the case of early M-type stars with color excesses of the order of 1.0 mag., a gain in speed of a factor of approximately 4 can be obtained in spectroscopic observations if the λλ 7500–8900 region is used rather than the photographic region of the spectrum. In the case of late M-type stars with no space reddening, a similar gain is obtained.

Studies concerning the infrared spectral classification of M-type stars have followed two lines of approach. First, in the work of Keenan and Hynek (1945), the spectra were photographed with sufficiently high dispersion (48 A/mm) to make possible a detailed study of the atomic lines and their changes with luminosity. On the other hand, the work of Nassau and his collaborators (1954) has been carried out with objective-prism spectra having dispersions of 1700 or 3400 A/mm. In this case a temperature classification can be made with high accuracy, but only the broadest molecular features are visible in the spectra.

This paper deals with the infrared spectral classification of M-type stars with slit spectrograms having a dispersion of 200 A/mm. This dispersion was chosen to be sufficiently high to reveal atomic and weaker molecular features which can serve as luminosity discriminants and, at the same time, sufficiently low to enable one to reach faint stars which are of interest in galactic research. These spectra were obtained with a grating spectrograph attached to the 40-inch Ritchey-Chrétien telescope of the Flagstaff Station, U.S. Naval Observatory, Flagstaff, Arizona. The spectrograph employs a 2-inch $f/6.8$ collimator, a 300-line/mm grating with high efficiency in the first-order infrared and second-order blue, and a camera of 6.7-inch focal length. A slit-width of 88 μ was used, which projects to 40 μ on the plate and to 2″.6 in the sky. The resolution of the spectra is approximately 1000. Eastman I-N plates were used throughout.

With this equipment, spectra of stars of apparent infrared magnitude 7.5 can be obtained in 2 hours. The intrinsically brightest M-type supergiants having this apparent magnitude lie at distances up to approximately 5 kpc in the galactic plane.

In order to establish temperature and luminosity criteria, M-type stars of known spectral type and luminosity class were observed. These are listed in Table 1, the columns of which contain the name of the star, the visual magnitude, the spectral classification, and the source of the latter. In the following sections the temperature and luminosity criteria applicable to this dispersion and wave-length range are discussed.

TEMPERATURE CLASSIFICATION

It was shown by Keenan and Hynek (1945) that the infrared bands of TiO behave consistently with the blue-green bands and can therefore be used to assign spectral types. Of these infrared bands, the group at λλ 7054, 7088, and 7126 is the strongest. However, if the spectrogram is exposed for optimum density in the λλ 7500–8900 region, it will generally be somewhat underexposed in the region of these TiO bands. This results from the drop in both the plate sensitivity and the energy-curve of the star. In the case of space-reddened M-type stars, this effect will be even greater, since it is in just this spectral region that interstellar extinction increases most rapidly with decreasing wave length. Consequently, the classification of early M-type stars must depend in most cases on TiO bands lying farther to the infrared. These have been catalogued by Bobrovnikoff (1933) for α Herculis and by Wurm and Meister (1936). The first two

TABLE 1

STANDARD STARS OBSERVED IN THE INFRARED

Star	m_v	Sp.	Source*	Star	m_v	Sp.	Source*
χ Peg	4.9	M2 III	1	ψ^1 Aur	5.0	M0 I*ab*	1
β And	2.2	M0 III	1	υ Gem	4.2	M0 III	1
14469	7.7	M3 I*ab*	3	Z Cnc	8.5–9.8	M6 III	5
14488	8.3	M4 I*ab*	3	RV Hya	7.6–8.3	M5 II	5
α Cet	2.8	M2 III	1	RS Cnc	5.3–6.8	M6 I*b*–II	5
ρ Per	3.2–4.1	M4 II–III	2	88230	6.6	dM0	1
γ Eri	3.2	M0 III	2	AD Leo	9.5	M4.5: V	1
SW Per	8.2–9.8	M5 III	5	95735	7.5	M2 V	1
α Tau	1.1	K5 III	1	Y UMa	7.7–9.3	M7 II–III:	5
119 Tau	4.3	M2 I*b*	1	11631	8.5	M0.5 V	1
α Ori	0.3	M2 I*ab*	1	RT Vir	6.5–8	M8	4
BQ Ori	6.9–8.9	M5 III	5	α Sco	1.2	M1: I*b*	2
π Aur	4.6	M3 II	4	α Her	3.5	M5 II	2
6 Gem	6.2	M1 I*a*	1	μ Cep	3.9	M2 I*a*	1
η Gem	3.7	M3 III	2	5 Lac	4.6	M0 II	4
μ Gem	3.2	M3 III	2	β Peg	2.6	M2 II–III	2

* Sources are as follows:
1. Morgan, W. W., and Johnson, H. L. 1953, *Ap. J.*, **117**, 313.
2. Keenan, P. C., and Morgan, W. W. 1951, *Astrophysics* (New York: McGraw-Hill Book Co., Inc., 1951).
3. Bidelman, W. P. 1947, *Ap. J.*, **105**, 492.
4. Morgan, W. W., Keenan, P. C., and Kellman, E. 1943, *An Atlas of Stellar Spectra* (Chicago: University of Chicago Press, 1943).
5. Keenan, P. C. 1942, *Ap. J.*, **95**, 461.

band heads in the next sequence lie at λ 7589 and λ 7628. These are immersed in the atmospheric A band and are therefore not useful for the assignment of spectral types. To the red of the A band, six features due to TiO are found in the early M's at λλ 7667, 7706, 7744, 7783, 7821, and 7900. Most of these are blends of two or more band heads. In later types two features, attributed to TiO (Nassau and Cameron 1954), appear at approximately λ8194 and λ 8430. At types M5 and later the λ 8859 band of TiO (Phillips 1950) limits the spectra at the red end. The VO bands appear at M6 (Keenan and Schroeder 1952). A description of the subclasses follows.

M0–M3.—In this range the temperature classification may be based on the rapid growth of the λ 7054 group of TiO bands whenever feasible. Otherwise it must depend on the less rapidly changing TiO blends between λ 7767 and λ 7900. At M0 the blends at λ 7744 and λ 7821 are faintly visible, and they become progressively stronger with later types. At M3 they are well marked.

M4.—The TiO absorption at λ 8430 is first visible here. The bands between λ 7667 and λ 7900 are stronger than in class M3, and the Ca II triplet is noticeably weaker.

M5.—The TiO absorptions at λ 8194 and λ 8859 are visible at this type, and the TiO feature at λ 8430 is stronger than in class M4. The Ca II triplet is weaker. At this type the atmospheric A band appears noticeably wider as a result of the underlying TiO bands at λ 7589 and λ 7628.

M6.—The TiO absorptions at λ 8194 and λ 8859 are stronger than in class M5, and the Ca II triplet is weaker. The VO bands are first visible at this type at λ 7865 and λ 7896.

M7.—The TiO absorptions are stronger than at M6, and the Ca II triplet is almost invisible. The VO bands at λ 7865 and λ 7896 are stronger and result in a narrowing of the emission-like feature near λ 7889.

M8.—The VO bands are quite strong and cause considerable weakening of the spectrum between λ 7896 and λ 8000 and also to the blue of the A band. The Ca II triplet is not visible.

Figure 1 illustrates the infrared temperature sequence for M-type giants. On the basis of the development of the TiO and VO bands and the visibility of the Ca II triplet, temperature classifications can be made with an accuracy comparable to that obtained in the blue.

LUMINOSITY CLASSIFICATION

In the infrared spectra of M-type stars with the low dispersion used here, almost all the atomic features are blends of several or more lines. Consequently, many of the sensitive indicators of absolute magnitude listed by Keenan and Hynek (1945) cannot be used here. On the other hand, the lower dispersion favors the use of weak molecular bands, i.e., cyanogen, as luminosity discriminants. The best criteria for the assignment of luminosity classes for types M0–M3 are listed below.

Cyanogen.—The most useful of the luminosity discriminants are the infrared CN bands in the region between λ 7800 and λ 8000. These have been identified and catalogued by Aller and Keenan (1951) for μ Cephei. In luminosity class III they are extremely weak or absent. In class II the CN appears as two blends at λ 7916 and λ 7941 which shade off toward longer and shorter wave lengths. In class I*b* the blend at λ 7895 is visible, and in class I*a* the feature at λ 7878 is well marked. λ 7895 can be compared with the feature at λ 7749. In α Scorpii λ 7895 is the weaker of the two, while in μ Cephei they are approximately equal. Two relatively strong features due to CN occur at λ 8044 and λ 8068. These also become progressively stronger with increasing luminosity and can be compared with λ 8026.

λ *7665.*—This feature, due to neutral potassium, is strong in the brightest supergiants and serves to distinguish between those of classes I*a* and I*ab*. It appears moderately strong in μ Cephei but is almost invisible in α Orionis.

λ *8308 and* λ *8330.*—These features, due to blends of titanium and iron lines, show a strong positive luminosity effect. They can be compared with the atomic features at λ 8435 and λ 8468.

Figure 2 illustrates a sequence of standard luminosity spectra for the early M-type stars.

In types M4 and later, luminosity effects are much less apparent. This is due to the smaller intrinsic spread in luminosity in the late M-type stars and to the fact that at M4 the CN bands to the blue of λ 8000 are obliterated by the TiO absorption. However, the blends at λ 8026 and λ 8044 are still visible at M4, and their ratio can be used as an indicator of luminosity. In the range M4–M6 the feature at λ 8254 shows a negative absolute-magnitude effect. It can be compared with λ 8308. Care must be exercised in the use of this feature because of its proximity to the telluric water-vapor bands.

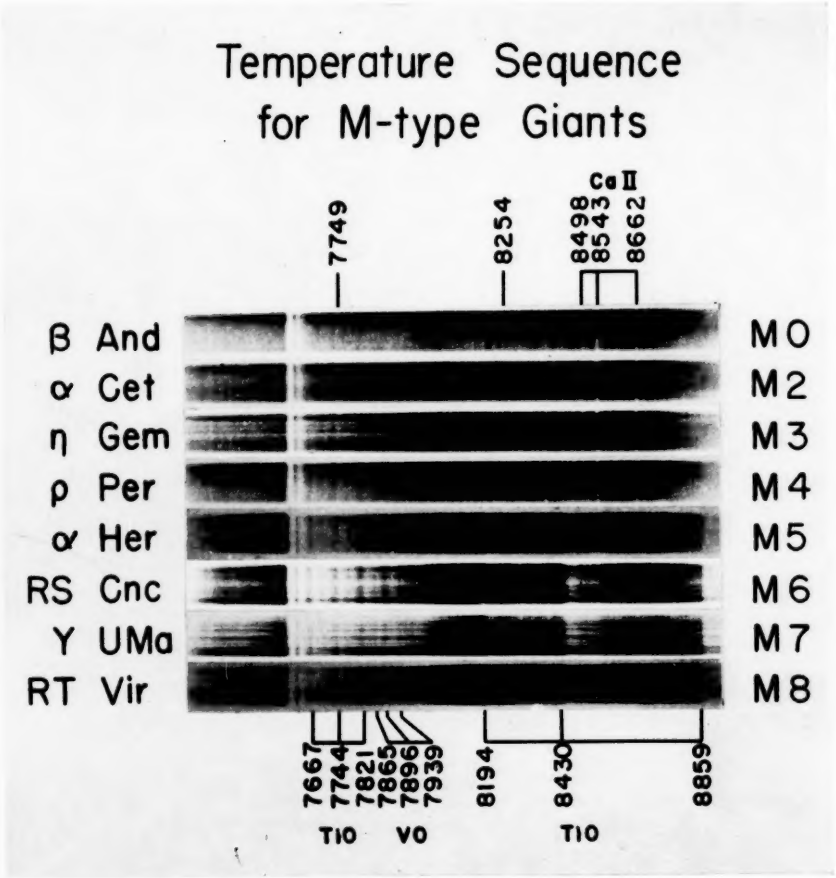

FIG. 1.—A sequence of spectra of M giants, showing the spectral changes with temperature in the infrared.

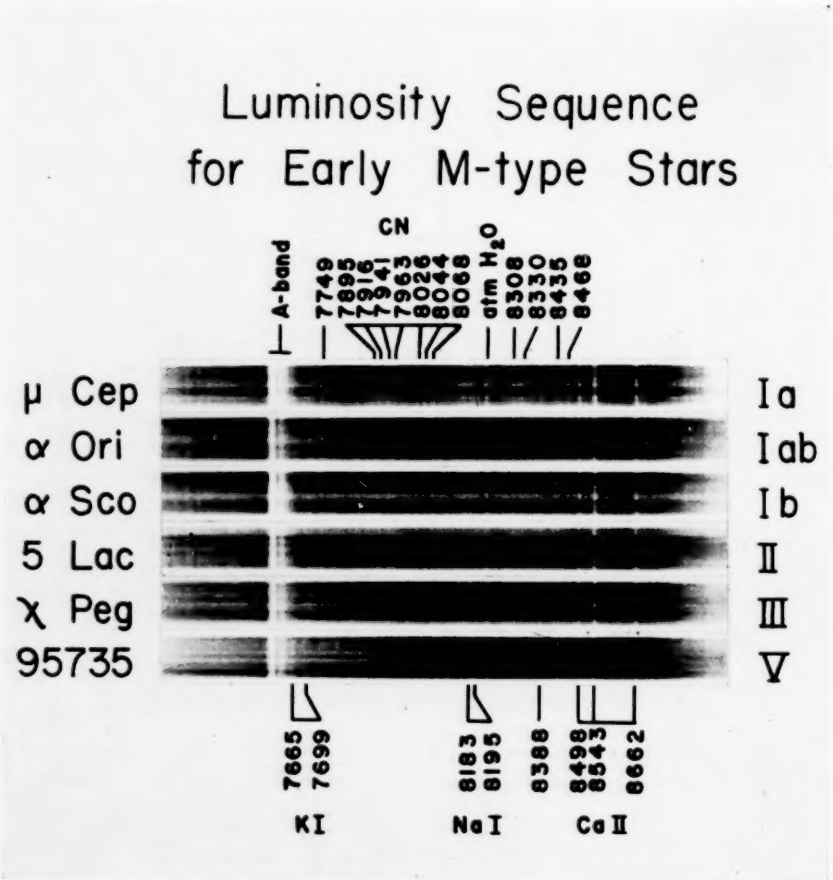

FIG. 2.—Luminosity effects in the infrared spectra of early M-type stars

M-TYPE DWARFS

The spectra of M-type dwarfs are easily distinguishable from those of higher-luminosity M-type stars on the basis of the strong lines of Na I at λ 8183 and λ 8195, and of K I at λ 7665 and λ 7699. The sodium lines are visible at M0 V and become progressively stronger with lower temperature. The potassium lines appear at approximately M1 V. The ratios of these lines to the Ca II triplet provide accurate criteria of spectral type in the range M0–M5 which can be used in addition to the temperature criteria listed earlier.

CONCLUSION

It has been shown that low-dispersion slit spectrograms of M-type stars in the infrared can be classified with respect to temperature and luminosity. By this means one can obtain spectroscopic parallaxes of many faint M-type stars which would otherwise be inaccessible. Spectroscopic and photometric observation of these stars in the infrared has several additional advantages: (1) although many M-type stars are variable in visible light, they remain more nearly constant in the infrared (Pettit and Nicholson 1933), and (2) the decreased interstellar extinction in the infrared decreases considerably the extinction corrections which have to be applied to apparent distance moduli obtained spectroscopically.

REFERENCES

Aller, L. H., and Keenan, P. C. 1951, *Ap. J.*, **113**, 72.
Bobrovnikoff, N. T. 1933, *Ap. J.*, **78**, 211.
Keenan, P. C., and Hynek, J. A. 1945, *Ap. J.*, **101**, 265.
Keenan, P. C., and Schroeder, C. W. 1952, *Ap. J.*, **115**, 82.
Nassau, J. J., and Blanco, V. M. 1954, *Ap. J.*, **120**, 118.
Nassau, J. J., Blanco, V. M., and Morgan, W. W. 1954, *Ap. J.*, **120**, 478.
Nassau, J. J., and Cameron, D. M. 1954, *Ap. J.*, **119**, 175.
Pettit, E., and Nicholson, S. B. 1933, *Ap. J.*, **78**, 320.
Phillips, J. G. 1950, *Ap. J.*, **111**, 314.
Wurm, K., and Meister, H. J. 1936, *Zs. f. Ap.*, **13**, 199.

SPECTRAL CLASSIFICATION OF RED VARIABLES ALONG THE GALACTIC EQUATOR

DONALD CAMERON AND J. J. NASSAU
Warner and Swasey Observatory, Case Institute of Technology
Received April 17, 1956

ABSTRACT

A catalogue is presented containing spectral classes, on the Case infrared system, for 723 red variable stars in a belt 12° in width, centered on the galactic equator, and extending from longitude 333° through zero to 201°. All known variables to the limiting photographic magnitude of 15.0 at maximum were selected. The statistical discussion is based on 541 M-type variables for which sufficiently reliable data are available. The spectral distribution is shown in the form of histograms for the Mira, long-period, semiregular, and irregular types of variability. The first two groups show a spectral range between M2 and M10, while the two latter groups are strongly concentrated at M6 and M6.5, with none later than M7. Only 20 per cent of the M-type variables are earlier than M5. Frequency distributions in galactic longitude seem to indicate that the Mira and long-period types tend to concentrate along the local spiral arm, while the semiregular and irregular types form a disk distribution. However, these conclusions must be regarded as tentative. An examination of the period-spectrum relation does not show significant differences at different galactic latitudes. However, the number of M variables in each subgroup is small. The galactic zone includes 110 carbon stars which are variable and 12 S-type stars. The period-frequency distribution of the carbon stars shows that about one-third of them have periods betwen 360 and 440 days.

I. INTRODUCTION

A catalogue is given containing the spectral classification of 723 red variables with photographic magnitude 15.0 and brighter at maximum light, in a zone 12° in width centered at the galactic equator from longitude 333° through zero to 201°. It includes M, S, and carbon stars, as well as a few stars with peculiar spectra. The discussion is based principally on 541 M-type stars for which the data on spectrum, type of variability, and identity are known with reasonable certainty. The list of known red variables was prepared from the *General Catalogue of Variable Stars* (Kukarkin and Parenago 1948), the six supplements (Kukarkin *et al.* 1949–1954), and the *Catalogue of Stars Suspected of Being Variable* (Kukarkin *et al.* 1951).

II. THE DATA

The region was covered by three sets of overlapping plates, one centered at the galactic equator (central zone), the second at latitude +4° (zone *a*), and the third at latitude −4° (zone *b*). The total number of plates with ample overlaps to cover the region completely was 192. The infrared spectra were secured with the 4° objective prism with a basic exposure of 10 minutes. Most of the plates had two additional shorter exposures, to permit the classification of the brighter stars. The 1-N emulsion used with a Wratten No. 89 filter covered the near infrared region from λ 6800 to λ 8800.

All M stars were classified on the Case infrared system, as described by Nassau and van Albada (1949), and upon the revision and extension of this system for very late M's (M6.5–M10) given by Cameron and Nassau (1955).

The identification of the variables was made in the following manner. The co-ordinates of the stars were computed for the epoch of 1855 and then plotted on special *BD* charts which had been enlarged to the scale of our plates. In the majority of cases no difficulties were encountered, as simple superposition identified the stars with certainty. However, in regions crowded with M stars and in cases where exact coincidence was not attained, certain identification was not always possible. Doubtful cases are indicated in

Table 2 as described later. When all methods of identification failed, the star was omitted. The choice of the limiting magnitude, $m_{pg} = 15$, was made after preliminary studies showed that a fainter limit would yield spectra too faint for classification with certainty. This refers to both early and late M-type stars. Table 1 gives a summary of the number of all the variables observed in the survey according to type of variability and spectrum.

III. DESCRIPTION OF CATALOGUES

The arrangement of the variables in Table 2*a* is according to constellations, and the star designations follow the practice of the *General Catalogue of Variable Stars* (Kukarkin and Parenago 1948). Likewise, the type of variability (col. 2) and the spectral class (col. 3) were secured from the same catalogue and the seven supplements (Kukarkin *et al.* 1949–1955). The fourth column gives the Case spectral class, and the fifth column the date of observation. An asterisk (*) attached to the name of the variable refers to the notes at the end of Table 2*b*. A dagger (†) after the name of the star indicates that the identification is uncertain. A double dagger (‡) after the name of the star indicates that

TABLE 1

NUMBER OF VARIABLES CLASSIFIED

Spectrum	Mira	L.P.	S.R.	Irreg.	Total
M	213	72	73	221	579
C	20	13	18	59	110
S	8	1	1	5	15
Total	241	86	92	285	704*

* Table 2 contains, in addition, 19 stars which, for various reasons, do not fit in Table 1, making the total 723 stars.

additional spectral observations are given in Table 3. They were secured from other available plates of the same region taken on different dates. Table 2*b* gives spectral data of stars which are in the first part of the *Catalogue of Stars Suspected of Being Variable* (Kukarkin *et al.* 1951).

The detection of S stars in the near infrared is made from the presence of the lanthanum oxide bands at λ 7400 and λ 7900 and the highly reddened appearance of the spectrum. However, not all S stars show the lanthanum oxide bands in the infrared (Keenan 1954; Nassau *et al.* 1954). These featureless, but highly reddened, spectra cannot readily be distinguished from highly reddened M0 or M1 stars, particularly when the spectrum is overexposed. For spectra of this type in Tables 2 and 3, the symbol "S:" was adopted, which designates "possible S star" or "supergiant early M."

An examination of Table 2 reveals certain rather large discrepancies between the spectrum given in the *General Catalogue of Variable Stars* and the Case spectrum for some irregular and semiregular stars. For example, in the *General Catalogue of Variable Stars* the spectrum of AZ Cep, an irregular variable, is M6, while the Case spectrum for this star is M0. Since previous investigations (Joy 1942) have shown that variables of these two types do not, in general, vary more than 1 or 2 spectral subdivisions, a careful reexamination of all such cases was made. In a very few of these cases there was found to be some doubt as to the identification, but in most cases the existence of the discrepancy was confirmed. The differences referred to are much too large to be attributed to differences in the systems of classification.

TABLE 2a
SPECTRA OF RED VARIABLES IN THE GALACTIC ZONE

Star	Type of Variable	Spec Class GCVS	Spec Class Case	Date of Observations
		AQUILA		
R Aql	M	M7e	M9	9-6-53
T	I?	M5	M5	7-20-54
RT*	M	M7e	M9p	7-20-54
SS	M		M6	7-20-54
UV	SR	N	C	7-20-54
UW	I	M0	M2:	9-2-54
XY	M		M8	7-20-54
AB	I?	M4	M5:	9-30-53
EM	M	M5	M7	7-20-54
EQ	LP		M5	7-22-54
ER*	M	Me	S	7-20-54
EU	M		M9	7-20-54
HP+	M		M6	9-2-54
KQ	SR	M1	M4	7-20-54
KT	LP		M5	7-20-54
KU	LP		M5	7-20-54
LO+	M		M0	7-20-54
LS	SR		M4	7-20-54
LU	SR	M4	M5	7-22-54
LX	LP		M9	7-22-54
MM	LP?		M8	7-22-54
MU	M		M4	7-22-54
MW	M?		M3	7-22-54
MX	LP		M9	7-22-54
V338	LP?	M5	M3	7-22-54
V353	I		M6	7-20-54
V373	I		M6.5	7-20-54
V446	SR	M1	M2	7-22-54
V449	I		M6.5	7-22-54
V451	I		M6	7-20-54
V455	M		M8	7-22-54
V462	I		M6.5	7-22-54
V473	I		M3:	7-20-54
V474	M		M6.5	7-20-54
V477	I	M6	M6.5	7-20-54
V482	I		M6	7-20-54
V483	I		M6	7-20-54
V486	I		M3	7-20-54
V637	M		M2	7-20-54
V642	I		M6	7-20-54
V806	M	M9	M6	9-6-53
V807	I?		M6.5	7-22-54
V812	LP		M7	7-20-54
V819	M		M9:	7-20-54
V830	I	M2	M5	7-22-54
V842	I	M7	M6	7-20-54
		AURIGA		
S Aur	LP	N	C	10-30-53
U ‡	M	M7e	M7:	11-16-54
W ‡	M	M3e	M5	10-30-53
RU	M	M8e	M8	11-8-54
SZ	M	M6e	M8	11-8-54

Star	Type of Variable	Spec Class GCVS	Spec Class Case	Date of Observations
		AURIGA (Cont'd.)		
TV Aur	SR	S	S	11-7-54
TX	I?	N	C	10-30-53
UV	SR	Ne	C	10-30-53
UZ	I	M4	M4	10-30-53
AQ ‡	M	M7	M7	11-8-54
AU	M	Ne	C	11-7-54
AW	M		M9	11-7-54
AY	M	M4	M6.5	11-16-54
BB	SR	M3	M5	11-16-54
BG	LP		M7	11-8-54
BI	M		M6	11-8-54
BO	SR		M6	11-16-54
BP	I		M6.5	11-16-54
BQ	I		C	11-16-54
BR	I		C	11-16-54
BS	M		M9	11-16-54
BT	M		M8:	11-16-54
CM	I	N	C	11-8-54
DD	I		M6	11-8-54
DF	I		M6	11-8-54
DH	SR		M3	11-8-54
DI	I	N:	C	10-30-53
DL	I		M6	11-8-54
DM	M	M7	M7	10-30-53
DQ ‡	I	M5	M6	10-30-53
DR	SR		M6	10-30-53
DS	I	R or N	C	11-8-54
DV	SR	M5	M5	10-30-53
DZ	I		M6	11-8-54
EE	SR?	M7	M7	10-30-53
EF	I		C	11-8-54
EG	SR	M6	M7	10-30-53
EH	I		M6	11-8-54
EN	I?	M3	M6	10-30-53
EX* +	LP	M1	C	11-8-54
EY	M		M6	12-17-52
EZ	I	M2	M6.5	12-17-52
FH	I		M6.5	12-17-52
FI* +	I	M1	M6.5	12-17-52
FL	I		M3	12-17-52
FQ	I		M3	11-7-54
FT	I		M6.5	11-16-54
FU	I?	N	C	11-16-54
GH +	M		M10:	11-16-54
		CAMELOPARDALIS		
AG Cam	SR	M4	M3	10-30-53
		CANIS MAJOR		
W C Ma	I	N	C	11-8-54
RS	I		M6.5	11-8-54
RV	I	M6	M6	11-16-54
SU	M		M6.5	1-1-55
SV	I		M4	1-1-55

TABLE 2a (Continued)
SPECTRA OF RED VARIABLES IN THE GALACTIC ZONE

Star	Type of Variable	Spec Class GCVS	Spec Class Case	Date of Observations
		CANIS MAJOR (Cont'd.)		
TT CMa	M		S	11-8-54
BF	LP		M6.5	11-8-54
BV	I	N	C	11-8-54
CS	SR		M4	11-8-54
DI	M		M2	11-16-54
DK	M		S:	11-16-54
DM	M		M0:	11-16-54
DN	M		M9	1-1-55
DR	I		M5	11-8-54
DS	M		M4	11-8-54
DU	LP		M6.5	11-8-54
DX	I		M4	11-13-54
		CASSIOPEIA		
V Cas	M	M6e	M6	6-28-54
W*	M	Se	C	9-29-53
X	M	Ne	C	12-18-52
Z	M	M7e	M10	9-29-53
TY	M?		M6	9-29-53
TZ	I	cM2	M2:	6-29-54
UW	M	M5	M9:	9-29-53
UX	I?	R	C	9-29-53
VY‡	SR	M6	M6.5	6-29-54
WW	I	N	C	9-28-53
WX	I?		M0:	12-18-52
WY*	M	M3	Sp	9-29-53
WZ	SR	N	C	9-29-53
AA	I	M6	M6	9-28-53
AV+	M	N	C	6-29-54
BB	M		M8	6-29-54
BL	SR?	M6	M6	6-29-54
BO	I		M6	9-28-53
BQ	I		M6.5	9-28-53
BT	M	M8	M9	12-18-52
BX	SR?	M6	M5	12-18-52
CI	I		M6.5	9-28-53
CQ	I		M6.5	9-28-53
CU	SR	M6	M6	9-29-53
CX	SR		M6	9-28-53
DE	SR	M6	M6	9-28-53
DG	LP?		M6	9-29-53
DQ	I		M5	6-29-54
DR	I	M2	S:	6-29-54
DS	I	N	C	6-29-54
DX	M		C	6-29-54
DY	SR	M5	M6.5	9-29-53
EH	I	M4	M2:	6-29-54
EM	LP	M6	M6.5	6-29-54
EO	M	S	S	6-29-54

Star	Type of Variable	Spec Class GCVS	Spec Class Case	Date of Observations
		CASSIOPEIA (Cont'd.)		
ER Cas	LP		M6	6-29-54
EZ‡	I		M6	6-29-54
FP	I		M6	9-29-53
FR	I	N	C	9-29-53
FX	LP		C	9-29-53
FZ	I		M6.5	9-29-53
GP	I	M3	M4	12-17-52
GQ	SR		M6	12-17-52
GS‡	I	M7	M6	12-17-52
GV	I	M4	M3	9-29-53
GW	I		C	9-29-53
HL	LP		C	9-28-53
HO	I	R	C	12-18-52
HS	I?		M3	12-18-52
HX	I		M3	9-28-53
II	M		M5	12-18-52
IM	SR	M5	M1	12-18-52
KN	I	M2	M1	9-29-53
KW	M		M6.5	9-1-54
		CEPHEUS		
W Cep	SR	Mep	M1	6-28-54
RW	I	cM0	M1:	6-28-54
ST	I	cM0	M2	6-28-54
TT*+	SR	M2	M6.5	9-1-54
TW	M	M0	M6.5	9-1-54
VX	M		M8	9-29-53
YY	M?	M6	M7	6-28-54
AB	M		M8	6-28-54
AC	M		M6.5:	6-28-54
AL	M		M6.5	6-28-54
AS	I	M4	M1:	6-28-54
AZ	I	M6	M0	9-1-54
BX	I		M5	9-29-53
BY	I	M3	M2	9-29-53
CD	I		M3	9-29-53
CH	SR	M3	M5	9-29-53
CI‡	M		M5	9-29-53
CK	SR	M7	M7	9-29-53
CU	M	M6	M4	6-28-54
CV	SR	M3	M4	6-28-54
DG	I	N	C	9-1-54
		CYGNUS		
U Cyg	M	Ne	C	9-1-54
RR	SR	M3	M1:	10-30-53
RS	SR	Ne	C	6-29-54
RU	SR	M8e	M6.5:	6-24-54
RW	LP	cM3	M5	6-29-54
RY	I?	N	C	6-29-54
RZ	M	M7	M7	6-19-54
SX	M	M7e	M8	9-2-54
TT	SR	Ne	C	8-31-54
TY	M	M8	M6.5	7-22-54

TABLE 2a (Continued)
SPECTRA OF RED VARIABLES IN THE GALACTIC ZONE

Star	Type of Variable	Spec Class GCVS	Spec Class Case	Date of Observations
		CYGNUS (Cont'd.)		
WX Cyg	M	Ne	C	6-29-54
YY	SR	N	C	9-2-54
AA*‡	SR	S	Mp	9-1-54
AD*‡	I	S	S:	9-2-54
AG	M	M6	M9:	9-1-54
AH	SR	M5	M6.5	9-1-54
AI‡	I	M5	M6.5	9-2-54
AU	M	M6e	M7	6-29-54
AY	I	N	C	9-1-54
AZ*	I	cM2	M2	10-30-53
BC*	I	M4	M3:	6-29-54
BG‡	LP	M8e	M8	8-31-54
BH	M	M4	M5	9-2-54
BI‡	I	M5	M3	6-29-54
BK	M		M9	9-5-54
BL	M		M6.5	9-5-54
BN	M	M4e	M4	9-5-54
BP	M		M5	9-5-54
BQ	M		M7	9-5-54
DG	M		M7	9-25-53
DH	M	M7	M6	6-19-54
DR	M	M3e	M7	9-2-54
DS	I	N	C	10-30-53
DV	M	M2	M2:	7-22-54
DW	M	M2	M6.5	7-22-54
EF	LP		M6.5	8-31-54
EH*†	M	M1	M6	9-10-53
EL†‡	M		M5	8-31-54
EO	M		M5	8-31-54
EQ	M	M5	M6.5	8-31-54
ER	LP		M8	8-20-53
ES	LP		M6.5	8-20-53
EV	M		M6.5	8-20-53
EW	SR		M6.5	8-20-53
FF*‡	M	M4e	S	9-2-54
FG	M		M9:	9-5-54
FH	LP		M5	7-22-54
FK	LP		M5	7-22-54
FM	M		M9	7-22-54
FN	M		M6	7-22-54
FQ	M		M9	8-31-54
FS	M		M6	8-31-54
FT	LP		M5	8-31-54
FV	LP		M3	9-10-53
FW	M		M7	8-31-55
FY	LP		M6	8-31-54
FZ	M		M9:	9-1-54
GN	SR	M5	M7	9-1-54
GU	M		M9	9-5-54
GY	I	M3	M7	9-5-54
HI Cyg	LP		M5:	8-31-54
HR	M		M10	8-31-54
HV	SR	N	C	8-31-54
HW†	LP		M2	8-31-54
HX	M		M7	8-31-54
HY	LP		M7	9-10-53
HZ*†	M		M6	8-31-54
II	SR		M6.5	8-31-54
IK	SR		M5	8-31-54
IL	M		M9:	8-31-54
IN†	M		M6.5	8-31-54
IP	M		M10	8-31-54
IQ	M		C	8-31-54
IX	SR		M6.5	8-31-54
IZ	M	M7	M3	9-1-54
KL	M		C	8-20-53
KM	M	M4	M5	9-1-54
KO	M	M6	M6	6-29-54
KW	LP		M2	9-1-54
KZ	M	M8e	M9	6-29-54
LM	M		M6	9-2-54
LP	M		M8	9-5-54
LT	M		M7	9-5-54
LV	M		M7	9-5-54
LX*‡	M		S	9-5-54
LY	M		M5	9-5-54
LZ	M		M9:	9-5-54
MM	LP		M7	9-5-54
MQ	M	N	C	6-24-54
MV	I		M6	9-5-54
OQ	I		M7	9-1-54
PP	M	M7e	M6.5:	9-1-54
PR	I	M4	M6	9-1-54
PU	I	N	C	9-1-54
QZ	I	M3	M3	9-1-54
V338	M	M5e	M8	9-1-54
V341	M	M5e	M7	9-1-54
V342	LP		M7	9-1-54
V349	I		M4	10-30-53
V354‡	SR	M6	M5	9-2-54
V362	SR		M6.5	6-19-54
V375	LP		M6.5	9-2-54
V384	LP		M5	9-2-54
V397	I	M2	M7	9-2-54
V405‡	I	M6	M6.5	6-29-54
V408	I	M3	M6	6-19-54
V410	M		M8	9-5-54
V413	I	N	C	6-24-54
V415	LP		M6	9-1-54
V417	I		M6	9-1-54

TABLE 2a (Continued)
SPECTRA OF RED VARIABLES IN THE GALACTIC ZONE

Star	Type of Variable	Spec Class GCVS	Spec Class Case	Date of Observations
		CYGNUS (Cont'd.)		
V420 Cyg	I		M2	9-1-54
V421	M		M8	9-1-54
V422	M	M6	M4	6-29-54
V423*†	LP		M6	9-1-54
V424	I		M6	9-1-54
V427	SR		M3	9-1-54
V430	I?	M4	M3	6-29-54
V431	I		M6.5	9-1-54
V432	I	R	C	6-29-54
V433	LP		M6.5	6-29-54
V434	M		M5	6-29-54
V436	LP		C	6-29-54
V440	I		M3	6-29-54
V441	LP	M5	M4:	9-2-54
V446	LP	M5	M6.5	9-2-54
V449‡	I	M3	M3:	8-31-54
V452	M		M7	9-1-54
V467	SR	N	C:	8-20-53
V487	SR	M3	M6:	8-20-53
V489	I	Mc	M6.5	9-2-54
V497	M		M8	9-1-54
V506	M		M7	9-1-54
V515	LP		M6	10-30-53
V527	I	M7	M6.5	9-2-54
V551‡	M		M6	9-2-54
V557	M	M7	M9	8-20-53
V562	M		M6.5	9-2-54
V573	M	R	C	6-19-54
V575	SR	S	S	6-19-54
V579	I	M5	M6	9-2-54
V582	I	M4	M4	6-19-54
V590	I	M5	M6	9-5-54
V591	I	M2	M1	9-5-54
V592	LP		M7	9-5-54
V594	I		M6	9-2-54
V595	I		M5	9-5-54
V597	M		M6.5:	9-2-54
V600	M		M6	9-5-54
V606	SR		M5	9-5-54
V612	I		M6.5	9-5-54
V615	M		M6	6-28-54
V617	I		M5	9-5-54
V619	I		M6.5	9-5-54
V622	I		M5	9-5-54
V623	I		M6.5	9-5-54
V624	I	N	C	9-5-54
V626	I	M0	M6	9-5-54
V627	LP		M5	9-5-54
V629	I	M4	M6	9-5-54
V634	I		M4	9-5-54
V637 Cyg	M		C	9-5-54
V643	LP		M6	9-5-54
V644†	LP		C	9-5-54
V649	I		M6	9-5-54
V653	LP		M6.5	9-5-54
V655	M		M7	9-5-54
V656	LP		M6.5	9-5-54
V662	M		M6:	9-5-54
V674	I		C	9-5-54
V682	I		M6	9-5-54
V685	I		M6	9-5-54
V701	I		C	9-2-54
V707	SR		M4	9-5-54
V717	I	M2	M2	8-20-53
V718*	SR	M3	M5	8-20-53
V722‡	I		M6.5	8-20-53
V723	I		M6	8-20-53
V727	M		M7	9-2-54
χ*‡	M	Mpe	M10	8-31-54
		GEMINI		
TU Gem	I	N	C	11-16-54
UU	M		M9	11-13-54
AB	I	N	C	12-26-54
AP	I		M6.5	11-13-54
AQ	I	M6	M6.5	11-13-54
AR	LP		M6	11-13-54
AS	I		M6	11-13-54
AT	SR		M6	12-26-54
BF	LP		M6	11-16-54
BI	I	M3	M6.5	11-16-54
BL	I	M4	M6	11-13-54
BV	I		M4	11-16-54
BX	I		M5:	11-16-54
BY*	I		M5p	11-16-54
BZ	I		M2	11-16-54
CC	SR	M3	M6.5	12-26-54
CF	I		S	12-26-54
CG	LP		M6.5	11-16-54
CL	LP	M3	M6.5	12-26-54
CN	LP		M7	12-26-54
CR	I	N	C	11-13-54
DH	SR	N	C	11-13-54
DO	M		M5	11-7-54
DY*	SR	M	M5	11-13-54
EE	M		M6	11-13-54
EK	LP		M7:	11-16-54
EP	SR?		M6.5	11-13-54
EV	I		C	12-26-54
FK	I	M7	M6.5	12-26-54
		HERCULES		
NN Her	I		M5	7-20-54

TABLE 2a (Continued)
SPECTRA OF RED VARIABLES IN THE GALACTIC ZONE

Star	Type of Variable	Spec Class GCVS	Spec Class Case	Date of Observations
LACERTA				
SV Lac	M		M7	9-1-54
TV	I	N	C	9-1-54
TX	I	R	C	9-1-54
TY	M		M8:	9-1-54
UU	M		M5:	9-1-54
UZ	M		M9:	9-1-54
VW	M		M9	9-1-54
WW	LP		M5:	9-1-54
WY	I?		M6.5	9-1-54
WZ	LP	M6	M6	6-28-54
XY	SR		M4	9-1-54
YY	I?		M6	9-1-54
YZ	LP		M7	9-1-54
AA	I		M6.5	9-1-54
AB	SR?		M6	9-1-54
AD	SR		M6	9-1-54
AF	I?		M5	9-1-54
AL	I		M6.5	9-1-54
AM	M		M5	9-1-54
AN	M?		M9	9-1-54
AO	M		C	9-1-54
AP	M		M9:	9-5-54
AS	M		M2	9-5-54
BX*	M		M10	6-28-54
CT	I	R	C	9-5-54
CU	I?		M6	9-1-54
CV	I		M5	9-1-54
CW	I		M0:	6-28-54
DM	M		M7	9-1-54
DS	M		M6	9-1-54
DU †	M		M2	9-1-54
DV	I	N	C	6-28-54
LYRA				
S Lyr* ‡	M	Me	S	7-22-54
X	I	M0	M2	7-22-54
BW	I		M2	7-22-54
MONOCEROS				
V Mon	M	M5e	M8	11-13-54
W	I	N	C	12-17-52
X	SR	M3e	M5	12-17-52
RV	SR	N	C	11-13-54
RY	LP	N	C	12-17-52
RZ	M		M6	12-26-54
ST	M		M6.5	12-26-54
SW	SR	M5	M6	11-8-54
SY	M	M6e	M7	11-13-54
TT	M	M5e	M7	11-13-54
WY	I		M6	11-16-54
AF	M	M7	M7	12-17-52
AH	M		M7	11-13-54
AK	M		M5	11-13-54
AL	M		M3	11-13-54

Star	Type of Variable	Spec Class GCVS	Spec Class Case	Date of Observations
MONOCEROS (Cont'd.)				
AM Mon	M		M10	11-13-54
AP	I		M3	12-17-52
AZ	M		M9	11-13-54
BF	M		M6	12-26-54
BG	LP	N	C	11-13-54
BK	M		M4	11-13-54
BN	SR	N	C	11-8-54
BR	I		M5:	11-13-54
BU	LP		M3:	11-13-54
BY	SR		M6	11-8-54
CD	M		M6.5	11-8-54
CG	M	N	C	11-13-54
CL	M	Ne	C	11-13-54
CN	M		M7	11-8-54
CO †	LP	N	C	11-13-54
CQ	I	M6	M6	11-8-54
CR	I		C	11-13-54
CT	I		M6	11-8-54
CY* †	I	M7	M5	11-8-54
DE	I	N	C	11-8-54
DF	I	N	C	11-8-54
DG	I		M2	11-8-54
DI	I	M2	M6	11-13-54
DM	I		M6.5	11-13-54
DS	LP		M6	11-16-54
DX	I		M2	11-8-54
EF	I		M7	11-16-54
EG	I	M6	M6	11-8-54
EL	I	M6	M5	11-8-54
EM	LP	R:	C	12-17-52
EN	I		M2	11-8-54
EO	I	M6	M5	11-8-54
ER	M		M9:	12-17-52
EU	I	N	C	11-8-54
EX	I		M5	12-17-52
FF	I		M3	11-13-54
FL	I		M4	11-8-54
FM	I		M5	11-8-54
FO	I		M4	11-13-54
FR	I		M6	11-13-54
FU*	SR	S	S:	11-13-54
FX	M		M6.5	12-26-54
GN	M		M9:	11-8-54
GS †	M		M9:	11-16-54
GT	LP		M5	11-8-54
GW	M		M7	11-16-54
GX	M		M9	12-26-54
GY	I	N	C	11-8-54
HN	M		M9:	12-17-52
HW	M		M10:	11-8-54

TABLE 2a (Continued)
SPECTRA OF RED VARIABLES IN THE GALACTIC ZONE

Star	Type of Variable	Spec Class GCVS	Spec Class Case	Date of Observations
	MONOCEROS (Cont'd.)			
IN † Mon	I	M4	M3	12-26-54
IT	I		C	12-26-54
KN	I		S:	11-8-54
KO	I		M6	11-8-54
KP	I		M2	11-8-54
KQ	I		C	11-8-54
	OPHIUCHUS			
X Oph	M	M6e	M9	7-20-54
TY	I	N	C	7-20-54
WY	I	M5	M6	7-20-54
BI	M	M3e	M5	7-20-54
BK	M	M6e	M9	7-20-54
V498	I		M4	7-20-54
V604	M		M5	7-20-54
V623	I		M6.5	7-20-54
V635	M		M5:	7-20-54
V639	M		M5:	7-20-54
V644	M		M4	7-20-54
V647 †	M		M9:	7-20-54
V649	I		M6.5	7-20-54
V652 †	M		M1	7-20-54
V654 †	I		M1:	7-20-54
V655	M		M8	7-20-54
V658	M		M5:	7-20-54
V659 †	M		M7:	7-20-54
V663	I		M3	7-20-54
V667	I		M6	7-20-54
V668	M		M5p	7-20-54
V669	SR		M6.5	7-20-54
V670	I		M6	7-20-54
V673	M		M7	7-20-54
V675	M		M6	7-20-54
V678	LP		M1	7-20-54
V679 *	I	S	S	7-20-54
V835	I		M6	6-28-54
V851	SR	M4	M6	7-20-54
	ORION			
U Ori	M	M8e	M9	11-7-54
RR	M	M5e	M8	11-7-54
BL	I	N	C	11-13-54
BQ	SR	M5	M6.5	11-7-54
DD	I?	M6	M6.5	12-17-52
DP	I?	M6	M6.5	1-1-55
DQ	LP	M3	M6.5	11-16-54
DR	I	M4	M6.5	1-1-55
DS	I		M6.5	1-1-55
DT	M		M10	11-16-54

Star	Type of Variable	Spec Class GCVS	Spec Class Case	Date of Observations
	ORION (Cont'd.)			
DU Ori	I	M3	M1:	11-13-54
DV * ‡	I		M2p	1-1-55
EE	I		M4	11-16-54
EI	I?		C	12-17-52
EL	SR		M3:	11-13-54
EM	LP		M6:	11-13-54
EN	I		M5	12-17-52
EO	I		M6.5	12-17-52
GK	LP	N	C	11-13-54
GL	SR		C	11-16-54
QU	I		M6	11-7-54
QW * †	I		M3	11-7-54
QX	M		M6.5	11-16-54
QZ	LP		M6.5	11-16-54
V337 †	I		M5	11-7-54
V340	LP	M0	M4	11-16-54
V342	LP		M6.5	11-7-54
V382	M		M9:	12-26-54
	PERSEUS			
S Per	SR	cM3e	M4	9-28-53
W ‡	SR	M8	M5	12-17-52
RS	I?	cM4	M4	9-28-53
SU	SR	cM3	M3:	9-28-53
SW ‡	SR	M5	M5	10-30-53
SY	LP	Ne	C	12-17-52
TY *	M		M6	9-28-53
UU	I	M5	M4	12-17-52
XX	I?	M4	M3	9-28-53
YZ ‡	I	cM2	M2	9-28-53
AD	I	cM2	M2	9-28-53
AO	I		M6	10-30-53
AP ‡	M	M7	M6.5	12-17-52
AQ	M		M7	10-30-53
AT	I	R	C	12-17-52
AU	M		M6.5	12-17-52
AV	I	N	C	12-17-52
BI	I	R	C	10-30-53
BK	I	R	C	12-17-52
BL	SR		M6.5	10-30-53
BT	I		C	9-28-53
BU	SR	cM4	M4	9-28-53
BX †	I		M6:	9-28-53
CN * †	M	M0	C	9-28-53
CT	I		M6	9-28-53

TABLE 2a (Continued)
SPECTRA OF RED VARIABLES IN THE GALACTIC ZONE

Star	Type of Variable	Spec Class GCVS	Spec Class Case	Date of Observations
PERSEUS (Cont'd.)				
CZ Per	I		M4	9-28-53
DI †	M		M9:	9-28-53
DP	I		M6.5	9-28-53
DQ	I		M6.5	9-28-53
DY	SR		C	9-28-53
EE	I		M6.5	9-28-53
ER	SR	M8	M6.5	9-28-53
EW †	I		C:	9-28-53
EY	I		M4	10-30-53
FI	M		M7	10-30-53
FL	I	N	C	10-30-53
FN	I		M6.5	10-30-53
FP	I		M3	10-30-53
FR	I	N	C	12-17-52
FS	LP		M6	12-17-52
FT	I		M6	10-30-53
FU	M		M9:	12-17-52
FV ‡	I	M6	M6.5	12-17-52
FZ	I	cM1	M2	9-28-53
GH	SR	M6	M6	12-17-52
GL	M		M6	11-7-54
GM	M	N	C	11-7-54
GN	I		M6.5	11-7-54
GO	I	M4	M4	11-7-54
GR	M		M9:	11-7-54
GS *	M		Sp	11-7-54
GU	I		M4	11-7-54
GV	I		M6	11-7-54
GZ	LP		M9	11-7-54
HL †	I		M6	11-7-54
HN	LP		C	11-7-54
HO	I	M7	M6.5	11-7-54
HR	I	M3	M6	12-17-52
HT	SR	M5	M7	10-30-53
HX	I		S	10-30-53
IO	I	M4	M3	12-17-52
PUPPIS				
TZ Pup	M		M7	11-13-54
UU	M		M3	11-13-54
UV	SR		M5	11-13-54
BF	I		C	11-13-54
EE	M		M1	11-13-54
EI	I		M6.5	11-8-54
FV	I		M6	11-8-54
FX	LP		M6	11-8-54
FY	I		M6.5	11-8-54
FZ	I		M6.5	11-8-54
GG †	I	S5,6	M0::	11-8-54
GM	I		M6	11-8-54
GN	I		C	11-8-54
GQ	SR		M6	11-8-54

Star	Type of Variable	Spec Class GCVS	Spec Class Case	Date of Observations
SAGITTA				
T ‡ Sge	I	M4	M6.5:	9-30-53
W	M	M4e	M6.5	10-2-53
Z †	I		M3:	7-22-54
TT	M		M6	7-22-54
UV	LP		M1	7-22-54
VV	I		M6.5	7-22-54
WX	M		M6	7-22-54
XZ	I		M3	7-22-54
AA	I		M6	7-22-54
AB	M		M8	7-22-54
AF	M		M5	7-22-54
AG	LP		M6	7-22-54
DD	SR	M3	M6	7-22-54
SAGITTARIUS				
SS Sgr	SR	R	C	6-28-54
SZ	SR	N	C	6-28-54
UZ	M		M6	6-24-54
VV	M	Me	M8	6-24-54
VX	SR	M4e	M4	6-27-54
AK	M	M5e	M9	6-28-54
FK	M		M9:	6-28-54
V746	M		M9:	6-24-54
V764	M	Me	M4	6-24-54
SCUTUM				
S Sct	SR	N	C	7-2-54
T	SR	N	C	7-2-54
RV	?	R	C	6-28-54
RX	I	N	C	7-2-54
TX †‡	LP		M6.5	6-28-54
VW ‡	M		M4	6-14-54
WW	M		M6.5	7-2-54
AA	M		M6	7-2-54
AB	M		M2	7-2-54
AI	M		C	7-2-54
AX	M		M3	7-2-54
BC	LP		M5	7-2-54
BP †	I?	M3	M4p	6-14-54
CG	M		M8	7-2-54
FR	I	M3	M2	6-24-54
SERPENS				
BE Ser	M		M5	6-28-54
BP	I		M6	7-20-54
BR	M		M5	7-20-54
BW	M		C	7-20-54
BX	I		M6	9-3-53
BY ‡	I	M6	M6	9-3-53
CZ	I	M3	M6.5	6-24-54
DE * †	M		M9	7-20-54

TABLE 2a (Concluded)
SPECTRA OF RED VARIABLES IN THE GALACTIC ZONE

Star	Type of Variable	Spec Class GCVS	Spec Class Case	Date of Observations
		TAURUS		
Y Tau	SR	N	C	11-8-54
Z	M		M7	11-8-54
RU	M	M0	M6.5	11-8-54
TU	I	N	C	11-7-54
VZ	?		M4	11-8-54
AB	LP	M5	M6.5	11-7-54
AT	I		M6	11-7-54
AW	M		M9:	11-7-54
AX	SR		M6.5	11-7-54
AY	I		M5	11-7-54
AZ	I	M8	M7	11-16-54
BB *	I	M0	S:	11-7-54
BC	I		M6	11-7-54
BD	I		M3	11-7-54
BE	SR?		M4	11-7-54
BF	SR		M6	11-16-54
BM *			M3p	11-16-54
CO	I		M5	11-16-54
CP	I	N	C	11-8-54
CS	I		M5	11-7-54
DU	I		M3:	11-8-54
DW	LP		M7	11-8-54
DX	I	M5	M3:	11-8-54
DY	I	M2	M5	11-8-54
DZ	I		M6	11-8-54
		TAURUS (Cont'd.)		
EE Tau	I		M4	11-8-54
EG	I		M5	11-8-54
EH	I	M3	M3	11-8-54
EI *	LP		S	11-8-54
EK	LP		M6.5	11-8-54
EL †	I	M0	M6.5	11-16-54
ER	I	N	C	11-8-54
		VULPECULA		
W Vul	LP	M5	M6	9-2-54
RW	M		M6.5	7-22-54
SS	M		M3	7-22-54
XY	M		M6.5	7-22-54
YY ‡	M		M8	7-22-54
YZ	M	M6	M8	9-10-53
AA	M		M9:	9-10-53
AG	M		M6	9-10-53
AR	I	N	C	8-20-53
CE *	I	S	S	8-20-53
CG	I?	N	C	7-22-54
CH	M		M5	9-2-54
CN	M		M5	7-22-54
CO	I		C	7-22-54
DE	M		M8	7-22-54
DI	I		M6.5	7-22-54
DK	LP	M6	M6.5	7-22-54
DL	LP		M6	7-22-54

TABLE 2b
SPECTRA OF RED SUSPECTED VARIABLES IN THE GALACTIC ZONES

Star	Type of Variable	Spec Class Case	Date of Observations
82	I	M6.5	9-29-53
124	I	M2	12-18-52
304	I	M6.5	10-30-53
411	SR	M5	7-20-54
601	LP	M7	11-7-54
709	I?	C	1-1-55
712	I?	M6:	11-13-54
728	I?	C	12-17-52
893	M	M6.5	4-1-55
912	LP	M6.5	1-1-55
933	LP	M9:	11-16-54
943	LP	M6.5	11-13-54
985	LP?	M6.5	11-13-54
1023 *	LP	M4	11-13-54
1042	M	M6:	11-13-54
1085	I?	M6	11-13-54
4006	I	C	6-28-54
4614	I?	M5	6-19-54
4786	LP	C	7-22-54
4847	I	M5	7-22-54
4856	LP	M7	7-22-54
4921 *	LP	M8	9-1-54
4970	I	M6	9-1-54
5067 †	I	M3	6-29-54
5286 *	M	M5	9-1-54
5454	I	M6.5	9-1-54
5482 ‡	LP	M6	9-1-54
5501	LP?	M6	6-28-54
5654 *	LP	M6p	9-1-54
5675 †	SR?	M5	9-1-54
5783	I?	M4:	6-29-54

NOTES TO TABLE 2*a*

RT Aql —Anomalous type; no λ 8300.
ER —No λ 7400 or λ 7900 bands on this plate, but a plate taken on 6-19-47 shows strong absorption at λ 7400 and λ 7900.
EX Aur —Identity uncertain; faint, early M near the C star may be EX.
FI —Identity uncertain; M2, *BD* star nearby.
W Cas —Appears to be a C star on Case plate taken on 9-29-53; was classified as S1e by Miss Davis (1934) and Se by Merrill (1940); Keenan (1954) lists it among "Stars with Spectra Related to Type S" and notes that "infrared CN bands and Swan bands of C2 were observed by Bidelman at Yerkes and by Keenan at Perkins (1950)."
WY —Strong absorption band at λ 7900; broad absorption from λ 7900 to λ 8400; the plate was taken 56 days after minimum light.
TT Cep —Very faint spectrum nearby—possible early M, may be TT Cep.
AA Cyg —Classified S7, 5 and S7.5, 6 by Keenan (1954); is known to have both M and S characteristics.
AD —Spectrum greatly overexposed; classed S5, 8 by Keenan (1954).
AZ —Tapered spectrum.
BC —Tapered spectrum.
EH —Identity uncertain; another M nearby.
FF —The spectrum is clearly that of an S star on three different infrared plates; this is in disagreement with M4e, which is listed in the *General Catalogue of Variable Stars* and was probably taken from the Dearborn survey (Lee and Bartlett 1944), M4, and Miss Cannon (1934), Me.
HZ Cyg —Identity uncertain; two late M stars close together.
LX —Has λ 8500 absorption band, in addition to strong λ 7400 and λ 7900.
V423 —Identity uncertain, two late M stars nearby.
V718 —Tapered spectrum.
χ —Classed S7, 1e; S9, 1e; and S10, 1e by Keenan (1954).
BY Gem —Spectrum has appearance of an M5, but with λ 7900 absorption band.
DY —Classed S8, 5 by Keenan (1954).
BX Lac —This is the latest-appearing M10 we have observed.
S Lyr —Plate taken on 7-22-54 shows weak λ 7900 and reddening; plate taken on 5-2-55 (see Table 3) shows strong absorption at λ 7900 and λ 7400.
CY Mon —Identity uncertain; an M6.5 nearby.
FU —Keenan (1954) lists this among "Stars with Spectra Related to Type S."
V679 Oph—Classed S4.5, 8 by Keenan (1954); blue plate taken on 7-14-49 shows faint C-star spectrum.
DV Ori —Several emission features between λ 7900 and λ 8500.
QW —Identity uncertain; and M6 nearby.
TY Per —Possible emission near λ 8800.
CN —There is no M star nearby; however, an M0 of $M_{pg} = 13.2$ at max. would probably be beyond the plate limit.
GS —Very broad and intense absorption band at λ 7900.
DE Ser —Identity uncertain; an M5 nearby.
BB Tau —No distinct absorption features, strong taper, possible S star on 4° plate; on 2° plate it appears to have carbon features; may be similar to W Cas (see note) which has both carbon and S-star features.
BM Tau —Listed as short period; not yet sufficiently investigated in *General Catalogue of Variable Stars;* absorption or emission near λ 7400.
EI —Strong absorption at λ 7400 and λ 7900; typical S-star spectrum.
CE Vul —Spectrum is greatly overexposed, but it shows the λ 7400 and λ 7900 absorption bands.

NOTES TO TABLE 2*b*

1023 —NO Mon in seventh supplement to *General Catalogue of Variable Stars.*
4921 —V738 Cyg in seventh supplement to *General Catalogue of Variable Stars.*
5826 —V750 Cyg in seventh supplement to *General Catalogue of Variable Stars.*
5654 —λ 7900 absorption present.

TABLE 3
ADDITIONAL SPECTRAL OBSERVATIONS OF RED VARIABLES

Star	Case Spec Class	Date of Observations	Star	Case Spec Class	Date of Observations
U Aur	M9	2-4-55	V551 Cyg	M4	8-20-53
	M9	2-24-55	V722	M6	9-2-54
W	M6.5	11-8-54	χ	M7	5-11-53
AQ	M6.5	10-30-53		M7	6-2-53
DQ *	M6p	11-8-54		M9	7-25-53
VY Cas	M6.5	8-29-54	χ	M10	8-20-53
EZ	M5	9-29-53		M9	9-8-53
GS	M6.5	11-1-54		M7	6-19-54
CI Cep	M6	6-29-54		M7	7-22-54
AA Cyg	M2p	6-19-54		M10	10-24-54
AA	Mp	7-21-55	S Lyr*	S	5-2-55
AD	S:	7-22-54	DV Ori	M1	11-16-54
AI	M6	7-22-54	W Per	M2	8-29-54
	M6	8-20-55		M2	11-1-54
BG	M7	7-22-54		M4	1-12-55
BG	M8	10-24-54	SW Per	M6.5	11-7-54
BI	M3	9-3-53	YZ	M1	12-17-52
EL	M4:	9-10-53	AP	M8	10-30-53
FF *	S	9-29-53	FV	M6	10-30-53
LX	S	8-20-55	T Sge	M6.5	8-20-53
V354	M4	10-30-53	TX Sct †	M6:	6-14-54
V405	M6.5	10-24-54	VW	M6	7-2-54
V449	M3	8-20-53	BY Ser	M6.5	7-20-54
	M3	7-22-54	YY Vul	M5	8-20-53
	M2	9-2-54	5482	M5	6-28-54

Notes: DQ Aur - absorption at λ8300 and several regions longwards of λ8400
FF Cyg - Very faint and narrow absorption band at λ8300.
S Lyr - See note at end of Table 2.

IV. TYPES OF VARIABILITY AND THEIR SPECTRAL DISTRIBUTION

Of the M-type variables given in Table 2*a*, 541 have the necessary data for study of their spectral distribution. Although much work has been done in this field, it was felt that such a study might prove useful for the following reasons:

a) The spectra of at least two-thirds of these variables were previously unknown. Thus the present data greatly strengthen spectral-distribution studies.

b) All spectra were secured with the same instrument and dispersion, and the system of classification is uniform.

c) The fact that the variables under consideration are confined within the same region (6° on each side of the galactic equator) as the general survey of late M's whose distribution is also under study here (Nassau *et al.* 1956) enables us to make comparisons between the two studies.

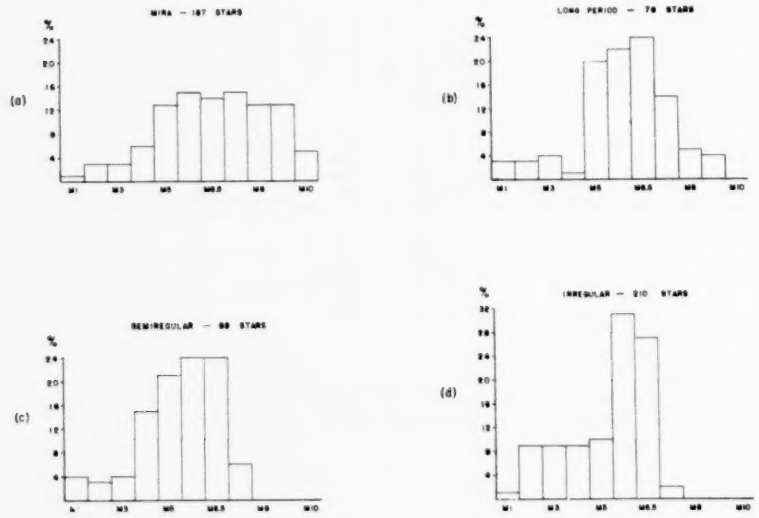

FIG. 1.—Frequency distribution of M variable stars. *a*, Mira type; *b*, long period; *c*, semiregular; *d*, irregular.

d) The limiting magnitude of the stars in the survey is the same.

e) Although the observed spectral classes do not refer to the time of maximum light, the relatively large number of stars provides means for estimating the range of spectral variability of the different types.

The division into types of variability given in the *General Catalogue of Variable Stars* is being followed. The Mira type includes those variables of long period with regular periodicity and amplitudes of variation greater than 2.5 mag. They generally show emission lines during certain phases. The long-period type is similar to the Mira variables except for the amplitude, which is less than 2.5 mag. The semiregular type has large irregularities in the period and small amplitudes. The irregular type shows no periodicity and has small amplitudes. Figure 1 shows the spectral distribution of the 541 variables of Table 2 according to these types, and Table 4 gives their distribution in the three galactic zones. Only those variables whose type of variability and Case spectra are

definitely known are included in the statistics. No marked differences between the three zones were observed when separate figures were compared. However, the number of stars in each of the zones was too small for a definite conclusion. The principal feature of the figure and table may be summarized as follows:

1. No marked asymmetry in the number of stars of the different types of variables is present between zones *a* and *b*. The somewhat larger number of irregular variables in zone *b* is attributable partly to the supergiants in the h and χ Persei clusters which are in this zone.

2. The central zone has fewer Mira-type and long-period variables than the other two zones. This is probably due to the combined effect of absolute magnitude and interstellar absorption rather than to selection. The number of semiregular and irregular variables is practically the same in the three zones if the h and χ supergiants are excluded.

3. The distribution of Mira and long-period variables covers all the M subclasses, being greatest from M5 through M7 or M8.

4. The distribution of semiregular and irregular M variables covers all M subclasses through M6.5 but ends abruptly at M7. There are no semiregular or irregular variables later than M7 and only nine that late.

TABLE 4

DISTRIBUTION OF M VARIABLES IN THE THREE ZONES

Type	Zone *a*	Central Zone	Zone *b*	All Zones
Mira	75	47	65	187
Long period	28	18	30	76
Semiregular	21	26	21	68
Irregular	65	62	83	210
Total	189	153	199	541

5. The irregular variables are concentrated at classes M6 and M6.5.

6. Twenty per cent of the M variables are earlier than M5.

The published material for Me variables by Merrill (1941) and for the irregular M variables by Joy (1942) provides means for comparison with our data. In this case the stars are not confined to the galactic belt, and the given spectra usually refer to the time of maximum light. Merrill's distribution (Fig. 2, *a*) of Me variables is much sharper than ours (Fig. 1, *a*) and the percentage of later-type stars much smaller than ours. This is as should be expected. For the irregular variables, Joy's distribution (Fig. 2, *b*) shows that the concentration occurs at M5 and M6 instead of at M6 and M6.5, as in our case (Fig. 1, *d*). Here a small difference between the Mount Wilson and Case systems of classification may exist, although the difference may be due, at least in part, to the fact that our spectra do not refer to the time of maximum light.

V. DISTRIBUTION OF THE M VARIABLES IN GALACTIC LONGITUDE

That selection effects are present and may influence the longitude distribution of the variables is well known. Nevertheless, not all aspects of the distribution can be attributed to selection alone, as will be shown in the following discussion. Figure 3, *a*, *b*, *c*, and *d*, shows the longitude distribution of the M variables according to type of variability. The similarity of Figure 3, *a* and *b*, suggests that they can be combined to form one group.

It is our understanding[1] that a second edition of the *General Catalogue of Variable Stars* will incorporate these two groups into one. Also the irregular variables will be grouped with the semiregulars. Figure 3, *c* and *d*, indicates that their distributions also are not dissimilar. A grouping of each of the two types of variability is shown in Figure 3, *e* and *f*, which show striking dissimilarities. The Mira-plus-long-period-variable group (Fig. 3, *f*) shows a marked maximum in the neighborhood of longitude 35° and a possible indication of a second maximum 180° from it, suggesting a grouping of these stars along the local spiral arm. Omitting the interval between $l = 333°$ to $l = 3°$, since this region is influenced to a great degree by broad obscuration, the semiregular plus irregular variable group (Fig. 3, *e*) shows a uniform distribution throughout.

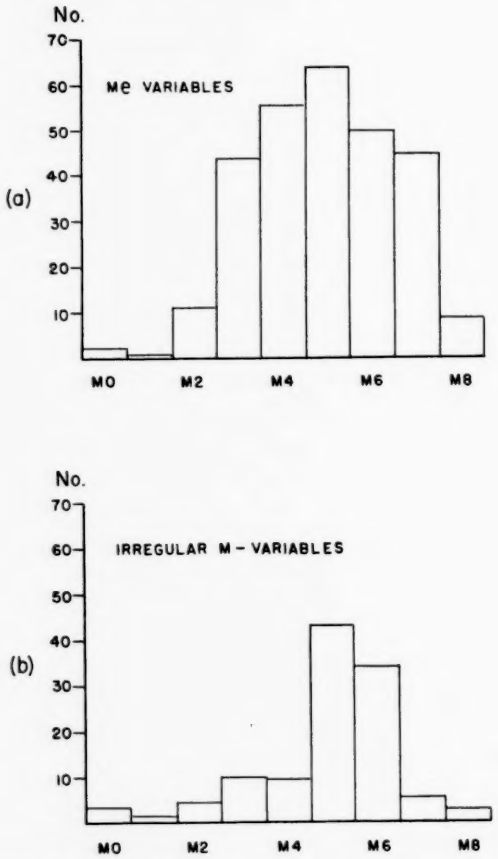

FIG. 2.—Frequency distribution of M variable stars according to Merrill and Joy. *a*, Me variable stars (Merrill); *b*, irregular M variable stars (Joy). (These figures have been replotted in the form of histograms from the original data of Merrill and Joy for comparison with Fig. 1, *a* and *d*.)

[1] This was stated by Kukarkin at the meeting of Commission 29, Dublin, 1955.

In Figure 4 the longitude distribution is shown for three different spectral groups: *a*, M0–M4; *b*, M5–M6.5; and *c*, M7–M10. Since the early M variables are predominantly irregular and semiregular, it is not surprising that Figures 4, *a*, and 3, *e*, are somewhat similar. Also Figures 4, *c*, and 3, *f*, are similar, since the M7–M10 variables are largely Mira or long period. In fact, of the 113 M7–M10 variables classified in this study, Table 5 shows that 92 per cent are Mira or long period. It is noteworthy that the distribution of the M7–M10 Mira variables also suggests a grouping of these stars along the local spiral arm. This is in agreement with Baade's (1951) suggestion that the Mira variables are intermediate between populations I and II and that the late-M Mira variables are population I. Unfortunately, the number of early-M Mira type is too small to yield a definite conclusion.

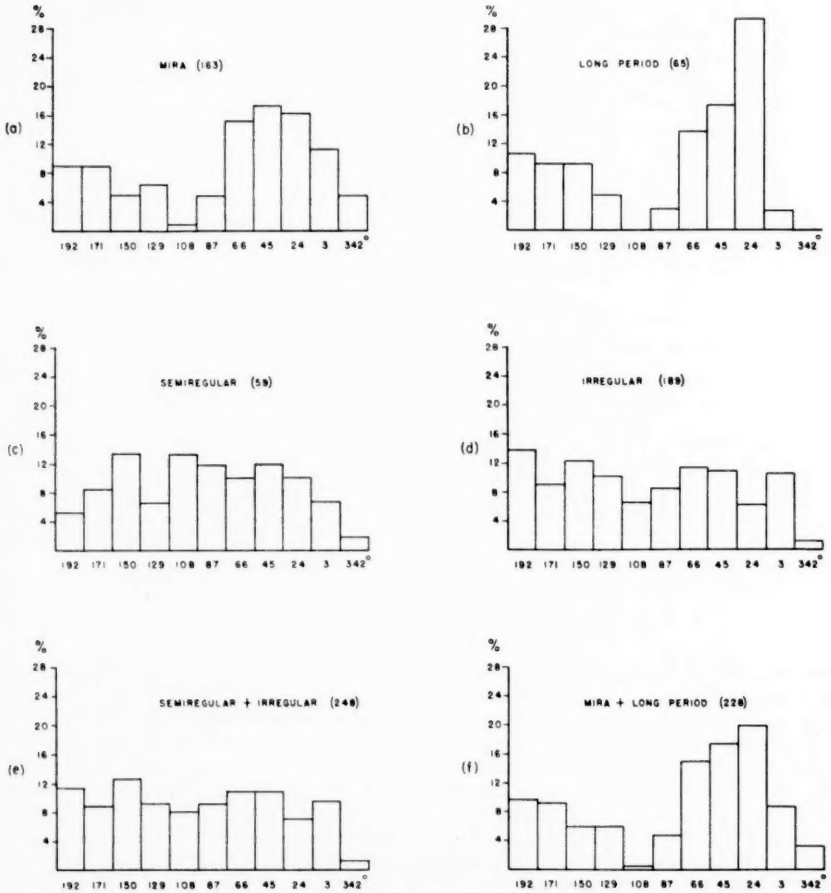

FIG. 3—Frequency distribution of the M variable stars in galactic longitude. *a*, Mira type; *b*, long period; *c*, semiregular; *d*, irregular; *e*, semiregular plus irregular types; *f*, Mira plus long-period types. Galactic longitude is plotted as abscissa, and the total number of stars is given in parentheses after the type of variability.

VI. PER CENT OF VARIABLES AMONG STARS OF SPECTRAL CLASSES M7–M10

The distribution of the M7–M10 stars is of particular interest, as will become apparent in the following section. These stars, which show the vanadium oxide absorption bands at λ 7400 and λ 7900, are among the coolest stars observed, and our experience with them has given us reason to believe that a large percentage, if not all, of them are variable. In fact, Nassau and Blanco (1954) have stated: "In a hundred or more cases examined, the presence of the VO bands indicates variability, usually of the Mira type or long-period variable." In addition, a limited study has been made covering an area of about 2 square degree in Cygnus (R.A. = 19^h55^m; dec. = 36°.8, epoch 1855) in which

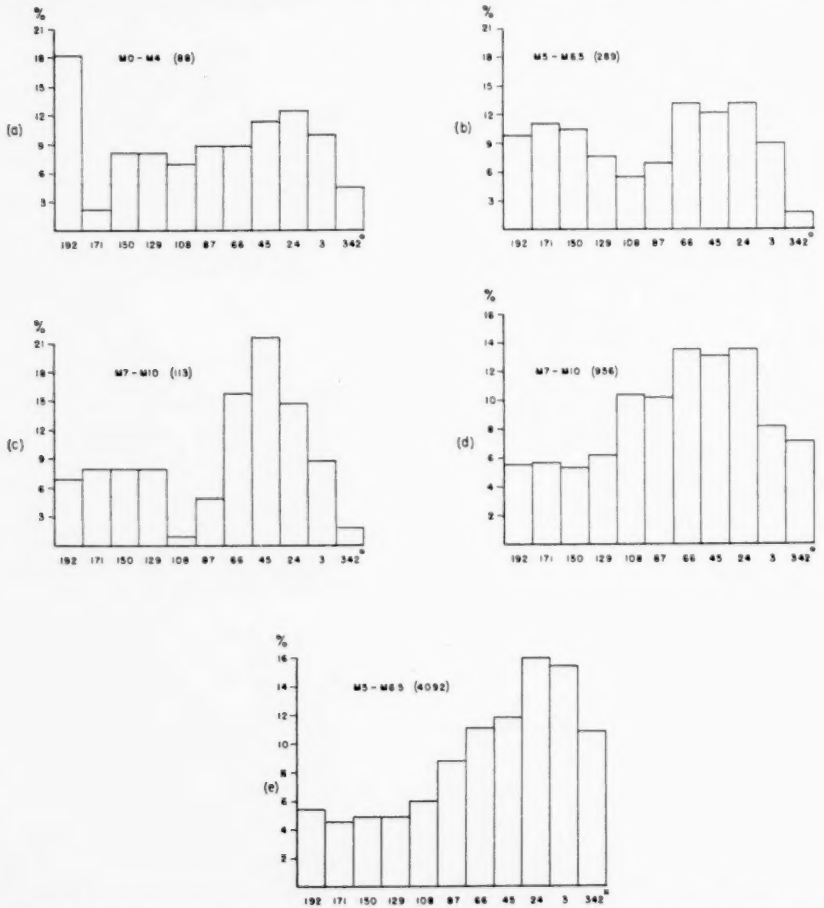

FIG. 4.—Comparison of the frequency distributions of the M variable stars and late M stars. *a*, M0–M4 variable stars; *b*, M5–M6.5 variable stars; *c*, M7–M10 variable stars; *d*, M7–M10 stars; *e*, M5–M6.5 stars. Galactic longitude is plotted as abscissa, and the total number of stars is given in parentheses after the spectral group.

all stars of class M5 and later were examined for variability. The area contained 73 such stars.

The results of this survey (Table 6) show that 56 per cent of the stars in the spectral range M7–M10 are definitely variable, and if those strongly suspected of variability are included, this figure increases to 76 per cent. While these results must necessarily be considered provisional, nevertheless they indicate that a majority of the stars of these spectral classes are variable. Additional evidence for the variability of M stars is furnished by Stebbins and Huffer (1930), who, using photoelectric photometry, found that 30 out of 32 stars of spectral classes M4, M5, and M6 varied by more than a tenth of a magnitude.

TABLE 5

M7–M10 VARIABLE STARS

Type	No.	Per Cent	Type	No.	Per Cent
Mira	86	76	Semiregular	4	4
Long period	18	16	Irregular	5	4

TABLE 6

VARIABLES AMONG STARS OF SPECTRAL CLASSES M7–M10

Variability	Total	At Least One Spectrum M7–M10	All Spectra between M7 and M10
Definite	30	24	5
Strongly suspected	11	9	1
Suspected	20	10	0
Non-variables	12	0	0
Total	73	43	6

VII. COMPARISON OF DISTRIBUTIONS OF VARIABLES AND LATE M STARS IN LONGITUDE

In this section a comparison is given of the distribution in longitude of the variables in the galactic belt of 12° width and all stars of classes M7–M10 for the same region. The latter distribution is from unpublished material by Nassau, Blanco, and Cameron. Figure 4, *c*, shows the distribution of the M7–M10 variables. Figure 4, *d*, shows the distribution of all stars of spectral classes M7–M10 in zones *a* and *b* (Nassau *et al.* 1956). Since the majority of these stars should be variable and of the same type as the known variables given previously, their distribution should be the same. The lack of agreement in Figure 4, *c* and *d*, may be due to the following or to their combined effect: (*a*) the galactic distribution of the variables is influenced by selection; (*b*) a systematic difference may exist between the M7–M10 groupings for the two surveys; it is also known that the two surveys were not carried out to the same limiting magnitude; (*c*) an appreciable number of M7–M10 stars may not be Mira-type or long-period variables.

With regard to the first possibility, it appears that the minimum at $l = 108°$ shown in

the distribution of the Mira and long-period variable group in Figure 3, *f*, cannot be attributed to selection, because the Mira variables, which constitute the largest part of this group, have large amplitudes of variation and would be discovered more easily than the much smaller-amplitude semiregular and irregular variable stars of Figure 3, *e*.

The second possibility has been given very serious consideration for several reasons. First, the distribution of M7–M10 stars, shown in Figure 4, *d*, which is taken from the Nassau, Blanco, and Cameron (1956) paper, is based on classification from 2° spectral plates, while the distribution of the M7–M10 variables, Figure 4, *c*, is based on 4° spectral plates. Thus both a difference in the limiting magnitudes of the two surveys which is known to exist and a systematic difference in the limiting spectral class, M7, could exist. The importance of the latter becomes evident if one recalls that the irregular and semiregular variables show a large concentration at M6.5 and then drop off to practically zero at M7. Thus a slight systematic shift of the spectral limit at M7 toward M6.5 would include a large number of irregular and semiregular variables in the M7–M10 group, which might alter the appearance of the distribution.

Because of these considerations, an independent check of the distribution of the M7–M10 and M5–M6.5 stars shown in Figure 4, *d* and *e*, was made. This time the 4° plates were used—the same plates as were used for the classification of the variables. Two regions were chosen for the check: one around $l = 108°$, the minimum of the variable-star distribution (Fig. 4, *c*), and the other around $l = 40°$, the maximum in the distribution. Both authors examined the plates for these two regions independently, selecting all stars M5 and later and classifying them. The results of this check indicate no significant difference from the original distribution of M7–M10 stars. It seems possible, therefore, that the difference in the two distributions (Fig. 4, *c* and *d*) may be attributed to the differences in the limiting magnitudes. The latter, dealing with fainter stars, may be reaching stars in the Perseus arm.

The third possibility leads to the conclusion that a considerable number of non-variables exists among stars of classes M7–M10, since hardly any irregular and semiregular variables are found in this spectral range. This seems less likely. However, red stars with very small amplitudes of variability may exist, which, under the prevailing methods of discovery, are considered non-variable. These stars do not, in general, come to the attention of the spectroscopists.

It is apparent that no definite conclusions are possible. However, the material available seems to indicate that the Mira and long-period variable group tends to show concentration along the local spiral arm and that the irregular and semiregular group shows a tendency for disk distribution.

VIII. PERIOD-SPECTRUM RELATION

The relation between period and spectrum for each of the types of variability was examined, with the idea of possible differences at different galactic latitudes. No such differences were found, although the number of stars in each subgroup was small. The period-spectrum distribution for all the stars in each group is given in Figure 5, *a*, *b*, and *c*. A few stars with periods greater than 700 days are omitted. For the Mira type (Fig. 5, *a*) the greatest concentration of stars is between 280 and 400 days and between spectral classes M6–M7, inclusive. The well-known trend of period with spectrum is evident; short periods correspond to early spectra, and long periods to late spectra. The long-period variables (Fig. 5, *b*) show a concentration in the period interval of 160–200 days and the spectral classes M6 and M6.5. The strong grouping of the semiregular variables (Fig. 5, *c*) between M5 and M6.5 has been pointed out. Here a similarly strong grouping between the period interval of 80 to 160 days is also present. Relatively few stars are outside this interval.

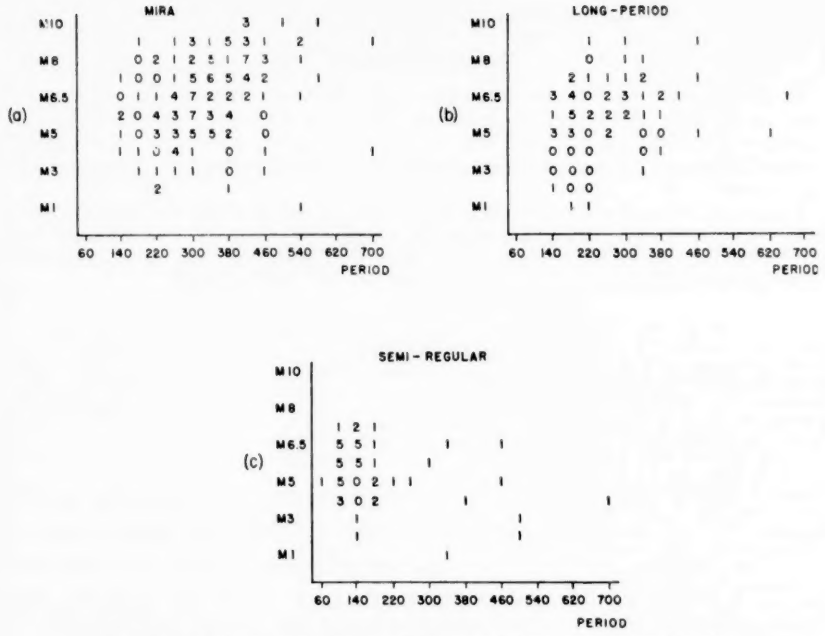

FIG. 5.—Period-spectrum relation. *a*, Mira type; *b*, long period; *c*, semiregular

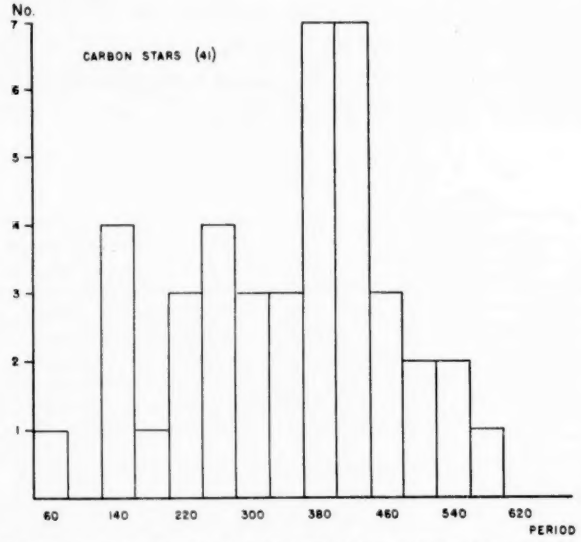

FIG. 6.—Period-frequency distribution of carbon variable stars (Mira, long-period, and semiregular types of variability are included).

IX. CARBON STARS

In the galactic zone there are 110 carbon stars which are known to be variable. Of these, 18 are Mira type, 9 are long-period variables, and 14 are semiregular. The period-frequency distribution for all these stars is given in Figure 6, which shows a maximum at about 420 days. The corresponding maximum for the M variables occurs about 100 days earlier.

Note added in proof.—The following carbon stars should be added in Table 2*a:* V478 Aqu, V Cyg, LW Cyg, GI Per, CZ Mon, V429 Cyg, V577 Cyg, DU Cas, LS Cas.

To Table 2*b* add the suspected variables 4376, 4712, 4995. Also add two S-type stars V633 Cyg and the suspected variable 4665, and the M0 star BU Gem.

REFERENCES

Baade, W. 1951, *Pub. Obs. U. Michigan*, **10**, 7.
Bidelman, W. P. 1950, *Ap. J.*, **112**, 219.
Cameron, D. M., and Nassau, J. J. 1955, *Ap. J.*, **122**, 177.
Cannon, A. J. 1934, *Harvard Bull.*, No. 897.
Davis, D. N. 1934, *Pub. A.S.P.*, **46**, 267.
Joy, A. H. 1942, *Ap. J.*, **96**, 344.
Keenan, P. C. 1950, *A.J.*, **55**, 172.
———. 1954, *Ap. J.*, **120**, 484.
Kukarkin, B. V., and Parenago, P. P. 1948, *General Catalogue of Variable Stars* (Moscow: Academy of Sciences, U.S.S.R.).
———. 1949–1951, First, second, and third supplements to the *General Catalogue of Variable Stars* (Moscow: Academy of Sciences, U.S.S.R.).
Kukarkin, B. V., Parenago, P. P., Efremov, U. E., and Kolorov, P. N. 1953–1955, fourth, fifth, sixth, and seventh supplements to the *General Catalogue of Variable Stars* (Moscow: Academy of Sciences, U.S.S.R.).
———. 1951, *Catalogue of Stars Suspected of Being Variable* (Moscow: Academy of Sciences, U.S.S.R.).
Lee, O. J., and Bartlett, T. J. 1944, *Ann. Dearborn Obs.*, Vol. **5**, Part 1B.
Merrill, P. W. 1940, The Spectra of Long-Period Variable Stars (Chicago: University of Chicago Press).
Merrill, P. W. 1941, *Ap. J.*, **94**, 171.
Nassau, J. J., and Albada, B. G. van. 1949, *Ap. J.*, **109**, 391.
Nassau, J. J., and Blanco, V. M. 1954. *Ap. J.*, **120**, 468.
Nassau, J. J., Blanco, V. M., and Cameron, D. M. 1956, *Ap. J.*, Vol. **124** (November).
Nassau, J. J., Blanco, V. M., and Morgan, W. W. 1954, *Ap. J.*, **120**, 478.
Stebbins, J., and Huffer, C. M. 1930, *Pub. Washburn Obs.*, **15**, Part 3, 139.

THE LAW OF INTERSTELLAR REDDENING AND ABSORPTION*

W. A. HILTNER AND H. L. JOHNSON
Yerkes and McDonald Observatories and Lowell Observatory
Received April 23, 1956; revised May 14, 1956

ABSTRACT

The law of interstellar reddening and the slope of the reddening lines in the plot of $U - B$ versus $B - V$ have been reinvestigated in the light of more extensive data. The data consist of a catalogue of 262 O stars for which we have three-color photometry and slit spectrograms. The anomalous behavior of stars in the Great Rift in Cygnus found by Johnson and Morgan is confirmed. The equation of the mean reddening line is

$$\frac{E_{(U-B)}}{E_{(B-V)}} = 0.72 + 0.05E_{(B-V)} .$$

A rediscussion of the ratio of total to selective absorption, with additional new data, gives

$$R = \frac{A_V}{E_{(B-V)}} = 3.0 \pm 0.2 \text{ (p.e.)} .$$

I. INTRODUCTION

There have been several suggestions (Baade and Minkowski 1937; Stebbins and Whitford 1945; Sharpless 1952; Johnson and Morgan 1955*a*) that the law of interstellar reddening and absorption is not the same everywhere. We wish here to reinvestigate, on the basis of more extensive data, the suggestion by Johnson and Morgan (1955*a*) that the law of interstellar reddening for the region of the Great Rift in Cygnus ($40° < l < 49°$) differs from that elsewhere in the Milky Way.

The ratio of total to selective absorption is also discussed here. Morgan, Harris, and Johnson (1953) and Blanco (1955) have found that the value of this ratio is

$$R = \frac{A_V}{E_{(B-V)}} = 3.0 ,$$

where A_V is the total visual absorption and $E_{(B-V)}$ is the color excess on the $B - V$ system, as determined from Whitford's (1948) interstellar absorption-curve, while Sharpless (1952) has derived a value of $R = 6.0$ for the region of the Orion Nebula.

When one uses the Q method for the determination of interstellar reddening (Johnson and Morgan 1953), he must know the characteristics of the reddening line (Morgan, Harris, and Johnson 1953) in the $U - B$ versus $B - V$ plot. The usual practice has been to assume, because of the relatively small number of data, that the reddening line is linear. Blanco, however, has shown, on the basis of the observed response of the photometer, the observed interstellar absorption-curve, and assumed stellar intensity distributions, that a slightly curved line is to be expected.

II. THE LAW OF INTERSTELLAR REDDENING

The data upon which our investigation of the law of interstellar reddening and the character of the reddening lines in the $U - B$ versus $B - V$ plot is based comes from catalogue of 262 O stars listed in Table 1. This catalogue was compiled from both published and unpublished data obtained by the two authors. The first column numbers

* Contributions from the McDonald Observatory, No. 266.

TABLE 1

CATALOGUE OF O-TYPE STARS

No.	Star	1900 α	1900 δ	l	b	Spectrum	V	B-V	U-B
		h m							
1...	108	0 00.9	+63°07'	85.6	+ 1.4	O8 fp	7.40	+0.18	-0.79
2...	+63°12	0 08.2	+63°37'	86.5	+ 2.0	O9 Ib	9.76	+0.55	-0.45
3...	1337	0 12.5	+50°53'	85.5	-10.9	O9 III	5.9*	+0.03	-1.01
4...	+60°39	0 16.2	+61°10'	87.1	- 0.7	O9 V	9.46	+0.24	-0.70
5...	+61°74	0 20.4	+62°00'	87.7	+ 0.1	O9 V nn	9.55	+0.32	-0.66
6...	+62°79	0 20.9	+62°53'	87.8	+ 1.0	O9.5 IV	9.22	+0.41	-0.56
7...	+61°105	0 25.6	+61°53'	88.3	- 0.1	O9 V	9.29	+0.27	-0.69
8...	No. 1 ref. 3	0 34.0	+60°25'	89.3	- 1.6	O9 IV	9.99	+0.37	-0.61
9...	No. 110 ref. 4	0 42.2	+62°27'	90.2	+ 0.5	O7	11.40	+0.48	-0.53
10...	5005	0 47.0	+56°05'	91.0	- 5.9	O6	7.76	+0.09	-0.83
11...	5689	0 53.5	+63°05'	91.5	+ 1.1	O6	9.13	+0.34	-0.68
12...	+62°249	1 19.5	+62°31'	94.5	+ 0.9	O9.5 V	10.04	+0.70	-0.34
13...	8768	1 21.4	+62°45'	94.7	+ 1.1	O9.5 IV	8.69	+0.40	-0.60
14...	+60°261	1 25.9	+60°37'	95.6	- 0.9	O7	8.63	+0.31	-0.67
15...	9974	1 32.4	+57°39'	97.0	- 3.6	O6 + W R	10.69	+0.02	-0.86
16...	10125	1 33.9	+63°40'	95.9	+ 2.3	O9.5 Ib	8.22	+0.31	-0.65
17...	E 236894	1 45.4	+57°57'	98.6	- 3.0	O8 V	9.37	+0.19	-0.76
18...	+59°367	1 51.6	+60°02'	98.8	- 0.7	O9.5 Ib	9.77	+0.53	-0.52
19...	12323	1 55.8	+55°08'	100.7	- 5.3	O9 V*	8.90	-0.02	-0.93
20...	+61°370	1 56.4	+61°24'	99.0	+ 0.9	O9 V	10.06	+0.70	-0.37
21...	12993	2 02.1	+57°27'	100.9	- 2.8	O5	8.98	+0.20	-0.80
22...	13268	2 04.6	+55°41'	101.8	- 4.4	O8 V nn	8.18	+0.13	-0.83
23...	No. 7 ref. 2	2 05.4	+59°26'	100.7	- 0.8	O9 V	11.03	+0.97	-0.13
24...	14434	2 14.8	+56°27'	102.8	- 3.2	O6	8.49	+0.16	-0.78
25...	14442	2 14.9	+59°06'	101.9	- 0.7	O5 V	9.22	+0.41	-0.62
26...	+60°470	2 15.8	+60°22'	101.6	+ 0.5	O8 V	9.88	+0.70	-0.36
27...	14633	2 16.7	+41°02'	108.9	-17.5	O8 V	7.44	-0.21	-1.09
28...	+61°411	2 19.0	+61°33'	101.5	+ 1.8	O8:	10.19	+0.99	-0.09
29...	14947	2 19.5	+58°25'	102.7	- 1.1	O6 f	8.01	+0.45	-0.60
30...	+60°497	2 24.2	+61°11'	102.2	+ 1.7	O7	8.80	+0.57	-0.49
31...	+60°498	2 24.5	+61°07'	102.3	+ 1.6	O9 V	9.92	+0.54	-0.46
32...	+60°501	2 25.0	+61°02'	102.4	+ 1.6	O6.5	9.60	+0.46	-0.58
33...	15558	2 25.1	+61°01'	102.4	+ 1.6	O6	7.81	+0.52	-0.56
34...	15570	2 25.2	+60°55'	102.4	+ 1.5	O5 f veiled	8.11	+0.70	-0.41
35...	15629	2 25.7	+61°05'	102.4	+ 1.6	O5	8.42	+0.43	-0.62
36...	+60°512	2 26.4	+60°57'	102.6	+ 1.6	O6	9.41	+0.50	-0.53
37...	+62°424	2 28.4	+62°31'	102.2	+ 3.1	O8	8.83	+0.45	-0.57
38...	16429	2 33.1	+60°51'	103.3	+ 1.8	O9.5 III	7.67	+0.62	-0.38
39...	16691	2 35.5	+56°28'	105.5	- 2.0	O5 f	8.70	+0.48	-0.57
40...	17505	2 43.4	+60°01'	104.8	+ 1.6	O7	7.06	+0.40	-0.64
41...	17520	2 43.5	+59°59'	104.9	+ 1.6	O8 V	8.27	+0.32	-0.68
42...	17603	2 44.4	+56°38'	106.5	- 1.4	O7 f:	8.45	+0.64	-0.42
43...	+59°562	2 45.6	+60°03'	105.1	+ 1.7	O8 V	9.73	+0.47	-0.53
44...	+60°586	2 46.4	+60°14'	105.1	+ 2.0	O7	8.48	+0.30	-0.67
45...	+56°739	2 47.4	+57°02'	106.7	- 0.8	O9.5 Ib	9.96	+1.00	-0.07
46...	+60°594	2 49.1	+61°01'	105.0	+ 2.8	O9 V	9.30	+0.36	-0.64
47...	18326	2 51.6	+60°10'	105.7	+ 2.2	O8	7.82	+0.38	-0.63
48...	18409	2 52.4	+62°19'	104.7	+ 4.1	O9 Ib	8.36	+0.42	-0.59
49...	19820	3 06.2	+59°11'	107.8	+ 2.3	O9 IV	7.1*	+0.50	-0.48
50...	24431	3 48.1	+52°21'	116.6	+ 0.2	O9 IV-V	6.72	+0.38	-0.61

TABLE 1– Continued

No.	Star	1900 α	1900 δ	l	b	Spectrum	V	B-V	U-B
51...	24534	$3^h49^m.1$	+30°45'	131.1	-15.9	O pe (var)	6.07	+0.31	-0.82
52...	No. 7 ref. 3	3 51.0	+56°56'	113.9	+ 4.0	O7.5	10.08	+0.27	-0.69
53...	+56°864	3 51.1	+56°56'	113.9	+ 4.0	O6 nn	9.68	+0.28	-0.69
54...	+56°866	3 51.4	+56°49'	114.0	+ 3.9	O9 V	10.28	+0.36	-0.60
55...	24912	3 52.5	+35°30'	128.3	-11.9	O7	4.02	+0.02	-0.92
56...	E 237211	3 55.3	+56°15'	114.8	+ 3.8	O9.5 I? p*	8.98	+0.49	-0.51
57...	34656	5 14.0	+37°20'	137.7	+ 1.5	O7	6.79	+0.02	-0.90
58...	E 242908	5 16.0	+33°25'	141.2	- 0.3	O5	9.04	+0.28	-0.72
59...	E 242926	5 16.1	+33°13'	141.4	- 0.4	O6	9.35	+0.34	-0.65
60...	E 242935	5 16.2	+33°19'	141.3	- 0.4	O8	9.43	+0.20	-0.73
61...	35619	5 21.0	+34°41'	140.7	+ 1.3	O7	8.55	+0.24	-0.71
62...	+34°1058	5 22.0	+34°35'	140.9	+ 1.4	O8 nn	8.78	+0.26	-0.73
63...	35921	5 23.0	+35°18'	140.4	+ 1.9	O9.5 III	6.81	+0.20	-0.78
64...	+39°1328	5 25.2	+39°59'	136.8	+ 4.9	O9 III ?*	9.84	+0.57	-0.46
65...	36483	5 26.9	+36°24'	140.0	+ 3.2	O9.5 III	8.18	+0.43	-0.55
66...	36619	5 27.9	-23°30'	194.1	-26.0	O7	8.60	+0.23	-0.69
67...	36861	5 29.6	+09°52'	162.8	-10.5	O8	3.39	-0.19	-1.03
68...	36879	5 29.7	+21°20'	153.0	- 4.4	O6	7.57	+0.20	-0.80
69...	37041	5 30.5	-05°29'	176.4	-18.4	O9.5 Vp	5.19	-0.16	-0.95
70...	37043	5 30.5	-05°59'	176.8	-18.7	O9 III	2.77	-0.25	-1.08
71...	37742-43	5 35.7	-02°00'	174.0	-15.3	O9.5 Ib	1.79	-0.20	-1.06
72...	E 248894	5 48.0	+20°51'	155.6	- 1.1	O8: V: nn	9.29	+0.24	-0.73
73...	39680(A)	5 49.0	+13°49'	161.8	- 4.4	O6: pe	7.99	+0.02	-0.96
74...	41997	6 03.2	+15°44'	161.8	- 0.5	O7	8.40	+0.39	-0.63
75...	42088	6 03.7	+20°31'	157.7	+ 2.0	O6	7.54	+0.06	-0.89
76...	No. 21 ref. 2	6 04.3	+13°08'	164.2	- 1.5	O9 V	10.23	+0.46	-0.56
77...	No. 22 ref. 2	6 05.1	+13°12'	164.3	- 1.3	O9 V	10.57	+0.46	-0.54
78...	E 254755	6 12.5	+22°43'	156.8	+ 4.8	O9 V: p?	8.84	+0.60	-0.44
79...	E 255055	6 13.6	+23°20'	156.4	+ 5.3	O9 V: p	9.38	+0.26	-0.70
80...	44597	6 17.5	+20°27'	159.3	+ 4.8	O9 V	9.02	+0.26	-0.69
81...	44811	6 18.8	+19°45'	160.1	+ 4.7	O7.5 V	8.42	+0.14	-0.80
82...	45314	6 21.6	+14°57'	164.7	+ 3.0	O9 ? pe	6.64	+0.15	-0.88
83...	46056	6 26.0	+04°54'	174.0	- 0.8	O8	8.17	+0.18	-0.75
84...	46149	6 26.6	+05°06'	173.8	- 0.6	O8	7.58	+0.18	-0.78
85...	46150	6 26.6	+05°00'	174.0	- 0.6	O6	6.74	+0.13	-0.82
86...	46202	6 26.9	+05°03'	174.0	- 0.5	O9 V	8.17	+0.17	-0.74
87...	46223	6 27.0	+04°53'	174.2	- 0.6	O5	7.26	+0.22	-0.76
88...	46485	6 28.6	+04°36'	174.6	- 0.4	O8	8.26	+0.32	-0.68
89...	46573	6 29.1	+02°36'	176.4	- 1.2	O7	7.93	+0.34	-0.66
90...	46966	6 31.1	+06°10'	173.5	+ 0.9	O8	6.86	-0.04	-0.92
91...	47129	6 32.0	+06°13'	173.6	+ 1.2	O8	6.06	+0.05	-0.88
92...	-00°1385	6 35.2	-00°16'	179.7	- 1.2	O8	9.87	+0.31	-0.67
93...	47839	6 35.5	+09°59'	170.6	+ 3.6	O7	4.65	-0.25	-1.06
94...	48099	6 36.6	+06°27'	173.9	+ 2.3	O6	6.37	-0.05	-0.94
95...	48279	6 37.5	+01°49'	178.1	+ 0.3	O8	7.90	+0.13	-0.80
96...	+00°1576	6 39.7	+00°43'	179.3	+ 0.3	O9 III:	9.26	+0.43	-0.59
97...	+01°1560	6 46.7	+01°30'	179.5	+ 2.2	O8:	9.66	+0.28	-0.68
98...	52266	6 55.4	-05°40'	186.8	+ 0.7	O9 V	7.23	-0.01	-0.90
99...	52533	6 56.5	-02°59'	184.5	+ 2.1	O9 V	7.70	-0.09	-0.95
100...	53975	7 02.0	-12°14'	193.4	- 1.0	O8	6.47	-0.10	-0.98

TABLE 1—Continued

No.	Star	1900 α	1900 δ	l	b	Spectrum	V	B-V	U-B
		h m							
101...	54662	7 04.6	-10°11'	191.8	+ 0.5	O6	6.21	+0.03	-0.88
102...	54879	7 05.5	-11°39'	193.2	0.0	O9.5 V	7.66	0.00	-0.86
103...	57061	7 14.5	-24°47'	205.8	- 4.4	O9 III	4.39	-0.14	-0.99
104...	57236	7 15.2	-21°49'	203.3	- 2.8	O8	8.75	+0.20	-0.73
105...	57682	7 17.2	-08°48'	192.1	+ 3.9	O9 V	6 44	-0.19	-1.04
106...	61347	7 33.7	-13°38'	198.4	+ 5.1	O9 Ib	8.43	+0.17	-0.76
107...	-29°4849	7 40.0	-29°05'	212.4	- 1.6	O9.5 II:	10.00	+0.22	-0.72
108...	63005	7 41.6	-26°15'	210.2	+ 0.2	O7	9.11	-0.02	-0.95
109...	64315	7 48.2	-26°10'	210.9	+ 1.5	O6: nn (e)	9.21	+0.22	-0.74
110...	65087	7 51.9	-28°16'	213.1	+ 1.0	O7 f	9.97	+0.16	-0.79
111...	66811	8 00.1	-39°43'	223.6	- 3.9	O5 f	2.25	-0.26	-1.11
112...	149757	16 31.7	-10°22'	334.0	+22.3	O9.5 V	2.56	+0.02	-0.86
113...	157857	17 20.7	-10°55'	340.6	+11.8	O7 f	7.78	+0.18	-0.80
114...	-29°13809	17 31.7	-29°03'	326.7	- 0.1	O9 V	9.74	+0.68	-0.34
115...	160730	17 36.4	-24°15'	331.3	+ 1.6	O8	9.68	+0.66	-0.40
116...	316232	17 39.4	-29°11'	327.5	- 1.6	O9 IV	10.30	+0.68	-0.37
117...	162978	17 48.7	-24°52'	332.2	- 1.1	O8	6.20	+0.04	-0.89
118...	163800	17 52.9	-22°30'	334.7	- 0.8	O8	7.04	+0.31	-0.69
119...	163892	17 53.4	-22°27'	334.9	- 0.8	O9 IV	7.44	+0.09	-0.79
120...	164438	17 56.0	-19°06'	338.1	+ 0.3	O9 IV	7.48	+0.34	-0.66
121...	164492	17 56.3	-23°01'	334.7	- 1.7	O7	7.63	0.00	-0.86
122...	166546	18 06.0	-20°27'	338.1	- 2.4	O9.5 II!	7.25	+0.05	-0.86
123...	-14°4922	18 06.3	-14°58'	342.9	+ 0.2	O9.5: II:	9.73	+0.85	-0.30
124...	166734	18 06.9	-10°46'	346.6	+ 2.1	O8 f	8.42	+1.09	-0.12
125...	-20°5043	18 08.1	-20°20'	338.4	- 2.8	O6	9.52	+0.85	-0.20
126...	167263	18 09.3	-20°25'	338.4	- 3.0	O9 II	5.98	+0.04	-0.88
127...	167330	18 09.6	-12°34'	345.4	+ 0.7	O9 I-II	8.23	+0.66	-0.45
128...	167633	18 11.0	-16°33'	342.0	- 1.5	O6	8.14	+0.27	-0.72
129...	167659	18 11.1	-19°00'	339.9	- 2.7	O8	7.39	+0.22	-0.74
130...	167771	18 11.6	-18°30'	340.3	- 2.5	O8	6.54	+0.12	-0.84
131...	-12°4964	18 11.8	-12°21'	345.8	+ 0.3	O8	9.82	+0.91	-0.22
132...	-12°4979	18 12.4	-12°17'	345.9	+ 0.2	O7 (f)	10.44	+0.68	-0.32
133...	-11°4586	18 12.5	-11°20'	346.8	+ 0.8	O8 (I?)	9.40	+1.00	-0.14
134...	167971	18 12.5	-12°17'	346.0	+ 0.2	O8 f	7.50	+0.77	-0.32
135...	-12°4984	18 12.7	-12°00'	346.2	+ 0.3	O9 V	9.93	+0.83	-0.26
136...	-13°4927	18 13.0	-13°48'	344.6	- 0.6	O5	10.08	+0.84	-0.32
137...	168112	18 13.1	-12°08'	346.2	+ 0.1	O6	8.52	+0.69	-0.40
138...	-13°4930	18 13.2	-13°52'	344.7	- 0.7	O9.5 V	9.44	+0.30	-0.70
139...	-12°4994	18 13.4	-12°09'	346.2	+ 0.1	O9: V:	9.81	+0.70	-0.39
140...	-13°4941	18 14.4	-13°06'	345.4	- 0.6	O9.5 IV	9.75	+1.08	-0.07
141...	-15°4930	18 14.6	-15°08'	343.6	- 1.5	O6 p	9.42	+0.74	-0.37
142...	-12°5009	18 14.7	-12°13'	346.3	- 0.2	O8	9.54	+0.68	-0.42
143...	-16°4826	18 15.2	-16°05'	342.9	- 2.2	O5	9.89	+0.76	-0.37
144...	168917	18 17.1	-14°25'	344.6	- 1.8	O9 V:	8.44	+0.43	-0.58
145...	-11°4620	18 17.9	-11°58'	346.9	- 0.8	O5	10.17	+0.80	-0.31
146...	-10°4682	18 18.8	-10°52'	347.9	- 0.5	O7	9.63	+0.56	-0.55
147...	169582	18 20.2	-09°49'	349.0	- 0.2	O5 f	8.70	+0.56	-0.49
148...	169727	18 21.0	-13°43'	345.7	- 2.3	O6	9.29	+0.79	-0.37
149...	169755	18 21.1	-14°34'	344.9	- 2.7	O8 V	9.26	+0.53	-0.51
150...	-08°4617	18 23.8	-08°38'	350.5	- 0.5	O8.5 (V)	9.36	+0.91	-0.21

TABLE 1–Continued

No.	Star	1900 α	1900 δ	l	b	Spectrum	V	B-V	U-B
151...	170452	$18^h24^m.4$	-13°01'	346.7	- 2.6	O9: V	8.75	+0.53	-0.48
152...	-13°5015	18 25.8	-13°38'	346.3	- 3.3	O7	10.02	+0.53	-0.54
153...	171198	18 28.3	-12°20'	347.7	- 3.2	O7:	9.54	+0.57	-0.48
154...	-08°4634	18 28.9	-08°10'	351.5	- 1.4	O9? V? p	9.44	+0.91	-0.18
155...	-04°4503	18 30.2	-04°53'	354.5	- 0.1	O7	10.83	+0.75	-0.31
156...	171589	18 30.6	-14°12'	346.3	- 4.6	O7 f	8.28	+0.32	-0.69
157...	172175	18 33.6	-07°57'	352.2	- 2.3	O6 f	9.44	+0.63	-0.43
158...	172275	18 34.2	-07°27'	352.7	- 2.2	O6	9.35	+0.77	-0.36
159...	173783	18 42.0	-09°25'	351.9	- 4.9	O9 I	9.31	+0.51	-0.52
160...	-06°4903	18 42.5	-06°25'	354.6	- 3.6	O8	9.94	+0.31	-0.72
161...	-05°4769	18 43.2	-05°37'	355.4	- 3.3	O8 (I:)	10.40	+0.75	-0.35
162...	-00°3584	18 48.4	-00°41'	0.4	- 2.2	O8	9.98	+0.62	-0.45
163...	175514	18 50.6	+09°13'	9.4	+ 2.0	O8: V nn	8.59	+0.59	-0.45
164...	175754	18 51.7	-19°17'	344.0	-11.3	O8 f	7.04	-0.07	-0.97
165...	175876	18 52.3	-20°33'	343.0	-12.0	O6	6.95	-0.10	-1.01
166...	+24°3843	19 37.7	+24°06'	27.9	- 0.5	O8 V	10.34	+0.99	-0.01
167...	+22°3782	19 39.0	+23°03'	27.1	- 1.3	O7	9.34	+0.56	-0.52
168...	+25°3952	19 41.5	+25°07'	29.2	- 0.7	O8	10.15	+0.63	-0.42
169...	+24°3866	19 41.5	+24°52'	28.9	- 0.9	O8 f	9.57	+1.18	+0.02
170...	186980	19 42.4	+31°52'	35.0	+ 2.7	O7.5	7.48	+0.08	-0.84
171...	+27°3512	19 42.6	+28°00'	31.8	+ 0.6	O7.5	8.77	+0.20	-0.78
172...	+24°3881	19 42.8	+24°36'	28.9	- 1.3	O6 f	9.12	+0.69	-0.43
173...	+29°3772	19 46.7	+29°09'	33.2	+ 0.4	O7 f	10.10	+0.50	-0.53
174...	188001	19 47.9	+18°25'	24.2	+ 5.4	O8 f	6.22	+0.01	-0.92
175...	188209	19 49.0	+46°47'	48.5	+ 9.2	O9.5 III	5.61	-0.05	-0.96
176...	E 227018	19 56.1	+35°02'	39.2	+ 1.9	O7	8.99	+0.38	-0.62
177...	E 227245	19 58.6	+35°24'	39.8	+ 1.7	O7	9.74	+0.62	-0.44
178...	+33°3717	20 00.6	+33°25'	38.4	+ 0.3	O7:	10.28	+0.47	-0.54
179...	190864	20 01.9	+35°19'	40.1	+ 1.1	O6	7.76	+0.20	-0.78
180...	E 227757	20 03.5	+36°04'	40.9	+ 1.3	O9.5 V	9.20	+0.18	-0.75
181...	191423	20 04.7	+42°19'	46.2	+ 4.6	O9 V:	8.03	+0.16	-0.76
182...	191978	20 07.5	+41°04'	45.5	+ 3.5	O8	8.02	+0.14	-0.78
183...	192001	20 07.6	+41°50'	46.1	+ 3.9	O9.5 IV	8.25	+0.32	-0.60
184...	192281	20 09.0	+39°58'	44.8	+ 2.6	O5 f	7.55	+0.38	-0.61
185...	E 228368	20 09.5	+34°43'	40.5	- 0.5	O7	8.39	+0.49	-0.51
186...	192639	20 10.8	+37°03'	42.6	+ 0.6	O8 f	7.11	+0.35	-0.63
187...	193117	20 13.5	+40°32'	45.7	+ 2.2	O9.5 II	8.70	+0.61	-0.42
188...	E 228766*	20 13.8	+37°00'	42.9	+ 0.1	(O6 f or WR)	9.14	+0.65	-0.37
189...	E 228779	20 14.0	+34°30'	40.9	- 1.4	O9.5 Ib	8.92	+1.31	+0.22
190...	193322	20 14.6	+40°25'	45.7	+ 2.1	O8	5.84	+0.11	-0.77
191...	E 228841	20 14.8	+38°34'	44.3	+ 0.9	O7.5 p	8.94	+0.56	-0.42
192...	E 228854	20 15.0	+36°02'	42.3	- 0.7	O8:	8.93	+0.70	-0.28
193...	193443	20 15.2	+37°57'	43.8	+ 0.5	O9 III	7.24	+0.40	-0.53
194...	193514	20 15.5	+38°57'	44.7	+ 1.0	O7 f	7.40	+0.45	-0.51
195...	193595	20 15.9	+38°44'	44.6	+ 0.8	O7	8.72	+0.36	-0.58
196...	193682	20 16.5	+37°30'	43.6	0.0	O5	8.41	+0.51	-0.48
197...	E 228989	20 16.7	+38°23'	44.4	+ 0.5	O9 V nn	9.72	+0.77	-0.20
198...	+36°4022	20 17.3	+36°29'	42.9	- 0.7	O9.5 II	9.94	+0.83	-0.20
199...	+38°4043	20 18.7	+38°24'	44.6	+ 0.2	O9 III	9.02	+0.59	-0.39
200...	E 229196	20 19.7	+40°34'	46.5	+ 1.3	O5	8.54	+0.90	-0.15

TABLE 1—Continued

No.	Star	1900 α	1900 δ	l	b	Spectrum	V	B-V	U-B
		h m							
201...	E 229202	20 19.8	+39°50'	45.9	+ 0.8	O8 V:	9.53	+0.87	-0.12
202...	194334	20 20.0	+38°34'	44.9	+ 0.1	O7.5 V	8.77	+0.84	-0.16
203...	E 229232	20 20.3	+38°47'	45.1	+ 0.1	O5 f	9.52	+0.82	-0.17
204...	E 229234	20 20.3	+38°12'	44.6	- 0.2	O9.5 III	8.92	+0.77	-0.19
205...	No. 17 ref. 7	20 20.5	+39°20'	45.6	+ 0.4	O7	9.86	+1.18	+0.11
206...	+39°4168	20 20.7	+39°26'	45.7	+ 0.5	O7	9.99	+1.07	+0.03
207...	+37°3929	20 21.3	+37°09'	43.9	- 1.0	O8 f	10.15	+1.25	+0.23
208...	194649	20 21.7	+39°54'	46.1	+ 0.6	O6.5	9.00	+0.95	-0.09
209...	+36°4063	20 21.9	+37°03'	43.9	- 1.2	O9.5 Ib	9.71	+1.14	+0.08
210...	+40°4179	20 24.1	+40°16'	46.7	+ 0.5	O8 V:	9.65	+0.57	-0.43
211...	195213	20 24.9	+40°28'	47.0	+ 0.4	O7	8.74	+0.84	-0.26
212...	195592	20 27.2	+43°59'	50.0	+ 2.3	O9.5 Ia	7.08	+0.87	-0.19
213...	No. 1 ref. 5	20 27.5	+41°10'	47.8	+ 0.5	O9 V?	11.09	+1.42	+0.31
214...	+40°4212	20 28.0	+40°52'	47.6	+ 0.2	O9 ?	10.29	+1.63	+0.54
215...	+40°4219	20 28.6	+41°06'	47.9	+ 0.3	O8	10.22	+1.18	+0.10
216...	+40°4220	20 28.8	+40°58'	47.8	+ 0.2	O7 f	9.1*	+1.67	+0.55
217...	No. 12 ref. 6	20 29.1	+40°55'	47.8	+ 0.1	O	11.4*	+3.01	+1.69
218...	No. 6 ref. 5	20 29.2	+41°05'	48.0	+ 0.2	O8 (V)	10.67	+1.22	+0.16
219...	No. 9 ref. 5	20 29.6	+40°55'	47.9	0.0	O5 f	10.80	+1.93	+0.65
220...	+40°4227	20 29.6	+40°58'	47.9	+ 0.1	O6 f	9.01	+1.28	+0.15
221...	No. 7 ref. 5	20 29.7	+41°00'	47.9	+ 0.1	O6 f	10.49	+1.44	+0.28
222...	+41°3804	20 30.2	+41°12'	48.2	+ 0.1	O9.5 Ia	9.88	+1.52	+0.40
223...	+45°3216	20 30.5	+45°19'	51.4	+ 2.6	O8	9.07	+0.39	-0.57
224...	+41°3807	20 30.6	+41.16'	48.3	+ 0.1	O6 f	10.04	+1.44	+0.26
225...	+36°4145	20 32.5	+37°04'	45.2	- 2.8	O9 V	8.95	+0.65	-0.37
226...	+42°3835	20 38.6	+42°49'	50.4	- 0.1	O9 p?	9.20	+0.91	-0.19
227...	+45°3260	20 42.2	+45°58'	53.2	+ 1.5	O9 V	9.06	+0.51	-0.50
228...	199579	20 53.1	+44°33'	53.4	- 0.9	O6	5.96	+0.05	-0.85
229...	202124	21 08.8	+44°07'	55.0	- 3.2	O9.5 Ib	7.80	+0.22	-0.69
230...	206267	21 35.9	+57°02'	66.9	+ 3.4	O6	5.62	+0.21	-0.74
231...	+49°3591	21 36.7	+50°03'	62.6	- 2.0	O7.5	9.67	+0.52	-0.48
232...	207198	21 42.2	+61°59'	70.7	+ 6.8	O9 II	5.96	+0.31	-0.64
233...	+28°4211	21 46.7	+28°24'	50.2	-20.0	O pec	10.54	-0.34	-1.26
234...	E 235673	21 54.1	+52°19'	66.1	- 1.9	O7	9.14	+0.21	-0.77
235...	209481	21 58.7	+57°31'	69.6	+ 2.0	O9 V	5.56	+0.07	-0.86
236...	209975	22 02.1	+61°48'	72.4	+ 5.3	O9.5 Ib	5.10	+0.09	-0.84
237...	+53°2790	22 04.3	+54°02'	68.3	- 1.3	O9.5 III? p	9.86	+0.25	-0.71
238...	210809	22 07.9	+51°56'	67.7	- 3.4	O9 Ib	7.54	+0.05	-0.89
239...	210839	22 08.1	+58°56'	71.5	+ 2.5	O6 f	5.04	+0.26	-0.74
240...	+53°2843	22 14.9	+53°46'	69.5	- 2.4	O8	9.50	+0.21	-0.74
241...	No. 21 ref. 1	22 18.5	+55°08'	70.7	- 1.5	O5	10.29	+0.26	-0.73
242...	E 235825	22 19.6	+54°44'	70.6	- 1.9	O9 V	9.28	+0.24	-0.73
243...	+54°2761	22 19.9	+55°11'	70.9	- 1.6	O5 f	9.98	+0.34	-0.68
244...	+62°2078	22 22.2	+62°54'	75.0	+ 4.9	O7	9.72	+1.11	0.00
245...	214680	22 34.8	+38°32'	64.8	-17.3	O9 V	4.88	-0.20	-1.04
246...	215835	22 42.9	+57°33'	74.8	- 1.0	O6 n	8.58	+0.32	-0.66
247...	216532	22 48.6	+61°54'	77.3	+ 2.7	O8	8.00	+0.54	-0.48
248...	+55°2840	22 51.0	+55°51'	75.1	- 3.0	O7.5 p	10.01	+0.45	-0.56
249...	216898	22 51.8	+61°46'	77.6	+ 2.4	O8	8.00	+0.53	-0.48
250...	217086	22 53.0	+62°12'	77.9	+ 2.7	O5	7.64	+0.62	-0.44

TABLE 1—Concluded

No.	Star	1900		l	b	Spectrum	V	B-V	U-B
		α	δ						
		h m							
251...	E 240160	22 57.4	+56°27'	76.2	- 2.8	O9	10.02	+0.48	-0.52
252...	E 240165	22 58.0	+56°39'	76.3	- 2.6	O9.5 V	10.13	+0.47	-0.53
253...	218195	23 01.0	+57°43'	77.1	- 1.8	O8	8.34	+0.27	-0.70
254...	218915	23 06.7	+52°31'	76.0	- 6.9	O9 I	7.20	+0.02	-0.90
255...	+60°2522	23 16.2	+60°38'	79.9	+ 0.3	O7 f	8.67	+0.41	-0.62
256...	No. 7 ref. 1	23 18.4	+61°35'	80.5	+ 1.1	O8 (f)	10.80	+0.75	-0.35
257...	+62°2299	23 43.1	+62°50'	83.6	+ 1.5	O8	9.58	+0.61	-0.47
258...	+61°2559	23 48.6	+61°52'	84.0	+ 0.5	O9 V	9.72	+0.29	-0.66
259...	+66°1661	23 52.4	+67°00'	85.4	+ 5.4	O9 V	8.72	+0.81	-0.20
260...	E 240464	23 53.7	+59°43'	84.2	- 1.8	O9 V	9.59	+0.30	-0.61
261...	+66°1675	23 57.0	+66°51'	85.8	+ 5.2	O7	9.05	+1.09	+0.04
262...	225160	23 58.9	+61°40'	85.1	+ 0.1	O8 f	8.19	+0.27	-0.72

REFERENCES

No. 1... Gonzalez, G. and Gonzalez, G. 1952, Bol. Obs. Ton. y Tac., No. 5, 1 - 7.
No. 2... Gonzalez, G. and Gonzalez, G. 1953, Bol. Obs. Ton. y Tac., No. 7, 3 - 10.
No. 3... Nassau, J. J., and Morgan, W. W. 1951, Ap. J. 113, 149.
No. 4... Munch, Luis 1954, Bol. Obs. Ton. y Tac., No. 10, 28 - 40.
No. 5... Munch, Luis and Morgan, W. W. 1953, Ap. J., 118, 161.
No. 6... Morgan, W. W., Johnson, H. L. and Roman, Nancy G. 1954, P. A. S. P., 66, 85.
No. 7... Nassau, J. J. and Harris, Daniel III, 1952, Ap. J., 115, 459 - 474, table 1.

NOTES

No. 3 AO Cas
No. 19 Fainter than 10 Lac
No. 49 CC Cas
No. 56 Ia from N III, C III weak.
No. 64 C III weak
No. 188 Spectroscopic binary
No. 217 Variable
No. 218 Photometric measurements include a fainter and probably bluer companion.
No. 246 CQ Cep. Variable in Magnitude and Spectrum.

The following stars have only one photometric observation: Nos. 3, 69, 147, 148, 149, 151, 153, 156, 159, 164, 165, 175, 183.

the stars consecutively. The second column gives the *Henry Draper Catalogue* number, the *Bonner Durchmusterung* number when not in the *HD*, or, if the star is in neither catalogue, a number is given followed by a reference. References in this column are listed at the end of the table, and the number of the star in this column is that used in the original publication. The next four columns give the positions in equatorial and galactic co-ordinates. The Lund pole was adopted for computing the galactic co-ordinates. Without exception, slit spectrograms were available for spectral classifications. Most of the spectral types were determined by Morgan (see Morgan, Code, and Whitford 1955) from McDonald, as well as Yerkes, slit spectrograms, and the remaining ones were classified by one of us (Hiltner) on McDonald spectrograms. The photometric observations were obtained either at McDonald or at Lowell Observatory, or both. The same filter and cell

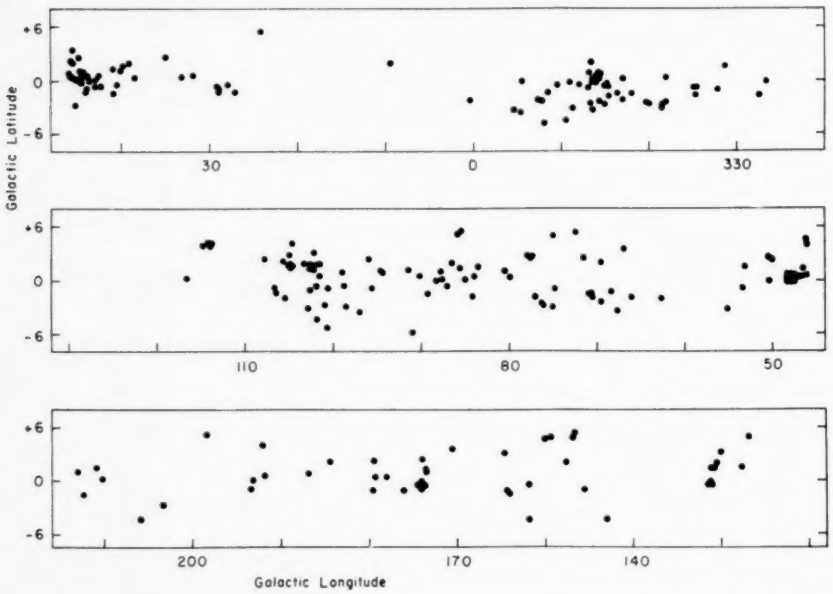

FIG. 1.—Distribution of O-type stars recorded in the catalogue

combinations were used by the two observers. No systematic differences in the two sources of data were detected.

Figure 1 shows the distribution of stars in galactic co-ordinates. Figure 2 gives the two-color plot for the stars in the catalogue except for BD+28°4211 and No. 12, reference 6. The open circles refer to the stars from galactic longitude 40.0 to 48.8 and galactic latitude $-3°$ to $+5°$. The filled circles refer to all other stars. It is apparent from the plot of the filled circles that the reddening line is not linear but curved, as suggested by Blanco (1955). The equation

$$\frac{E_{(U-B)}}{E_{(B-V)}} = 0.72 + 0.05E_{(B-V)}$$

represents the data satisfactorily.

It is also apparent from Figure 1 and from Figure 3, where only the Rift stars are plotted, that the stars in the Great Rift are anomalous. The stars in this region clearly give a straight line for the reddening law in contrast to that of those outside this region. In any case, the introduction of a curvature for the Rift stars would not be compatible with the observations. The cause of this discrepancy is obscure but most probably will be found in variations in interstellar absorption. However, intrinsic peculiarities of the Rift stars relative to others cannot be eliminated with the data at hand. For example, the intersection of the most probable line for the Rift stars and those outside intersect at $B - V = -0.1$, not at that color where the color excess is zero. But in our discussion we shall assume that the effect is caused by a variation in the reddening law.

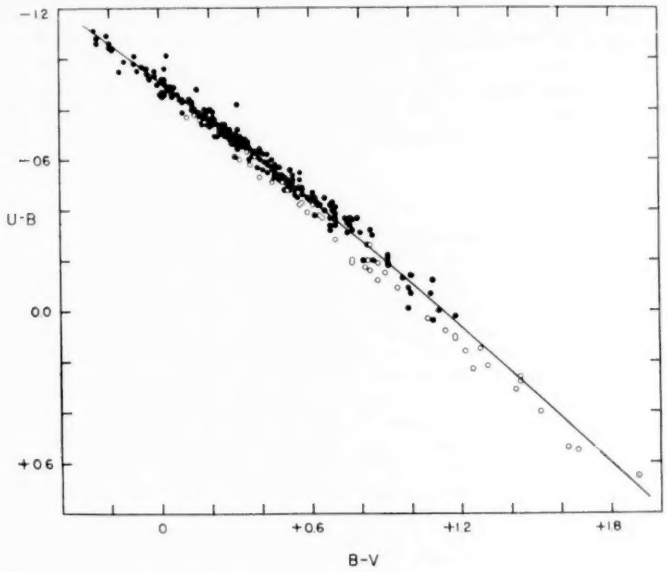

FIG. 2.—$U - B$ versus $B - V$ for the stars of Table 1. The open circles designate stars behind the Great Rift in Cygnus; the filled circles, stars elsewhere in the Milky Way. The line represents the reddening line:

$$\frac{E_{(U-B)}}{E_{(B-V)}} = 0.72 - 0.05\,E_{(B-V)}\,.$$

It is also apparent from the plot of $B - V$ versus $U - B$, for the stars outside the Great Rift in Cygnus, that the scatter in the diagram increases with reddening. This can be interpreted as evidence for a small general variability in the reddening law.

III. THE RATIO OF TOTAL TO SELECTIVE ABSORPTION

Aside from the determinations of

$$R = \frac{A_V}{E_{(B-V)}} = 3.0$$

from Whitford's (1948) interstellar absorption-curve by Blanco (1955), there have been several determinations of this ratio. Oort (1938) discusses several, leading to a value of

$A_{pg}/E_1 = 9$, where A_{pg} is the total photographic absorption and E_1 is the color excess on the C_1 system of Stebbins, Huffer, and Whitford (1940). Since the scale of C_1 is 0.483 that of $B - V$ (Morgan, Harris, and Johnson 1953, eq. [2]), this value gives $R = 3.3$. Stebbins (1950) mentions a value of

$$\frac{A_{pg}}{C_{int}} = 4.0 \pm 0.2$$

obtained from observations of the colors and brightness of the near and far sides of the Andromeda Nebula, from which we get $R = 3.0$. Sharpless has found $R = 6$ from unreddened and moderately reddened stars in the region of the Orion Nebula.

We can add another direct determination to this list by taking advantage of the fact that the region of the double cluster in Perseus is more heavily reddened on one side of

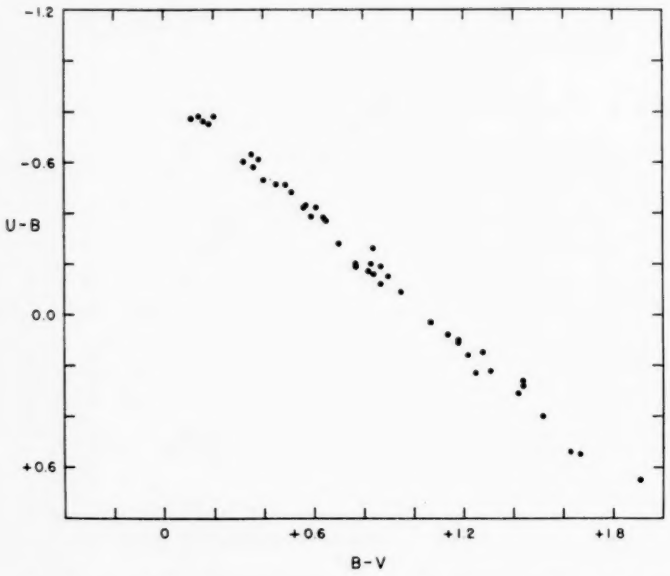

FIG. 3.—$U - B$ versus $B - V$ for stars from galactic longitude 40°.0 to 48°.8 and galactic latitude $-3°$ to $+5°$.

the clusters than on the other. There are a large number of stars (cluster members) of the same spectral types and luminosity classes situated in both regions. For example, there are 12 B1 V stars (Johnson and Morgan 1955*b*; Johnson and Hiltner 1956) whose observed colors range from $B - V \sim +0.2$ to $B - V \sim +0.7$. From all the available stars we find

$$R = 3.0 \pm 0.3 \text{ (p.e.)} .$$

The foregoing evaluations of R suggest the value

$$R = \frac{A_V}{E_{(B-V)}} = 3.0 \pm 0.2 \text{ (p.e.)} ,$$

if we omit Sharpless' determination of $R = 6$ for the Orion Nebula. The existence, however, of Sharpless' determination raises the question of the value of R that applies to other possibly peculiar regions. We are especially concerned with the region of the Great Rift in Cygnus, where a variation in the law of interstellar reddening (see Sec. II) may be in evidence. If we assume that the Rift stars of Table 1 are all of the same absolute luminosity and at the same distance, we obtain $R = 2.1$. The assumption of equal distance for the stars is certainly not correct, since these stars are distributed along the spiral arm behind the Great Rift.

If we correct the distances of these stars by arbitrarily placing the Rift stars on the spiral arm, according to the model of the Galaxy of Morgan, Sharpless, and Osterbrock (1952) (a correction of about 0.2 mag. per degree of galactic longitude), we obtain $R \simeq 3.0$. While this determination from the Great Rift in Cygnus has low weight because of the uncertainties in the distance corrections, it does argue against an abnormally high value for R in this region. A departure from the normal reddening line does not necessarily reflect a departure from the normal total to selective ratio that we have determined here. This follows, of course, since a third spectral region (ultraviolet) is employed in establishing the reddening line, and peculiarities in the absorption at this region alone may affect the reddening line.

IV. CONCLUSIONS

Additional evidence has been given for the divergence of the reddening in the region of the Great Rift in Cygnus from that generally elsewhere in the Milky Way, in the sense that the Great Rift absorbs more ultraviolet light compared to blue and yellow light than other interstellar clouds do. The curvature of the reddening line suggested by Blanco is also confirmed by our observations, except for the Cygnus stars that give a linear relationship. In this connection we should point out that our new reddening line (eq. [1]) is identical, for small reddening, with that of Johnson and Morgan (1953) and that their derived relationships for spectral type, reddening, etc., apply directly. The only change required at the present time is the making of a second approximation to include the effect of the second term on the right of equation (1).

The effect of the divergence of the reddening line in Cygnus from equation (1) will be small for reddening ranging from zero to moderate, since in the equation

$$Q = (U-B) - \frac{E_{(U-B)}}{E_{(B-V)}}(B-V)$$

the coefficient of

$$\frac{E_{(U-B)}}{E_{(B-V)}},$$

$B - V$, is small. Furthermore, in the Q method of determining color excess, we use the equation $E_{(B-V)} = (B - V) - 0.337Q + 0.009$, and errors in Q appear in $E_{(B-V)}$ reduced by a factor of 3. Tests show that divergences of the reddening lines from equation (1), by the amount found in Cygnus, will not introduce errors in $E_{(B-V)}$ greater than 0.02 or 0.03 mag., for $E_{(B-V)} < -0.7$ or $A_V < 2.1$ mag. These remarks apply only to O and B stars, of course.

The ratio of total to selective absorption has been found to be $R = 3.0$, with the only discordant determination that of Sharpless. More recent and unpublished data analyzed with that published by Sharpless (1952) show that a value near 3 is not necessarily discordant in this region. Blaauw (1956) has also shown that evolutionary effects within the association may vitiate the earlier results. However, the probable error, ± 0.2, should be regarded as a minimum value.

One of us (Hiltner) expresses his thanks to the National Science Foundation for financial support.

REFERENCES

Baade, W., and Minkowski, R. 1937. *Ap. J.*, **86**, 123.
Blaauw, A. 1956, private communication.
Blanco, V. M. 1955, *Ap. J.*, **123**, 64.
Johnson, H. L., and Hiltner, W. A. 1956, *Ap. J.*, **123**, 267.
Johnson, H. L., and Morgan, W. W. 1953, *Ap. J.*, **117**, 313.
———. 1955*a*, *ibid.*, **122**, 142.
———. 1955*b*, *ibid.*, p. 429.
Morgan, W. W., Code, A. D., and Whitford, A. E. 1955, *Ap. J. Suppl.*, **2**, 41 (No. 14).
Morgan, W. W., Harris, D. L., and Johnson, H. L. 1953, *Ap. J.*, **118**, 92.
Morgan, W. W., Sharpless, S. L., and Osterbrock, D. E. 1952, *Sky and Telescope*, **11**, 138.
Oort, J. H. 1938, *B.A.N.*, **8**, 233.
Sharpless, S. L. 1952, *Ap. J.*, **116**, 251.
Stebbins, J. 1950, *Observatory*, **70**, 206.
Stebbins, J., Huffer, C. M., and Whitford, A. E. 1940, *Ap. J.*, **91**, 20.
Stebbins, J., and Whitford, A. E. 1945, *Ap. J.*, **102**, 318.
Whitford, A. E. 1948, *Ap. J.*, **107**, 102.

THREE-COLOR PHOTOMETRY IN THE GLOBULAR CLUSTER M3*

H. L. JOHNSON
Lowell Observatory
AND
A. R. SANDAGE
Mount Wilson and Palomar Observatories
Carnegie Institution of Washington, California Institute of Technology
Received May 21, 1956

ABSTRACT

New three-color photometric data are presented for about 225 stars in the globular cluster M3. These stars permit conversion of the older m_{pg}, m_{pv} magnitude in M3 to the well-defined B, V system. A new color-magnitude diagram in V and $B - V$ is given. An ultraviolet excess exists for the giant, subgiant, and main-sequence stars. This excess ranges from about $\Delta(U - B) = 0.20$ mag. for the giants at $B - V = 1.0$ to $\Delta(U - B) = 0.55$ mag. for main-sequence stars at $B - V = 0.6$. As in M13, the M3 stars along the blue-end horizontal branch appear to have an ultraviolet deficiency which may be due to the effect of low surface gravity on the Balmer jump. The difference in the energy distributions for the M3 stars compared with the nearby stars makes any identification of sequences dubious at this time.

I. INTRODUCTION

A photometric study in three colors of about 225 stars in M3 is reported. The present work is an extension and revision of the earlier two-color study of this cluster (Sandage 1953), hereafter referred to as "Paper I." A combination of photoelectric and photographic techniques was used. Photoelectric observations in U, B, and V of 35 standard stars were made with the 82-inch telescope at the McDonald Observatory. These standards range from $V = 9.9$ to $V = 21.9$ and embrace the entire magnitude interval covered by the older photographic material. New photographic plates were obtained in three colors with the 100-inch Hooker telescope and the 200-inch Hale telescope at the Mount Wilson and Palomar Observatories. These new data are used to convert the m_{pg} and m_{pv} values of Paper I to the B, V system. Furthermore, the new observations give the $U - B$ versus $B - V$ relation for the cluster stars from $M_v = -3$ to $M_v = +5$.

II. THE PHOTOELECTRIC OBSERVATIONS

The three-color photoelectric observations were all made with the 82-inch telescope of the McDonald Observatory during March and April, 1954, and February, 1956. The 1954 observations were made with the same filters and 1P21 that were used to establish the U, B, V system (Johnson and Morgan 1953; Johnson 1955). The 1956 observations were made with the same filters, but the photomultiplier was an extremely sensitive, nineteen-stage tube made for the Lowell Observatory by Dr. A. Lallemand, of the Paris Observatory. In both seasons an integrator-type D.C. amplifier (Gardiner and Johnson 1955) was used; however, this amplifier was torn down, rebuilt, and recalibrated between the two observing seasons, and we may consider that two distinct amplifiers (of the same type) were used.

The photoelectric observations are listed in Table 1. The designation system is that of Paper I, with the exception of the faintest stars, F-1 to F-12. These additional stars are identified in Figure 1. The estimated probable errors in magnitude range from $\pm 0.010(V)$, $\pm 0.010(B - V)$, and $\pm 0.020(U - B)$ for the brightest stars, to $\pm 0.08(V)$, $\pm 0.11(B - V)$, and $\pm 0.14(U - B)$ for the stars between $V = 20$ and $V = 21.5$.

* Contributions from the McDonald Observatory, No. 267.

Because of the relatively short time of exposure (1½ hours) on the faintest star, its probable errors are $\pm 0.2(V)$ and $\pm 0.3(B-V)$. All the stars brighter than $V = 18$ and about half of those between $V = 18$ and $V = 20.5$ were observed in 1954 with the 1P21. The rest of the faint stars were observed in 1956 with the Lallemand tube. There is sufficient overlap between the two seasons, during which different photomultipliers and amplifiers were used, to establish the equality of the two scales. This may be regarded as confirmation of the linearity of both the amplifiers and the photomultipliers, since it does not seem likely that all would be in error by the same amount in the same direction. The 1P21 was used with a multiplication of about 1.4×10^6, while the Lallemand tube was used at a multiplication of about 1×10^7.

TABLE 1

PHOTOELECTRIC STANDARDS

Star	V	$B-V$	$U-B$	Star	V	$B-V$	$U-B$
206.....	9.86	+1.15	+1.04 Std.	I-II-4.....	15.86	+0.08	−0.03
1397.....	12.65	+1.56	+1.63	I-IV-18....	15.95	− .01	− .02
1402.....	12.66	+0.63	+0.08 Std.				
I-III-28....	12.81	+1.37	+1.26	I-II-9.....	16.74	+ .71	+ .05
297.....	12.87	+1.44	+1.42	a.....	16.86	+ .75	− .01
				I-VI-4.....	17.00	+ .71	+ .07
216.....	14.05	+1.00	+0.68	F-1.....	17.75	+ .70	− .04
I-II-18.....	14.09	+0.94	+0.49	F-2.....	18.38	+ .60	− .12
237.....	14.09	+0.65	+0.10				
193.....	14.76	+0.90	+0.35	F-3.....	18.39	+ .71	+ .20
I-II-57.....	14.93	−0.27	−1.11	F-4*.....	18.46	+ .48	− .22
				F-5.....	18.99	+ .41	− .27
180.....	15.23	+1.11	+1.03	F-6.....	19.18	+ .44	− .35
I-III-9.....	15.58	+0.51	−0.03	F-7.....	19.76	+ .56	− .31
I-II-6.....	15.61	+0.08	+0.14				
I-II-11.....	15.68	+0.42	−0.03	F-8.....	20.09	+ .36	− .44
I-VI-14....	15.68	+0.72	+0.20	F-9.....	20.11	+ .58	− .16
				F-10.....	20.44	+ .63	−0.34
182.....	15.69	+0.09	+0.10	F-11.....	21.32	+ .74	.....
I-VI-18....	15.70	+0.16	+0.05	F-12.....	21.9	+0.5	.....
235.....	15.76	+0.08	+0.13				

* Star F-4 is double. Measures refer to combined light.

Laboratory checks on the linearity have also been made, and no significant deviations from linearity have been found. These tests were made with light-intensities covering the range corresponding to $V = 10$ to $V = 22$ with the 82-inch telescope.

The sensitivity of the 1P21 that was used in 1954 is such that, with the yellow filter on a star of visual magnitude $V = 21.40$ in the 82-inch, the photoemission from the cathode is about 3×10^{-19} amp. Under the same conditions the photoemission from the Lallemand tube is about 7×10^{-19} amp. Since a current of 1 electron/sec corresponds to 1.60×10^{-19} amp, the first two rows in Table 2 follow immediately. The third row contains data computed from Table II of Baum's (1954) study of M13. In his table Baum gives the average number of counts at $V = 21.40$ as 390/100 sec. The data in Table 2 are only approximate, but they show clearly that the photometer used at the 82-inch in 1956 is sufficiently more sensitive than Baum's photometer to make up the difference in the light-gathering powers of the two telescopes.

All observations on all stars, including the standard stars, were made with a focal-plane diaphragm 7″ in diameter. This size diaphragm is large enough to minimize the systematic corrections for seeing that Baum (1954) found to be necessary; furthermore

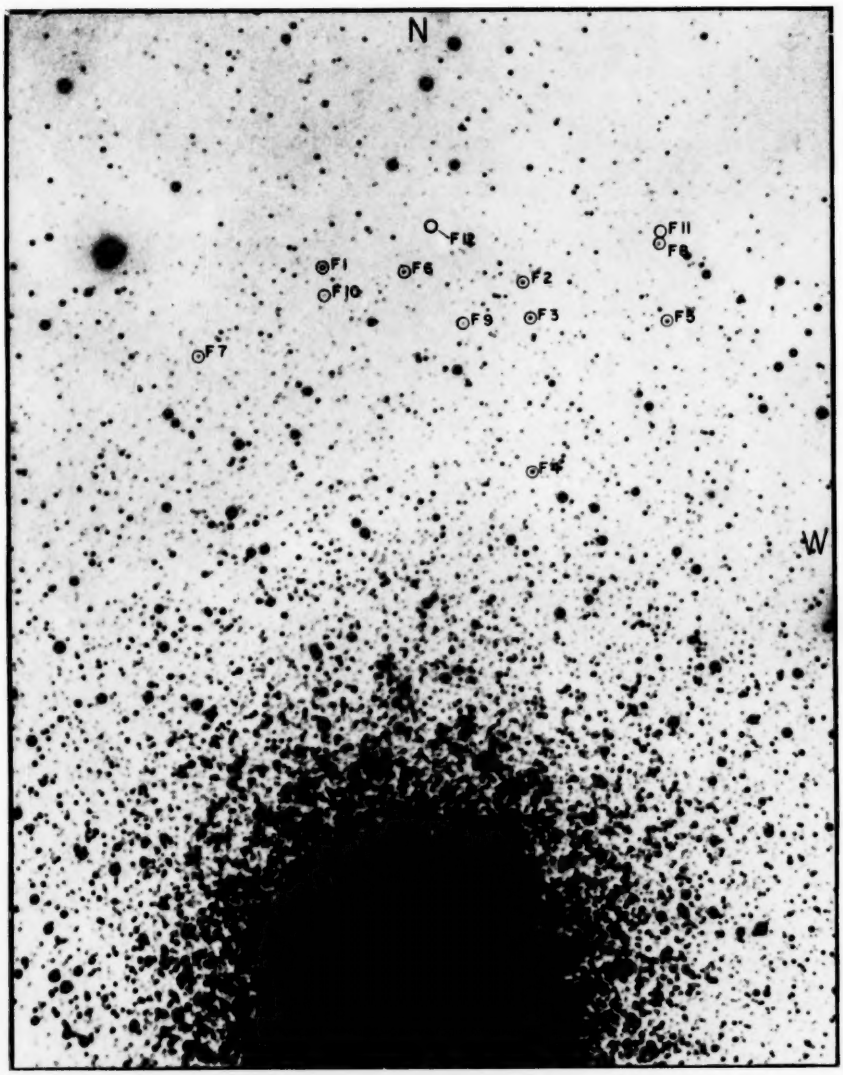

FIG. 1.—Identification chart for the 12 faint standard stars of Table 1. The remaining photoelectric standards were identified on charts in Paper I.

since the standard stars were observed with the *same diaphragm* at intervals of 1–1½ hours, all remaining systematic errors should cancel out.

A rough measurement of the scattered light at various distances from a bright star indicates that, at a distance of 6′ from the center of the cluster (nearly the outer limit of the photographic photometry for the color-magnitude diagram), systematic errors at $V = 21.4$ of as much as 0.3 mag. in V and 0.1–0.3 mag. in $B - V$ and $U - B$ may be made. This error would be made if, because of crowding by other stars, the comparison-sky position would have to be taken along the radius vector from the cluster center. This scattered-light problem can be avoided by taking the sky measurement on a line perpendicular to the radius vector from the cluster center, but this restriction so severely limited our choice of faint stars for photoelectric standards that all the faint stars were located about 12′ north of the cluster and the magnitude scale was transferred inward by special photographic plates. All sky measures were taken at right angles to the direction of the cluster center, and sometimes two sky measures, one on each side of the star, were taken.

Stars fainter than $V = 16.5$ were found by means of offsets measured from 100- and 200-inch plates. The 100-inch plates, taken at the Newtonian focus, were used directly

TABLE 2

ELECTRON COUNTS AT $V = 21.40$ (YELLOW FILTER)

Tube	Telescope	Electrons per Second
1P21-Y	82-inch	1.9
Pierette V (Lallemand)	82-inch	4.4
EMI (Baum)	200-inch	3.9

(except for a scale change) for the 82-inch Cassegrain offsets. The 200-inch plate was taken with the Ross corrector, and a correction for the field distortion produced by this lens has been applied. After this correction has been made, the computed offsets for the stars present on plates taken with both telescopes are in very satisfactory agreement. The two faintest stars that were measured with the 82-inch telescope are too faint to be photographed with the 100-inch, and they could not have been measured if the 200-inch plate had not been available.

III. THE PHOTOGRAPHIC OBSERVATIONS

Plates in three colors were taken with the 100-inch telescope diaphragmed to 58 inches. These plates were centered on the cluster and were used for stars brighter than $V = 17.0$. The plate and filter combinations were: ultraviolet, Eastman 103*a*-O + 2-mm Schott UG2; blue, Eastman 103*a*-O + 2-mm Schott GG13; yellow, Eastman 103*a*-D + 2-mm Schott GG11. These combinations are known to give negligible color equations to the U, B, V system (Johnson and Sandage 1955; Johnson, Sandage, and Wahlquist 1956). For stars fainter than $V = 17.0$, plates were obtained with the 200-inch telescope. These were centered midway between the faint standards and the stars of series III, sector II, which are identified in Paper I. Negligible distance corrections were encountered for plates centered in this way. One ultraviolet plate was obtained with the 200-inch with the Ross corrector lens removed (since the ultraviolet transmission of the $f/3.67$ lens is very small) and with the mirror diaphragmed to 120 inches. A second faint ultraviolet plate, exposed for 90 minutes in good seeing, was obtained with the 100-inch diaphragmed to 58 inches.

About 200 stars were chosen for measurement from the photometric catalogue of Paper I. They were picked to cover adequately the interval from $V = 12.7$ to $V = 20.8$,

so that conversion curves from the m_{pg}, m_{pv} system to the B, V system would be well determined.

Six plates in each of the three colors were measured for stars brighter than $V = 17.0$. Two plates in each of the three colors were used for stars fainter than this limit. The resulting colors and magnitudes are given in Table 3, where the identifying notation is that of Paper I. The internal probable errors are of the order of ± 0.02 for the final magnitudes and ± 0.03 for the colors for stars brighter than $V = 17$, and about twice these values for stars fainter than this limit.

Data for the photoelectric standards, read back through the calibration-curves, are also given in Table 3. Comparison of these data with those of Table 1 gives the color and magnitude equations for the remaining data. Figures 2 and 3 show these comparisons. The sense of the plotted differences is photoelectric *minus* photographic. The residuals are all satisfactorily small and show no systematic trend with either V or $B - V$. We conclude that all data of Table 3 are on the U, B, V system to within the errors of the determination.

Table 3 compared with Tables II and VI of Paper I gives the conversion functions relating m_{pg} and m_{pv} to B and V. These are shown in Figure 4. The visual magnitudes of Paper I are nearly on the V system for stars brighter than $V = 17.0$. For stars fainter than this, a systematic error exists in m_{pv} which reaches 0.40 mag. at $m_{pv} = 21.2$. The fact that the divergence begins with stars as bright as $V = 17.0$ and continues to faint magnitudes probably means that the two faintest photoelectric standards of Paper I, which are stars c and d (Baum 1952; Sandage 1953) are too faint compared with the present system and that the extrapolation of the scale used in Paper I beyond $m_{pv} = 19.0$ continued the error to the photographic limit. The same systematic difference exists in $B - m_{pg}$, and this circumstance leaves the color difference between CI and $B - V$ nearly constant over the entire range. The mean difference in the color systems of about 0.12 mag. is primarily a result of the change in zero point of $B - V$ compared with the International system (Johnson and Morgan 1953; Johnson 1955). The effect of these magnitude corrections on the luminosity function (Sandage 1954) will be discussed in a separate paper.

IV. THE COLOR-MAGNITUDE DIAGRAM

All magnitudes in Paper I have been converted to B and V by the relations of Figure 4, and the resulting color-magnitude diagram is shown in Figure 5. The diagram is very similar to that previously given, but several changes in detail should be noted. (1) The bluest stars on the extension of the horizontal branch now reach only to $B - V = -0.40$ instead of to $CI = -0.80$. This large change is, of course, a result of the cutoff of the blue filter at 3800 A, which is characteristic of the U, B, V system. (2) The color boundaries of the variable-star domain are well defined at $B - V = +0.17$ and $B - V = +0.39$. (3) The change in the slope of the subgiant branch from $V = 16$ to $V = 18$ is evident. In the diagram of Paper I, this sequence was nearly vertical, whereas Figure 5 shows a slight blueward slope for faint magnitudes.

The apparent visual magnitude of the RR Lyrae domain is $V = 15.67$. This is the apparent modulus of M3 on the assumption that $\bar{M}_v = 0.00$ for the RR Lyrae stars. The break point from the main sequence occurs at about $V = 19.0$, which corresponds to $M_v = +3.3$. This is about 0.2 mag. brighter than was given by the old diagram. The difference is a result of the corrections to the magnitudes shown in Figure 4. The age of the stars in M3, computed in the manner of Paper I, becomes about 20 per cent smaller. However, it has become increasingly clear that stellar models of a more detailed nature than those of Schönberg and Chandrasekhar (1942) are needed before a precise age can be obtained for the globular-cluster stars. Recent models by Hoyle and Schwarzschild (1955) and by Hoyle and Hazelgrove (1956) are a step in this direction. The new data of Figure 5, together with Hoyle and Hazelgrove's models, give an age of about 6×10^9

TABLE 3

MAGNITUDES OF SELECTED STARS IN M3 DETERMINED PHOTOGRAPHICALLY

Star	V	B-V	U-B
STANDARDS OF TABLE I			
1397	12.70	+1.69	+1.57
I-III-28	12.79	+1.37	+1.28
297	12.87	+1.46	+1.37
216	14.04	+1.00	+0.58
I-II-16	14.15	+0.89	+0.45
237	14.13	+0.59	+0.14
193	14.76	+0.88	+0.28
I-II-57	15.06	-0.40	-1.10
180	15.10	+1.22	+1.04
I-III-9	15.62	+0.47	-0.06
I-II-6	15.59	+0.08	+0.11
I-II-11	15.69	+0.42	-0.05
I-VI-14	15.57	+0.82	+0.21
182	15.71	+0.11	+0.08
I-VI-18	15.70	+0.16	+0.11
235	15.67	+0.17	+0.12
I-II-4	15.95	+0.01	0.00
I-IV-18	15.92	+0.05	+0.01
I-II-9	16.80	+0.72	+0.02
a	16.79	+0.82	+0.05
I-VI-4	16.90	+0.82	-0.01
F 1	17.74	+0.69	+0.02
F 2	18.43	+0.60	-0.16
F 3	18.37	+0.81	0.00
F 4	18.47	+0.43	-0.20
F 5	18.93	+0.44	-0.24
F 6	19.07	+0.44	-0.19
F 7	19.60	+0.57	-0.36
F 8	19.92	0.52	-0.35
F 9	20.30	+0.69	-0.41
F 10	20.56	+0.59	-0.47
F 11	21.27	+0.74	-
A. J., 58, 61, 1953. Table II			
B	13.56	+0.67	+0.25
D	15.08	+0.86	+0.25
E	16.37	+0.83	+0.13
G	16.12	+0.85	+0.14
H	14.91	+0.90	+0.29
L	15.15	0.83	+0.22
M	16.00	+0.81	+0.23
N	16.87	+0.70	-0.09
O	16.75	+0.71	-0.09
P	16.29	+0.87	+0.08
R	16.70	+0.64	-0.12
S	14.11	+0.95	+0.69
T	14.62	+0.77	+0.29
U	13.53	+1.11	+0.90
V	14.87	+0.70	+0.19
W	15.62	+0.88	+0.63
X	16.81	+0.80	+0.02
Y	16.34	+0.88	+0.01
Z	15.77	+0.02	+0.14
AA	12.69	1.57	1.56
AB	16.40	+0.80	+0.11
AC	14.62	+0.87	+0.36
AE	13.85	+0.98	+0.61
AF	15.66	+0.12	+0.13
AG	15.78	+0.91	+0.04
AH	13.74	+1.08	+0.90
AI	16.06	+0.80	+0.16
AJ	16.26	+0.77	+0.14
AM	15.02	+0.51	-0.03
AN	15.97	-0.05	+0.06
AO	14.70	+0.72	+0.30
AQ	15.68	+0.48	-0.06
AR	15.63	+0.37	+0.01
AT	15.60	+0.75	+0.15
AU	15.79	+0.76	+0.10
AV	14.01	+1.04	+0.63
AW	14.80	+0.76	+0.16
AX	15.57	+0.13	+0.11
AZ	15.92	+0.77	+0.21
BB	14.73	+0.82	+0.34
BC	13.84	+1.05	+0.79
BF	13.62	+1.16	+0.75
BG	14.24	+0.92	+0.47
BH	14.63	+0.78	+0.23
BI	14.11	+1.03	+0.58

Star	V	B-V	U-B
A. J., 58, 61, 1953. Tab. II (Cont'd)			
BJ	15.47	+0.83	+0.17
BK	16.85	+0.78	+0.15
BL	15.42	+0.88	+0.20
155	14.51	+0.98	+0.48
167	15.12	+0.84	+0.17
179	14.76	+0.62	+0.06
1331	15.23	+0.87	+0.16
SERIES I			
I, 2	15.47	+0.89	+0.17
21	13.05	+1.37	+1.10
30	15.79	0.00	+0.04
34	14.65	+0.91	+0.36
36	16.03	+0.80	+0.16
39	14.44	+0.91	+0.37
46	13.82	+1.06	+0.74
55	15.54	+0.54	-0.07
58	17.08	-0.23	-0.59
65	15.50	+0.54	-0.05
71	15.42	+0.54	0.00
72	14.59	+0.87	+0.48
77	15.56	+0.43	-0.01
78	15.23	+0.53	+0.10
80	15.35	+0.48	+0.08
91	15.60	+0.18	+0.11
97	15.77	+0.05	+0.06
103	15.53	+0.14	+0.11
II, 1	15.98	+0.57	-0.14
2	16.64	+0.75	+0.09
3	15.23	+0.89	+0.10
5	16.01	+0.77	+0.09
7	15.48	+0.84	+0.16
8	15.73	+0.14	+0.07
12	15.57	+0.71	+0.19
13	15.72	+0.08	+0.13
15	15.62	+0.45	-0.05
22	16.48	+0.82	+0.12
24	17.04	+0.72	-0.06
26	16.84	+0.75	-0.03
28	16.54	+0.74	+0.09
32	15.86	+0.81	+0.22
34	17.00	+0.67	+0.06
35	16.31	+0.72	+0.12
39	16.66	+0.80	+0.02
40	16.98	+0.62	+0.06
42	14.78	+0.63	+0.31
43	15.76	+0.66	+0.20
45	15.61	+0.15	+0.10
47	15.59	+0.47	+0.04
48	16.87	+0.71	+0.05
50	16.88	+0.70	+0.01
52	16.77	+0.65	-0.01
53	15.68	+0.40	+0.03
54	15.13	+0.75	+0.23
56	17.00	+0.76	+0.04
58	16.66	+0.69	+0.04
63	15.72	+0.08	+0.12
III, 6	15.69	+0.12	+0.13
8	15.40	+0.84	+0.19
10	15.93	+0.79	+0.09
12	15.73	+0.08	+0.15
15	15.18	+0.80	+0.21
19	15.46	+0.46	-0.04
32	15.40	+0.59	+0.01
33	14.40	+0.90	+0.56
43	15.48	+0.55	+0.03
51	15.56	+0.43	-0.01
56	14.68	+0.67	+0.27
57	16.65	-0.15	-0.37
71	14.93	+0.77	+0.36
72	15.47	+0.18	+0.10
74	14.94	+0.57	+0.13
77	13.30	+1.15	+1.16
87	17.60	-0.38	-1.04
IV, 7	15.51	+0.62	0.00
25	13.60	+1.13	+0.87

Star	V	B-V	U-B
IV, 27	13.99	+1.00	+0.75
29	15.54	+0.56	0.00
33	15.67	+0.44	-0.02
50	15.58	+0.45	-0.01
56	15.65	+0.15	+0.12
82	13.46	+1.23	+1.26
86	15.62	+0.18	+0.12
92	15.62	+0.18	+0.10
98	15.61	+0.43	+0.01
101	13.26	+1.30	+1.19
V, 41	13.79	+0.88	+0.55
75	15.66	+0.12	+0.12
VI,54	17.39	-0.21	-0.68
74	15.40	+0.16	+0.11
85	15.43	+0.12	+0.14
SERIES II			
II, 10	17.88	+0.72	-0.10
12	18.56	+0.46	-0.20
58	17.90	+0.20	+0.05
III, 23	17.73	+0.49	-0.14
25	16.97	+0.70	+0.07
26	17.45	+0.71	-0.07
27	18.40	+0.60	-0.11
33	17.78	+0.61	-0.11
SERIES III			
II, 4	20.30	+0.62	-
5	19.51	+0.51	-0.42
8	20.30	+0.61	-0.28
10	20.09	+0.64	-0.75
11	19.63	+0.61	-0.40
15	20.13	+0.72	-
18	18.24	+0.20	-0.01
19	19.37	+0.56	-0.27
21	20.59	+0.81	-
22	20.53	+0.77	-
23	20.74	+0.73	-
24	20.58	+0.74	-
25	19.50	+0.56	-0.40
31	20.46	+0.62	-
32	19.54	+0.46	-
35	19.31	+0.51	-0.28
90	18.76	+0.43	-0.15
92	18.77	+0.41	-0.22
93	19.81	+0.62	-0.43
95	19.86	+0.57	-
100	18.77	+0.82	-0.14
108	17.28	+0.64	-0.04
113	19.50	+0.48	-0.31
122	20.47	+0.58	-
126	17.13	+0.72	-0.03
127	20.12	+0.85	-
141	20.00	+0.61	-0.40
143	20.68	+0.63	-
154	19.30	+0.44	-
155	18.92	+0.37	-0.16
164	18.97	+0.40	-0.21
167	18.49	+0.45	-0.18
181	17.95	+0.74	-0.12
195	18.82	+0.40	-0.26
199	18.90	+0.41	-0.23
217	18.22	+0.92	-
230	18.65	+0.43	-0.27
232	18.77	+0.43	-0.09
239	18.89	+0.43	-0.31
251	19.13	+0.39	-0.26
254	19.37	+0.39	-0.32
258	18.70	+0.40	-0.23
267	20.20	+0.65	-0.35
275	18.84	+0.42	-0.29
299	18.03	+0.62	-0.03
306	17.32	+0.69	-0.08
325	17.82	+0.69	-0.12
332	19.27	+0.38	-
344	18.82	+0.39	-0.36

years for the M3 stars (Hoyle 1956). This is probably the best available estimate at the present time.

Mean points obtained from the data of Figure 5 are given in Table 4. Here n is the number of stars used in forming the means. The mean points, together with the photoelectric data of Table 1, are plotted in Figure 6. Shown also is the relation of the M3 diagram to the main sequence of unevolved stars as defined by the faint members of the Hyades and Pleiades clusters. The geometrical modulus for the Hyades of 3.03 given by van Bueren (1952) is adopted, and the M3 modulus is assumed to be $m - M = 15.67$. The main sequence of M3 is very close to the initial sequence as defined by the Hyades

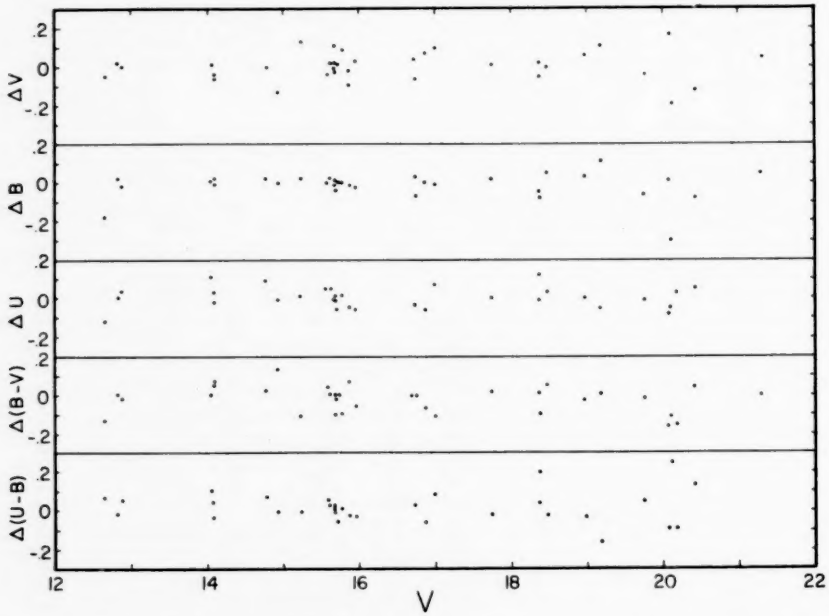

FIG. 2.—The residuals for the standard stars in the sense photoelectric *minus* photographic data. Data are from Tables 1 and 3. These relations define the magnitude equations.

and the Pleiades. However, the discussion of the two-color diagram in the next section shows that the stars in M3 are fundamentally different in their energy-distribution-curves from stars in the solar neighborhood; hence the comparison shown in Figure 6 may have only formal significance. At the present stage it seems highly dubious to fit globular-cluster main sequences to any known sequence of the nearby stars in order to determine an absolute magnitude for the RR Lyrae stars, as has been suggested (Baade 1948). It also seems premature to compare the present M3 diagram with those of other globular clusters until additional and independent photometry is completed on M13, M92, and other clusters.

V. THE TWO-COLOR DIAGRAM

The data of Tables 1 and 3 give the $U - B$ versus $B - V$ relation for the M3 stars. Mean points have been computed from the data of Table 3 for stars lying on the giant,

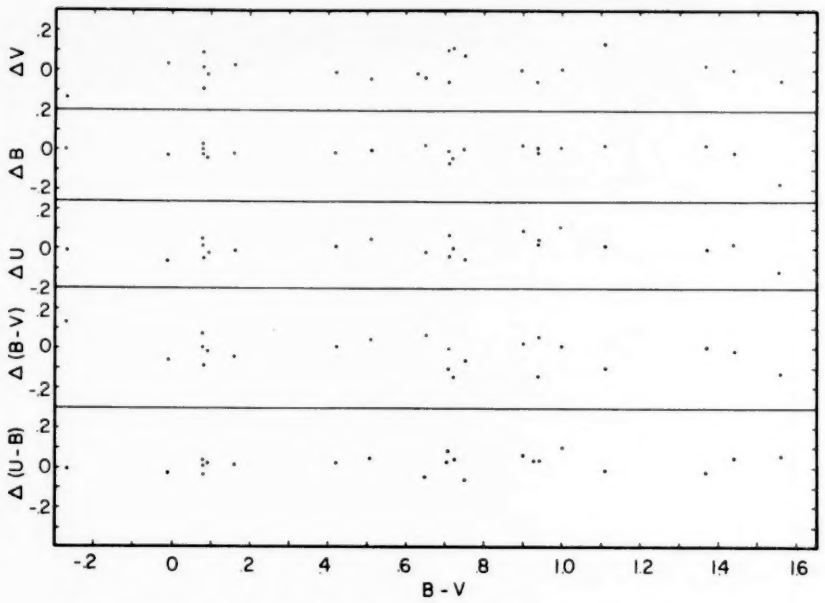

FIG. 3.—Same as Fig. 2 plotted against $B - V$. These relations define the color equations

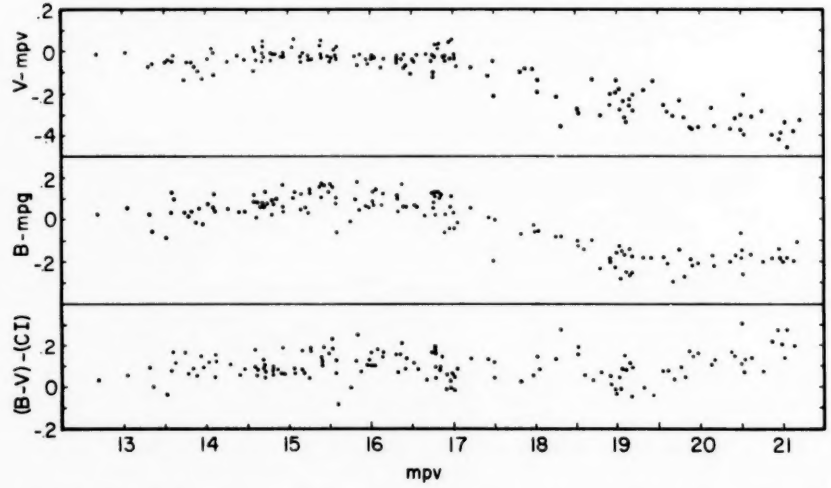

FIG. 4.—Magnitude and color correction-curves to convert m_{pg}, m_{pv}, and CI from Paper I to B, V, and $B - V$.

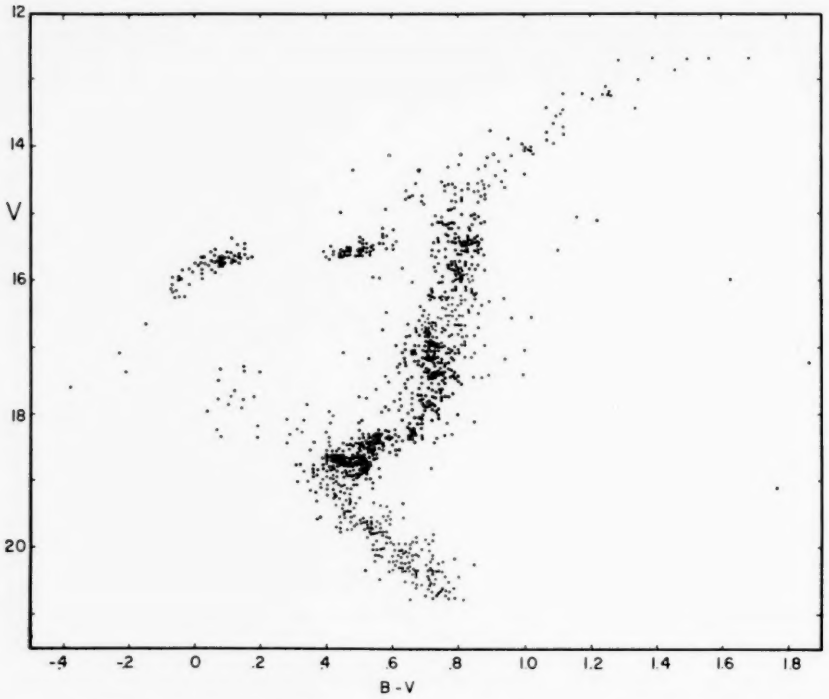

FIG. 5.—Color-magnitude diagram for M3 stars in the arguments V and $B - V$

TABLE 4

MEAN COLOR-MAGNITUDE DIAGRAM FOR M3

GIANTS AND HORIZONTAL-BRANCH STARS			SUBGIANTS AND MAIN SEQUENCE		
V	$B-V$	n	V	$B-V$	n
12.68.....	+1.70	1	15.29.....	0.80	54
12.70.....	+1.60	1	15.77.....	.80	58
12.75.....	+1.50	1	16.26.....	.77	51
12.90.....	+1.40	3	16.77.....	.74	86
13.10.....	+1.30	5	17.24.....	.72	91
13.32.....	+1.20	5	17.75.....	.70	59
13.75.....	+1.07	8	18.32.....	.60	84
14.25.....	+0.95	14	18.75.....	.47	142
14.75.....	+0.86	18	18.95.....	.42	.....
15.50.....	+0.55	27	19.24.....	.45	46
15.59.....	+0.45	24	19.73.....	.54	69
15.61.....	+0.15	18	20.25.....	.65	68
15.75.....	+0.05	26	20.64.....	0.73	26
16.09.....	−0.05	16			

transition, subgiant, and main sequences, and these are tabulated in Table 5. Again, n is the number of stars forming each mean. These data are plotted as triangles in Figure 7. The individual photoelectrically measured stars, with data taken from Table 3, are plotted as crosses. The curve through the points traces out the giant to main-sequence stars in order of decreasing luminosity as we go from the lower right to the upper left. The bend in the curve at $B - V = +0.4$ occurs at the junction of the subgiants with the main sequence at $V = 19.0$. Also plotted in this figure are the individual stars on the horizontal branch. The solid curve is the normal relation for the main sequence and the

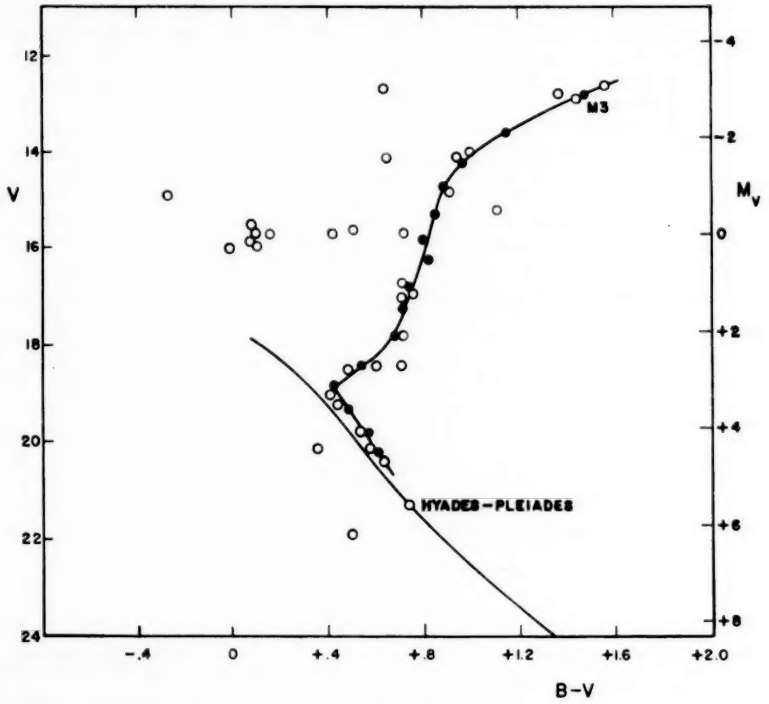

FIG. 6.—Color-magnitude diagram for M3 defined from the photoelectric standards of Table 1 (*open circles*) and from the mean points of Table 4 (*closed circles*). The main sequence from the Hyades and Pleiades stars is shown. See text.

yellow giants, defined by the nearby stars and by several of the brighter galactic clusters (Johnson and Morgan 1953). As in M13 (Arp and Johnson 1955), there appears to be an ultraviolet deficiency for these horizontal-branch stars. The explanation of this deficiency may lie in the effect of the low surface gravity on the Balmer discontinuity.

The M3 stars, ranging from the giant sequence to the main sequence, lie from 0.20 to 0.55 mag. above the normal relation. This anomaly, commonly described as an ultraviolet "excess," has also been found in the bright stars of two other globular clusters, NGC 4147 (Sandage and Walker 1955) and M92 (Sandage and Walker 1956), and for certain weak-line F-type stars in the general field (Roman 1954). The excess has been

TABLE 5

MEAN TWO-COLOR DATA FROM TABLE 3 FOR GIANT, SUBGIANT, AND MAIN SEQUENCES

V	$B-V$	$U-B$	$(U-B)_0$	$\Delta(U-B)$	n
12.78.....	1.47	+1.40	+1.73	0.33	3
13.56.....	1.15	+0.95	+1.16	.21	11
14.19.....	0.96	+0.55	+0.75	.20	7
14.70.....	0.88	+0.35	+0.60	.25	7
15.29.....	0.85	+0.18	+0.54	.36	11
15.76.....	0.80	+0.21	+0.44	.23	10
16.22.....	0.81	+0.11	+0.46	.35	10
16.79.....	0.74	+0.02	+0.33	.31	16
17.20.....	0.71	−0.04	+0.27	.31	6
17.83.....	0.69	−0.09	+0.24	.33	5
18.36.....	0.54	−0.14	+0.02	.16	5
18.81.....	0.42	−0.23	−0.01	.22	14
19.32.....	0.48	−0.29	−0.01	.28	7
19.78.....	0.57	−0.39	+0.05	.44	6
20.21.....	0.61	−0.44	+0.11	0.55	5

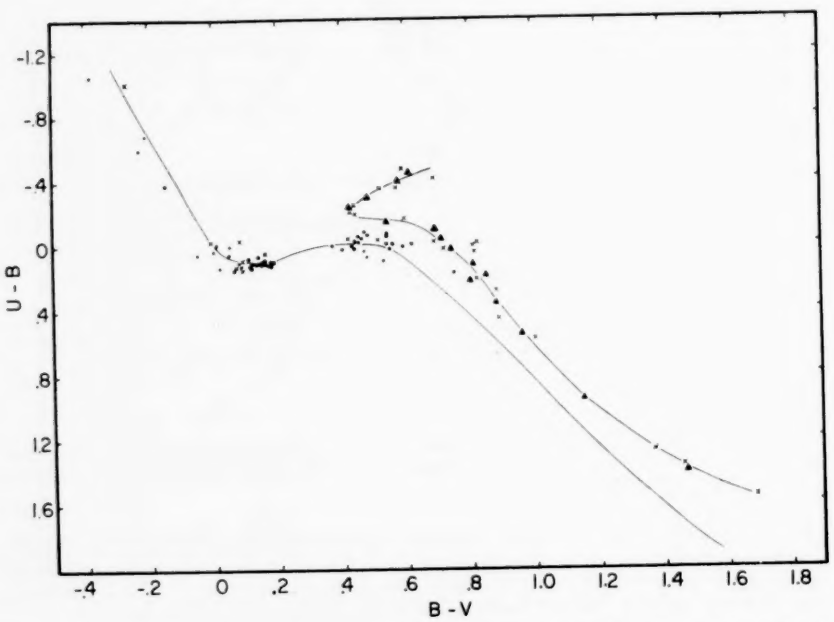

FIG. 7.—The two-color diagram. The triangles are mean points for the M3 giant, subgiant, and main sequences from Table 5. The crosses are the photoelectric standards. Individual stars on the horizontal branch are plotted. The normal relation between $U - B$ and $B - V$ is also shown.

shown to be small, however, in M13 (Arp and Johnson 1955). Our present data show that the anomaly persists for the fainter stars in M3 and may increase until an "excess" of 0.55 mag. is reached for the faintest observed main-sequence stars The last two columns of Table 5 give the normal $U - B$, designated by "$(U - B)_0$" (the "normal" curve of Fig. 7), and the "excess" defined by $\Delta(U - B) = (U - B)_0 - (U - B)_{\text{observed}}$. The dependence of $\Delta(U - B)$ on V is not large until the main sequence is reached, where $\Delta(U - B)$ appears to increase with fainter V. We must point out, however, that the large "excess" of 0.55 mag. for the M3 main-sequence stars may be due partly to observational errors. The mean $U - B$ for the M3 main sequence depends upon photoelectric observation of four stars, for each of which the probable error of $U - B$ is ± 0.14 mag. Furthermore, the scattered-light problem is worst in the ultraviolet. It seems likely, however, that the ultraviolet excess for the M3 main-sequence stars is at least 0.30 mag.

The most plausible explanation for the excess may be that a change in the blanketing of metal lines will cause a change in $U - B$ (a suggestion apparently first made by Strömgren). This suggestion is subject to observational check by a spectrophotometric method such as that used by Schwarzschild, Searle, and Howard (1955). Sufficient numbers of bright field stars with $\Delta(U - B) > 0.20$ mag. are now known (Roman 1954, 1956) to make the spectrophotometric check both feasible and highly desirable. A further check may be available from the stars in M92. If the blanketing suggestion is correct, there should be a difference in the $\Delta(U - B)$ between M3 and M92, since the M92 lines are about 60 per cent weaker than those in M3 (Greenstein 1956). Three-color photometry in M92 is nearly complete, and an answer to this question is forthcoming.

It is interesting to note that among the high-velocity stars observed by Miss Roman (1954, 1956) there are a number with $\Delta(U - B)$ in just the range covered by the M3 stars. Indeed, Miss Roman (1954) foreshadowed the results of Figure 7 by the final comments in her 1954 paper. With the exception of the RR Lyrae stars, these F-type field stars may be the only known cases of stars like those in the globular clusters which have been identified in the general field.

The construction of the photometer used at the 82-inch in 1956 was aided by funds granted by the Research Corporation.

REFERENCES

Arp, H. C., and Johnson, H. L. 1955, *Ap. J.*, **122**, 171.
Baade, W. 1948, *Pub. A.S.P.*, **60**, 230.
Baum, W. A. 1952, *A.J.*, **57**, 222.
———. 1954, *ibid.*, **59**, 422.
Bueren, H. G. van. 1952, *B.A.N.*, **11**, No. 432, 385.
Gardiner, A. J., and Johnson, H. L. 1955, *Rev. Scient. Instr.*, **26**, 1145.
Greenstein, J. L. 1956, unpublished discussion.
Hoyle, F. 1956, unpublished discussion.
Hoyle, F., and Hazelgrove, C. B. 1956, *M.N.*, in press.
Hoyle, F., and Schwarzschild, M. 1955, *Ap. J. Suppl.*, **2**, 1 (No. 13).
Johnson, H. L. 1955, *Ann. d'ap.*, **18**, 292.
Johnson, H. L., and Morgan, W. W. 1953, *Ap. J.*, **117**, 313.
Johnson, H. L., and Sandage, A. R. 1955, *Ap. J.*, **121**, 616.
Johnson, H. L., Sandage, A. R., and Wahlquist, H. D. 1956, *Ap. J.*, **124**, 81.
Roman, N. G. 1954, *A.J.*, **59**, 307.
———. 1956, *Ap. J. Suppl.*, **2**, 198 (No. 18).
Sandage, A. R. 1953, *A.J.*, **58**, 61.
———. 1954, *ibid.*, **59**, 162.
Sandage, A. R., and Walker, M. F. 1955, *A.J.*, **60**, 230.
———. 1956, unpublished observations.
Schönberg, M., and Chandrasekhar, S. 1942, *Ap. J.*, **96**, 161.
Schwarzschild, M., Searle, L., and Howard, R. 1955, *Ap. J.*, **122**, 353.

EXCITATION IN NEBULAE: CHARGE TRANSFER AND THE CASSIOPEIA RADIO SOURCE

JOSEPH W. CHAMBERLAIN
Yerkes Observatory
Received May 2, 1956

ABSTRACT

The recent analysis by Minkowski and Aller of the spectrum of this filamentary nebulosity is extended and modified. A consistent explanation of the large [O I]/Hα and [O I]/[O II] intensity ratios for filament 1 is obtained on the basis of collisional excitation with normal abundances and $T_e < 12000°$ K. The hydrogen is over 90 per cent neutral. It is shown that O^+ will be readily transformed to O through charge-transfer collisions with H; hence large electron densities need not be invoked to explain the weak [O II].

Attention is directed toward difficulties presented by the hypothesis that the observed O^{++} is left from an earlier state of the nebula. Alternatively, it is suggested that [O III] arises from the narrow high-temperature region immediately following a strong shock wave. A larger and cooler portion of the nebulosity, farther behind the shock wave, gives rise to [O I]. The excitation of filaments 2 and 3 is discussed briefly; without more data, their solution is not so clearly defined, but they probably are excited by weaker disturbances in the nebulosity. The question of the relationship between the optical and the radio emission is discussed briefly.

I. INTRODUCTION

Baade and Minkowski (1954) have recently published photographs and spectra of a new type of nebulosity identified with the intense radio source Cassiopeia A. The main features are a filamentary structure with large radial velocities and unusual emission-line spectra. The region designated as "filament 1" shows strong [O I] and [O III] lines of about equal intensity and at least five times stronger than the unobserved [O II] or Hα. Filaments 2 and 3, on the other hand, have much smaller radial velocities and show Hα and [N II] with much weaker [O I] lines and no detectable [O III].

Minkowski and Aller (1954) have discussed the excitation of filament 1, and their analysis may be briefly summarized: The approximate equal intensities of [O I] and [O III] imply roughly equal abundances of O and O^{++}. On the assumption of "normal" cosmic abundance ratios, the intensity of Hα relative to [O I] and [O III] can then be explained by collisional excitation at an electron temperature below 15000° K. Alternatively, radiative excitation would require a very high temperature, which seems excluded on the basis of the strong forbidden-line emissions.

This interpretation, however, still presented two difficulties. (1) The presence of O^{++} seems incompatible with a temperature as low as 15000° K; hence Minkowski and Aller attributed the high ionization to an earlier state of the nebulosity, which has since cooled but not had time to recombine completely. (2) The absence of [O II] lines seems peculiar, in view of the strong [O I] and [O III], and this item was explained in terms of an electron density sufficiently high[1] (10^4 cm^{-3}) to de-excite [O II] much more than [O I] or [O III]. They indicated, however, that, with such a high density, O^{++} would recombine in only a very few years!

[1] In view of Minkowski and Aller's Table 3, a density of 10^4 cm^{-3} would seem to be a minimum acceptable value on the basis of their interpretation. Some of the numerical values quoted by Minkowski and Aller are incorrect owing to errors in taking the excitation rate coefficient for 10000 °K from an earlier paper by Chamberlain (1953) and in computing the lifetimes for recombination versus electron density. Also in their Table 2 the columns for γ (O I) and γ (O III) are interchanged.

Thus consider the rate at which H^+ and O^{++} recombine with electrons. We have

$$\frac{dN(O^{++})}{dt} = -\alpha_{rec}(O^{++})\, N(O^{++})\, N_e \tag{1}$$

and

$$\frac{dN_e}{dt} = -\alpha_{rec}(H^+)\, N_e^2, \tag{2}$$

where we set the proton density $N(H^+)$ equal to the electron density N_e. The recombination coefficients, α_{rec}, in these equations can be estimated for any given temperature. For hydrogen the coefficient is readily evaluated on the basis of Menzel's (1937, eq. [25]) form for the recombination equation.[2] Although the coefficient for O^{++} is less accurately known, calculations by Aller[3] (1956) indicate $\alpha_{rec}(O^{++})$ is about six times the coefficient for H^+ at nebular temperatures. Thus we adopt $\alpha_{rec}(H^+) \sim 3 \times 10^{-13}$ cm^3/sec and $\alpha_{rec}(O^{++}) \sim 1.8 \times 10^{-12}$ cm^3/sec for $T_e = 15000°$ K.

Since the coefficient for O^{++} is much larger than that for H^+, we may take N_e as a constant in equation (1), so long as we are concerned only with the time for the density to drop to about half its initial value. Then integration shows that the lifetime for recombination is

$$\tau \sim \frac{1}{\alpha_{rec}\, N_e}. \tag{3}$$

Similarly, from equation (2), even though the rate of decay goes as N_e^2, integration shows that the lifetime is still of the same order as given by equation (3), except that α_{rec} is different. (Aller[3] [1956] has solved eqs. [1] and [2] simultaneously and presented the results graphically; but for short time intervals the exact solution reduces to that indicated here, and the "lifetime" is essentially unchanged.)

If $N_e = 10^4$ cm^{-3}, then $\tau(O^{++}) \sim 2$ years, which seems incredibly short. Although at temperatures around 15000° K an appreciable amount of hydrogen ionization could be maintained by collisions, the abundance of O^{++} would be governed entirely by the decay equations with the Minkowski-Aller hypothesis. Nor does it seem likely that the lifetime of [O III] emission can be significantly lengthened by supposing that the oxygen was originally in higher stages of ionization, since the tendency of a greater net charge on the ion is to increase the recombination coefficient.

Hence additional analysis of this peculiar spectrum was undertaken. In this paper it will be shown that charge transfer can be of major importance in nebulae where hydrogen is only partially ionized, and the effect of charge-transfer collisions on the Cassiopeia spectrum is discussed. The analysis substantiates the conclusion that the nebula is excited by collisions rather than by stellar radiation; explains the absence of [O II] without recourse to collisional de-excitation; and bears out our suspicion that [O III] must arise from a different region of the nebula than that producing [O I].

II. CHARGE TRANSFER IN NEBULAE

In a gaseous nebula where much of the material is un-ionized, slow inelastic collisions between atomic systems may have an important influence on the ionization and consequently the excitation of certain elements. Bates and Massey (1954) have discussed the various types of reactions that can result from transitions between energy states of the quasi-molecule formed momentarily during a collision. Such reactions involving the transfer of an electron from one atom to another can be of importance in nebulae where

[2] The numerical computations may be greatly simplified by the use of auxiliary equations and computations in later papers in the series "Physical Processes in Gaseous Nebulae" by Menzel *et al.*, appearing in *Astrophysical Journal*, 1937–1945.

[3] I am indebted to Professor Aller for forwarding this information prior to publication of his book.

the hydrogen ionization is controlled by inelastic electron collisions, in "decaying" nebulae (whose external source of energy has been extinguished), and possibly at the boundaries of radiative H II regions.

The theory of collisional excitation of hydrogen in gaseous nebulae has been discussed in detail in an earlier paper by the author (1953, referred to hereafter as "Paper I"). Of importance here is the fact that, at electron temperatures below 20000° K, much of the hydrogen will be neutral (Paper I, Table 6).[4] In this event the transfer of an electron between hydrogen and oxygen by a slow collision will govern the ionization equilibrium of oxygen.

In particular, as Bates (1954) has pointed out, the reactions

$$H^+ + O \rightarrow H + O^+ \tag{4a}$$

and

$$H + O^+ \rightarrow H^+ + O \tag{4b}$$

have large rate coefficients at low collision speeds because of the near resonance in the ionization energies of H and O (13.595 and 13.614 ev, respectively).

Cross-sections for reaction (1) have not been determined directly, but Dalgarno and Yadav (1953) have investigated slow collisions with charge transfer between protons and hydrogen atoms:

$$H^+ + H \rightarrow H + H^+ . \tag{5}$$

The cross-sections $Q(v)$ for reactions (4*a*) and (4*b*) and (5) should not be greatly different. The rate coefficient α is given by

$$\alpha = \int_0^\infty Q(v)\, v f(v)\, dv , \tag{6}$$

where $f(v)$ is the Maxwellian distribution of velocities. In the temperature range of 10000–20000 °K the coefficient for reactions (4*a*) and (4*b*) will be $\alpha_4 \sim 10^{-8}$ cm^3/sec (where subscripts refer to the equation numbers).

For comparison we may estimate the rate coefficient for ionization of O by electron impact:

$$O + e \rightarrow O^+ + 2e . \tag{7}$$

At low energies the ionization cross-section for O is approximately twice that for H (Massey and Burhop 1952, p. 265), and the ionization rate coefficients for H have been evaluated in Paper I. Thus we find roughly, for 10000° K, $\alpha_7 \sim 5 \times 10^{-15}$ cm^3/sec and, for 20000° K, $\alpha_7 \sim 10^{-11}$ cm^3/sec. Even if the nebula is only moderately ionized, the proton and electron densities will be approximately equal, so the relative importance of ionization of O by reactions (4*a*) and (7) will depend only on the relative reaction rates. The foregoing calculations show that process (4*a*) will be about 10^3 times as important as process (7) even at 20000° K.

Similarly, we may compare the rate of electron capture for O^+ by reaction (4*b*) and by ordinary recombination:

$$O^+ + e \rightarrow O + h\nu . \tag{8}$$

The cross-section for capture of a low-energy electron into the ground configuration of O is comparable to the corresponding value for H (Massey and Burhop 1952, p. 336). Moreover, for computing capture into higher levels, one may use a hydrogenic approximation. Aller (1956) has carried out the detailed computations and finds $\alpha_{rec}(O^+) \equiv \alpha_8$

[4] Since the publication of Paper I the calculations of Balmer decrements and the ionization equilbrium of hydrogen have been carried out for higher temperatures. Some of the results have been quoted by Minkowski (1955); others are available upon request.

is around four or five times $\alpha_{rec}(H^+)$. Thus at $T_e = 15000^\circ$ K we have $\alpha_8 \sim 1.5 \times 10^{-12}$ cm^3/sec, and, by the time the ionization ratio $N_e/N(H)$ falls below 10^{-4}, charge transfer will be the dominant process neutralizing O^+.

Of course, the ionization equilibrium of O and H considered together will still be governed by recombination and ionization by electron impact. But charge transfer will be dominant in establishing the *relative* ionization equilibria. Or, since hydrogen is far more abundant than oxygen, we may consider the H-H$^+$ equilibrium as maintained by the free-electron processes and O-O$^+$ as governed by charge transfer.

The absolute values of the rate coefficients for charge transfer are of interest here only to indicate when the various reactions are important; hence we need not know these values accurately. Of more immediate concern are the relative coefficients for reactions (4*a*) and (4*b*). The coefficients are quantum-mechanical quantities that vary only with the electron temperature. Therefore, we may establish relative values by invoking thermodynamic equilibrium and the Saha ionization formula. In statistical equilibrium

$$N(H^+)\, N(O)\, \alpha_{4a} = N(H)\, N(O^+)\, \alpha_{4b}\,. \tag{9}$$

Applying the Saha equation and remembering that O and H have essentially equal ionization potentials, we find

$$\frac{\alpha_{4b}}{\alpha_{4a}} \approx \frac{\varpi(H^+)\,\varpi(^3P)}{\varpi(^2S)\,\varpi(^4S)} = \frac{9}{8}\,, \tag{10}$$

where ϖ represents the statistical weights of the ground terms.[5] Hence, to a good approximation, we may write, from equations (9) and (10),

$$\frac{N(O)}{N(O^+)} \approx \frac{N(H)}{N(H^+)}\,. \tag{11}$$

Charge-transfer reactions similar to equations (4*a*) and (4*b*) will usually proceed much more slowly for other cases, where near-resonance is not present. However, reactions of the type

$$H + X^{++} \rightarrow H^+ + X^+\,, \tag{12}$$

where X represents an unspecified element, can also be important in certain cases. For example, in the case of silicon, Bates and Moiseiwitsch (1954) found a rate coefficient at nebular temperatures of $\alpha_{12}(X = Si) \sim 5 \times 10^{-9}$ cm^3/sec. In general, when the excess energy of reaction (12) is, say, 2 or 3 ev, it may possibly (but not invariably) have a high rate coefficient. For those elements reacting rapidly through process (12), any doubly charged ions present would rapidly disappear from the nebula as soon as an appreciable number of neutral H atoms was formed. On the other hand, if the reaction is exothermic by a large amount, as in the case of O, it will most likely have a very small coefficient (see Dalgarno 1954) and have a negligible effect in nebulae.

III. CASSIOPEIA FILAMENT 1

On the basis of the foregoing discussion we may conclude that the presence of strong [O I] lines in the Cassiopeia spectra is substantial evidence for the presence of large amounts of neutral hydrogen. Therefore, it is most likely that excitation occurs by collisions, in agreement with Minkowski and Aller's conclusion. Also, since charge transfer is likely to be the dominant mechanism in establishing the O-O$^+$ equilibrium, the relative intensities of [O I] and [O II] can be used to ascertain the ionization equilibrium of hydrogen and hence a maximum value for the electron temperature.

In the absence of de-exciting collisons and ignoring the small contribution arising from

[5] I am indebted to Dr. A. Dalgarno for suggesting the argument in the previous paragraph.

the hydrogen ionization is controlled by inelastic electron collisions, in "decaying" nebulae (whose external source of energy has been extinguished), and possibly at the boundaries of radiative H II regions.

The theory of collisional excitation of hydrogen in gaseous nebulae has been discussed in detail in an earlier paper by the author (1953, referred to hereafter as "Paper I"). Of importance here is the fact that, at electron temperatures below 20000° K, much of the hydrogen will be neutral (Paper I, Table 6).[4] In this event the transfer of an electron between hydrogen and oxygen by a slow collision will govern the ionization equilibrium of oxygen.

In particular, as Bates (1954) has pointed out, the reactions

$$H^+ + O \rightarrow H + O^+ \tag{4a}$$

and

$$H + O^+ \rightarrow H^+ + O \tag{4b}$$

have large rate coefficients at low collision speeds because of the near resonance in the ionization energies of H and O (13.595 and 13.614 ev, respectively).

Cross-sections for reaction (1) have not been determined directly, but Dalgarno and Yadav (1953) have investigated slow collisions with charge transfer between protons and hydrogen atoms:

$$H^+ + H \rightarrow H + H^+ . \tag{5}$$

The cross-sections $Q(v)$ for reactions (4*a*) and (4*b*) and (5) should not be greatly different. The rate coefficient α is given by

$$\alpha = \int_0^\infty Q(v)\, v f(v)\, dv , \tag{6}$$

where $f(v)$ is the Maxwellian distribution of velocities. In the temperature range of 10000–20000 °K the coefficient for reactions (4*a*) and (4*b*) will be $\alpha_4 \sim 10^{-8}$ cm³/sec (where subscripts refer to the equation numbers).

For comparison we may estimate the rate coefficient for ionization of O by electron impact:

$$O + e \rightarrow O^+ + 2e . \tag{7}$$

At low energies the ionization cross-section for O is approximately twice that for H (Massey and Burhop 1952, p. 265), and the ionization rate coefficients for H have been evaluated in Paper I. Thus we find roughly, for 10000° K, $\alpha_7 \sim 5 \times 10^{-15}$ cm³/sec and, for 20000° K, $\alpha_7 \sim 10^{-11}$ cm³/sec. Even if the nebula is only moderately ionized, the proton and electron densities will be approximately equal, so the relative importance of ionization of O by reactions (4*a*) and (7) will depend only on the relative reaction rates. The foregoing calculations show that process (4*a*) will be about 10^3 times as important as process (7) even at 20000° K.

Similarly, we may compare the rate of electron capture for O^+ by reaction (4*b*) and by ordinary recombination:

$$O^+ + e \rightarrow O + h\nu . \tag{8}$$

The cross-section for capture of a low-energy electron into the ground configuration of O is comparable to the corresponding value for H (Massey and Burhop 1952, p. 336). Moreover, for computing capture into higher levels, one may use a hydrogenic approximation. Aller (1956) has carried out the detailed computations and finds $\alpha_{rec}(O^+) \equiv \alpha_8$

[4] Since the publication of Paper I the calculations of Balmer decrements and the ionization equilbrium of hydrogen have been carried out for higher temperatures. Some of the results have been quoted by Minkowski (1955); others are available upon request.

is around four or five times $a_{rec}(H^+)$. Thus at $T_e = 15000°$ K we have $a_8 \sim 1.5 \times 10^{-12}$ cm^3/sec, and, by the time the ionization ratio $N_e/N(H)$ falls below 10^{-4}, charge transfer will be the dominant process neutralizing O^+.

Of course, the ionization equilibrium of O and H considered together will still be governed by recombination and ionization by electron impact. But charge transfer will be dominant in establishing the *relative* ionization equilibria. Or, since hydrogen is far more abundant than oxygen, we may consider the H-H^+ equilibrium as maintained by the free-electron processes and O-O^+ as governed by charge transfer.

The absolute values of the rate coefficients for charge transfer are of interest here only to indicate when the various reactions are important; hence we need not know these values accurately. Of more immediate concern are the relative coefficients for reactions (4*a*) and (4*b*). The coefficients are quantum-mechanical quantities that vary only with the electron temperature. Therefore, we may establish relative values by invoking thermodynamic equilibrium and the Saha ionization formula. In statistical equilibrium

$$N(H^+)\, N(O)\, a_{4a} = N(H)\, N(O^+)\, a_{4b}\,. \tag{9}$$

Applying the Saha equation and remembering that O and H have essentially equal ionization potentials, we find

$$\frac{a_{4b}}{a_{4a}} \approx \frac{\varpi(H^+)\,\varpi(^3P)}{\varpi(^2S)\,\varpi(^4S)} = \frac{9}{8}\,, \tag{10}$$

where ϖ represents the statistical weights of the ground terms.[5] Hence, to a good approximation, we may write, from equations (9) and (10),

$$\frac{N(O)}{N(O^+)} \approx \frac{N(H)}{N(H^+)}\,. \tag{11}$$

Charge-transfer reactions similar to equations (4*a*) and (4*b*) will usually proceed much more slowly for other cases, where near-resonance is not present. However, reactions of the type

$$H + X^{++} \rightarrow H^+ + X^+\,, \tag{12}$$

where X represents an unspecified element, can also be important in certain cases. For example, in the case of silicon, Bates and Moiseiwitsch (1954) found a rate coefficient at nebular temperatures of $a_{12}(X = Si) \sim 5 \times 10^{-9}$ cm^3/sec. In general, when the excess energy of reaction (12) is, say, 2 or 3 ev, it may possibly (but not invariably) have a high rate coefficient. For those elements reacting rapidly through process (12), any doubly charged ions present would rapidly disappear from the nebula as soon as an appreciable number of neutral H atoms was formed. On the other hand, if the reaction is exothermic by a large amount, as in the case of O, it will most likely have a very small coefficient (see Dalgarno 1954) and have a negligible effect in nebulae.

III. CASSIOPEIA FILAMENT 1

On the basis of the foregoing discussion we may conclude that the presence of strong [O I] lines in the Cassiopeia spectra is substantial evidence for the presence of large amounts of neutral hydrogen. Therefore, it is most likely that excitation occurs by collisions, in agreement with Minkowski and Aller's conclusion. Also, since charge transfer is likely to be the dominant mechanism in establishing the O-O^+ equilibrium, the relative intensities of [O I] and [O II] can be used to ascertain the ionization equilibrium of hydrogen and hence a maximum value for the electron temperature.

In the absence of de-exciting collisons and ignoring the small contribution arising from

[5] I am indebted to Dr. A. Dalgarno for suggesting the argument in the previous paragraph.

cascading from higher levels, we have, for the intensity ratio of λ 6300 + λ 6364 [O I] to λ 3727 [O II],

$$\frac{I_{\mathrm{O\,I}}}{I_{\mathrm{O\,II}}} = \frac{\tilde{\delta}_{PD}\,(\mathrm{O\,I})\,h\nu_{6300}}{\tilde{\delta}_{SD}\,(\mathrm{O\,II})\,h\nu_{3727}}, \tag{13}$$

where the number of collisional excitations per cubic centimeter per second is

$$\tilde{\delta}_{AB} = N_e N_A a_{\mathrm{exc}} \equiv N_e N_A \int_{v_{AB}}^{\infty} Q_{AB}(v)\, v f(v)\, dv. \tag{14}$$

Here v_{AB} is the minimum electron velocity capable of exciting level B from level A. An approximate method for evaluating the integral a_{exc} rather simply has been given by

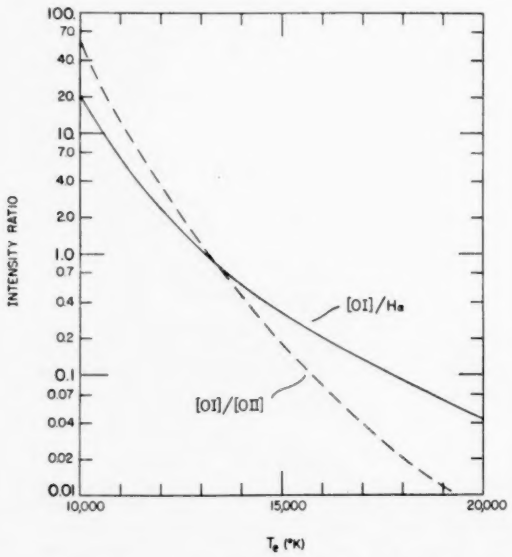

FIG. 1.—Relative intensities of λ 6300 + 6364 [O I], λ 3727 [O II], and Hα for collisional excitation. Assumptions regarding relative abundances are explained in the text. The O I collision strength, Ω, has been taken as constant; it actually increases with electron energy, which will make [O I] slightly stronger toward higher temperatures than is given by these curves.

Hebb and Menzel (1940, eq. [32]), and Seaton's (1953*a*, *b*) cross-sections for oxygen ions have been adopted. (Following Minkowski and Aller for O I, we adopt an average *collision strength* of $\Omega = 0.4$.) For various values of the electron temperature T_e we obtain the ratio $N(\mathrm{O})/N(\mathrm{O}^+)$ from equation (11), where $N(\mathrm{H})/N(\mathrm{H}^+)$ has been interpolated from Paper I, Table 6. The intensity ratio $I_{\mathrm{O\,I}}/I_{\mathrm{O\,II}}$ is shown in Figure 1.

The approximate ratio $I_{\mathrm{O\,I}}/I_{\mathrm{H}\alpha}$ may be calculated in the same fashion, where the excitation rate coefficient $a_{\mathrm{exc}}(\mathrm{H}_3)$ for the third orbit of hydrogen has also been computed earlier (Paper I, Table 1). For the sake of definiteness, we adopt an abundance ratio $N(\mathrm{O})/N(\mathrm{H}) = 3 \times 10^{-4}$ and assume that nearly all the oxygen is in the form of O or O^+. (The strong [O III] lines will be considered later.) These results are also illustrated in Figure 1. At 20000° K the error in neglecting cascading and recombinations

makes the Hα intensities less than 5 per cent too small; for higher temperatures it is advisable to use the modified excitation-ionization equation for hydrogen and the calculations (Paper I) of the departures of this equation from thermodynamic-equilibrium values.[6]

It is seen from Figure 1 that a consistent picture of the [O I]/Hα and [O I]/[O II] ratios in filament 1 is obtained for $T_e < 12000°$ K. The computations shown in the figure have assumed that the hydrogen ionization is in equilibrium with T_e; Minkowski and Aller suggest, however, that the presence of [O III] lines indicates that the general level of ionization is not completely in equilibrium. If this is true, there will be more free electrons, H^+, and O^+ present than one would expect from the electron temperature. This would mean that the intensity ratio [O I]/[O II] plotted in Figure 1 is actually a maximum value for each T_e, and the conclusion that $T_e < 12000°$ K is still valid.

From equations (13) and (14) we find that, in the temperature range around 12000° K, $I_{OI}/I_{OII} \approx 0.3\ N(O)/N(O^+)$. Hence the observation that $I_{OI}/I_{OII} > 5$ implies $N(O)/N(O^+) = N(H)/N(H^+) > 15$, whether or not equilibrium conditions obtain. Therefore, we conclude that the hydrogen is at least 93 per cent neutral and that $T_e < 12000°$ K, the low temperature being confirmed by the [O I]/Hα intensity ratio.

The Minkowski-Aller explanation of the [O III] lines then presents difficulties in addition to the lifetime considerations presented in the introduction. One might suppose that, since charge transfer removes the necessity of having a large electron density to de-excite [O II], the lifetime of [O III] can be increased in accordance with equation (3). But, since O^{++} recombines considerably faster than H^+ and since hydrogen is now over 90 per cent neutral, only a minute fraction of the oxygen can still be in the form O^{++}. This conclusion is independent of the electron density in the filaments.

Therefore, we should seriously consider the possibility that [O I] and [O III] originate from two separate portions of the nebula, an alternative that may at first appear highly artificial. Baade and Minkowski's spectra show several radial-velocity components in each of the spectral lines, and, from the similarity between the [O I] and [O III] components, we must reject the notion that these two emissions arise from completely separate clouds. Nevertheless, the radial velocities are at least as high as 2200 km/sec, which suggests that a strong shock wave has been set up by a gas cloud moving through the interstellar medium (or possibly colliding with another cloud).

Pikelner (1954) has investigated theoretically the conditions existing behind the shock front produced by the motion of a cloud through the interstellar medium (and also the conditions resulting from a collision of two such fronts). His treatment predicts the ion and electron temperatures (which can be greatly different) and the hydrogen ionization versus time after the shock wave has passed a given point in the low-pressure gas, when a set of initial conditions is assumed. Too little is known about the Cassiopeia filaments to attempt an accurate analysis of the shock-wave phenomena, but the general picture presented by Pikelner (1954, Fig. 3*b*) is of qualitative interest here.

As the kinetic energy of mass motion is transformed to ionization and electron energy, a rather sharp region appears where the electron temperature T_e is quite high. Back of this region, T_e drops off rapidly, and the ions will begin to recombine. But a little farther from the front, T_e begins to decrease more slowly, and we have a region that is large compared with the high-temperature peak and in which T_e is effectively constant at a few thousand degrees. Over a portion of the low-temperature region, however, the ions will not have had time to recombine, and the electron density will be higher than the value expected in ionization equilibrium.

Thus we might idealize the Cassiopeia filament 1 as consisting of a narrow, high-tem-

[6] A rough idea of the error introduced by neglecting cascading and recombinations may be had by comparing the total rate coefficients for ionization and excitation to levels $n > 3$ with the coefficient for $n = 3$ and remembering that only a few per cent of these higher-energy electrons will produce an Hα quantum in cascading back to the ground.

perature region just behind the shock front and a wide, low-temperature region through which the shock wave passed earlier and which is now cooling by the emission of radiation. This same general picture of the effect of a plane shock wave on a gas is also demonstrated by the experiments of Kantrowitz (1955, Fig. 8) and associates.

It remains for us to consider the relative intensities of spectral lines in the two regions. To account for the production of large amounts of O^{++}, T_e in the high-temperature region is probably near 40000° K or higher. At these temperatures the excitation of forbidden-line radiation is more efficient than in the cool region, because of both larger rate coefficients for excitation and larger electron densities. If we assume equal mass densities in 40000 and 12000° K nebulae and suppose that all the oxygen is in O^{++} in the former and O in the latter region, then equal intensities of [O III] and [O I] imply that the hot region is only 1/150 times as thick as the cool one. Of course, this picture is an oversimplification, and these intensities vary as the square of the mass densities, so that, if the density in the hot region is appreciably smaller, the actual relative sizes would not differ so much. Nevertheless, it is clear that a fairly thin high-temperature region near the advancing shock front could account for [O III].

Moreover, an appreciable contribution to the hydrogen-line intensities would not arise from this idealized model. At 40000° K we would have a maximum ratio of $I_{O\,III}/I_{H\alpha} \approx 10$ (although this ratio would be reduced according to the amount of oxygen not in the stage O^{++}), and the ratio increases with T_e.

Thus the analysis given for the low-temperature region is unaffected by the presence of a high-temperature fringe.

IV. CASSIOPEIA FILAMENTS 2 AND 3

In filaments 2 and 3 the radial-velocity dispersion is not nearly so extreme, and one may well ask whether it is possible to give a consistent analysis on the basis of a single effective electron temperature. If so, the temperatures are probably considerably higher than in the low-temperature region of filament 1. The [O I]/Hα ratio as interpreted by Figure 1 would suggest a temperature slightly above 15000° K. This, at first, seems inconsistent with the [O I]/[O II] ratio; however, collisional de-excitation will selectively suppress [O II] for an electron density greater than 10^4 cm^{-3}. For example, for a density of the order of 10^5 electrons/cm^3 at 15000° K, 93 per cent of the excited [O II] will be collisionally de-excited, whereas only 6 per cent of the [O I] will be prohibited from radiating. Hence at this density the [O I]/[O II] ratio would be raised by a factor of 13 (which is nearly independent of T_e). A temperature of 15000° K or higher could also maintain appreciable ionization of nitrogen. The [N II] inelastic cross-section is quite large (Seaton 1953*b*), and the lifetime of the upper term is short enough that collisional de-excitation will not entirely quench the radiation. (For a density of 10^6 electrons/cm^3, [N II] will be about 40 per cent de-excited.)

Alternatively, we might suppose that the temperature could be somewhat lower than 15000° K if the density were high enough to suppress [O I] partially, as well as [O II] (say, 10^6 electrons/cm^3). This interpretation presents inconsistencies with the [N II] lines, however, which would also then be de-excited.

On the other hand, the analysis of filament 1 suggests that the other filaments may also involve a varying temperature and ionization, although here the conditions are not likely to be so extreme. But if the ionization equilibrium lags appreciably behind the electron temperature, as shown in Pikelner's theory, the temperature peak may contain a considerable number of neutral atoms, and Hα and [O I] would be enhanced. For the milder shock wave the broad region behind the temperature maximum is probably less important. A more thorough analysis of the N-N^+ ionization equilibrium (and comparison with that for H-H^+) and interpretation of the spectrum in terms of a shock-front analysis seem necessary to decide whether collisional de-excitation, with the large N_e it implies, is necessary to explain the low [O II]/[N II] intensity ratio.

V. SUMMARY

The picture we have obtained for filament 1 has developed along these lines: in view of the large rate coefficients for charge transfer by reactions (4*a*) and (4*b*), the presence of strong [O I] is excellent evidence for large amounts of neutral hydrogen, which, in turn, substantiates Minkowski and Aller's conclusion that H is excited by collisions. Through the resulting relation (11) between the hydrogen and oxygen ionization equilibria, we find from the [O I]/[O II] intensity ratio that H is over 90 per cent neutral and that $T_e < 12000°$ K. The [O I]/Hα ratio independently imposes a similar maximum temperature. Since the absence of [O II] is explained in terms of the ionization equilibrium, large electron densities are not required to de-excite [O II] collisionally.

The [O III] lines are probably not a remnant of an earlier, high-temperature stage of the nebula. Rather, they are interpreted as arising from the high-temperature region immediately following a shock front that is set in motion by a high-velocity cloud moving through the interstellar medium. Lines of [O I], H, and probably [O II] will be weak in this high-temperature region, so that the analysis of the cooler region, through which the shock wave passed earlier, is unaffected.

Even if the intensities of [O II] or Hα could be observed, it is doubtful whether the interpretation could be carried much further without an elaborate discussion of the shock-wave phenomena along the lines presented by Pikelner (1954). Otherwise, one could not be certain which region of the nebula was producing these emissions. Indeed, [O II] may originate mostly in an intermediate region, where the temperature has dropped and O^{++} has recombined but where O and H have not had time to form. Still, for a shock-wave analysis to be especially fruitful, we would require measurements of the absolute intensities and some information on the emitting volumes involved.

It is also suggested that the various radial-velocity components in Baade and Minkowski's spectrum arise from separate shock fronts, produced perhaps by inhomogeneities in the cloud or the interstellar gas. The deceleration of the advancing cloud will give rise to a system of expansion waves, which will eventually overtake the shock waves and affect their velocity and intensity (Burgers 1951). Burgers also points out that if the density of the interstellar gas decreases in the direction of the shock wave's motion, the velocity of propagation of the shock may increase. These considerations may explain in part why the various line components have considerable dispersion in velocity and intensity. Also the impinging cloud may have generated separate shock waves in various directions to the line of sight.

The solution for filaments 2 and 3 is more ambiguous. It seems likely that the shock waves, if they exist at all in these filaments, are less severe. An effective electron temperature, intermediate between the high and low values of filament 1, can explain the spectrum if the densities are high enough; but other solutions involving varying ionization and temperature may be preferable.

Twiss (1954) has discussed the excitation of the radio-frequency spectrum from the standpoint of synchrotron radiation. If this is the proper mechanism, magnetic fields of the order of 10^{-2} gauss are required. The radio-frequency excitation, requiring relativistic electrons, would then probably not be intimately associated with the visual filaments. (This is apparently the case in the Crab Nebula, Taurus A.) Nevertheless, if such strong magnetic fields are present in the region, it would seem plausible that significant fields are also associated with the filaments. Twiss proposes that these magnetic fields are responsible for holding together the filaments, which would otherwise rapidly disperse because of the large "internal" motions suggested by the observed radial velocities. With the model proposed here, the magnetic field is not required to explain the structure; but if a field is present, a discussion of the filaments in terms of hydromagnetic shock waves (cf. Sen 1956) is called for. Thus another unknown parameter—the magnetic field in the filaments—is introduced.

For the radio-frequency spectrum to be associated with the visible structure, the most likely means of radio-frequency excitation lies in plasma oscillations. Twiss points out that, to produce the observed radio frequencies, very high electron densities (say, 10^7 cm^{-3}) are apparently required. An adequate theory for exciting and sustaining strong electron oscillations is lacking. But if small fluctuations in the space charge can actually be amplified to large oscillations by a collision of gas clouds, as suggested by Kahn (1955; also cf. Lampert 1956), it may be possible to attribute the radio-frequency and visual radiation to a single basic phenomenon.

I am pleased to thank Professor L. H. Aller for reviewing a preliminary draft of the manuscript and offering several suggestions.

REFERENCES

Aller, L. H. 1956, *Gaseous Nebulae* (London: Chapman & Hall), pp. 160–163.
Baade, W., and Minkowski, R. 1954, *Ap. J.*, **119**, 206.
Bates, D. R. 1954, *The Earth as a Planet*, ed. G. P. Kuiper (Chicago: University of Chicago Press), chap. 12, p. 625.
Bates, D. R., and Massey, H. S. W. 1954, *Phil. Mag.*, **45**, 111.
Bates, D. R., and Moiseiwitsch, B. L. 1954, *Proc. Phys. Soc., A*, **67**, 805.
Burgers, J. M. 1951, *Problems of Cosmical Aerodynamics*, ed. J. M. Burgers and H. C. van de Hulst (Dayton, Ohio: Central Air Documents Office), p. 68.
Chamberlain, J. W. 1953, *Ap. J.*, **117**, 387.
Dalgarno, A. 1954, *Proc. Phys. Soc., A*, **67**, 1010.
Dalgarno, A., and Yadav, H. N. 1953, *Proc. Phys. Soc., A*, **66**, 173.
Hebb, M. H., and Menzel, D. H. 1940, *Ap. J.*, **92**, 408.
Kahn, F. D. 1955, *Gas Dynamics of Cosmic Clouds*, ed. J. M. Burgers and H. C. van de Hulst (New York: Interscience Publishers), p. 115.
Kantrowitz, A. 1955, *Gas Dynamics of Cosmic Clouds*, ed. J. M. Burgers and H. C. van de Hulst (New York: Interscience Publishers), p. 85.
Lampert, M. A. 1956, *J. Appl. Phys.*, **27**, 5.
Massey, H. S. W., and Burhop, E. H. S. 1952, *Electronic and Ionic Impact Phenomena* (Oxford: Clarendon Press).
Menzel, D. H. 1937, *Ap. J.*, **85**, 330.
Minkowski, R. 1955, *Gas Dynamics of Cosmic Clouds*, ed. J. M. Burgers and H. C. van de Hulst (New York: Interscience Publishers), p. 108.
Minkowski, R., and Aller, L. H. 1954, *Ap. J.*, **119**, 232.
Pikelner, S. B. 1954, *Izvestia Crimean Ap. Obs.*, **12**, 93.
Seaton, M. J. 1953*a*, *Phil. Trans. R. Soc. London, A*, **245**, 469.
———. 1953*b*, *Proc. R. Soc. London, A*, **218**, 400.
Sen, H. K. 1956, *Phys. Rev.*, **102**, 5.
Twiss, R. Q. 1954, *Phil. Mag.*, **45**, 249.

ROTATIONAL TEMPERATURE AND PHASE VARIATION OF THE CARBON DIOXIDE BANDS OF VENUS*

JOSEPH W. CHAMBERLAIN AND GERARD P. KUIPER
Yerkes and McDonald Observatories
Received April 17, 1956

ABSTRACT

The CO_2 absorption bands in the spectrum of Venus are discussed in terms of a model atmosphere that is optically thick and scatters radiation isotropically. The rotational temperature thus derived from two bands is 285° ± 9° K (p.e.). A series of low-dispersion spectra shows a marked change in the strength of CO_2 versus phase angle. This phase effect is also interpreted by the radiative-transfer treatment of scattering and absorption in the atmosphere. The approximate theory and observations are in qualitative agreement.

I. INTRODUCTION

Carbon dioxide was first observed in the spectrum of Venus by Adams and Dunham (1932). They measured the two vibration-rotation bands having heads at 7882.8 and 7820.0 A, which arise from transitions from the ground vibrational level to $[5\nu_3 + (\nu_1, 2\nu_2)]$, where the ν_1 and $2\nu_2$ levels are in Fermi resonance. Also, they found the $5\nu_3$ band at 8688.7 A. Later Herzberg (1952, p. 411) observed the $[3\nu_3 + (2\nu_1, \nu_1 + 2\nu_2, 4\nu_2)]$ group of three bands around 10500 A and the two $[3\nu_3 + (\nu_1, 2\nu_2)]$ bands near 12000 A. Other bands have been recorded in the 1.0–2.5 μ region by Kuiper (1947, 1952, p. 356).

The first determination of a rotational temperature in Venus was made by Adel (1937) from an inspection of published prints of the spectrum. For the band at 7820 A he estimated $T_{rot} > 320°$ K. Similarly, Herzberg (1951) found that the relative line intensities in the Adams-Dunham spectra were roughly the same as in his laboratory spectra made at room temperature. On this basis he estimated the Venus CO_2 temperature at 300° ± 50° K. Dunham (1949) derived the temperature by measuring the intensities from original plates and also estimated 300° ± 50° K.

In these earlier estimates it was assumed in all cases that the relative intensities of the lines were proportional to the relative populations, N_J, of the lower levels of the transitions. Van de Hulst (1952, p. 102) has pointed out, however, that in an optically thick atmosphere, where scattering and absorption are both important, this simple relation would not be expected to hold true. In particular, for an optically thick planetary atmosphere scattering light isotropically, the line absorption for weak lines is proportional to $N_J^{1/2}$.

In this paper we shall examine the problem of line formation in the Venus atmosphere and apply the results to the available spectra of high dispersion in a new determination of the rotational temperature. The spectra discussed here were obtained by Mr. Kuiper, except for two spectra loaned from the Mount Wilson Observatory. The analysis was carried out by Mr. Chamberlain in consultation with Mr. Kuiper.

The general solution can be expressed in terms of Chandrasekhar's (1950) H-functions and, as a limiting case, can be reduced to the relation quoted by van de Hulst. This approximate formula is then used in Section III to derive a rotational temperature from high-dispersion Venus spectra. In Section IV an approximate radiative-transfer solution is applied to an analysis of the variation in strength of the 8689 A band of CO_2 with phase, an effect that was previously reported by Kuiper (1952, p. 370).

* Contributions of the McDonald Observatory, No. 268.

II. LINE FORMATION IN THE VENUS ATMOSPHERE

Consider an area on Venus where the incident flux, πF, of sunlight enters from direction θ_0 (zenith angle), ϕ_0 (azimuth). We wish to find the depth of an absorption line when this region of the planet is observed from direction θ, ϕ. Radiation in the atmosphere will be subject to scattering by particles with a mass scattering coefficient of $\sigma(\mathrm{cm}^2/\mathrm{gm})$. Also there will be absorption (without re-emission) produced by CO_2, where the mass absorption coefficient is κ_ν. The scattering particles in Venus are probably of the order of 10 or 20 μ in diameter (cf. Kuiper 1952, p. 371; van de Hulst 1952, p. 105). In this case the phase function for scattering can be adequately approximated by an isotropic distribution plus a large forward-scattering lobe. However, in discussions of the radiation transfer, forward-scattered light is indistinguishable from light not scattered at all. Hence we assume only isotropic scattering and investigate the line formation that would result from diffuse reflection by an optically thick plane-parallel atmosphere.

The equation of transfer for specific intensity I_ν, then, is (cf. Chandrasekhar 1950, chap. 1)

$$dI_\nu = I_\nu(\sigma + \kappa_\nu)\,\rho \sec\theta\, dz - \left[\int_0^{2\pi}\int_0^{\pi} I_\nu \sin\theta\, d\theta\, d\phi + \pi F e^{-(\sigma+\kappa_\nu)\rho z \sec\theta_0}\right]\frac{\sigma\rho\sec\theta\, dz}{4\pi}, \tag{1}$$

where z is depth in the atmosphere and ρ is the density in grams per cubic centimeter. Defining $d\tau_\nu = (\sigma + \kappa_\nu)\rho dz$, $\mu = \cos\theta$, and $\varpi_\nu = \sigma/(\sigma + \kappa_\nu)$, we have

$$\mu\frac{dI_\nu}{d\tau_\nu} = I_\nu - \frac{\varpi_\nu}{2}\int_{-1}^{+1} I_\nu(\mu)\, d\mu - \frac{F}{4}\varpi_\nu e^{-\tau_\nu/\mu_0}. \tag{2}$$

For a semi-infinite atmosphere the exact solution of equation (2) has been expressed by Chandrasekhar (1950, p. 85) in terms of the H-functions:

$$I(\tau_\nu = 0, \mu) = \frac{\varpi_\nu}{4} F \frac{\mu_0}{\mu + \mu_0} H(\mu) H(\mu_0). \tag{3}$$

In the continuum we have $\varpi_\nu = 1$ and write $I_\nu = I_c$. Thus the relative depression below the continuum at a particular point in the line is

$$s_\nu = \frac{I_c - I_\nu}{I_c} = 1 - \frac{\varpi_\nu H_\varpi(\mu) H_\varpi(\mu_0)}{H_1(\mu) H_1(\mu_0)}. \tag{4}$$

We now wish to simplify equation (4), in order to make it amenable to further analytic treatment. For the case of $\varpi_\nu \approx 1$ we assume an expression of the form

$$H_\varpi(\mu) = \frac{H_1(\mu)}{1 + f_\varpi(\mu)} \approx H_1(\mu)\,[1 - f_\varpi(\mu) + f_\varpi^2(\mu)], \tag{5}$$

where $f_\varpi \ll 1$. Combining this expression with the integral relations given by Chandrasekhar (1950, pp. 105 ff.), we derive two integral equations for f_ϖ:

$$\int_0^1 f_\varpi(\mu)\, d\mu = 1 - \frac{\varpi}{1-\varpi}\int_0^1 f_\varpi^2(\mu)\, d\mu \tag{6}$$

and

$$\int_0^1 \mu f_\varpi(\mu)\, d\mu = \frac{(2/\sqrt{3})(1-\varpi)^{1/2} - \frac{1}{2}(1-\varpi)}{1+\varpi} + \frac{\varpi}{1+\varpi}\int_0^1 \mu f_\varpi^2(\mu)\, d\mu. \tag{7}$$

We now postulate that $f_\varpi = A\ \mu^p$, where $p > 0$. Substitution of this relation in equations (6) and (7) is sufficient to determine both A and p as functions of ϖ. For the case where $\varpi \approx 1$, the solution gives $p = 1$ and $A = [3(1 - \varpi)]^{1/2}$. Then from equation (5) we have van de Hulst's (1952) formula,

$$H_\varpi(\mu) = \frac{H_1(\mu)}{1 + \mu\,[3\,(1 - \varpi_\nu)\,]^{1/2}}. \tag{8}$$

Substitution of equation (8) in equation (4) gives

$$s_\nu \approx (\mu + \mu_0)\ [3\,(1 - \varpi_\nu)\,]^{1/2} \approx 3^{1/2}\,(\mu + \mu_0)\left(\frac{\kappa_\nu}{\sigma}\right)^{1/2}, \tag{9}$$

which is valid for $\kappa_\nu \ll \sigma$ (or $\varpi_\nu \approx 1$) and $\mu \gg 0$.

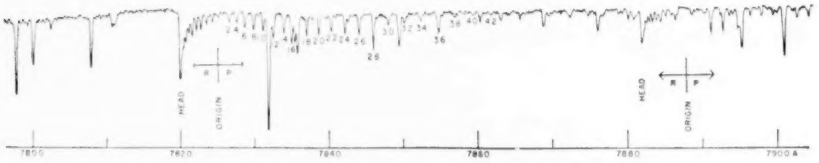

FIG. 1.—The $5\nu_3 + (\nu_1, 2\nu_2)$ bands of CO_2 in the spectrum of Venus, obtained by Dunham, Mount Wilson Observatory, coudé No. Ce 1750, August 8, 1938. Dispersion on the plate, 4.4 A/mm.

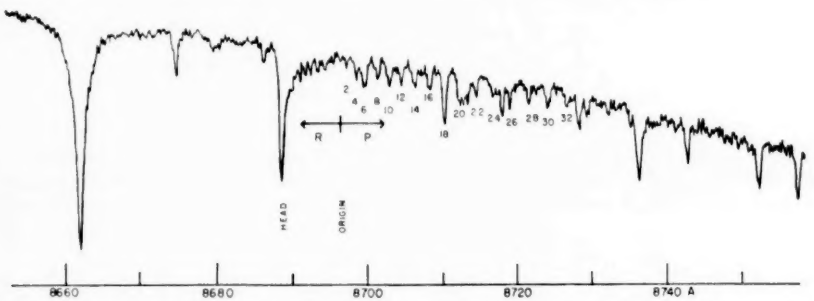

FIG. 2.—The $5\nu_3$ band of CO_2 in the spectrum of Venus, McDonald Observatory, coudé No. 1267, February 14, 1955. Dispersion on the plate, 9.6 A/mm.

Actually, there will be a slight variation in the oscillator strengths for the different lines, and in the case of several diatomic molecules this variation has been computed. However, we have no such information for CO_2, so we make the usual assumption that the oscillator strengths are the same for all lines. Then from equation (9) we find, for the equivalent width of a line at small phase angles,

$$W(J) \equiv \int_0^\infty s_\nu(J)\,d\nu = \text{Const.}\ N_J^{1/2}, \tag{10}$$

where the constant is the same for all lines in a particular band.

III. ROTATIONAL TEMPERATURE

In Figures 1, 2, and 3 are presented microphotometer tracings of the 7800, 8700, and 10500 A regions, respectively, showing the vibration-rotation bands discussed in the

introduction. Of the bands shown, only the P branches in λ 7820 and λ 8689 are sufficiently strong and free from blends with solar lines for reliable temperature analyses.

Herzberg (1945, p. 395) quotes, for the rotational constant in the ground vibrational level, $B_0 = 0.389$. The Boltzmann distribution, when substituted in equation (10), thus leads to

$$\log_{10} \frac{W(J)}{(2J+1)^{1/2}} = \text{Const.} - 0.122 \frac{J(J+1)}{T_{\text{rot}}}. \tag{11}$$

Figure 4 shows plots of equation (11) from plates made at McDonald Observatory for the two bands analyzed. In both cases a number of lines had to be discarded because of blends. The validity of approximation (10) is evidenced by the linearity of the plotted points. Alternatively, when it is assumed that the equivalent width is proportional to N_J, there is a definite upward curvature.

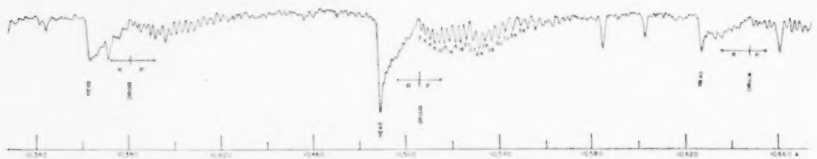

FIG. 3.—The $3\nu_3 + (2\nu_1, \nu_1 + 2\nu_2, 4\nu_2)$ bands of CO_2 in the spectrum of Venus, McDonald Observatory, coudé No. 416, May 23, 1943. Dispersion on the plate, 17.3 A/mm.

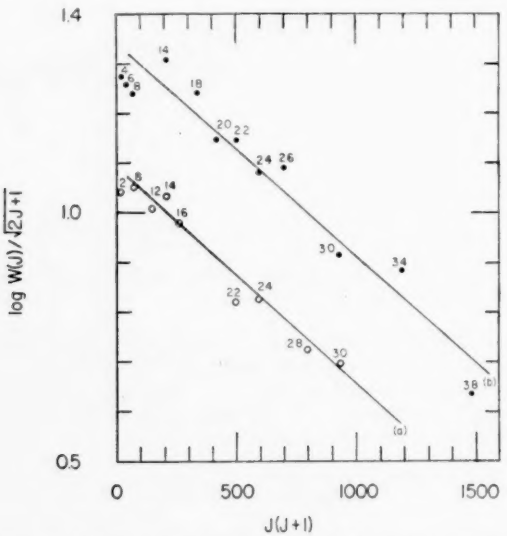

FIG. 4.—Determination of rotational temperatures from McDonald Observatory plates. (*a*) Open circles 8689 A band; (*b*) closed circles, 7820 A band. The relative intensities in *a* are not on the same scale as those in *b*. The J-values of the lines are indicated next to the small circles. Lines with odd values of J are absent from the spectrum of these bands. The straight lines represent least-squares solutions of equation (11), as explained in the text.

Several plates obtained at McDonald and Mount Wilson Observatories have been measured, and the rotational temperatures and probable errors were determined by least-squares solutions. Table 1 summarizes the results; the mean temperature from all three groups is 285° ± 9° K(p.e.).

The most important systematic errors in T_{rot} probably arise from our neglect of the variation of oscillator strengths with the different lines in a band and from departures of the absorption law from the asymptotic relations (9) and (10). However, for all the plates measured, the phase angle was around 75°–80°, and the approximate equations should be reasonably reliable (see below).

IV. PHASE VARIATION OF CARBON DIOXIDE

It has previously been reported that a pronounced weakening of the CO_2 band λ 8689 relative to λ 8498 of Ca II occurs at large phase angles (Kuiper 1952, p. 370). Here this phase effect is interpreted in terms of the transfer of radiation in the Venus atmosphere.

TABLE 1

ROTATIONAL TEMPERATURES OF VENUS

Spectrograph	Band	No. of Plates	T_{rot} (° K)
McDonald coudé	8689	6	286 ± 13
McDonald coudé	7820	2	292 ± 16
Mount Wilson coudé	7820	2*	277 ± 15

* Ce 1750, Ce 1753.

As in the case of the rotational temperature, since the ratio κ_ν/σ (or ϖ_ν) is not known, it is expedient to use an approximate relation for the equivalent width rather than attempt to use the exact solution (4). Substituting equation (8) in equation (4), we find, for $\mu = \mu_0$ and $\kappa_\nu \ll \sigma$,

$$s_\nu \approx \frac{3^{1/2} 2\mu\, \kappa_\nu^{1/2}}{\sigma^{1/2}} - \frac{(9\mu^2 - 1)\, \kappa_\nu}{\sigma}, \tag{12}$$

which reduces to equation (9) when $\mu \gg 0$. It is of interest, however, that, according to equation (12), for large phase angles or as $\mu \to 0$ (near inferior conjunction) $s_\nu \to \kappa_\nu/\sigma$. If large phase angles be excluded, we may represent s_ν by equation (9).

For pure collisional broadening, the equivalent width of a line described by equation (9) will be proportional to the square root of the density of atoms and molecules producing damping. In the planetary atmosphere this density varies considerably over the region in which the line is formed, so we simply take the broadening proportional to the square root of the density at some effective depth of line formation—say, where the incident intensity is reduced one-half. The broadening at different phases will then be roughly proportional to $\mu^{1/2}$, since, for an atmosphere following the barometric law, the density at the effective depth will be proportional to μ. But as $\mu \to 0$ and $s_\nu \to \kappa_\nu/\sigma$ in accordance with equation (12), we approach the usual condition that the equivalent width of a weak line is independent of the amount of broadening and hence independent

of μ. Thus the equivalent width of a band composed of weak lines and observed at different phases with $\mu \approx \mu_0$ is roughly

$$W_\mu = \text{Const.}\ \mu^{3/2}\ , \qquad \mu \gg 0\ ,$$
$$= \text{Const.}\ , \qquad \mu \sim 0\ . \tag{13}$$

Figure 5 shows the results of measures of the estimated strength of λ 8689 relative to the Ca II line λ 8498 on 59 low-dispersion (230 A/mm) plates obtained by Kuiper. All these plates were taken near five different phase angles, and the results for each phase are averaged. It must be cautioned that, since the CO_2 band falls in the region of the spectrum where the plate sensitivity is rapidly falling off, the accuracy of individual measurements is quite low. As the figure illustrates, however, the probable error of the series of measurements for each phase is usually appreciably less than the differences between phases.

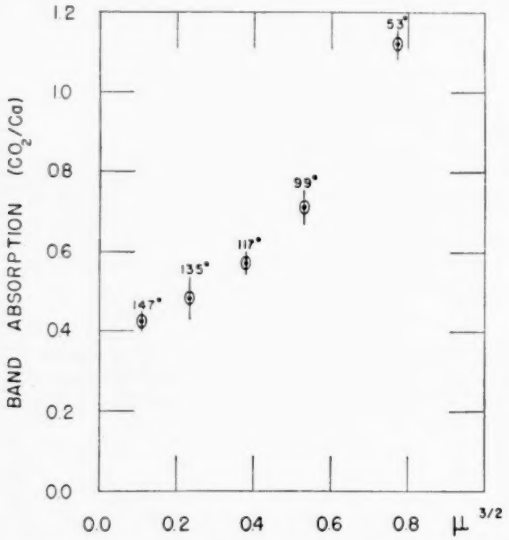

FIG. 5.—Variation of equivalent width of 8689 A band of CO_2 with phase angle. The abscissa is $\mu^{3/2}$, where $\mu = \cos(i/2)$ and i is the phase angle. Vertical lines represent probable errors of the average CO_2 absorption at each phase.

For large μ the equivalent widths plotted against $\mu^{3/2}$ probably do tend toward a straight line passing near the origin, whereas the curve changes very slowly near $\mu = 0$, in qualitative agreement with equation (13). A more quantitative comparison of theory and observation would require information on the relative absorption and scattering coefficients. The presence of a fairly narrow, but finite, forward lobe in the scattering phase function also probably causes serious deviations at large phase angles from the equivalent widths expected in purely isotropic scattering.

We wish to express our appreciation to Director Bowen and to Dr. Dunham for the loan of two Mount Wilson coudé spectra and to Mrs. Patricia A. Grant for assistance with the measurements.

REFERENCES

Adams, W. S., and Dunham, T., Jr. 1932, *Pub. A.S.P.*, **44**, 243.
Adel, A. 1937, *Ap. J.*, **86**, 337.
Chandrasekhar, S. 1950, *Radiative Transfer* (Oxford: Clarendon Press).
Dunham, T., Jr. 1949, *The Atmospheres of the Earth and Planets*, ed. G. P. Kuiper (Chicago: University of Chicago Press), chap. xi. (Also cf. 2d ed., 1952.)
Herzberg, G. 1945, *Raman Spectra* (New York: D. Van Nostrand Co.).
———. 1951, *J.R.A.S. Canada*, **45**, 100.
———. 1952, *The Atmospheres of the Earth and Planets*, ed. G. P. Kuiper (2d ed.; Chicago: University of Chicago Press), chap. xiii.
Hulst, H. C. van de. 1952, *The Atmospheres of the Earth and Planets*, ed. G. P. Kuiper (2d ed.; Chicago: University of Chicago Press), chap. iii.
Kuiper, G. P. 1947, *Ap. J.*, **106**, 252.
———. 1952, *The Atmospheres of the Earth and Planets*, ed. G. P. Kuiper (2d ed.; Chicago: University of Chicago Press), chap. xii.

THE SOURCE FUNCTION FOR AN EQUILIBRIUM GRAY ATMOSPHERE

JEAN I. F. KING
Geophysics Research Directorate, Air Force Cambridge Research Center
Bedford, Massachusetts
Received May 8, 1956

ABSTRACT

The exact form of the source function for a finite gray atmosphere in radiative equilibrium (planetary thermal problem) is derived. It proves to be expressible in terms of the X- and Y-functions of Chandrasekhar. An unexpected result is that Hopf's function $q(\tau)$ is shown to be, apart from a numerical factor, equivalent to the second functional moment of X and Y.

I. INTRODUCTION

In his treatise on radiative transfer, Chandrasekhar (1950) solves a host of scattering problems in terms of certain X- and Y-functions, first introduced and tabulated by him. That this proves possible stems from the fact that these functions, themselves solutions of a pair of non-linear integral equations, reflect a deep invariance in the scattering process. Although exact solutions of the external radiation field are obtained under a wide variety of conditions, solutions for the internal radiation field are in a less satisfactory state. For these, expressions have been given only in terms of finite approximations or in lengthy numerical integrals, clumsy of evaluation. We shall now fill in this lacuna by deriving the exact form of the source function in terms of the X- and Y-functions and their moments.

II. THE SOURCE FUNCTION

As our model we take a plane-parallel gray atmosphere in radiative equilibrium, of optical thickness τ_1. This finite atmosphere is irradiated solely from below by the uniform isotropic radiation I_0. The emergent intensity for such an atmosphere, derived by using an invariant approach (King 1956) is

$$I(0, \mu) = \frac{F}{2} \frac{X(\mu, \tau_1) + Y(\mu, \tau_1)}{\alpha_1(\tau_1) + \beta_1(\tau_1)}, \tag{1}$$

where F is the constant flux filtering upward through the atmosphere and α and β are moments of the X- and Y-functions, defined by

$$\alpha_n = \int_0^1 X(\mu)\, \mu^n d\mu, \qquad \beta_n = \int_0^1 Y(\mu)\, \mu^n d\mu. \tag{2}$$

The constancy of the flux integral of the transfer equation is automatically assured by the form of equation (1), since

$$2\int_0^1 I(0, \mu)\, \mu d\mu = F, \tag{3}$$

while the K-integral requires that

$$K(0) = \frac{1}{2}\int_0^1 I(0, \mu)\, \mu^2 d\mu = \frac{FQ}{4}. \tag{4}$$

We thus find that the Q-constant of the K-integral is simply related, through expression (1), to the moments of the X- and Y-functions,

$$Q = \frac{\alpha_2 + \beta_2}{\alpha_1 + \beta_1}. \tag{5}$$

Using the method of discrete ordinates, the solution for the source function can be expressed in the nth approximation as

$$B(\tau) = \frac{3F}{4}\left\{\tau + Q + \sum_{a=1}^{n-1} L_a \left[e^{-k_a \tau} - e^{-k_a(\tau_1 - \tau)} \right] \right\}. \tag{6}$$

The method of elimination of constants has been used to express the values of L_a and Q in terms of the roots of a certain characteristic equation (King 1956).

In a brilliant speculation, Yamamoto (1955) assumed that the source function could be written in exact form as

$$B(\tau) = \frac{3F}{4}\{\tau + Q(\tau_1) + L(\tau_1)\,[q(\tau) - q(\tau_1 - \tau)]\}, \tag{7}$$

where $q(\tau)$ is Hopf's function, for a long time familiar in the context of a semi-infinite atmosphere. By the substitution of equation (7) in the Milne-Schwarzschild equation, Yamamoto was able to obtain integral expressions for the constants Q and L, which he evaluated numerically.

We now circumvent this lengthy procedure and relate the constants Q, L, and, surprisingly enough, q directly to the moments of X and Y.

To establish a connection between the source function at the top of the atmosphere and the emergent intensity, we note, using equation (1), that

$$B(0) = \frac{1}{2}\int_{-1}^{1} I(0, \mu)\, d\mu = \frac{F}{2(\alpha_1 + \beta_1)}, \tag{8}$$

since, from a theorem on the X- and Y-functions,

$$\alpha_0 + \beta_0 = 2. \tag{9}$$

Equating relation (8) and the source function (eq. [7]) taken at the top of the atmosphere, we find that

$$\frac{2}{3(\alpha_1 + \beta_1)} = Q + L\,[q(0) - q(\tau_1)]. \tag{10}$$

Rearranging this equation slightly and substituting the momental expression for Q, we have

$$L\,[q(0) - q(\tau_1)] = \frac{2/\sqrt{3}}{\alpha_1 + \beta_1}\left[\frac{1}{\sqrt{3}} - \frac{\alpha_2 + \beta_2}{2/\sqrt{3}}\right]. \tag{11}$$

We have written this equation, making use of the exact value of the Hopf function,

$$q(0) = \frac{1}{\sqrt{3}}. \tag{12}$$

From equation (11) we see immediately that the common factor L can be identified as

$$L = \frac{2/\sqrt{3}}{\alpha_1 + \beta_1}. \tag{13}$$

Furthermore, the Hopf function is determined as

$$q = \frac{a_2 + \beta_2}{2/\sqrt{3}}. \tag{14}$$

With relations (5), (13), and (14) we have reached the goal of expressing the source function in terms of moments of X and Y. Using these moments explicitly, we can write $B(\tau)$ in the provocative form,

$$B(\tau) = \frac{3F}{4}\left\{\tau + \frac{a_2(\tau_1) + \beta_2(\tau_1) + a_2(\tau) + \beta_2(\tau) - a_2(\tau_1 - \tau) - \beta_2(\tau_1 - \tau)}{a_1(\tau_1) + \beta_1(\tau_1)}\right\}. \tag{15}$$

We note further that

$$qL = Q. \tag{16}$$

Thus any two of the constants suffice to determine the third.

III. EVALUATION OF THE CONSTANTS

Certainly the logically most direct method is a numerical solution of the X- and Y-functions from their defining integral equations, followed by an integration to obtain their moments. However, because of the exhaustive effort devoted to the semi-infinite atmosphere problem, the Hopf function has been evaluated to sixth-place decimal accuracy. What is wanted, therefore, is some simple relation which will yield Q or L to the corresponding degree of accuracy as q.

We begin with the emergent intensity from a finite atmosphere expressed as an integral of the transfer equation,

$$I(0, \mu) = \int_0^{\tau_1} B(\tau)\, e^{-\tau/\mu} \frac{d\tau}{\mu} + I_g e^{-\tau_1/\mu}. \tag{17}$$

Upon using equation (1) for $I(0, \mu)$, equation (7) for $B(\tau)$, and the relation, derivable from invariance considerations,

$$I_g = \frac{3F}{4}(\tau_1 + 2Q), \tag{18}$$

we find that

$$\frac{L}{\sqrt{3}}[X(\mu) + Y(\mu)] = \mu(1 - e^{-\tau_1/\mu}) + Q(1 + e^{-\tau_1/\mu}) + L\int_0^{\tau_1} [q(\tau) - q(\tau_1 - \tau)]\, e^{-\tau/\mu} \frac{d\tau}{\mu}. \tag{19}$$

Multiplying the equation by μ and integrating over μ between the limits 0 and 1, we obtain

$$\tfrac{2}{3} = \tfrac{1}{3} - E_4(\tau_1) + Q[\tfrac{1}{2} + E_3(\tau_1)] + L\int_0^{\tau_1} [q(\tau) - q(\tau_1 - \tau)]\, E_2(\tau)\, d\tau. \tag{20}$$

Rearranging terms and using the fact that $qL = Q$, we have, finally,

$$L(\tau_1) = \frac{\tfrac{1}{3} + E_4(\tau_1)}{q(\tau_1)[\tfrac{1}{2} + E_3(\tau_1)] - \int_0^{\tau_1} [q(\tau_1 - \tau) - q(\tau)]\, E_2(\tau)\, d\tau}. \tag{21}$$

The exactitude of L is limited only by the degree of accuracy of the Hopf function. The integral

$$I(\tau_1) = \int_0^{\tau_1} [q(\tau_1 - \tau) - q(\tau)] E_2(\tau)\, d\tau \tag{22}$$

varies monotonically from $I(0) = 0$ to $I(\infty) = q(\infty)/2 - \frac{1}{3} = 0.02188971$.

Table 1 lists the values of the constants exact to the sixth decimal place. The Hopf function, an iterated variational solution of the sixth order, is taken from Kourganoff (1952). The L-constant has been numerically integrated by equation (21) by means of electronic computing equipment. The Q-constant is, of course, the product of the two.

The L-constant has previously been evaluated in at least four unrelated fashions. The comparison in Table 2 tests the accuracy of the various schemes. The values in the first

TABLE 1

RADIATIVE EQUILIBRIUM CONSTANTS FOR THE GRAY ATMOSPHERE

τ	q	L	Q	τ	q	L	Q
0.00	0.57735027	1.15470054	0.66666667	0.60	0.685801	1.019388	0.699097
0.01	.588236	1.135963	.668214	0.70	.690109	1.015711	.700951
0.02	.595391	1.124654	.669609	0.80	.693535	1.012865	.702457
0.03	.601242	1.115850	.670896	0.90	.696294	1.010625	.703692
0.04	.606287	1.108544	.672096	1.00	.698540	1.008837	.704713
0.05	.610758	1.102278	.673225	1.25	.702572	1.005711	.706584
0.06	.614789	1.096782	.674290	1.50	.705131	1.003790	.707803
0.07	.618468	1.091889	.675298	1.75	.706802	1.002563	.708614
0.08	.621854	1.087484	.676256	2.00	.707916	1.001759	.709161
0.09	.624993	1.083486	.677171	2.25	.708673	1.001220	.708538
0.10	.627919	1.079828	.678045	2.50	.709191	1.000858	.709799
0.20	.649550	1.054717	.685091	2.75	.709551	1.000607	.709982
0.30	.663365	1.040311	.690106	3.00	.709806	1.000429	.710111
0.40	.673090	1.030876	.693872	3.25	.709985	1.000309	.710204
0.50	0.680293	1.024252	0.696791	∞	0.71044609	1.00000000	0.71044609

column are computed from Chandrasekhar's (1948) tables based on van de Hulst's (1948) approximate method considering successive orders of scattering. The second-column figures are the moments obtained directly from Chandrasekhar's (1952) electronic-machine solutions of the X- and Y-functions. The third column lists values of the L-constant computed by Yamamoto (1955) from a lengthy numerical integral. The method of discrete ordinates applied to this problem yields another explicit form:

$$L(\tau_1) = \frac{G(0)}{F(0)}, \tag{23}$$

where G and F are two fundamental polynomials derived by Chandrasekhar (1947) in the context of a finite atmosphere. These have been calculated to the fourth approximation by the author and are tabulated in the fourth column.

IV. CONCLUSIONS

Our most surprising result is the equivalence of the Hopf function and the second functional moment of X and Y. Why has this relation remained undiscovered? The answer is that q has been associated with the semi-infinite atmosphere, while the function, through its connection with X and Y, actually has its roots in the finite-atmosphere

problem. These remarks, quite incidentally, are evidence that the logically most satisfactory approach to the radiative-transfer problem is through the finite atmosphere. The semi-infinite results can be reclaimed as a special case from any point in the finite formalism, by requiring the thickness τ_1 to become infinite.

It is worthy of note that, without exception, every expression and constant derived herein is a function of the *sum* of the X- and Y-functions. Chandrasekhar (1952) has shown that this sum is invariant, thus free of the indeterminacy which is characteristic individually of X and Y in the conservative case. In this particular conservative problem, nature has rid herself of ambiguity by dealing only with invariant sums.

TABLE 2

THE L-CONSTANT

τ	van de Hulst and Chandrasekhar	Chandrasekhar	Yamamoto	Discrete Ordinate	Exact Solution
0.00	1.15470054	1.15470054	1.153320	1.14154	1.15470054
0.005	1.143782	.....	.....	1.13877	.....
0.01	1.136627	.....	1.100046	1.13606	1.135963
0.02	1.125726	.....	.....	1.13084	1.124654
0.03	1.117209	.....	.....	1.12584	1.115850
0.04	1.110117	.....	.....	1.12099	1.108544
0.05	1.104006	1.10397	.....	1.11654	1.102278
0.06	1.098630	.....	.....	1.11215	1.096782
0.07	1.093827	.....	.....	1.10802	1.091889
0.08	1.089491	.....	.....	1.10403	1.087484
0.09	1.085539	.....	.....	1.10023	1.083486
0.10	1.081919	1.08193	1.054924	1.09659	1.079828
0.11	1.078582	.....	.....	1.09311	.....
0.12	1.075479	.....	.....	1.08977	.....
0.13	1.072595	.....	.....	1.08656	.....
0.14	1.069903	.....	.....	1.08352	.....
0.15	1.067380	1.06740	.....	1.08059	.....
0.16	1.065012	.....	.....	1.07779	.....
0.17	1.062776	.....	.....	1.07509	.....
0.18	1.060670	.....	.....	1.07251	.....
0.19	1.058676	.....	.....	1.07004	.....
0.20	1.056788	1.05682	.....	1.06768	1.054717
0.25	1.048644	1.04864	.....	1.05719	.....
0.30	1.042173	.....	.....	1.04864	1.040311
0.35	1.036911	.....	.....	1.04162	.....
0.40	1.032557	.....	.....	1.03519	1.030876
0.45	1.028906	.....	.....	1.03104	.....
0.50	1.025819	1.0256	.....	1.02710	1.024252
0.60	1.020902	.....	.....	1.02088	1.019388
0.70	1.017254	.....	.....	1.01644	1.015711
0.80	1.014469	.....	.....	1.01320	1.012865
0.90	1.012337	.....	.....	1.01076	1.010625
1.00	1.010685	1.0079	1.006524	1.00888	1.008837
1.25	.....	.....	.....	1.00574	1.005711
1.50	.....	.....	.....	1.00385	1.003790
1.75	.....	.....	.....	1.00265	1.002563
2.00	.....	.....	.....	1.00190	1.001759
2.25	.....	.....	.....	1.00129	1.001220
2.50	.....	.....	.....	1.00091	1.000858
2.75	.....	.....	.....	1.00064	1.000607
3.00	.....	.....	.....	1.00046	1.000429
3.25	.....	.....	.....	1.00033	1.000309
∞	.....	1.0	1.0	1.0	1.0

The approach used in this paper, while correct, is somewhat oblique. The fact that the source function can be expressed exactly and completely in terms of X- and Y-functional moments argues that one should be able to obtain the source function from invariance considerations alone.

REFERENCES

Chandrasekhar, S. 1947, *Ap. J.*, **106**, 152.
———. 1948, *ibid.*, **108**, 92.
———. 1950, *Radiative Transfer* (Oxford: Clarendon Press).
Chandrasekhar, S., and Elbert, D. 1952, *Ap. J.*, **115**, 269.
Hulst, H. C. van de. 1948, *Ap. J.*, **107**, 220.
King, J. I. F. 1956, *Ap. J.*, **124**, 272.
Kourganoff, V. 1952, *Basic Methods in Transfer Problems* (Oxford: Clarendon Press).
Yamamoto, G. 1955, *Sci. Rept. Tohoku University*, Ser. 5, Geophysics, **7**, 1.

ON CLUSTER-TYPE VARIABLES AND MAGNETIC FIELDS

G. R. BURBIDGE
Mount Wilson and Palomar Observatories
Carnegie Institution of Washington, California Institute of Technology
Received March 26, 1956; revised May 8, 1956

ABSTRACT

It is shown that a comparison of the observed with the available theoretical values of the period-density relation for giant models, applied to the cluster-type variables, cannot be expected to show good agreement at the present time. However, the effect of a magnetic field, similar to that observed in RR Lyrae, is explored, and it is shown that, for field distributions such that $H_{\text{central}}/H_{\text{surface}} \simeq 10^3$, changes of the period of a few per cent can be expected. A brief qualitative discussion of the effect of a strong magnetic field on a degenerate stellar core is given.

At the present time we do not have adequate theoretical models of the cluster-type variables, and their role in the evolutionary picture of population II systems is not clear. They lie quite near to the population I main sequence, but their energy sources and structures should be very different from main-sequence stars of the same luminosity (Hoyle and Schwarzschild 1955). At a particular stage, stars evolve into those of RR Lyrae type, which are very sharply defined in color and magnitude (cf. Roberts and Sandage 1955, for M3).

Recently H. W. Babcock (1956) discovered the existence of a large surface magnetic field in RR Lyrae itself. This immediately raises the interesting question of the possible role of the magnetic field as a factor in the evolution of stars in this part of the HR diagram. Two separate approaches can be distinguished: (*a*) the effect of the magnetic field on the periods of pulsation and (*b*) the role of the magnetic field in promoting instability and its effect in convection zones in regions of the HR diagram from the giant branch onward.

In this note, a preliminary reconnaissance mainly concerning approach *a* will be attempted. Without considering the magnetic field, the most determinate value of $Q = P\sqrt{\bar{\rho}/\bar{\rho}_\odot}$ is obtained from the observational data by using masses for the RR Lyrae stars of $1.25M_\odot$, which have been derived from evolutionary arguments based on the observed globular-cluster diagram for M3 (Sandage 1953), and a radius for RR Lyrae, obtained by Stebbins (1953) by means of Wesselink's method, of $5 \pm 0.6 \times 10^{11}$ cm. These values give

$$Q = 0.033^{+0.007}_{-0.005}.$$

Sandage (1956) has taken into account the change in emergent flux as a function of the effective gravity. He has shown that a theoretical value of Q of 0.041 obtained by Epstein (1950) is consistent with the observations both of the RR Lyrae stars in M3 and of RR Lyrae itself, if the stars in M3 are bluer by $\Delta(B - V) = 0.12$ mag. than main-sequence stars of the same effective temperature, and because RR Lyrae appears to be reddened by about $\Delta(B - V) \simeq 0.12$ mag. The large value of Q of about 0.060 used by some authors for RR Lyrae (cf. Savedoff 1953, Table 1; Ledoux, Simon, and Bierlaire 1955) can be traced to the use of a mass of about $3M_\odot$, which was computed by Kuiper's empirical mass-luminosity law. However, as has been implied by Savedoff (1953) in his concluding discussions, this is certainly incorrect for horizontal branch stars of population II.

Epstein concluded that the fundamental period is largely determined by the conditions in regions about $0.75R$ from the center. The recent calculations of Ledoux and his

collaborators (Ledoux 1955; Ledoux, Simon, and Bierlaire 1955) have shown that if it is assumed that the star has a very deep outer convective zone extending to a depth $r/R = 0.04$ and $\rho_c/\bar{\rho} = 1.198 \times 10^6$, then $Q = 0.056$. This value must be compared with 0.041, obtained by Epstein. It must also be remembered that the models of Epstein and Ledoux are those which have been computed to represent the classical cepheids, and it is unlikely that the classical cepheids, the population II cepheids (W Virginis stars), and the RR Lyrae stars are all homologous in their outer envelopes, so that we should not expect Q to be single-valued for all these types. Thus an adequate comparison between the observed and computed values of Q cannot be made with any degree of certainty at the present time. However, to show what the effects of the magnetic field may be, the model of Ledoux will be used for RR Lyrae in what follows.

A first approximation to the fundamental frequency $\sigma = 2\pi/P$ of a radially pulsating star was originally derived by using the virial theorem by Ledoux and Pekeris (1941). It is

$$\sigma^2 = -(3\gamma - 4)\frac{\Omega}{I}. \tag{1}$$

A similar approximate formula applicable when the star has a total magnetic energy, $\mathfrak{M}$, has been derived by Chandrasekhar and Limber (1954). It is

$$\sigma'^2 = -\frac{(3\gamma - 4)(\Omega + \mathfrak{M})}{I}. \tag{2}$$

Thus it is clear that if the presence of the magnetic field has a negligible influence on the values of Ω and I, i.e., if it does not alter the mass distribution for a particular model, and if γ remains unaltered, the period can be lengthened. However, it is well known that equation (1) and hence also equation (2) are good approximations only for a star having a fairly uniform mass distribution, while, for a high degree of central condensation such as we have here, the approximation is poor. In order partially to overcome this difficulty, we shall adopt the following procedure. Dividing equation (2) by equation (1), we find

$$\left(\frac{P}{P'}\right)^2 = 1 + \left(\frac{\mathfrak{M}}{I}\right)\left(\frac{I}{\Omega}\right). \tag{3}$$

Now in equation (3) we shall replace (I/Ω) not by its exact value computed for this particular model but by $\sigma_0^2/(3\gamma - 4)$, where σ_0 is the fundamental frequency computed by Ledoux *et al.* for their model. They find

$$\omega = \left(\frac{3\sigma_0^2}{4\pi G\bar{\rho}}\right)^{1/2} = 2.07,$$

so that $\sigma_0^2 = R^3/(GM)4.285$. Since $\gamma = \frac{5}{3}$,

$$\left(\frac{P}{P'}\right)^2 = 1 + \frac{\mathfrak{M}}{I}\frac{R^3}{(GM)\,4.285}.$$

Now $I = xR^2M = H^2M$, where H is the radius of gyration, so that

$$\left(\frac{P}{P'}\right)^2 = 1 + \frac{\mathfrak{M}}{4.285x}\frac{R}{GM^2};$$

and, if we substitute $M = 1.25M_\odot$ and $R = 5 \times 10^{11}$ cm for RR Lyrae, then

$$\left(\frac{P}{P'}\right)^2 = 1 + 2.80\,(10^{49}x)^{-1}\mathfrak{M}. \tag{4}$$

The mean effective surface magnetic field observed by Babcock is of the order of 1500 gauss (the sight-line component of the polar-field intensity would be about 5000 gauss if the field were of regular dipolar form), while the internal field distribution is completely unknown. It is probable that this distribution is very different from that of a decaying dipole field in a solar-type model with a conductivity distribution of the sort described by Cowling (1945), but this is the only case for which the total magnetic energy has been calculated (Wrubel 1952; Burbidge 1954). If the star normally has a convection zone, the presence of the field will affect the equilibrium of this zone, and the complicated effects found in systems in hydromagnetic equilibrium will be present. Also the concentration of the field toward the center may be quite great, whereas in the solar-type model the amplification between the center and the surface is of the order of 100. So, to get some idea of the possible changes in the period, three extremely simplified models in which no explicit assumptions about the type of field are made will be considered. We shall suppose (i) that $\mathfrak{M}$ has its lowest possible value corresponding to a mean field of 4000 gauss extending through the whole volume of the star; (ii) that, inside a radius such that $r/R = 0.1$, there is a uniform field $H = 100H_{\text{surface}}$, while the remainder of the volume has a mean field H_{surface}; (iii) that, inside a radius $r/R = 0.1$, $H = 1000H_{\text{surface}}$, while the remainder of the volume has a mean field H_{surface}. For these three cases $\mathfrak{M} = 3.33 \times 10^{41}$, 3.66×10^{42}, and 3.33×10^{45} ergs, respectively.

If we write equation (4) in the form

$$\left(\frac{P}{P'}\right)^2 = 1 + y, \tag{5}$$

then for cases i, ii, and iii, $y = 0.93\ (10^7x)^{-1}$, $1.03\ (10^6x)^{-1}$, and $0.93\ (10^3x)^{-1}$.

Without a detailed model for the RR Lyrae stars the radius of gyration and hence x cannot be computed. The most complete list of computations of this quantity for a series of models which approximate at all to the extremely centrally condensed ones are those of Motz (1952). He finds that $x \simeq 0.01$ for the models of Li Hen and Schwarzschild (1949) and Richardson and Schwarzschild (1948), which represent the classical cepheids and which have central condensation such that $\rho_c/\bar{\rho} \simeq 10^6$. The arguments of Hoyle and Schwarzschild suggest that the evolution of the RR Lyrae stars through a helium-burning phase and possibly a later degenerate core will lead to central condensations at least as great as this, and we cannot rule out the possibility that for these stars x will turn out to be less than 0.01. If we put $x = 0.01$ into equation (5), the corresponding changes in the period due to the influence of the magnetic field are such that $P/P' = 1.000005$, 1.00005, and 1.05 for cases i, ii, and iii. Thus, bearing in mind the considerable uncertainties in the approximations that we have been forced to make, we conclude that, unless $x \ll 0.01$, field distributions represented by case i or case ii will not affect the period by factors large enough to be detected. However, if the internal field is concentrated centrally to the extent proposed for model iii, when a change of period of about 5 per cent is produced, this may well be detectable. It is also clear that for a model of this sort the effect of the field on the structure of the static model should be investigated before solutions of the pulsation equation are attempted.

Finally, brief mention will be made of a possible instability effect which may be significant for stars on the giant branch in the HR diagram. If a magnetic field is present in the central regions, the existence of a degenerate core may lead to changes in the form and the strength of the field and also to instability while such changes are taking place. For in the degenerate core the transport of energy will take place predominantly by thermal conduction, which will be radially symmetrical if no field is present. If a strong field is present, however, the flow of heat by thermal conductivity will be reduced in the direction of the temperature gradient by a factor of $(1 + \omega^2\tau^2)^{-1}$, and a flow will be produced in the transverse direction which is $\omega\tau$ as large as the direct flow (Chapman and

Cowling 1939). Here $\omega = eH/m$ and $\tau = 3\lambda/5c_v p$, where λ is the thermal conductivity and c_v and p are the specific heat and pressure. The nonuniform energy flow which would be imposed in this way cannot be maintained. Either an instability will develop, or the currents generated by the electrons will modify the original field distribution. It is possible that the magnetic field may be amplified in this way at the expense of the nuclear or gravitational energy sources. This problem will be considered in detail elsewhere.

The author is indebted to Margaret Burbidge and Allan Sandage for a number of provocative comments and to H. W. Babcock for information concerning the magnetic field of RR Lyrae.

REFERENCES

Babcock, H. W. 1956, *Pub. A.S.P.*, **68**, 70.
Burbidge, G. R. 1954, *Ap. J.*, **120**, 589.
Chandrasekhar, S., and Limber, D. N. 1954, *Ap. J.*, **119**, 10.
Chapman, S., and Cowling, T. G. 1939, *Mathematical Theory of Non-uniform Gases* (Cambridge: At the University Press), p. 337.
Cowling, T. G. 1945, *M.N.*, **105**, 166.
Epstein, I. 1950, *Ap. J.*, **112**, 6.
Hoyle, F., and Schwarzschild, M. 1955, *Ap. J. Suppl.*, **2**, 1.
Ledoux, P. 1955, *Ann. d'ap.*, **18**, 232.
Ledoux, P., and Pekeris, C. L. 1941, *Ap. J.*, **94**, 124.
Ledoux, P., Simon, R., and Bierlaire, J. 1955, *Ann. d'ap.*, **18**, 65.
Li Hen and Schwarzschild, M. 1949, *M.N.*, **109**, 631.
Motz, L. 1952, *Ap. J.*, **115**, 562.
Richardson, R. S., and Schwarzschild, M. 1948, *Ap. J.*, **108**, 373.
Roberts, M., and Sandage, A. R. 1955, *A.J.*, **60**, 185.
Sandage, A. R. 1953, Liège colloquium: "Les Processus nucléaires dans les astres," *Mém. Soc. R. Sci. Liège*, sér. 4, **14**, 254.
———. 1956, *Ap. J.*, **123**, 278.
Savedoff, M. P. 1953, *B.A.N.*, **12**, 58.
Stebbins, J. 1953, *Pub. A.S.P.*, **65**, 118.
Wrubel, M. 1952, *Ap. J.*, **116**, 291.

ON SYNCHROTRON RADIATION FROM MESSIER 87

G. R. BURBIDGE
Mount Wilson and Palomar Observatories
Carnegie Institution of Washington, California Institute of Technology
Received April 23, 1956

ABSTRACT

The recent discovery by Baade that the optical radiation emitted by the jet in M87 is strongly polarized—and thus is synchrotron radiation—is a confirmation of a prediction made by Shklovsky and others. In this paper calculations of the required conditions of magnetic-field and particle energies are made, for both the optical and the radio emission. To account for the optical radiation in the jet, the total energy required in particles and field ranges from about 10^{54} to 10^{59} ergs for a series of assumed magnetic fields ranging from 10^{-2} to 10^{-6} gauss. To account for the radio emission for the same series of magnetic-field strengths, total energies in the range 10^{56}–10^{61} ergs are demanded. It is suggested that reasonable values are about 2×10^{55} ergs in particles and field, with $H \simeq 10^{-3}$ gauss, in the jet and about 10^{57} ergs in a volume 200 times greater than that of the jet, also with $H \simeq 10^{-3}$ gauss, which will explain the radio emission. By considering nuclear collisions of the high-energy protons with the static material present in the jet, it is shown that a continuous supply of electrons and positrons will be produced. If a density of about 3×10^{-22} gm/cc is assumed in the jet, the rate of electron-positron energy generation will be sufficient to balance the loss of energy by synchrotron radiation. The jet will also be a source of high-energy gamma radiation. Energy sources which might give rise to the primary particles and magnetic fields are discussed. It is suggested that the presence of antimatter in M87 would lead to a very powerful source of high-energy electrons and positrons.

I. INTRODUCTION

The observations by Baade (1956) of the polarization of the jet in M87 are convincing proof of the hypothesis that this optical radiation is synchrotron radiation emitted by relativistic electrons and positrons moving in magnetic fields in this region of the E0 galaxy. The prediction that this radiation might be polarized was made by Shklovsky (1955), who estimated some of the conditions necessary, and by Spitzer and Hoyle in unpublished discussions. In this paper we shall present some calculations leading to results which may be compared with the predictions of Shklovsky, and we shall discuss some of the implications of the results.

M87 is situated in the Virgo cluster, which has a mean red-shift velocity of 1136 km/sec (Humason, Mayall, and Sandage 1956). For a value of the Hubble constant of 180 km/sec/megaparsec (Humason *et al.* 1956) this gives a distance of 6.3×10^6 pc, which will be used for M87 in what follows. The dimensions of the jet are about 20″ by 2″, according to Baade and Minkowski (1954). Thus the linear dimensions are about 610 × 61 pc. The condensations in which Baade has detected about 30 per cent polarization lie near the end of the jet, which appears to extend all the way from the center of the galaxy (cf. the reproduction in the paper of Baade and Minkowski 1954), so that the effective large dimension may be less than 610 pc.

The absolute magnitude of the E0 galaxy is −19.2, so that it is one of the brightest of the known ellipticals. No accurate measures of the brightness of the jet are yet available. However, inspection of the plates suggests that it is comparable in brightness with the central region of M87 at a wave length near 4000 A. This central region probably has a luminosity near that of the center of M31, whose luminosity has been measured by Thiessen (1955). His curve shows that the luminosity is +17 mag/square second of arc. If we use this value for the jet, we find that its absolute magnitude is −16.0, if an area of 40 square seconds of arc is used. This value may be reduced if we suppose that only the condensations at the end of the jet with an area of 10 square seconds of arc are

effective. Then $M = -14.5$. It is clear that in the photographic region the jet is not much fainter than this, and it may be brighter. To determine accurately the energy emitted corresponding to these luminosities, it would be necessary to know the form of the spectrum in this range. In view of the uncertainties, we shall neglect the differences in the photographic region between the jet spectrum, which may be a power-frequency spectrum of the form $P(\nu)d\nu = k\nu^{-x}d\nu$, and that of a black body. With these assumptions, the total power obtained in comparison with the sun in the photographic region is given by

$$\log \int_{\nu_1}^{\nu_2} P\,d\nu = 33.587 + 0.4\,(4.62 + 19.2 + m)\ ,$$

where $m = M(\mathrm{M87}) - M(\mathrm{jet}) = -3.2$ or -4.7. Thus the total power $= 6.8 \times 10^{41}$ or 1.7×10^{41} ergs/sec if $M(\mathrm{jet}) = -16.0$ or -14.5. We shall suppose that this energy is emitted in a wave-length range $\lambda\lambda$ 4000–5500 corresponding to frequencies ν_2 and ν_1. We shall find it convenient to compute theoretically the power which will be radiated through the synchrotron mechanism at a frequency $\nu = 6.52 \times 10^{14}$ c/s ($\lambda = 4600$ A). Also a frequency-power spectrum of the form $P(\nu)d\nu = k\nu^{-x}d\nu$ will be assumed, where we shall put $x = 0.5$ and 1, respectively. For these two cases the equivalent band widths, $\Delta\nu$, such that

$$\int_{\nu_1}^{\nu_2} P\,d\nu = P_{(6.52\times 10^{14})}\Delta\nu$$

are 2.06×10^{14} and 2.08×10^{14}, respectively.

II. CALCULATION OF THE TOTAL ENERGY IN THE JET

The expressions for the power radiated and the critical frequency of radiation in the synchrotron mechanism have been given by Schwinger (1949) and others, and integrals similar to those needed here have already been used by Oort and Walraven (1956) in their analysis of the Crab Nebula. Thus only a brief treatment will be given here, since our discussion necessarily follows theirs quite closely.

The power radiated by an electron or positron of energy E per c/s moving in a magnetic field of strength H is given by

$$p\,(\nu) = 2.343 \times 10^{-22} H \sin\theta \frac{\nu}{\nu_c} \int_{\nu/\nu_c}^{\infty} K_{5/3}\,(\eta)\,d\eta\ , \tag{1}$$

where θ is the angle between the velocity vector and H. The critical frequency, ν_c, is given by

$$\nu_c = 6.269 \times 10^{18} H \sin\theta\, E^2 = 4.19 \times 10^{6} H \sin\theta\, \gamma^2\ , \tag{2}$$

where $\gamma = E/mc^2$. The radiation is totally polarized, with the electric vector parallel to the radius of curvature of the orbit, and it is emitted in a very sharp cone, with its axis the velocity vector and an angle of mc^2/E.

We shall suppose that the differential energy-spectrum of the electrons which give rise to the radiation is of the form

$$N\,(E)\,dE = KE^{-n}dE\ , \tag{3}$$

and we shall put $n = 2$ or 3.

If we define $\phi(\nu_c)$ as the number of electrons with critical frequency ν_c in a unit frequency interval about ν_c, then

$$\phi(\nu_c)\, d\nu_c = KE^{-n} dE\,; \tag{4}$$

and, using equation (2), we find

$$\phi(\nu_c) = \frac{K}{2}\, \nu_c^{-(n+1)/2}\, (kH_e)^{\frac{n-1}{2}}, \tag{5}$$

where $k = 6.269 \times 10^{18}$ and $H_e = H\langle \sin\theta \rangle_{\mathrm{av}} = H\pi/4$. The intensity of radiation at a particular frequency is

$$J(\nu) = \int_0^\infty P(\nu)\, \phi(\nu_c)\, d\nu_c\,. \tag{6}$$

If we now write

$$F(a) = a \int_a^\infty K_{5/3}(\eta)\, d\eta\,, \tag{7}$$

where

$$a = \frac{\nu}{\nu_c},$$

TABLE 1

ELECTRON ENERGIES NECESSARY TO PRODUCE RADIATION IN OPTICAL RANGE

H (gauss)	$E_c(\lambda = 4000$ A) (ev)	$E_c(\lambda = 5500$ A) (ev)	$E(\lambda = 4600$ A) (ev)	
			$a = 10$	$a = 0.01$
10^{-2}	6.84×10^{10}	5.84×10^{10}	2.02×10^{10}	6.37×10^{11}
10^{-3}	2.16×10^{11}	1.84×10^{11}	6.37×10^{10}	2.02×10^{12}
10^{-4}	6.84×10^{11}	5.84×10^{11}	2.02×10^{11}	6.37×10^{12}
10^{-5}	2.16×10^{12}	1.84×10^{12}	6.37×10^{11}	2.02×10^{13}
10^{-6}	6.84×10^{12}	5.84×10^{12}	2.02×10^{12}	6.37×10^{13}

and substitute from equations (1), (5), and (7) in equation (6), we find

$$J(\nu) = 1.1711 \times 10^{-22} K \left(\frac{\nu}{kH_e}\right)^{(1-n)/2} \int_0^\infty F(a)\, a^{(n-3)/2} da\,. \tag{8}$$

The function $F(a)$ for $0.001 < a < 10.67$ has been tabulated by Oort and Walraven, and they have pointed out that the following approximations can also be made:

$$a < 0.01\,, \qquad F(a) \simeq 2.15\, a^{1/3}\,;$$

$$a > 10\,, \qquad F(a) \simeq 1.26\, a^{1/2} \exp(-a)\,. \tag{9}$$

The electron energies which are demanded in order that ν_c may lie in the optical range have been computed from equation (2) for values of H_e ranging from 10^{-2} to 10^{-6} gauss. The energy limits outside which electrons will no longer contribute appreciably to the power emitted in the photographic range have been delineated by computing values of E_c from equation (2) for $a = 10$ and $a = 0.01$, where $\nu = 6.52 \times 10^{14}$ c/s. All these values are given in Table 1.

The integral in equation (8) has been evaluated by numerical integration for $n = 2$ and 3. Hence $J(\nu)$ has been determined for $\nu = 6.52 \times 10^{14}$ c/s. Now we have, from our previous estimate of the total power radiated,

$$J\,(\nu = 6.52 \times 10^{14}) = y \times 10^{41} \times (\Delta\nu)^{-1}\,, \tag{10}$$

where $y = 6.8$ or 1.7; $\Delta\nu = 2.06 \times 10^{14}$ for $n = 2$; and $\Delta\nu = 2.08 \times 10^{14}$ for $n = 3$. By substituting equation (10) in equation (8), we have determined K. We find that

$$\begin{aligned} &\text{If } n = 2\,, && K = y H_e^{-3/2} \times 1.999 \times 10^{45}\,; \\ &\text{If } n = 3\,, && K = y H_e^{-2} \times 2.689 \times 10^{43}\,. \end{aligned} \tag{11}$$

Now the total energy in the electrons is as follows:

$$\begin{aligned} \epsilon &= K \int_{E_1}^{E_2} \frac{dE}{E^{n-1}} \\ &= K \left(\frac{1}{E_1} - \frac{1}{E_2} \right) \qquad \text{when } n = 3\,, \\ &= K \log \left(\frac{E_2}{E_1} \right) \qquad \text{when } n = 2\,. \end{aligned} \tag{12}$$

TABLE 2

TOTAL PARTICLE AND MAGNETIC ENERGIES IN THE JET

H (gauss)	$\epsilon/y(n=3)$ (ergs)	$\epsilon/y(n=2)$ (ergs)	$(\epsilon/y)(M/m)$ $(n=3)$ (ergs)	$\mathfrak{M}$ (ergs)	Particle Energy Density $(\epsilon/y)(M/m)(1/\pi r^2 d)$ (ev/cc)
10^{-2}	8.3×10^{49}	6.9×10^{49}	1.5×10^{53}	2.1×10^{56}	1.8×10^{3}
10^{-3}	2.6×10^{51}	2.2×10^{51}	4.8×10^{54}	2.1×10^{54}	5.7×10^{4}
10^{-4}	8.3×10^{52}	6.9×10^{52}	1.5×10^{56}	2.1×10^{52}	1.8×10^{6}
10^{-5}	2.6×10^{54}	2.2×10^{54}	4.8×10^{57}	2.1×10^{50}	5.7×10^{7}
10^{-6}	8.3×10^{55}	6.9×10^{55}	1.5×10^{59}	2.1×10^{48}	1.8×10^{8}

We have put $E_1 = E_c$ when $\alpha = 10$ and $E_2 = E_c$ when $\alpha = 0.01$. From equations (11) and (12) we have computed ϵ/y for values of H_e ranging from 10^{-2} to 10^{-6} gauss. These values are shown in Table 2. Also included in this table are values of the total magnetic energy, $\mathfrak{M}$, which has been computed on the assumption that the jet has a cylindrical form with $l = 610$ pc and $r = 30.5$ pc, so that $\mathfrak{M} = H_e^2 r^2 l/8$. Most considerations regarding the origin of the particles in the jet lead us to believe that, besides the electrons and positrons, a large density of protons must also be present. Thus we have also included in Table 2 values of the total particle energy and energy density calculated on the assumptions that the protons have energies M/m times those of the electrons and that the numbers of protons and electrons are equal. This might be the case if they were both primary components accelerated together but would certainly not be true if the electrons and positrons arose as secondary particles. These points will be discussed more fuliy in Sections VI and VII. Before discussing the implications of these results, it is of some interest to consider the origin of the radio energy emitted by M87.

III. RADIO POWER EMITTED BY M87

M87 is well known as a strong radio source. However, there is no evidence that the radio source is localized on the jet. The source has been generally believed to have an angular diameter of about 5′ (Pawsey 1955), corresponding to a dimension of 9180 pc, and to be roughly coincident with the optical E0 galaxy. Measurements of the power received at 18.3, 60, 81.5, 100, 101, and 3200 Mc/s have been listed by Pawsey. These enable us to make an estimate of the form of the power-frequency spectrum. If this is written in the form $P(\nu) = k\nu^{-x}$, it is found that a unique value of x cannot be assigned to cover the whole of the observed range of frequencies. This is characteristic of other extragalactic sources (cf. Burbidge 1956). The two curves which give a reasonable fit are

$$P(\nu) = 3.23 \times 10^{11}\nu^{-1.3}, \qquad 1.83 \times 10^{7} < \nu < 2 \times 10^{8}$$

and

$$P(\nu) = 5.00 \times 10^{5}\nu^{-0.6}, \qquad 2 \times 10^{8} < \nu < 3.2 \times 10^{9}.$$

Here $P(\nu)$ is measured in units of 10^{-24} watt/m^2/c/s. Also $\nu = 2 \times 10^8$ has been chosen as a convenient point at which to join the slopes of two roughly determined curves. It has no other significance. We have now obtained the total power radiated in the radio spectrum by integrating these two curves between two *assumed* cutoffs, $\nu_1 = 10^7$ c/s and $\nu_3 = 3.5 \times 10^9$ c/s. This integration gives a total power output from the radio source of 5.1×10^{40} ergs/sec.

IV. CALCULATION OF TOTAL ENERGY NECESSARY TO PRODUCE RADIO POWER

To determine the total energy in the electrons necessary to produce the radio power, we proceed in a slightly different way from that used in Section II. The total energy emitted per second by an electron of energy E is given by

$$-\frac{dE}{dt} = 2.368 \times 10^{-3} H_e^2 E^2 = 1.58 \times 10^{-15} H_e^2 \gamma^2. \tag{13}$$

Thus, if the electron-energy spectrum is of the form

$$N(E)\, dE = K_1 E^{-m} dE, \tag{14}$$

the total energy emitted by the electrons per second is

$$5.1 \times 10^{40} = 2.368 \times 10^{-3} H_e^2 K_1 \int_{E_1}^{E_2} E^{-m+2} dE. \tag{15}$$

Now the total energy in the electrons, ϵ, is given by

$$\epsilon = K_1 \int_{E_1}^{E_2} E^{-m+1} dE, \tag{16}$$

where E_1, E_2, and E_3 have been determined from equation (2) by putting $\nu_1 = 10^7$, $\nu_2 = 2 \times 10^8$, and $\nu_3 = 3.5 \times 10^9$. These values are given in Table 3. The electron spectrum has been written in the form

$$N(E)\, dE = K_1 E^{-m_1} \qquad (E_1 < E < E_2),$$

$$N(E)\, dE = K_1 E_2^{(-m_1+m_2)} E^{-m_2} \qquad (E_2 < E < E_3).$$

By eliminating K_1 between equations (15) and (16), we find that

$$\epsilon = 2.154 \times 10^{43} H_e^{-2}$$
$$\times [(m_1 - 2)^{-1}(E_1^{2-m_1} - E_2^{2-m_1}) + E_2^{(-m_1+m_2)}(m_2 - 2)^{-1}(E_2^{2-m_2} - E_3^{2-m_2})] \quad (17)$$
$$\times [(m_1 - 3)^{-1}(E_1^{3-m_1} - E_2^{3-m_1}) + E_2^{(-m_1+m_2)}(m_2 - 3)^{-1}(E_2^{3-m_2} - E_3^{3-m_2})]^{-1}.$$

Since it is easily shown that the relation between the indices in the electron spectrum and in the power-frequency spectrum is $m = (2x + 1)$, we have put $m_1 = 3.6$ and $m_2 = 2.2$. The right-hand side of equation (17) has then been evaluated for H_e ranging from 10^{-2} to 10^{-6} gauss. These values are shown in Table 4. Also included in this table

TABLE 3

ELECTRON ENERGIES NECESSARY TO PRODUCE RADIATION IN THE RADIO-FREQUENCY RANGE

H (gauss)	E_1 (ev)	E_2 (ev)	E_3 (ev)	H (gauss)	E_1 (ev)	E_2 (ev)	E_3 (ev)
10^{-2}	7.9×10^{8}	3.5×10^{7}	1.5×10^{8}	10^{-5}	2.5×10^{8}	1.1×10^{9}	4.7×10^{9}
10^{-3}	2.5×10^{7}	1.1×10^{8}	4.7×10^{8}	10^{-6}	7.9×10^{8}	3.5×10^{9}	1.5×10^{10}
10^{-4}	7.9×10^{7}	3.5×10^{8}	1.5×10^{9}				

TABLE 4

TOTAL PARTICLE AND MAGNETIC ENERGIES TO PRODUCE THE RADIO EMISSION

H (gauss)	ϵ (ergs)	$(M/m)\epsilon$ (ergs)	$\mathfrak{M}$ (ergs)	$(M/m)(3\epsilon/4\pi r^3)$ (ev/cc)
10^{-2}	5.6×10^{61}	1.0×10^{65}	4.7×10^{61}	5.4×10^{-1}
10^{-3}	1.8×10^{63}	3.2×10^{66}	4.7×10^{59}	1.7×10
10^{-4}	5.6×10^{64}	1.0×10^{68}	4.7×10^{57}	5.4×10^{2}
10^{-5}	1.8×10^{66}	3.2×10^{69}	4.7×10^{55}	1.7×10^{4}
10^{-6}	5.6×10^{67}	1.0×10^{61}	4.7×10^{53}	5.4×10^{5}

are estimates of the total magnetic energy, $\mathfrak{M}$, computed on the assumption that the radio emission arises in a sphere of radius $r = 4590$ pc, so that $\mathfrak{M} = H_e^2 r^3/6$. We have also included in Table 4 total particle energies and energy densities computed by supposing that the protons have M/m times the energy of the electrons and that the numbers of protons and electrons are equal. Equation (17) has been used to calculate the total energy of the electrons in preference to one similar to equation (8), because the range of frequencies involved is such that $\nu_3/\nu_1 \gg 1$. In this case the slight inaccuracy present is due to the fact that we are neglecting electrons lower than E_1 and greater than E_3, which may contribute a small amount to the radio emission. On the other hand, we are also neglecting the radiation emitted slightly outside our chosen cutoffs by the electrons of energies E_1 and E_3. It is clear that ϵ is roughly proportional to the value of E_1^{-1}, so that this value is important in defining the minimum energy that the electrons can have. A conservative estimate has been made by putting $\nu_1 = 10^7$ c/s, since this is quite close to the lowest frequency 1.83×10^7 c/s for which measurements are available.

V. COMPARISON OF THE OPTICAL WITH THE RADIO SPECTRUM

It is of some interest to consider briefly whether the form of the frequency-power spectrum is compatible with the idea that both the optical and the radio emission arise from a unique electron spectrum, over most of the frequency range 10^7–10^{15} c/s. It has already been pointed out that the radio spectrum does not appear to be unique. However, the frequency-power spectrum $P(\nu) = 5.00 \times 10^5 \nu^{-0.6}$ for $2 \times 10^8 \leq \nu \leq 3.5 \times 10^9$ is rather uncertain, since the value 0.6 depends rather critically on one (low) value of the power measured at 32×10^9 c/s. Thus, for the time being, we shall ignore this relation and write

$$P(\nu) = k\nu^{-x} \qquad (\nu_1 < \nu < \nu_2)$$

and determine x for (*a*) $\nu_1 = 10^8$, $\nu_2 = 6.52 \times 10^{14}$, and (*b*) $\nu_1 = 3.2 \times 10^9$, $\nu_2 = 6.52 \times 10^{14}$. We have no observational knowledge concerning the spectrum within the optical range (previous dependences have been *assumed*), so we shall put $P(\nu = 6.52 \times 10^{14}) = 10^{41} \times y/(2.04 \times 10^{+14}) = 4.902 \times 10^{26} \times y$. With these assumptions, we find, for case *a*, $x = 0.62$ and 0.71 for $y = 6.8$ and 1.7; for case *b*, $x = 0.62$ and 0.73 for $y = 6.8$ and 1.7. Thus, despite all the uncertainties connected with the various aspects of the problem, it appears that an index between 0.6 and 0.7 would be sufficient to represent all the observations between $\nu = 10^{15}$ and 10^8 c/s, while an index of 1.3 would represent the observations between $\nu = 10^8$ and 10^7 c/s. Thus a unique electron spectrum with an index of -2.2 is indicated over most of the energy range. However, this index becomes more negative, reaching a value of -3.6 at the low-energy end. The energy ranges over which these indices are appropriate cannot be determined unless assumptions are made about the effective magnetic fields. These will be discussed in Section VII.

VI. NUCLEAR COLLISIONS IN THE JET

In Tables 2 and 4 we have tabulated the total energy in the particles on the assumption that the proton energy is M/m times that of the electrons and that protons and electrons are present in equal numbers. If both protons and electrons are of primary origin and if they have both been accelerated in the turbulent gas in the jet by induction-type mechanisms, of which the Fermi mechanism and the Swann betatron mechanism are examples, this procedure would be correct in the idealized case. However, it is well known that electrons are more difficult to accelerate by these mechanisms, because of their large energy losses in the low-energy region by bremsstrahlung and collisional ionization processes. Thus other mechanisms of electron and positron production must be considered. One of the most obvious assumptions is to suppose that they are of secondary origin and are produced as the end-products following nuclear collisions between high-energy primary protons and the nuclei at the kinetic temperature of the jet.

We shall suppose that the number-density of the material at kinetic temperature in the jet is n/cc. Now the lifetime for a high-energy proton between nuclear collisions in the jet is given by

$$\tau = \frac{1}{\sigma_A n_A c}, \tag{18}$$

where σ_A is the appropriate cross-section for collision. For proton-proton collisions we shall put $\sigma = 4 \times 10^{-26}$ cm^2, while for elements of atomic weight A, $\sigma_A = \pi r^2 A^{2/3}$, where $r = 1.4 \times 10^{-13}$ cm (this value of r may be an overestimate for very high-energy collisions). Thus, for p-p collisions,

$$\tau = \frac{8.33 \times 10^{14}}{n}, \tag{19}$$

and, for p–heavy-particle collisions,

$$\tau_A = \frac{5.41 \times 10^{11}}{n_A A^{2/3}}. \tag{20}$$

If we assume that normal cosmic abundances were present originally in the jet, it is clear that, except for $A = 4$, $n \gg n_A A^{2/3}$. Thus, although the total multiplicity of electrons and positrons may be greater for collisions involving heavy particles, in this approximation we can neglect their influence. However, equation (20) will be used when we discuss spallation. We shall suppose that the total proton energy is V ergs, and, to simplify the discussion, no specific proton-energy spectrum will be assumed, but we shall put

$$V = N\langle E \rangle , \tag{21}$$

where $\langle E \rangle$ is the mean energy of the primary protons such that the secondary electrons lie in the range to produce optical radiation. In a collision between two protons with total kinetic energy $\langle E \rangle \gg Mc^2$ the following particles and their decay products will be produced:

$$(a) \quad \pi^{\mp} \rightarrow \mu^{\mp} + \nu \rightarrow e^{\mp} + 3\nu ,$$

$$\pi^0 \rightarrow 2\gamma ;$$

$$(b) \quad \tau^{\mp} \rightarrow 2\pi^{\pm} + \pi^{\mp} \rightarrow 2\mu^{\pm} + \mu^{\mp} + 3\nu \rightarrow 2\,e^{\pm} + e^{\mp} + 9\nu ,$$

$$\theta^0 \rightarrow \pi^+ + \pi^- \rightarrow \mu^+ + \mu^- + 2\nu \rightarrow e^+ + e^- + 6\nu ;$$

$$(c) \quad p, \bar{p},$$

$$n \rightarrow p + e^- + \nu ,$$

$$\bar{n} \rightarrow \bar{p} + e^+ + \nu ;$$

$$(d) \quad \Lambda^0 \rightarrow p + \pi^- \rightarrow p + \mu^- + \nu \rightarrow p + e^- + 3\nu ,$$

$$\Sigma^+ \rightarrow p + \pi^0 \rightarrow p + 2\gamma ,$$

$$\Sigma^{\pm} \rightarrow n + \pi^{\pm} \rightarrow p + e^- + \mu^{\pm} + 2\nu \rightarrow p + e^- + e^{\pm} + 6\nu ,$$

$$\Xi^- \rightarrow \Lambda^0 + \pi^- \rightarrow p + 2\mu^- + 2\nu \rightarrow p + 2\,e^- + 6\nu .$$

Some of the hyperon-decay schemes listed under category d are still uncertain. The multiplicity of electrons can be estimated from the statistical theory of Fermi (1950). Although it is not in especially good agreement with experiment at energies not too far above the threshold, it should be a better approximation in the very high-energy region which we are considering here. Fermi considered only the production of π mesons and nucleons and antinucleons, since the particles in categories b and d had not yet been discovered. He showed that the multiplicities of π mesons, s_1, and of nucleons and antinucleons, s_2, were given by

$$s_1 = 0.54\sqrt{W}$$

and

$$s_2 = 1.30\sqrt{W} , \tag{22}$$

where

$$W = \sqrt{\frac{2\langle E \rangle}{Mc^2}} .$$

The greater number of nucleons and antinucleons is due to their greater statistical weight. Since the K mesons (τ, θ) have masses intermediate between π mesons and nucleons, they will have a lower threshold for production than nucleons and antinucleons. Their statistical weights are uncertain, but their presence will mean that their multiplicity will be increased at the expense of the other particles. The effect of the presence of hyperons is difficult to estimate and will be neglected.

We shall suppose that the total multiplicity of particles is still equal to $1.84\sqrt{W}$ but that the relative statistical weight of the K mesons relative to the nucleons and antinucleons is $\frac{3}{8}$. Then, from the decay schemes given here, we estimate that the total electron multiplicity, s_3, is given by

$$s_3 = 1.78\sqrt{W}, \tag{23}$$

and the total electron energy after a collision, E_t, is

$$E_t = \frac{0.16}{1.84}\langle E\rangle. \tag{24}$$

Thus the average electron energy, E_e, is given by

$$E_e = \frac{\langle E\rangle}{\sqrt{W}} \times 0.049. \tag{25}$$

TABLE 5

PRIMARY PROTON ENERGIES AND ELECTRON MULTIPLICITIES NECESSARY TO PRODUCE ELECTRONS WHICH WILL EMIT IN THE OPTICAL RANGE

H (gauss)	$E_e(\lambda = 4000$ A) (ev)	$\langle E\rangle$ (ev)	s_3	Mean γ-Ray Energy (ev)
10^{-2}	6.84×10^{10}	3.1×10^{13}	16	5.3×10^{11}
10^{-3}	2.16×10^{11}	1.5×10^{14}	23	1.7×10^{12}
10^{-4}	6.84×10^{11}	6.8×10^{14}	34	5.3×10^{12}
10^{-5}	2.16×10^{12}	3.1×10^{15}	50	1.7×10^{13}
10^{-6}	6.84×10^{12}	1.5×10^{16}	74	5.3×10^{13}

Here we have assumed that the total energy available is divided equally among all the particles produced and then equally among all their decay products. Values of E_e taken from Table 1 (corresponding to the production of optical radiation at λ 4000 A) have been used to calculate from equations (23) and (25) the electron multiplicities and energies of primary protons. These values are shown in Table 5.

With the assumptions we have made, the total energy available in a collision will be carried away in the following proportions: neutrinos, $\simeq$45 per cent; protons and antiprotons, $\simeq$35 per cent; electrons, $\simeq$10 per cent; and gamma radiation, $\simeq$10 per cent. It might be thought that the γ radiation emitted in the decay of the π^0 mesons would produce electron-positron pairs in the jet. However, the mean free path for γ radiation against pair production is about $6\times10^{25}/n$ cm, so that, unless $n \geq 10^4$, the major proportion of the γ rays will escape from the jet without producing pairs. Thus, if our assumptions are correct, the jet should be a source of γ rays emitting at a power level which is approximately equal to the rate of electron-energy production. It would be interesting to see whether the gamma radiation from M87 could be detected by the

cosmic-ray workers. Our calculations suggest that the intensity of gamma radiation to be expected would be 10^{-9}–10^{-11}/cm^2/sec at the top of the atmosphere. Average energies of the γ rays have been estimated and are given in Table 5.

From equations (19) and (21) we find that the total number of collisions taking place per second is given by

$$\frac{Yn}{\langle E\rangle \times 8.33\times 10^{14}},$$

and, from equation (24), the total energy in electrons produced per second is given by

$$Yn\times 1.044\times 10^{-16}.$$

Now, if there is to be no energy loss or gain,

$$y\times 10^{41} = Yn\times 1.044\times 10^{-16}$$

or

$$Y = \frac{9.58\times 10^{56} y}{n}, \tag{26}$$

where $y = 6.8$ or 1.7. Values of Y for a number of assumed values for n and the corresponding total mass of the jet are shown in Table 6. It is clear that the secondary production of electrons is an important effect, whether or not primary high-energy electrons were originally present.[1] The characteristic time scale, t_1, for the optical emission is of the order of $Y\times 10^{-41}$ seconds.

TABLE 6

ESTIMATED PROTON FLUX ENERGIES IF ELECTRONS AND PROTONS ARE PRODUCED IN NUCLEAR COLLISIONS

n	$Y(y=6.8)$ (ergs)	$Y(y=1.7)$ (ergs)	Mass of Jet (gm)	n	$Y(y=6.8)$ (ergs)	$Y(y=1.7)$ (ergs)	Mass of Jet (gm)
1	6.5×10^{57}	1.6×10^{57}	8.7×10^{37}	10^2	6.5×10^{55}	1.6×10^{55}	8.7×10^{39}
10	6.5×10^{56}	1.6×10^{56}	8.7×10^{38}	10^3	6.5×10^{54}	1.6×10^{54}	8.7×10^{40}

The other important time scale, t_2, is that for the electrons and positrons to lose an appreciable fraction of their energy by synchrotron emission. If there is no source of energy gain after the electrons and positrons have been produced, this time (t_2) will be given by the integral of equation (13). However, it is probable that, apart from the high-energy particles, the majority of the material in the jet will be in a state of hydromagnetic turbulence and that its turbulent energy will be roughly in equipartition with the magnetic energy. In this case we shall have

$$v^2 = \frac{3H^2}{8\pi\rho} = \frac{H^2}{n}\,7.16\times 10^{22}.$$

The electrons and positrons will therefore gain energy in Fermi collisions with the turbulent clouds, and this rate of gain is given approximately by

$$\frac{\delta E}{\delta t} = E\left(\frac{v}{c}\right)^2\frac{c}{l}, \tag{27}$$

[1] It is probable that the effect of nuclear collisions in the Crab Nebula will be important. This question will be considered elsewhere.

where l is the distance traveled between successive collisions. Thus, using equations (13) and (27) and substituting for v^2, we find that the net loss of energy is given by

$$-\frac{dE}{dt} = 1.58 \times 10^{-15} H^2 \left(\frac{E}{m c^2}\right)^2 - \frac{E H^2}{n l} \times 7.16 \times 10^{22} \text{ ergs/sec}.$$

If there is to be no energy loss,

$$l \leq 1.51 \times 10^{27} \frac{E}{n} \left(\frac{m c^2}{E}\right)^2. \tag{28}$$

Now, if we anticipate our concluding discussion and suppose that the total energies of the particles and the field are the minimum values obtained by interpolating in Table 2, we have $H = 10^{-3}$ gauss and $E = 2 \times 10^{11}$ ev. Thus, for $n = 10^2$ for no energy loss,

$$l \leq 3 \times 10^{13} \text{ cm}.$$

This value is extremely small and does imply that the turbulence in the jet has extremely fine structure. On the other hand, if we suppose that $l > 3 \times 10^{13}$ cm, then the time scale for the buildup process through nuclear collisions is governed by the fact that it must be less than t_2, which, for the values of E and H taken above, is of the order of 100 years. As well as implying that the jet is a very short-lived phenomenon, this also demands that the total energies involved in particles and field are greater than those obtained by interpolating in Table 2.[2] An estimate of the proton energy required can be made by supposing that the electron flux is built up in about 100 years. In this case we have

$$Y = 3.04 \times 10^6 \left(\frac{\epsilon}{n}\right),$$

and, if $H = 10^{-2}$ and 10^{-3} gauss, $n = 10^2$, $Y \simeq 2 \times 10^{56}$ and 7×10^{57} ergs, respectively. It is clear that if H were 10^{-3} gauss, the majority of the protons would rapidly escape from the jet. On the other hand, if the field were about 10^{-2} gauss, the total magnetic and particle energies would be approximately equal.

It remains to discuss briefly the possible spallation effects which may take place in the jet. These will continuously increase the relative abundances of the light elements at the expense of the heavier ones. One of the most interesting of the effects is the gradual building up of the lithium, beryllium, and boron group, which is extremely rare in the normal abundance-curve. The cosmic-ray work (Kaplon, Noon, and Racette 1954, and other references) suggests that in a spallation collision between a fast proton and a slow (thermal) carbon, nitrogen, or oxygen nucleus there is a large probability that a lithium, beryllium, or boron nucleus will be emitted. Thus from equations (20) and (21), putting $A = 16$, and $n(\text{C, N, O}) = 10^{-3}\, n$, we find that the approximate rate of production of lithium, beryllium, and boron is

$$\frac{dn}{dt}(\text{Li, Be, B}) = 2.15 \times 10^{-22} \langle E \rangle^{-1}/\text{cc}.$$

Since the minimum value of $\langle E \rangle$ is about 10 ergs (Table 5), it is clear that the rate of buildup relative to the "static" material is negligible. The fragments which are produced will, in general, have energies much lower than those of the colliding protons but much higher than those of the "static" material. The density of the fast particles is only

[2] If fine-structured turbulence were present, it is probable that the protons as well as the electrons would gain energy from the gas by a modified Fermi process. This would not be so efficient as the electron acceleration process, since, for protons having energies greater than 10^{13}–10^{14} ev, the radii of the proton orbits would be comparable with, or greater than, the value of l suggested here.

$(Y/\langle E\rangle \times 1.9 \times 10^{-62}$ cc, and if the carbon, nitrogen, and oxygen comprised 10^{-3} of this density, then the lithium, beryllium, and boron group would attain equilibrium with it in a time $t = 9 \times 10^{-42}\ Y$ seconds, i.e., a time comparable with the time scale for optical radiation. Deuterium will also be produced, but sufficient experimental evidence is not available to estimate its rate of production.

VII. DISCUSSION

The most remarkable result of the computations described in this paper is the tremendous amount of energy contained in the magnetic field and the charged particles which is necessary to explain both the optical radiation from the jet and the radio emission. The numbers which we have derived here can be compared with the total energy in cosmic radiation and magnetic field in our own Galaxy, which we estimate (assuming an energy density of about 1 ev/cc in the particles and a magnetic field $\sim 10^{-5}$ gauss) to be about 10^{54} ergs. As far as they can be compared, our results are in good agreement with the estimates of Shklovsky, who used a magnetic field of the order of 10^{-4} gauss and then estimated that the total particle energy should be about 10^{56}–10^{57} ergs.

If we suppose that in the jet there is rough equipartition between the magnetic and kinetic energy modes, then we can interpolate in Table 2 to obtain the total energy of the system. The result is that the total energy is about 2×10^{55} ergs, and the mean magnetic field is about 1×10^{-3} gauss. However, this is a minimum value of the energy, and the difficulties associated with the production of electrons and positrons if these values are assumed are discussed in Section VI. It may be that a larger value of the total energy of about 4×10^{56} ergs and a mean magnetic field of about 10^{-2} gauss are more reasonable. If a mean density of about 200/cc corresponding to a total mass of the jet of about 10^{-4} times that of the whole galaxy is assumed, the system may be in equilibrium for short time scales as far as the optical radiation is concerned. This condition depends both on the efficiency of Fermi collision processes and on the total proton energy. The equipartition condition between magnetic and turbulent kinetic energy demands that, for assumed values of H of 10^{-3} or 10^{-2} gauss, the turbulent velocities will be 150 or 1500 km/sec.

As far as the radio emission is concerned, two extreme possibilities can be considered: (i) We can suppose that the radio source is located in the jet alone, in which case, if we use the value of the magnetic field determined from the equipartition argument for the optical radiation, the total particle energy is about 5×10^{56} ergs; (ii) or we can suppose that the area of radio emission is spread over the whole volume, corresponding to an angular diameter of about 5′. In this case the minimum total energy demanded by the equipartition argument would be about 10^{58} ergs, with an effective magnetic field of about 10^{-4} gauss. It is possible that the radio emission arises in a volume greater than that of the jet but less than that of the whole galaxy. For example, if the volume were about two hundred times greater than that of the jet, the total energy would be about 10^{57} ergs equally divided between a magnetic field of about 10^{-3} gauss and the high-energy particles. It has been shown elsewhere (Burbidge and Burbidge 1956) that in the radio sources NGC 5128 and NGC 1316, which do not show non-thermal optical emission, energy sources of the same orders of magnitude must be present.

The origin of the particles giving rise to the radio emission is uncertain. Shklovsky has made the interesting suggestion that they have been degraded in energy in radiating in the jet and have then diffused outward. A second possibility is that they are also secondary and are being continuously produced in nucleon-nucleon collisions in a lower-energy range, though here the multiplicities are lower than those estimated for the jet and also the rate of interaction is much lower because of the smaller density of static material which must reasonably be inferred.

Equipartition of energy between magnetic field and material motion need not always

be assumed in systems of this kind. The balance will depend on the age of the system and the original energy source. It is clear that this type of indirect observation of great amounts of non-thermal energy may lead to revision of current ideas concerning the possible magnetic-field strengths, for example, in an early epoch of galactic formation. It may be that large fields—very much greater than those indicated by theoretical stability arguments and by indirect observational methods in our Galaxy ($\simeq 10^{-5}$ gauss)—are initially built in the very early stages of galactic evolution and that these later decay by hydromagnetic means, thus providing a source of turbulent kinetic energy. The role of stars in these processes is not understood. However, the large amounts of energy which Oort and Walraven have shown to be present in particles and field in the Crab Nebula are comparable on a stellar scale to those discussed here on a galactic scale, and in the case of the Crab Nebula the energy source may be connected with the "moving ripples" observed by Baade near the central star with velocities of the order of $c/5$.

It is clear that, in order to investigate this phenomenon more fully, extensive observing programs should be undertaken in an attempt to detect more objects showing the large degree of polarization characteristic of the synchrotron radiation. Thus, in addition to optical studies of known radio sources, if a strong non-stellar continuum is present, it would be worthwhile to investigate other galaxies which may not be detectable radio sources but which are chosen after preliminary study of their optical spectra. Since the synchrotron radiation may reach a maximum in any region of frequency, depending on the cutoffs and on the conditions of magnetic field and particle acceleration, all accessible regions of the spectrum, including, for example, the infrared, demand investigation.

Very few of the potential sources of energy which we know of in nature are comparable in magnitude to those present here. The kinetic energy of two galaxies in interaction with a relative velocity of about 1000 km/sec is about 10^{60} ergs, and the potential energy of a galactic mass is about 10^{59} ergs. The total amount of energy emitted in a supernova outburst is estimated to be 10^{49}–10^{50} ergs. Thus the total energy of about 10^7 supernovae would be demanded to explain the phenomena if stars were involved.

The mass equivalent of this energy is about 100–1000 $M_\odot$.

In some radio sources there is evidence of interaction between two galactic systems, suggesting that a fraction of the energy of collision, if it can be converted, is available as an energy source. However, there is no evidence that in M87 any collision process is taking place. It may be that the system is in the process of formation and that this is a process of energy loss which is required. It is very rich in globular clusters, and, by measuring the colors of some of these and comparing them with the globular clusters in our own Galaxy, it might be possible to make an estimate of the age of the system. The richness of M87 in globular clusters has led Shklovsky to suggest that perhaps the energy source arises in collisions between globular clusters. This possibility should be investigated further, in order to see whether the rate of collisions with the very small cross-sections for stellar encounters is sufficient. It is probable that at this epoch in its evolution the stellar population of the jet is small. The absence of stellar absorption lines in the jet spectrum suggests this. Also, if the total amount of radiation from stars in the jet were comparable to the amount of synchrotron radiation, the total degree of polarization would be small. This suggests that there are $\ll 10^{41}/10^{33}$ stars in the jet.

Finally, it remains to speculate on one other possible energy source—the presence of antimatter. If this were present in a separate galactic system, there is no known observational method which would enable us to detect it. However, theoretical arguments suggest that if antimatter were present in any gaseous medium with a density of the order of the interstellar density in our own Galaxy ($\simeq 10^{-24}$ gm/cc), its rate of reaction with the normal matter would be such that, in a time scale $\ll 10^9$ years, the constituent in the smaller proportion would be reduced to a negligible fraction. However, if in M87 a globular cluster consisting of stars completely composed of antimatter were captured

after it had been moving in the intergalactic medium, where the reaction rates are quite small, it would eventually collide with one of the globular clusters of normal matter. In this case very few stellar collisions would be made, but in a stellar collision the rates of the reactions would probably become so fast that the whole of the mass would be converted to mesons with energies of 10^8–10^9 ev and hence to electrons, positrons, neutrinos, and gamma radiation. This is not entirely certain, since it is possible that the pressures set up in the interactions between the outer regions of the stars would become so large that the remaining material would be separated again. The threshold for the production of nucleon-antinucleon pairs is too high for any proton or antiproton component to be produced in such an interaction, so that the total particle energy necessary to produce the synchrotron emission would be ϵ and not $\epsilon(M/m)$. The discussion given in Section VI would then become superfluous. Only one or two stellar encounters would be required to produce the electron-positron component, which would then have to be further accelerated, perhaps by the Fermi mechanism in the turbulent magnetic fields.

I am indebted to Dr. W. Baade for information concerning the observed polarization and to Dr. Margaret Burbidge, Professor R. F. Christy, and Professor R. P. Feynman for helpful criticism.

REFERENCES

Baade, W. 1956, *Ap. J.*, **123**, 550.
Baade, W., and Minkowski, R. 1954, *Ap. J.*, **119**, 215.
Burbidge, G. R., and Burbidge, E. M. 1956, *Ap. J.*, in preparation.
Fermi, E. 1950, *Prog. Theoret. Phys.*, **5**, 570.
Humason, M. L., Mayall, N., and Sandage, A. R. 1956, *A.J.*, **61**, 97.
Kaplon, M. F., Noon, J. H., and Racette, G. W. 1954, *Phys. Rev.*, **96**, 1408.
Oort, J. H., and Walraven, T. 1956, *B.A.N.*, **12**, 285.
Pawsey, J. L. 1955, *Ap. J.*, **121**, 1.
Schwinger, J. 1949, *Phys. Rev.*, **75**, 1912.
Shklovsky, I. S. 1955, *Astr. J. USSR*, **32**, 215.
Thiessen, G. 1955, "Les Particules solides dans les astres," *Mém. Soc. R. Sci. de Liège*, 4th sér., **15**, 411.

TWISTED MAGNETIC FIELDS

P. H. ROBERTS*
Yerkes Observatory, Williams Bay, Wisconsin
Received March 13, 1956

ABSTRACT

A study is made of the stability of a twisted tube of magnetic force lying within an infinitely conducting fluid. It is shown that the system is unstable.

I. INTRODUCTION

It is generally recognized that cosmical magnetic fields exist and may play an important role in astrophysical phenomena. In most cases the problem of how these fields may have been generated is unimportant, since the fields extend over such large regions that the time of their decay is comparable with the age of the universe. In some cases, however, Joule heat losses may not be neglected, and the question of how the magnetic fields are maintained against these losses must be answered.

One likely mechanism has been suggested by Larmor (1919). It supposes that the magnetic field is maintained by a self-exciting dynamo action. The mathematical difficulties involved in the investigation of this idea are great (see, e.g., a paper by Bullard and Gellman 1955), but it appears that some light may be thrown upon it by examining the stability of certain types of magnetic fields. In this connection, Jenson (1955) has examined the stability of a general toroidal field in a sphere of infinitely conducting fluid. He finds that the field is unstable to certain types of perturbation. The result of this instability may well be the generation of new magnetic lines of force, perhaps by the mechanisms suggested by Alfvén (1950). The existence of instabilities, particularly in the toroidal components of a magnetic field, may be regarded as necessary to the realization of a self-exciting field, although it is by no means certain that they will be sufficient to maintain its toroidal components (see Bullard and Gellman 1955, p. 219).

In this paper, two simple examples are chosen to demonstrate toroidal instabilities in a more clear-cut way than was possible in Jenson's more complicated model. In each case it will be supposed that the lines of force inside a cylinder of infinitely conducting fluid are circular helices of pitch $2\pi p$. In the first case, as an illustration, a limiting form of the boundary condition is used. In the second case, infinitely conducting fluid extends to infinity. Small perturbations are applied to the systems, and it is shown that each is unstable. In the first case the modes of maximum instability are examined. In certain respects, these problems are similar to some investigated by Dungey and Loughhead (1954).

II. THE CHOICE OF MODELS IN HYDROMAGNETICS

It is well known that the hydromagnetics of infinitely conducting fluids is easier to understand mathematically and pictorially than that of finitely conducting fluids: mathematically, because no external agency need be invoked to counteract Joule heat losses; pictorially, since lines of magnetic force can be visualized as being tied to the fluid particles in all their motions. Thus, when investigating a hydromagnetic phenomenon, it is convenient to assume that the fluids are infinitely conducting, provided that it is physically realistic to do so. For example, the process envisaged by Alfvén (1950) in his "twisted-kink" theory may be thought of in two parts: first, a bundle of lines of force are twisted until they become unstable; and, second, the kinks set up by the insta-

* Now at Atomic Weapons Research Establishment, Aldermaston, England.

bilities break away from the parent loop and form new loops. The breaking-apart of the lines of force visualized in the second part of this process is essentially a finite conductivity effect, since, at the end of the process, the lines of force pass through different fluid particles from those at the beginning. In investigating the first part of the process, not only is it permissible to consider that the fluid has infinite conductivity, but it is also desirable to do so, since the instabilities may thereby be clearly separated from the effects of natural decay.

The object of this paper is to investigate the formation of the instabilities mentioned. Some care must, however, be exercised in choosing the precise equilibrium system to be investigated. It should be realized that not all systems have any correspondence with reality, since some cannot be obtained by a limiting process from a system that could be set up in a finitely conducting fluid. This is illustrated by the following example.

Suppose that the region $|z| < l$ is filled with an inviscid fluid of density ρ and infinite electrical conductivity and that a uniform magnetic field of strength H is directed along the z-axis. Let two thin films of fluid, $z = \pm l$ and $r \leq R$, be rotated through an angle of l/p in opposite directions. Considering the lines of force to be attached to the fluid particles, it is seen that an equilibrium state is set up in which the components of particle displacement, $\boldsymbol{\xi}$, and magnetic field, $\boldsymbol{H}_0$, in a cylindrical co-ordinate system are, respectively,

$$\boldsymbol{\xi} = \begin{cases} \left[0, \quad \dfrac{rz}{p}, \quad 0\right] & (r \leq R), \\ [0, \quad 0, \quad 0] & (r > R), \end{cases} \tag{1}$$

$$\boldsymbol{H}_0 = \begin{cases} H\left[0, \quad \dfrac{r}{p}, \quad 1\right] & (r \leq R), \\ H\,[0, \quad 0, \quad 1] & (r > R), \end{cases} \tag{2}$$

and in which the hydrostatic pressure, $\mathfrak{P}_0$, is given by

$$\mathfrak{P}_0 = \begin{cases} \mathfrak{P}_\infty + \dfrac{H^2}{8\pi p^2}(R^2 - 2r^2) & (r \leq R), \\ \mathfrak{P}_\infty & (r > R). \end{cases} \tag{3}$$

A uniform current flows in the z-direction within the cylinder and returns along its surface. The presence of a current sheet is typical of problems involving infinitely conducting materials. Such a sheet cannot exist in a fluid of finite conductivity, σ. It is replaced by a thin layer of material through which the magnetic field changes rapidly. The currents flowing in this layer would diffuse outward, with a characteristic time of σR^2, and the system could be considered to be in equilibrium for times short compared with σR^2. Thus the model defined by equations (1)–(3) corresponds in some sense to a similar configuration in a fluid of finite conductivity; but, before any reality can be attached to the model, it must be shown that it is possible to set up motions or potential differences in a fluid of finite conductivity that will give rise to a configuration which, as $\sigma \to \infty$, is that of equations (1)–(3).

In a finitely conducting fluid the finite rotation of the two thin disks $z = \pm l$ and $r \leq R$ would only twist the tube of force momentarily. Once the rotation ceased, the lines of force would uncoil themselves and return to their initial positions. The only means of generating a permanent twist in the tube is to set up a uniform rotation of the disks and look for an equilibrium state in which the uncoiling effects of finite conductivity are balanced by the twisting effect of the moving disks. Such an equilibrium state must satisfy the well-known dynamo equation (see Bullard and Gellman 1955),

$$\operatorname{curl} \boldsymbol{H} = 4\pi\sigma\,(-\operatorname{grad}\phi + \boldsymbol{u} \times \boldsymbol{H}), \tag{4}$$

where

$$\operatorname{div} \boldsymbol{H} = 0 \,, \tag{5}$$

$$\operatorname{div} \boldsymbol{u} = 0 \,, \tag{6}$$

and the equation of hydrostatics,

$$\rho \boldsymbol{u} \cdot \operatorname{grad} \boldsymbol{u} = -\operatorname{grad} \mathfrak{P} + \boldsymbol{j} \times \boldsymbol{H} \,, \tag{7}$$

where ϕ is the electrostatic potential and $\boldsymbol{j}$ is the electric current (electromagnetic units have been used). Suppose that the disks are rotated in opposite directions with a peripheral velocity of U, which is much less than the Alfvén velocity V defined by

$$V^2 = \frac{H^2}{4\pi\rho} . \tag{8}$$

Equations (4)–(7) and the appropriate boundary conditions are satisfied by

$$\boldsymbol{u} = \begin{cases} \left[0 \,, \quad \dfrac{U r z}{Rl} \,, \quad 0\right] & (r \leq R) \,, \\ [0 \,, \quad 0 \,, \quad 0] & (r > R) \,, \end{cases} \tag{9}$$

$$\boldsymbol{H}_0 = \begin{cases} H\left[0 \,, \quad \dfrac{\lambda' r}{2R^3}(2R^2 - r^2) \,, \quad 1\right] & (r \leq R) \,, \\ H\left[0 \,, \quad \dfrac{\lambda' R}{2r} \,, \quad 1\right] & (r \geq R) \,, \end{cases} \tag{10}$$

$$\mathfrak{P}_0 = \begin{cases} \mathfrak{P}_\infty + \dfrac{\lambda'^2 H^2}{48\pi R^6}(R^2 - r^2)^2 (5R^2 - 2r^2) & (r \leq R) \,, \\ \mathfrak{P}_\infty & (r \geq R) \,, \end{cases} \tag{11}$$

where

$$\lambda' = \frac{U\pi\sigma R^2}{l} . \tag{12}$$

In the limit $\sigma \to \infty$, $U \to 0$, $\lambda' \to R/p$, $\lambda' \boldsymbol{u}/U \to \boldsymbol{\xi}$, the equilibrium state does not become the configuration of equations (1)–(3). It is only asymptotic to it for small r. The essential difference is the absence of the current sheet on $r = R$. In fact, it appears that no *equilibrium* state involving current sheets *within* an infinitely conducting fluid is realistic.

III. FIELD EQUATIONS AND BOUNDARY CONDITIONS

Consider an equilibrium state defined by

$$\boldsymbol{H}_0 = H\,[0, \, r\,g\,(r) \,, \, 1] \,, \tag{13}$$

$$\mathfrak{P}_0 = \mathfrak{P}_\infty + \frac{H^2}{4\pi} \int_r^\infty g \, \frac{d}{dr}(r^2 g)\, dr \,, \tag{14}$$

where $g(r)$ is everywhere continuous, finite, and vanishes at $r = \infty$ at least as $1/r^2$.

Suppose that when the system is perturbed the resulting magnetic field is

$$\boldsymbol{H} = \boldsymbol{H}_0 + \boldsymbol{h} \,. \tag{15}$$

On the usual hydromagnetic approximations, it can be shown that

$$\frac{\partial \boldsymbol{h}}{\partial t} = \boldsymbol{H}_0 \cdot \operatorname{grad} \boldsymbol{u} - \boldsymbol{u} \cdot \operatorname{grad} \boldsymbol{H}_0 , \tag{16}$$

$$\frac{\partial \boldsymbol{u}}{\partial t} = -\operatorname{grad} \varpi + \frac{1}{4\pi\rho} [\boldsymbol{H}_0 \cdot \operatorname{grad} \boldsymbol{h} + \boldsymbol{h} \cdot \operatorname{grad} \boldsymbol{H}_0] , \tag{17}$$

where

$$\rho\varpi = \mathfrak{P} - \mathfrak{P}_0 + \frac{1}{4\pi} (\boldsymbol{H}_0 \cdot \boldsymbol{h}) . \tag{18}$$

On introducing the particle displacement, $\boldsymbol{\xi}$, which, to the first order, satisfies the equation

$$\boldsymbol{u} = \frac{\partial \boldsymbol{\xi}}{\partial t} , \tag{19}$$

it is found that

$$\frac{\partial^2 \boldsymbol{\xi}}{\partial t^2} = -\operatorname{grad} \varpi + \frac{1}{4\pi\rho} (\boldsymbol{H}_0 \cdot \operatorname{grad})^2 \boldsymbol{\xi} - \frac{1}{4\pi\rho} (\boldsymbol{\xi} \cdot \operatorname{grad}) (\boldsymbol{H}_0 \cdot \operatorname{grad} \boldsymbol{H}_0) . \tag{20}$$

For displacements in which the last term vanishes, equation (20) reduces to an inhomogeneous wave equation. The system will be stable for all such disturbances, which will travel independently along lines of $\boldsymbol{H}_0$ with the Alfvén velocity V. For other displacements, the role of the last term is more complicated and requires detailed investigation. The third and fourth terms on the right-hand side of equation (20) play the same part as the second and first terms on the right-hand side of equation (24) of a paper by Lundquist (1951), who approached hydromagnetic stability problems in a somewhat different manner. On dividing equation (20) into components, it is found that

$$\frac{\partial^2 \xi_r}{\partial t^2} = -\frac{\partial \varpi}{\partial r} + V^2 \left[D^2 + 2 r g \frac{d g}{d r} \right] \xi_r - 2 V^2 g D \xi_\theta , \tag{21}$$

$$\frac{\partial^2 \xi_\theta}{\partial t^2} = -\frac{1}{r} \frac{\partial \varpi}{\partial \theta} + V^2 D^2 \xi_\theta + 2 V^2 g D \xi_r , \tag{22}$$

$$\frac{\partial^2 \xi_z}{\partial t^2} = -\frac{\partial \varpi}{\partial z} + V^2 D^2 \xi_z , \tag{23}$$

where

$$D = \frac{\partial}{\partial z} + g \frac{\partial}{\partial \theta} . \tag{24}$$

Suppose that ϖ has the form

$$\varpi = \varpi_0 (r) \exp i (\omega t + k z + m \theta) . \tag{25}$$

The other variables will then depend on t, z, and θ in the same way, and, on omitting the subscript zero, equations (21)–(23) give

$$\frac{\partial \varpi}{\partial r} = -\left[V^2 K^2 - \omega^2 - 2 V^2 r g \frac{d g}{d r} \right] \xi_r - 2 i K V^2 g \xi_\theta , \tag{26}$$

$$\frac{i m \varpi}{r} = -[V^2 K^2 - \omega^2] \xi_\theta + 2 i K V^2 g \xi_r , \tag{27}$$

$$i k \varpi = -[V^2 K^2 - \omega^2] \xi_z , \tag{28}$$

where

$$K = K(r) = k + mg . \tag{29}$$

Define Δ, a, b, c, and d by

$$\Delta = [V^2K^2 - \omega^2]\left[V^2K^2 - \omega^2 - 2V^2 r g \frac{dg}{dr}\right] - 4K^2V^4g^2 , \tag{30}$$

$$a = [V^2K^2 - \omega^2]\Delta^{-1} , \tag{31}$$

$$b = \left[V^2K^2 - \omega^2 - 2V^2 r g \frac{dg}{dr}\right]\Delta^{-1} , \tag{32}$$

$$c = 2KV^2 g\Delta^{-1} , \tag{33}$$

$$d = \Delta^{-1} = ab - c^2 . \tag{34}$$

The solutions of equations (26)–(28) may then be written

$$\xi_r = -\left[a\frac{\partial \varpi}{\partial r} + c\frac{m\varpi}{r}\right], \tag{35}$$

$$\xi_\theta = -i\left[c\frac{\partial \varpi}{\varpi r} + b\frac{m\varpi}{r}\right], \tag{36}$$

$$\xi_z = -\frac{ik\varpi}{[V^2K^2 - \omega^2]} . \tag{37}$$

But, to the first order, $\boldsymbol{\xi}$ is solenoidal, so that

$$\frac{1}{r}\frac{\partial}{\partial r}(r\xi_r) + \frac{1}{r}\frac{\partial \xi_\theta}{\partial \theta} + \frac{\partial \xi_z}{\partial z} = 0 . \tag{38}$$

It follows that

$$\left[ar\frac{\partial}{\partial r} - mc\right]\left[ar\frac{\partial}{\partial r} + mc\right]\varpi = (m^2 + k^2r^2)\,d\varpi . \tag{39}$$

On applying the condition that ϖ be bounded at the origin and vanish at least as $1/r$ at infinity, equation (39) determines ϖ uniquely and therefore, by equations (35)–(37), determines $\boldsymbol{\xi}$ also.

If V or $g'(r)$ or both are discontinuous across $r = R$, certain boundary conditions must be applied at that surface.

Case 1: V Continuous, g'(r) Discontinuous

Denote by $\boldsymbol{n}$ a unit normal to the disturbed surface. Denote the electric field by $\boldsymbol{E}$ and the total pressure by P, where

$$P = \mathfrak{P} + \frac{1}{8\pi}\boldsymbol{H}^2 . \tag{40}$$

The field equations demand that $\boldsymbol{H}$, $\boldsymbol{n}\times\boldsymbol{E}$, $\boldsymbol{n}\cdot\boldsymbol{j}$, $\boldsymbol{n}\cdot\boldsymbol{u}$, and P shall be continuous on the disturbed surface. These conditions are not independent.

If $\boldsymbol{H}$ is continuous, so are its tangential derivatives and therefore $\boldsymbol{n}\cdot\boldsymbol{j}$ also. Since $\boldsymbol{H}$ is parallel to the surface, it follows that

$$\boldsymbol{n}\times\boldsymbol{E} \equiv -\boldsymbol{n}\times(\boldsymbol{u}\times\boldsymbol{H}) = \boldsymbol{H}(\boldsymbol{n}\cdot\boldsymbol{u}) . \tag{41}$$

The condition on the electric field is therefore automatically satisfied by the condition on $\boldsymbol{n}\cdot\boldsymbol{u}$. Notice that equation (41) supports the conclusion already reached that current

sheets must be excluded from the interior of equilibrium configurations, since it shows that $\boldsymbol{n} \times \boldsymbol{E}$ could be made continuous across such sheets by demanding that $\boldsymbol{n} \cdot \boldsymbol{u}$ be zero on them, that is, the sheets could not be perturbed by any disturbance. (Because of an algebraic error, a result of this nature obtained by Roberts [1955] is incorrect.)

The equivalence of the conditions on $\boldsymbol{n} \times \boldsymbol{E}$ and $\boldsymbol{n} \cdot \boldsymbol{u}$ may also be seen in another way. If $\boldsymbol{n} \times \boldsymbol{E}$ is continuous, so are its tangential derivatives and therefore also $\boldsymbol{n} \cdot \operatorname{curl} \boldsymbol{E}$. The Maxwell equation

$$\operatorname{curl} \boldsymbol{E} = -\frac{\partial \boldsymbol{H}}{\partial t} \tag{42}$$

then implies that $\boldsymbol{n} \cdot \boldsymbol{h}$ and, by equation (16), $\boldsymbol{n} \cdot \boldsymbol{u}$ are continuous.

The change $\boldsymbol{h}^*$ in $\boldsymbol{H}$ *following the motion* is given by

$$\boldsymbol{h}^* = \boldsymbol{h} + \boldsymbol{\xi} \cdot \operatorname{grad} \boldsymbol{H}_0 = \boldsymbol{H}_0 \cdot \operatorname{grad} \boldsymbol{\xi} \,. \tag{43}$$

The condition that $\boldsymbol{H}$ be continuous across the disturbed surface is equivalent to the condition that $\boldsymbol{h}^*$ be continuous on the undisturbed surface, and, since $\boldsymbol{H}_0$ is tangential to the undisturbed surface, this requires $\boldsymbol{\xi}$ to be continuous on that surface in virtue of equation (43). This condition does not imply that $\boldsymbol{h}$ is continuous on $r = R$, but, in fact, h_r and h_z will be.

Continuity of P is equivalent to the same demand for

$$\mathfrak{P}_0 + \rho\varpi - \frac{1}{4\pi} (\boldsymbol{H}_0 \cdot \boldsymbol{h}) + \frac{1}{8\pi} (\boldsymbol{H}_0 + \boldsymbol{h})^2 \tag{44}$$

on the disturbed surface. To the first order, this requires the continuity of

$$\xi_r \left[\frac{d p_0}{d r} + \frac{H^2}{4\pi} r g \frac{d}{d r} (r q) \right] + \rho\varpi \tag{45}$$

on the undisturbed surface. Equation (14) shows that condition (45) is equivalent to the requirement that

$$\rho \left[\varpi - V^2 r g^2 \xi_r \right] \tag{46}$$

be continuous on $r = R$. This is automatically so, since the continuity of ϖ has already been realized by the continuity of ξ_z. Altogether, the boundary conditions reduce to two: namely, that ϖ and ξ_r be continuous on $r = R$.

Case 2: V Discontinuous

The author has shown in an earlier paper (Roberts 1955) that, when $\boldsymbol{H}_0$ is not parallel to the surface of discontinuity S, no current sheet is generated on S and consequently $\boldsymbol{h}^*$ must be continuous across it. When $\boldsymbol{H}_0$ is parallel to S, this argument breaks down, because the Lorentz force between the current sheet $\boldsymbol{J}$ and the field $\boldsymbol{H}_0$ acts at right angles to S and therefore does not produce infinite fluid accelerations in S. The hydromagnetic disturbances are propagated as surface waves along S, and a periodic surface current is generated on it. The boundary conditions are now that $\boldsymbol{n} \cdot \boldsymbol{H}$, $\boldsymbol{n} \times \boldsymbol{E}$, $\boldsymbol{n} \cdot \boldsymbol{u}$, and P shall be continuous and that the flow of current into any element of the current sheet, both perpendicular to the sheet and along the sheet itself, be zero.

As in case 1, the boundary condition on $\boldsymbol{E}$ is automatically satisfied by that on $\boldsymbol{n} \cdot \boldsymbol{u}$. Again, $\boldsymbol{n} \cdot \boldsymbol{H}$ is zero on the disturbed surface if ξ_r is continuous on the undisturbed surface. Expression (46) must be continuous on the undisturbed surface, and this requires the same of $\rho\varpi$. The conservation of current at the current sheet is automatically satisfied by the condition on $\boldsymbol{n} \cdot \boldsymbol{u}$. Altogether, the boundary conditions reduce to two, namely, that $\rho\varpi$ and ξ_r be continuous.

When empty space exists outside the cylinder, the boundary conditions may be derived from the case just discussed by taking the limit $V \to \infty$ for the region outside the cylinder.

IV. PARTICULAR CASES

Model 1

Consider, first, the model defined by

$$\boldsymbol{H}_0 = H\left[0, \quad \frac{r}{p}, \quad 1\right] \qquad (r \leq R), \tag{47}$$

$$\mathfrak{P}_0 = \frac{H^2}{4\pi p^2}(R^2 - r^2) + \text{constant} \qquad (r \leq R), \tag{48}$$

in which the conducting fluid occupies the interior of the cylinder.

It can easily be shown, from the theory of the last section, that

$$\varpi = AJ_m(\alpha k r) \qquad (r \leq R), \tag{49}$$

where

$$\alpha^2 = \frac{4K^2}{p^2[K^2 - (\omega^2/V^2)]^2} - 1, \tag{50}$$

$$K = k + \frac{m}{p} = \text{Constant}, \tag{51}$$

and $J_m(z)$ is a Bessel function of the first kind of order m. The boundary condition in this illustrative example will be taken to be $\varpi(R) = 0$:

$$0 = AJ_m(\alpha k R). \tag{52}$$

Denote by $j_{m,0}, j_{m,1}, \ldots$, the non-zero zeros of $J_m(z)$ in ascending order of magnitude. The frequencies $\omega_{m,n}$ associated with the wave lengths k and m are then given by equation (50). They are

$$\frac{j_{m,n}^2}{k^2R^2} = \frac{4K^2}{p^2[K^2 - (\omega_{m,n}^2/V^2)]^2} - 1. \tag{53}$$

The marginal stability of this particular mode is governed by

$$\frac{j_{m,n}^2}{k^2R^2} = \frac{4}{(m + kp)^2} - 1. \tag{54}$$

In examining these conditions, we may suppose, without loss of generality, that k is positive and m is an integer positive, negative, or zero. If mK is negative, the lines of equidisplacement are helices that are more closely wound around the axis than the undisturbed lines of force. For this reason, such modes might be called "winding modes." Similarly, disturbances of positive mK may be called "unwinding modes." The only modes relevant to Alfvén's twisted-kink theory are those for which m is $+1$ or -1, for these are the only ones for which the central axis of the cylinder moves. If $m = 1$, the axis uncoils itself into a negatively wound helix of pitch $2\pi/k$, while, if $m = -1$, the axis becomes a positively wound helix of the same pitch. If $m = -1$ and $kp < 1$, the perturbation belongs to an unwinding mode, even though the axis is wound into a positive helix. There is no contradiction in terminology here, as, under these circumstances, the

axis is wound less tightly around its undisturbed position than the undisturbed lines of force are.

Equation (53) shows that the system is unstable for all (k, m, n) modes satisfying the inequalities

$$-\frac{\lambda}{p} < K < \frac{\lambda}{p}, \tag{55}$$

where $\lambda = \lambda_{m,n}(k)$ is an increasing function of k defined by

$$\lambda = \frac{2kR}{\sqrt{[(kR)^2 + j_{m,n}^2]}}. \tag{56}$$

It is clear that if the mode (k, m, n_1) is unstable, so are all modes (k, m, n) for which n is less than n_1.

Remembering that k may not be negative, we may divide inequality (55) into three distinct cases:

A_1: $$-\lambda < m < \lambda .$$

Since $j_{m,n}$ is real, this cannot be satisfied unless $|m| < 2$. Instabilities then show themselves if

$$0 < kp < (\lambda - m) , \tag{57}$$

B_1: $$m < -\lambda .$$

Instabilities occur in these modes if

$$-(\lambda + m) < kp < (\lambda - m) , \tag{58}$$

C_1: $$m > \lambda .$$

These modes are always stable. It follows that the system is stable for all disturbances in which m exceeds 2.

The mode $m = 0$ shows instabilities of type A_1 for all p satisfying

$$\frac{p}{R} < \frac{2}{\sqrt{[(kR)^2 + j_{0,0}^2]}}. \tag{59}$$

If the cylinder is of infinite length, this implies that

$$R > \tfrac{1}{2} j_{0,0}\, p = 1.202p . \tag{60}$$

If the cylinder is finite and of length l, k cannot be less than $2\pi/l$, so that, for small l/R, for example, instabilities occur when

$$l > \pi p . \tag{61}$$

The mode $m = 1$ is stable for all kR less than $j_{1,0}/\sqrt{3} = 2.2122$, since, for these wave lengths, λ is less than m and case C_1 applies. If kR is greater than this value, the system will show instabilities of type A_1 if p is sufficiently small. The greatest value of p is attained when

$$kR = (2^{2/3} - 1)^{-1/2} j_{1,0} = 4.9995 . \tag{62}$$

This provides the condition

$$R > (2^{2/3} - 1)^{-3/2} j_{1,0}\, p = 8.5112p \tag{63}$$

for the existence of this type of instability in an infinite cylinder. If the length of the cylinder is less than

$$\frac{2\pi\,(2^{2/3}-1)^{1/2}}{j_{1,\,0}}R, \tag{64}$$

a more stringent condition applies. For small l/R, it takes the form

$$l > 2\pi p\ . \tag{65}$$

The mode $m = -1$ is always unstable for some k. If kR exceeds $j_{1,\,0}/\sqrt{3}$, the system is unstable for all p satisfying

$$\frac{p}{R} < \frac{2}{\sqrt{[(kR)^2 + j_{1,\,0}^2]}} + \frac{1}{kR}, \tag{66}$$

while, if kR is less than this value, p must also satisfy

$$\frac{p}{R} > \frac{-2}{\sqrt{[(kR)^2 + j_{1,\,0}^2]}} + \frac{1}{kR}. \tag{67}$$

However large p is, the system is always unstable for a sufficiently small value of k. An infinitely long cylinder is therefore always unstable to this mode. If the cylinder is of finite length, the maximum value of p at which instabilities can manifest themselves is

$$\frac{p}{R} = \frac{2}{\sqrt{[(2\pi R/l)^2 + j_{1,\,0}^2]}} + \frac{l}{2\pi R}. \tag{68}$$

For small l/R, this gives the condition

$$l > \frac{2\pi p}{3}. \tag{69}$$

If m is less than -1, case B_1 applies, and the system is always unstable for some values of k. If the pitch is large, these values of k are small, and, if the cylinder is of finite length, they may be impossible. This leads to the condition

$$l > \frac{2\pi p}{2-m}. \tag{70}$$

We will now investigate the modes of maximum instability, that is, those with the greatest value of $-\omega^2$. Equation (53) shows that

$$\left(\frac{\omega}{V}\right)^2 = K^2 \pm \frac{\lambda K}{p}, \tag{71}$$

from which it is immediately clear that

$$\left(\frac{\omega}{V}\right)^2 \geq -\frac{1}{p^2}. \tag{72}$$

We need only consider those cases in which the second term on the right-hand side of equation (71) is negative. For large negative m, inequality (58) shows that the system is unstable for modes in which kp is large. If m is sufficiently small, kR will also be large for these instabilities. Under these circumstances, equation (71) gives

$$\left(\frac{\omega}{V}\right)^2 \simeq K^2 - \frac{2\,|K|}{p\sqrt{(1+\gamma^2)}}, \tag{73}$$

where

$$\gamma = \lim_{m \to -\infty} \frac{j_{m,0}}{kR}, \tag{74}$$

and the kR in this definition of γ refers to the unstable band. The modes of maximum instability are those for which

$$|K| = \frac{1}{p\sqrt{(1+\gamma^2)}}. \tag{75}$$

On using the result (see Watson 1944, p. 516) that

$$\lim_{m \to \infty} \frac{m}{j_{m,0}} = 1, \tag{76}$$

we see, by combining equations (74) and (75), that

$$\gamma = \frac{p}{R}. \tag{77}$$

It follows that the most unstable modes are those for which

$$|K| = \frac{R}{p\sqrt{(p^2+R^2)}} \tag{78}$$

and that, for these, ω is given by

$$i\omega = \frac{VR}{p\sqrt{(p^2+R^2)}}. \tag{79}$$

When p/R is small, the modes of maximum instability have the same time constant for all values of m less than 2. In this case, $i\omega$ is given by

$$i\omega \simeq \frac{V}{p}, \tag{80}$$

in agreement with equation (79) derived for large negative m.

When p/R is large, the modes $m = 0$ and $m = 1$ are stable, while, for the others, the maximum time constants are given by

$$i\omega \simeq \frac{VR}{p^2} \frac{m}{j_{m,0}}. \tag{81}$$

It can be shown (see Watson 1944, p. 516) that $m/j_{m,0}$ is an increasing function of m. The modes of greatest instability are therefore those with the smallest m, and, for these,

$$i\omega \simeq \frac{VR}{p^2}, \tag{82}$$

in agreement with equation (79).

For intermediate values of p/R, the position is considerably more complicated. Write equation (71) in the form

$$\left(\frac{\omega}{V}\right)^2 + \left[\frac{R}{p\sqrt{(p^2+R^2)}}\right]^2 = \left[|K| - \frac{R}{p\sqrt{(p^2+R^2)}}\right]^2 + \frac{2|K|}{p}\left[\frac{R}{\sqrt{(p^2+R^2)}} - \frac{kR}{\sqrt{[(kR)^2 + j_{m,0}^2]}}\right]. \tag{83}$$

Using the fact that

$$j_{m,0} - |m| > 2\,, \tag{84}$$

we see that

$$j_{m,0} > \lambda - m \tag{85}$$

and that, consequently, by inequalities (57) and (58),

$$kp < j_{m,0} \tag{86}$$

for unstable modes. The right-hand side of equation (83) is therefore positive. It follows that

$$i\omega \leq \frac{VR}{p\sqrt{(p^2+R^2)}}\,. \tag{87}$$

Thus, for all values of p/R, the most unstable modes are those of the largest negative m.

Model 2

The model that has just been discussed is mathematically the simplest. It is not, however, relevant to the discussion of twisted fields imbedded in large bodies of fluid. To examine these, a model must be chosen in which conducting fluid is present outside the twisted cylinder of force. Consider, therefore, the model defined by

$$\boldsymbol{H}_0 = \begin{cases} H\left[0, \quad \dfrac{r}{p}, \quad 1\right] & (r \leq R)\,, \\ H\left[0, \quad \dfrac{R^2}{rp}, \quad 1\right] & (r \geq R)\,, \end{cases} \tag{88}$$

$$\mathfrak{P}_0 = \begin{cases} \mathfrak{P}_\infty + \dfrac{H^2}{4\pi p^2}(R^2 - r^2) & (r \leq R)\,, \\ \mathfrak{P}_\infty & (r \geq R)\,, \end{cases} \tag{89}$$

in which an infinitely conducting fluid of uniform density occupies the whole of space. It can be shown in the case of marginal stability that

$$\varpi = \begin{cases} A\left(k + \dfrac{m}{p}\right) J_m(\beta k r) & (r \leq R)\,, \\ B\left(k + \dfrac{mR^2}{pr^2}\right) K_m(kr) & (r \geq R)\,, \end{cases} \tag{90}$$

where A and B are constants, $K_m(z)$ is a modified Bessel function of the second kind of order m, and β is the value of α when $\omega = 0$, namely,

$$\beta^2 = \frac{4}{(m+kp)^2} - 1\,. \tag{91}$$

Continuity of ϖ and ξ_r requires that

$$AJ_m(\beta kR) = BK_m(kR)\,, \tag{92}$$

$$\frac{AJ'_m(\beta kR)}{\beta kR} + \frac{2mA}{(m+kp)}\frac{J_m(\beta kR)}{(\beta kR)^2} = -\frac{BK'_m(kR)}{kR}\,, \tag{93}$$

respectively. These equations are consistent if

$$\frac{J'_m(\beta kR)}{\beta kRJ_m(\beta kR)} + \frac{m(1+\beta^2)^{1/2}}{(\beta kR)^2} = -\frac{K'_m(kR)}{kRK_m(kR)}. \tag{94}$$

Denote by $\beta_{mn}(kR)$ the solutions to this equation in ascending order of magnitude,

$$\beta_{mn_1} > \beta_{mn_2} \quad \text{if} \quad n_1 > n_2 . \tag{95}$$

Equation (91) shows that the system is unstable for all (k, m, n) modes satisfying

$$-\frac{\Lambda}{p} < K < \frac{\Lambda}{p}, \tag{96}$$

where $\Lambda = \Lambda_{m,n}(k)$ is an increasing function of k defined by

$$\Lambda = \frac{2}{\sqrt{(1+\beta^2_{m,n})}}. \tag{97}$$

It is clear that, if the mode (k, m, n_1) is unstable, so are all modes (k, m, n) for which n is less than n_1.

We may divide inequality (96) into three distinct cases:

A_2: $$-\Lambda < m < \Lambda .$$

Since $\beta_{m,n}$ is real, this cannot be satisfied unless $|m| < 2$. Instabilities then show themselves if

$$0 < kp < (\Lambda - m), \tag{98}$$

B_2: $$m < -\Lambda .$$

Instabilities occur in these modes if

$$-(\Lambda + m) < kp < (\Lambda - m) \tag{99}$$

C_2: $$m > \Lambda .$$

These modes are always stable. It follows that the system is stable for all disturbances in which m exceeds 2.

The argument proceeds much as before. An infinitely long cylinder is always unstable for modes of negative m, no matter how large p may be. Criteria (60) and (63) for the presence of instabilities in the modes $m = 0$ and $m = 1$ are replaced, respectively, by

$$R > 1.2024p , \tag{100}$$

$$R > 3.0747p . \tag{101}$$

The system behaves in the same general manner as Model 1, and it may be conjectured that the modes of maximum instability are again those of the largest negative m. It does not seem possible to verify this without investigating equation (39) in the case $\omega \neq 0$ and

$$g(r) = \frac{R^2}{pr^2}. \tag{102}$$

No such simple solution as equation (90) is then possible.

V. CONCLUSIONS

A twisted cylinder of magnetic force is always unstable, but its instabilities do not show themselves in the manner conjectured by Alfvén (1950), although it is nevertheless possible that they could generate loops in a somewhat similar fashion.

I am grateful to Dr. S. Chandrasekhar for suggesting to me the problems investigated in this paper and for some interesting discussions about them. I am indebted to Drs. R. Hide and R. J. Tayler for some valuable suggestions. The research reported in this paper was supported in part by the Geophysics Research Directorate of the Air Force Cambridge Research Center, Air Research and Development Command, under contract AF 19(604)-299 with the University of Chicago.

REFERENCES

Alfvén, H. 1950, *Tellus*, **2**, 74.
Bullard, E. C., and Gellman, H. 1955, *Phil. Trans. R. Soc. London, A*, **247**, 213.
Dungey, J. W., and Loughhead, R. E. 1954, *Australian J. Phys.*, **7**, 5.
Jenson, E. 1955, *Ap. J. Suppl.*, Vol. **2**, No. 16.
Larmor, J. 1919, *Rep. Brit. Assoc.*, p. 159.
Lundquist, S. 1951, *Phys. Rev.*, **83**, 307.
Roberts, P. H. 1955, *Ap. J.*, **121**, 720.
Watson, G. N. 1944, *A Treatise on the Theory of Bessel Functions* (2d ed.; Cambridge: At the University Press).

ON AZIMUTHAL SOLAR MAGNETIC FIELDS*

V. C. A. Ferraro and P. C. Kendall
Queen Mary College, London, England
Received April 10, 1956

ABSTRACT

The theory of sunspot magnetic fields recently developed by Bullard (1956) and more briefly by Cowling (1946) is reviewed. It is shown that if the sunspot field is generated by convection to the surface of a subsolar azimuthal field, the magneto-mechanical forces arising from a field large enough to give rise to an observed sunspot field are considerable. They cannot be balanced by other forces or pressure gradients, and they would inevitably produce large-scale meridional motion in the sun far exceeding the observed "motion" of sunspots in latitude. This consideration seems to lead one to suppose that an azimuthal field in the subsurface layers is more likely to be produced by hydromagnetic waves.

I. INTRODUCTION

It has been suggested by Cowling (1946) and also recently by Bullard (1956) that the sun may possess a magnetic field with a large azimuthal or toroidal component and that when this component is convected to the surface by rising material, it produces a pair of sunspots. Such a toroidal field will arise, as was first pointed out by one of us (Ferraro 1937), if the sun possesses a general meridional magnetic field and the rotation of the sun is neither uniform nor in shells generated by the rotation of a magnetic line of force of the general field about the axis of rotation. The purpose of this note is to reconsider in some detail this theory of sunspots and, in particular, the effect of the mechanical forces arising from the action of the magnetic field on the currents.

It will be shown that these forces tend to set up a circulation in meridian planes unless opposed by other forces. In the absence of such forces the motion resulting from the generation of a toroidal field of the same order of magnitude as that of sunspots would be far more rapid than that which would result if one interpreted the "motion" in latitude of sunspots during a solar cycle as a true meridional motion; and there is, in fact, little evidence of meridional circulation in the sun. This suggests that the conclusions reached by one of us in an earlier paper are still cogent and that the law of isorotation must be true to a high degree of approximation in any region where the permanent magnetic field is regular, that is, the lines of force are simple closed curves in merdian planes. In this connection it is perhaps significant to note that sunspots are not observed in high-latitude regions where the solar field appears to be most regular and to simulate that of a dipole field.

II. THE GENERATION OF AN AZIMUTHAL SOLAR MAGNETIC FIELD

We first consider the generation of an azimuthal magnetic field due to the sun's rotation in a permanent magnetic field $\boldsymbol{H}_0$ whose lines of force lie in meridian planes. Neglecting displacement currents, the field equations are

$$\operatorname{curl} \boldsymbol{H} = 4\pi \boldsymbol{j}\,, \qquad \operatorname{curl} \boldsymbol{E} = -\frac{\partial \boldsymbol{H}}{\partial t}\,, \qquad \boldsymbol{j} = \sigma\,(\boldsymbol{E} + \boldsymbol{v} \times \boldsymbol{H})\,, \tag{1}$$

where $\boldsymbol{E}$ and $\boldsymbol{H}$ are the electric- and magnetic-field intensities, $\boldsymbol{j}$ is the current density, in e.m.u., σ is the electrical conductivity, and $\boldsymbol{v}$ is the velocity of the gas. Eliminating

* Published with the aid of a grant from the American Astronomical Society.

$\boldsymbol{E}$ and $\boldsymbol{j}$ between these equations, we obtain an equation for the magnetic field, $\boldsymbol{H}$, namely,

$$\text{curl curl } \boldsymbol{H} = -4\pi\sigma \frac{\partial \boldsymbol{H}}{\partial t} + 4\pi\sigma \text{ curl } (\boldsymbol{v} \times \boldsymbol{H}) . \tag{2}$$

Let $\boldsymbol{h}$ denote the azimuthal component of the magnetic field, so that we may write

$$\boldsymbol{H} = \boldsymbol{H}_0 + \boldsymbol{h} ; \tag{3}$$

introducing spherical polar co-ordinates (r, θ, ϕ) with the line $\theta = 0$ as axis of rotation, which is assumed to coincide with the axis of symmetry of the magnetic field, the equation div $\boldsymbol{H}_0 = 0$ shows that there is a stream function, U, such that

$$H_r = \frac{1}{r^2 \sin \theta} \frac{\partial U}{\partial \theta}, \qquad H_\theta = \frac{1}{r \sin \theta} \frac{\partial U}{\partial r} . \tag{4}$$

Since the velocity of the material is wholly azimuthal, we may introduce an angular velocity, $\boldsymbol{\Omega}$, such that

$$\boldsymbol{v} = \boldsymbol{\Omega} \times \boldsymbol{r} , \tag{5}$$

when $\boldsymbol{r}$ is the position vector of a field point relative to the center of the sun. Writing h for the magnitude of the azimuthal component of the field and $\mu = \cos \theta$, equation (2) becomes

$$\left(\frac{\partial^2}{\partial t^2} + \frac{1-\mu^2}{r^2} \frac{\partial^2}{\partial \mu^2} \right) (rh \sin \theta) = 4\pi\sigma \frac{\partial}{\partial t} (rh \sin \theta) + 4\pi\sigma (1-\mu^2) \frac{\partial (\Omega, U)}{\partial (r, \mu)} . \tag{6}$$

Some general considerations follow at once from this equation; suppose that d is a scale length characteristic of space variations and τ is a time scale characteristic of the time variations of the field. Then the order of magnitude of the left-hand side of this equation is h/d and that of the first two terms on the right-hand side is $4\pi\sigma hd/\tau$ and $4\pi\sigma\Omega H_0 d$, respectively; here H_0 denotes the order of magnitude of the permanent field. These three terms are, respectively, in the ratios

$$1 \ : \ \frac{4\pi\sigma d^2}{\tau} \ : \ \frac{4\pi\sigma\Omega d^2 H_0}{h} . \tag{7}$$

Now $4\pi\sigma d^2$ corresponds to the time of free decay of the magnetic field, h, extending over a region of space of linear dimension, d. Hence, if this time is large compared with τ, the term on the left-hand side of equation (6) is negligible; this means that we may treat the medium as if it were one of infinite conductivity. Further, the ratio of the remaining two terms must be of order unity, so that

$$\frac{h}{H_0} \sim \Omega\tau . \tag{8}$$

III. NUMERICAL ILLUSTRATION

As a numerical illustration of the orders of magnitude involved, we shall take $\sigma = 10^{-6}$ e.m.u., a value corresponding to the conductivity in the surface layers of the star, and $d \sim 10^{10}$ cm, a value comparable with the solar radius. This gives $4\pi\sigma d^2 = 1.26 \times 10^{15}$ sec, or nearly 4×10^7 years, which is large compared with the duration of a sunspot cycle; d would have to be considerably smaller than the dimensions of a sunspot (about 10^9 cm) for a decay time of the order of a duration of a sunspot cycle. Thus, in all cases of interest, we can treat the conductivity of the medium as infinite.

Since an axially symmetric magnetic field derived from a potential field has no azi-

muthal component, it follows that outside the sun this azimuthal component is zero; the internal azimuthal field must become vanishingly small near the surface and may not be observed there. Such a field will increase in intensity with depth at a rate depending on the electrical conductivity and the rate of deviation of the angular velocity, Ω, from isorotation. We have solved equation (6) in the special case when the permanent field, $\boldsymbol{H}_0$, is due to a dipole centered at the sun's center with its axis directed along the negative direction of the θ-axis and when the angular velocity varies according to the law

$$\Omega = \Omega_0 + \omega\,(t)\,\sin^2\,\theta\,, \tag{9}$$

where Ω_0 is the isorotational angular velocity and $\omega(t)$ is the variable part. This makes the angular velocity symmetrical with respect to the θ-axis and with the equator, as must be the case. Assuming that $\omega = \omega_0 e^{t/\tau_1}$, where ω_0 and τ_1 are constants, the solution, which will not be reproduced here, indicates that the toroidal field becomes appreciable at a depth L below the surface, of the order of $(4\pi\sigma/\tau_1)^{-1/2}$. Taking $\sigma = 10^{-6}$ e.m.u. and measuring τ_1 in years, we find L to be of the order of $1.6 \times 10^6 \sqrt{\tau_1}$ cm. Changes of polarities of sunspots from one cycle to the next could be explained either in terms of a meridional circulation, as was originally suggested by Bjerknes (1926) and more recently by Bullard (1956), or by a torsional hydromagnetic oscillation, as suggested by Plumpton and Ferraro (1955). In either case we may take τ_1 to correspond to the duration of a solar cycle, say 11 years. With this estimate of τ_1, we find L to be of the order of 5.44×10^6 cm, which is very small—smaller, in fact, than the dimensions of a granule; this estimate can be increased by decreasing σ or increasing τ_1, but it seems clear that, for time changes which are small compared with the decay time through resistance, the transition region in which the azimuthal component grows appreciably is small compared with a solar radius. Except in this transition region, the ratio of the intensity of the toroidal field to the field of the dipole H_0 is given by

$$\frac{h}{H_0} = 2\omega\tau_1 \frac{\sin^3\,\theta\,\cos\,\theta}{(1 + 3\cos^2\,\theta)^{1/2}}. \tag{10}$$

This formula shows that h changes sign as we cross the equator, as in Bullard's hypothesis. Also the ratio h/H_0 is of the order $\omega\tau_1$ (cf. eq. [8]), which represents the differential angle of rotation ϕ, say, corresponding to departure from isorotation. Sunspot motion in longitude indicates a variation of angular velocity corresponding to an equatorial differential velocity Δv of 0.01 km/sec (Cowling 1954), and it seems unlikely that this could be increased by more than a factor of order unity. Adopting 0.05 km/sec as a reasonable value for Δv, we find $\omega = 7.3 \times 10^{-8}$ rad/sec. Supposing that this variation in angular velocity takes place over a period of 11 years, we find $\tau_1 = 3.4 \times 10^8$ sec, whence $\phi = 24.8$ radians very nearly; thus $h/H_0 \sim 50$ at most, and, to produce an azimuthal field of 2000 gauss, we require H_0 to be at least 40 gauss. The surface value of the sun's magnetic field is of the order of a few gauss, so that, unless the magnetic field H_0 increases rapidly with depth, as seems unlikely, the sun's field could attain this value only in the deep interior. This raises an immediate difficulty unless we can raise the value of the ratio h/H_0 by increasing either or both of ω and τ_1.

IV. MECHANICAL FORCES ASSOCIATED WITH THE GENERATION OF AN AZIMUTHAL FIELD

General mechanical considerations, however, also seem unfavorable to the hypothesis of the generation of a large azimuthal field by dynamo action. If j_r and j_θ denote the radial and transverse resolutes of the current density vector (in a meridian plane) and H_r and H_θ denote the corresponding resolutes of the field $\boldsymbol{H}_0$, the mechanical force per unit volume has resolutes

$$h\,j_\theta - h\,j_r\,, \qquad j_r H_\theta\,, \qquad j_\theta H_r\,, \tag{11}$$

the first two being the radial and transverse resolutes in a meridian plane; the last (azimuthal) resolute will act so as to destroy the variation of angular velocity and has been discussed by Bullard. Using equation (10), we find

$$j_r = \frac{h}{4\pi r}(4 \cot \theta - \tan \theta), \qquad j_\theta = \frac{h}{2\pi r},$$

so that the mechanical force tending to set up a circulation in meridian planes is of the order of $h^2/2\pi r$. We shall underestimate this force if we take r to be equal to a solar radius. To illustrate the orders of magnitude involved, take $h = 2000$ gauss; the mechanical force is of the order of 10^{-5} dyne/cm^3, and, if the local density of the material is ρ, the acceleration produced in an element will be of the order of $10^{-5}/\rho$ cm/sec^2. In a time T the velocity acquired by the element would be $10^{-5}T/\rho$ cm/sec. Taking $T = 11$ years or 3.4×10^8 sec, this becomes $3400/\rho$ cm/sec. If one interprets the motion of sunspots in latitude as evidence of a meridional circulation, we should expect the meridional velocity to be of the order of 100 cm/sec. Since ρ is likely to be considerably smaller than unity in the surface layers, the mechanical forces are clearly too large. They cannot be balanced by pressure gradients, since they are not derived from a potential except in the unlikely event when the field depends solely on the distance from the axis. Hence we must suppose that they cannot be sustained. Nevertheless, a circulation could be set up in the interior of the sun and transferred to the surface layer by viscous forces. Such a circulation is likely to exceed the circulation in meridian planes produced by unequal heating at the equator and the poles, which is known to be excessively slow. But though electromagnetic forces may provide a more efficient mechanism in exciting a meridian circulation, these are likely to be confined to the deeper layers of the sun. In the surface layers the law of isorotation seems likely to be obeyed to a high degree of approximation. Hence, if an azimuthal field is produced in these layers, the mechanism is more likely to be that of hydromagnetic waves.

REFERENCES

Bjerknes, V. 1926, *Ap. J.*, **64**, 93.
Bullard, E. C. 1955, *Vistas in Astronomy* (London: Pergamon Press), p. 685.
Cowling, T. G. 1946, *M.N.*, **106**, 218.
———. 1954, *The Sun*, ed. G. P. Kuiper (Chicago: University of Chicago Press), chap. 8.
Ferraro, V. C. A. 1937, *M.N.*, **97**, 458.
Plumpton, C., and Ferraro, V. C. A. 1955, *Ap. J.*, **121**, 168.

A STUDY OF MAGNETIC MAPS OF THE SUN

MARION B. WOOD
National Bureau of Standards, Boulder, Colorado
Received October 29, 1955; revised April 25, 1956

ABSTRACT

Bipolar- and unipolar-type magnetic regions have been identified and related to other types of solar activity. Unipolar regions have been studied relative to the geomagnetic disturbance figure, Ap; no definite relationships could be recognized from the available data, and thus no identification of these regions with solar "M" regions could be established.

A study has been made of weak solar magnetic fields, using the magnetogram records of H. W. and H. D. Babcock. Their techniques for recording these weak, localized fields in the form of magnetic "maps" of the solar disk have been described in the literature (1953*a*, *b*, 1955*a*, *b*). They very kindly made their records available to us for independent study.

Our results are in general agreement with those of the Babcocks. We have observed the high-latitude polar fields and the low-latitude localized fields; these latter may be described as predominantly of bipole type (BM) or unipole type (UM). In studying the magnetograms, we traced around the peripheries of the important BM and UM regions, drawing them to the same scale as is used for the solar maps in the *High Altitude Observatory Quarterly Solar Activity Summaries*. These latter show the contours of the green and red coronal-line emission regions and the locations of sunspots, plages, and flares. One such map was made for each solar rotation. We then drew the outlines of the BM and UM regions onto the solar maps, forming composite pictures. These we placed one beneath the other, so that persistent regions appeared along vertical straight lines. We thus had a graphic method of identifying magnetic regions and studying their life-cycles in relation to associated optical activity. The maps were particularly useful in establishing in position and in life-cycle the correspondence of BM regions with the other forms of activity appearing on the solar maps, and they facilitated the observation of the growth of the UM regions out of the previously active areas, after the optically visible activity had died out. Each of the three major UM sequences was, in this manner, found to grow out of a previously active BM region.

Table 1 summarizes the individual magnetic regions, their development, and the appearance of associated optical phenomena. With the exception of one small BM area, all the regions that we studied exhibited the following general characteristics.

BIPOLE REGIONS (BM)

1. BM regions were found to lie in areas where other forms of activity were present, such as sunspots, flares, plages, and coronal intensity maxima. The strength of the bipoles corresponded roughly to the degree of such activity. The regions exhibited good position correspondence with the coronal maxima and calcium plage areas.
2. BM regions developed at about the same time as did other forms of activity, i.e., within a solar rotation thereof. It had been hoped (Billings 1954) that, if they preceded other evidences of activity, they would be of use in prediction work.
3. BM regions diminished with the dying-away of other activity.

UNIPOLE REGIONS (UM)

1. UM regions developed from the previously active BM regions and thus existed in those areas from which other forms of activity had disappeared. They were quite stable

TABLE 1

CMP DATES OF UM SEQUENCES *A*, *B*, AND *C*
(Antecedent BM* and Transition Stages Also Listed)

Sequence A

May 1, 1953:	BM region (53-J, 53-G), moderate intensity; no earlier magnetic records to determine whether the BM region appeared with the first optical appearance of the region.
May 28, 1953:	Strong, small BM (53-G); possible small weak UM on trailing edge.
July 22, 1953:	BM (53-G) had disappeared; strong, well-defined UM; no other polarities were present.
August 18, 1953:	Strong BM region (53-S) was evident; strong, well-defined UM on trailing edge.
September 15, 1953:	UM region was again the tail of a BM area (53-S), but now more widely separated from it; another BM (53-V) lay east of it; UM region was in the northern solar hemisphere, which was directed toward the earth.
October 11, 1953:	Moderate UM region, with other complex polarities in vicinity; in the northern hemisphere, which was oriented toward the earth.
November 7, 1953:	No UM region clearly recognized; new active region developed in vicinity (53-Y).

Sequence B

(This UM sequence lay rather symmetrically across solar equator during all its passages)

September 21, 1953:	Two BM regions (53-V, 53-Z); magnetic regions first appeared with the first passage of the active regions.
October 17, 1953:	Two BM regions (53-V, 53-Z).
November 12, 1953:	Fairly weak but well-defined UM region; no other polarities were present.
December 9, 1953:	Weak UM region; no other polarities were present.
January 5, 1954:	Well-defined UM region; no other polarities were present.
February 1, 1954:	Weak UM region, but well defined; no other polarities were present.
February 28, 1954:	Weak UM region; background of other polarities in vicinity.
March 27, 1954:	No observable UM region.

Sequence C

April 28, 1953:	Strong BM region in the north (53-H); no earlier magnetic records to determine whether BM appeared with first appearance of active region.
May 25, 1953:	BM region (53-H).
June 20, 1953:	Fairly intense BM region (53-H).
July 16, 1953:	Two very intense BM regions (53-H, 53-Q).
August 12, 1953:	Complex polarities; intense (53-H was still present in the north; 53-Q had disappeared).
September 7, 1953:	Three strong UM regions, with the region in the north the strongest (this was in the area of 53-H, which was still present but very weak in this passage); the northern region was in the hemisphere oriented toward earth.
October 4, 1953:	Two UM regions, with northern very intense; it was in the hemisphere oriented toward earth.
November 1, 1953:	Weak, poorly defined UM region (sensitivity low).
November 28, 1953:	Single, strong, well-defined UM region in the north; no other polarities were present.
December 25, 1953:	Strong, well-defined UM region; no other polarities were present.
January 22, 1954:	Strong, well-defined UM region; no other polarities were present.
February 18, 1954:	Whole disk magnetically disturbed; next passage showed growth of new active region (54-G).

* The antecedent BM stages are designated in parentheses by their corresponding identification codes for active solar regions (*High Altitude Observatory Quarterly Solar Activity Summaries*).

in position and maintained the same polarities throughout their lifetimes (usually several rotations).

2. The data on UM regions were insufficient to establish any clear-cut relationship between them and geomagnetic effects. Our attempt to relate unipoles to earth effects led us to question the generality of the tentative conclusions of the Babcocks (1955*a*, *b*) and of Simpson, Babcock, and Babcock (1955), who suggested that UM regions may be identified with the hypothetical solar "M" regions. These authors based their identification mainly on the recurrence, for several consecutive solar rotations, of a geomagnetic storm occurring about two days after successive central meridian passages of a strong UM region on the sun. The recurrences also of cosmic-ray maxima in time association with the UM region were noted by Simpson *et al.* (1955).

We wish to point out that, during the period studied, at least two other well-defined UM regions occurred that were not strongly related to any evident geomagnetic effects.

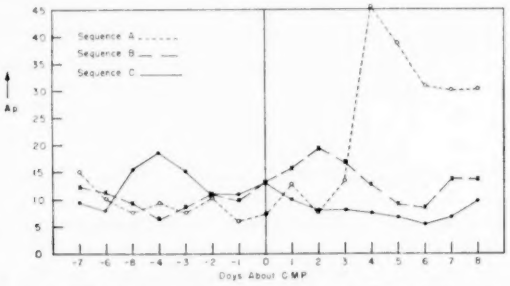

FIG. 1.—UM-Ap correspondence relative to CMP of UM regions

The relative magnetic-field intensities of these regions, their solar hemisphere positions, and descriptions of important neighboring polarities are given in Table 1. Figure 1 shows the relation of each of these major UM sequences (*A*, *B*, and *C*) to the geomagnetic figure, *Ap*, in a superposed epoch presentation. Sequence *A*, that studied by the Babcocks, showed a marked relation to geomagnetic disturbance about 4 days after CMP; sequence *B* showed a slight rise about 2 days after CMP; sequence *C* showed a slight rise about 4 days before CMP. It should be remarked that a single geomagnetic storm sequence was associated with the *Ap* rises following CMP of regions *A* and *B*. This storm sequence began at least three rotations before the appearance of UM region *A* and persisted for two rotations after its disappearance; these last two storm occurrences corresponded in time with the first two passages of UM region *B*, which developed as sequence *A* was dying out. The solar longitude of sequence *B* reached CMP about 3 days later than that of *A;* the *Ap* rise relative to CMP of sequence *B* (Fig. 1) was correspondingly earlier than that of *A* but was related to the same geomagnetic storm sequence. The rises in *Ap* relative to passages of UM regions *A* and *B* cannot, therefore, be considered as independent cases.

As Table 1 reveals, sequence *A* had three CMP dates during the fall equinox, when its position in the northern hemisphere was most nearly directed toward the earth. Such orientation is considered by Bell and Glazer (1954) to be favorable for producing terrestrial effects. (These authors were concerned solely with green coronal-line emission as related to geomagnetic disturbances, low values of the corona corresponding to high values of geomagnetic disturbance about 2 days after CMP.) At no time was there any other UM region near UM region *A;* however, for three of its passages, UM region *A* existed as a "tail" on a strong, well-defined BM region. Sequence *B* lay fairly symmetrically across

the equator and hence might be expected to have no equinoctial effect. It was weaker than *A*, but large and well defined. At no time were there other UM regions of opposite polarity in its vicinity. Sequence *C* was strong and well defined; however, during its passages up through October an opposite-polarity UM area was also present. By the November passage only the one polarity, in the northern hemisphere, remained; this was strong and well defined for three rotations. During these later passages it was not so directly oriented toward the earth as during the September and October CMP's. The characteristics of these three sequences just described lead us to believe that all of them should be included in any general study of UM-geomagnetic relationships.

In an attempt to test further for a possible relationship between UM regions and geomagnetic activity, we have gone back to solar and geomagnetic data for 1952 and early 1953, a period in which solar magnetograms were not yet available but for which "M"-region-type geomagnetic activity was most pronounced. Longitudes which had been active previously, but from which the optically visible activity had died, were studied

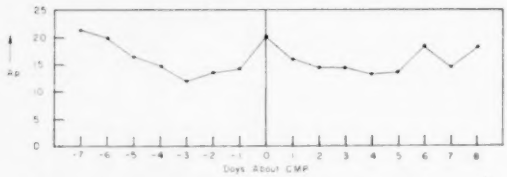

FIG. 2.—UM-Ap correspondence relative to CMP of hypothetical UM regions

relative to geomagnetic activity. No clear-cut relationship (see Fig. 2) was found, although the smallness of the data sample must be emphasized.

In view of the lack of consistent results from all three UM regions, we are led to doubt the generality of the relationship between UM region *A* and geomagnetic activity. Thus we consider the evidence inadequate for identifying UM regions with the hypothetical solar "M" regions.

I wish to express by appreciation to Dr. W. O. Roberts and Dr. D. E. Billings, of the High Altitude Observatory, for their interest in this work and their very helpful discussions during its course.

REFERENCES

Babcock, H. W. 1953*a*, *Ap. J.*, **118**, 387.
Babcock, H. W., and Babcock, H. D. 1953*b*, *The Sun*, ed. G. P. Kuiper (Chicago: University of Chicago Press), pp. 704–711.
———. 1955*a*, *Nature*, **175**, 296.
———. 1955*b*, *Ap. J.*, **121**, 349.
Bell, B., and Glazer, H. 1954, *J. Geophys. Res.*, **59**, 551.
Billings, D. E. 1954, *Ap. J.*, **120**, 184.
Simpson, J. A., Babcock, H. W., and Babcock, H. D. 1955, *Phys. Rev.*, **98**, 1402.
Solar Activity Summary, High Altitude Observatory of Harvard University and University of Colorado, quarterly reports for 1952, 1953, 1954.

THE TEMPERATURE AND EQUILIBRIUM OF HYDROGEN IN SOLAR PROMINENCES

HAROLD ZIRIN*
High Altitude Observatory
Received March 14, 1956

ABSTRACT

The Hα, Hβ, and D3 emission lines of solar prominences in active coronal regions have been photographed with the 16-inch coronagraph and high-dispersion spectrograph of the Upper Air Research Observatory, Sunspot, New Mexico. The Doppler profiles, after elimination of turbulent motion, give temperatures ranging from 7000° to 50000° K, depending on the nature of the prominence involved. The statistical equilibrium of hydrogen in a solar prominence at temperatures of 25000°–200000° is analyzed. Among the most important processes are found to be collisional excitation from the ground state and photoexcitation from the second level by photospheric radiation. Hardly any of the models are optically deep in Hα; the critical question turns out to be the Lyman-α depth; if this is large, the prominence radiates strongly in Hα, and vice versa.

I. INTRODUCTION

The temperatures and densities in solar prominences have been a matter of wide interest for a long time. Prominences are a phenomenon in the same space occupied by the corona, where the temperature is roughly 2000000° K; yet the fact that they exhibit hydrogen emission lines implies a much lower temperature than their surroundings. On the other hand, prominences are often seen, in Hα, to form by apparent condensation from the corona, a fact which implies a very high temperature in these cases. To measure physical conditions in prominences, many workers have studied the brighter emission lines from solar prominences. Several methods have been used to estimate temperatures from the emission lines, the two most common being the measurement of Doppler half-widths and the method of curve-of-growth analysis. It should also be possible to ascertain temperatures from the excitation of the various members of the Balmer series and from the intensity ratios of singlet and triplet helium (Zirin 1956*a*), as well as from the ratio of λ 4686 of ionized helium to the neutral helium lines (Zirin 1956*b*).

The Doppler half-width approach is both simple and easy and has therefore been employed by many workers. In recent years measurements of profiles and half-widths have been made by Conway (1952), Ellison (1952), Severny (1954), and ten Bruggencate (quoted by Unsöld 1955). Ellison computed that prominence temperatures fell in the range 10000°–20000°, with evidence from the shape of the profiles that the interior of the prominences was at a slightly higher temperature than the exterior, a somewhat puzzling conclusion in view of the fact that the exterior of the prominences is in contact with the million-degree corona. Severny finds a temperature of 14000° for a large, bright, quiescent prominence. Ten Bruggencate obtained a kinetic temperature of 14000° from Hα and helium D3 half-widths.

Aside from the ordinary instrumental problems, two sources of error are inherent in the Doppler profile method of half-width determination: first, the profile should be pure Doppler, with any possible self-absorption removed, and, second, one must be quite certain to compare identical points of the prominence in different lines.

The most detailed treatment of prominences from the curve-of-growth point of view has been made by Brück and Moss (1945). It is necessary in this treatment to make the

* This work was supported in part by the Air Force Cambridge Research Center, Geophysics Research Directorate, through contract AF 19(604)-146 with Harvard University and AF 19(604)-969 with the High Altitude Observatory.

assumption that the number of Hα-emitting atoms is proportional to the D3 intensity. For this to be true, two conditions must apply: (1) the prominence must be optically thin in D3, probably a reasonable assumption in general, and (2) the excitation of D3 must be the same as that of Hα, an assumption quite probably incorrect. In any event there were only two prominences, both very bright, in which Brück and Moss could distinguish between temperatures of 5000° and 30000°. In these two cases the temperature, granting the foregoing assumption with regard to D3, could be fixed at 5000°. Unsöld (1955) presents a curve of growth for $T = 3700°$ calculated by Bohm from the Brück and Moss data. The curve-of-growth method, therefore, suffers from three drawbacks: (1) the usual caveat that one must look at the same point in space for both lines, (2) the very shaky assumption with regard to D3, and (3) the fact that the curves of growth for different temperatures are distinguishable only for very bright prominences, and the method is therefore useless for most prominences.

Almost all this work, with either method, has been carried out on bright prominences of quiescent type, since they are usually large and relatively easy to observe. The study of the somewhat fainter prominences usually associated with strong solar activity, which display surges, streamers, and loops, requires the use of very low light-scattering systems, such as Lyot coronagraphs. Spectra for the study of the intensity variations of the emission lines of the corona, taken for a number of years at Climax, Colorado, and Sacramento Peak, New Mexico, also show the emission lines of prominences in regions of strong coronal activity, as well as elsewhere. Since the plates were all exposed for coronal emission lines, it is obvious that very faint prominences could be observed in this manner. Billings (1956) has recently reported on a number of prominences so observed. Reducing the Hα and D3 profiles, he reports temperatures ranging from 50000° to 200000° in regions of extremely high activity. Unfortunately, the resolution of the old Climax spectrograph was low; furthermore, since the plates had been exposed for the coronal lines, most of the prominence lines were overexposed, necessitating the measurement of the ghost images. On the other hand, the profiles measured by Billings were all much wider than the instrumental profiles, so wide, indeed, that they could not be attributed to instrumental effects. Furthermore, spectra of quiescent prominences yielded the same results as those of the other observers quoted previously, i.e., from 5000° to 15000°. Although the low temperatures from Billings' work are to be regarded as upper limits only, because of the low resolution, the fact that low temperatures are obtained verifies that the instrumental resolution of the old, Climax spectrograph was sufficient to distinguish "hot" from "cold" prominences.

A small forewarning of Billings' result is in the reports of measurements of streamers and surges from flares made at the McMath-Hulbert Observatory. Several papers (Dodson and Hedeman 1949; Dodson and McMath 1952; Dodson, Hedeman, and Chamberlain 1953) report bright flare prominences and surges with Hα profiles from 1 to 5 A wide. Since these were, no doubt, quite bright occurrences and no measures were made in any other spectrum lines, it is unfortunately impossible to guess how much of the width is due to gas kinetic motion and how much to other effects, such as microscopic turbulence and damping wings (curve of growth). Certain prominences are reported as brighter than the Hα disk, indicating an excitation temperature greater than that of the solar boundary.

The various observational results on prominence temperatures raise the following questions: (1) Will higher-resolution coronagraph spectra, taken explicitly for the purpose, substantiate the high temperatures obtained by Billings? (2) Granted that the observed rate of Hα emission is perfectly reasonable for 5000° prominences, under what conditions can we expect observable radiation in Hα from prominences at 50000° or 100000°?

Part II of this paper discusses some observational results obtained in an attempt to answer the first question; Part III examines the equilibrium of hydrogen from the theo-

retical standpoint, to see what the conditions must be for Hα emission at the temperatures discussed.

II. OBSERVATIONS OF ACTIVE PROMINENCES WITH THE U.A.R.O. SPECTROGRAPH

Through the kindness of Dr. John W. Evans, I have made use of the spectrograph of the Upper Air Research Observatory at Sacramento Peak, New Mexico, to observe and photograph the spectra of prominences. The 16-inch coronagraph produces a solar image about 10 inches in diameter on the head of the spectrograph, which has a dispersion of 0.6 A/mm. The instrumental profile is roughly 0.05 A in width and therefore negligible for this work. The program was to take successive spectra in Hα, D3, and Hβ of prominences in active regions.

Fortunately, every day of the 2-week observing period was clear, and there was appreciable green-line emission on the limb every day, signifying substantial solar activity. The spectra were taken only minutes apart, and the large scale of the instrument enabled me to pick out identical knots and formations in each spectrum. I traced the plates on the microphotometer of the High Altitude Observatory in Boulder. Standardization was carried out with a tube sensitometer.

The D3 line presents a special problem to high-resolution spectroscopic analysis because it is a multiplet, with two lines of separation 0.27 A and a relative intensity of 8:1 (actually, it is a triplet with two very close components). The apparent broadening, due to the merging of these lines, can be computed by making a number of model profiles for various temperatures. The effect is as large as 14 per cent for 40000°; since we obtain our final temperature by comparing the hydrogen and helium temperatures, the effect on the kinetic temperature can be still larger. The necessary correction has been applied to all D3 profiles given here.

Table 1 gives the temperatures determined from the measurements of line widths. The "apparent temperatures" in the fourth column are obtained directly from the individual profiles. The computed kinetic temperatures in the fifth column are obtained from the standard two-atom solution. The temperatures cover a wide range, which is not surprising, since prominences themselves cover a very wide range of regions and appearances. The highest temperature, 50000°, is less than the high temperatures obtained by Billings. On the other hand, Billings' observations were made in extremely active regions at the height of the solar cycle; the present work included only moderately active regions at a relatively low point in the cycle.

The question of self-absorption naturally arises in a discussion of prominence profiles. The Hα profiles used here are all approximately Gaussian, with a self-absorption of, at most, 10 per cent (i.e., the line is a Doppler profile with central intensity only 90 per cent) and usually none at all. By using a large scale, we have managed to separate individual prominence "fibers." The slit-width of 50 μ subtends only 1000 km on the solar image. Since the prominence is quite faint to begin with, we do not look through a large amount of matter.

The prominences recorded in Table 1 were, in general, in regions of strong green coronal activity but not otherwise particularly active, except for the hottest ones. We seem continually to get results between 15000° and 25000° for prominences of this type. It seems plausible that solar prominences occur with a great range of temperatures, from the 2000° mentioned by Öhman (1955) to the 200000° found by Billings. An extensive program of further spectroscopy is presently in progress at Climax.

III. THEORETICAL MODELS

On the basis of the data set forth in Table 1 it now seems logical to set up a series of prominence models with temperatures in the observed ranges. We have no knowledge of the electron densities and will therefore carry out the computations for various reason-

able densities. This will enable us to determine how dense a prominence must be to radiate sufficiently brightly to be observed in Hα at, for instance, 100000°.

Consider the following model: the prominence is a thread about 5000 km thick, of any length (for simplicity we shall consider a sphere, the only difference will be thickness along the axis), at temperatures from 10000° to 20000°, and at densities of from 10^9 to 5×10^{10} H atoms/cm^3. We consider the equilibrium of the five lowest levels of hydrogen, as well as the continuum. Calculations of this type have been carried out by many authors for hydrogen and helium under other conditions. Chamberlain (1953), for instance, considered the equilibrium of hydrogen in a nebula surrounding a hot star with an ultraviolet excess. In our case the star has no ultraviolet excess, but, because the

TABLE 1

TEMPERATURES OBTAINED FROM PROMINENCE SPECTRA TAKEN WITH THE U.A.R.O. CORONAGRAPH

Date (September, 1955)	Position Angle	Height above Limb (km)	Apparent Temperature (° K)		Computed Kinetic Temperature (° K)
			H	D3	
13	245°	14000	19000	24200	17270
		25000	17000	26720	13800
16	325°	Bottom	51670	56800	50000
		14000	27560	34700	23500
		25000	28630	58800	18600
		33000	27560	Too faint	.....
17	85°	Bottom	18150	44950	7400
			24800	37300	20600
			31960	40000	29380
			19730	Too faint	.....
18	290°	Bottom	Hβ 44700	64200	38200
		8000	.....	62200	.....
		22000	.....	34800	.....
21	270°	Bottom	23500	41200	38200
		11000	21000	28600	.....
		22000	14700	32600	.....
22	270°	Bottom	Hβ 31900	34800	30900
		7000	17900	24600	15600
		11000	.....	23200	.....

dilution is small (one-half), the radiation of the sun in the visible region becomes quite important. Otherwise our method of calculation is very similar to Chamberlain's.

The most important processes in hydrogen are found to be the following:

1. *Recombination in All Levels*

The formula (Cillié 1936) for the number of electrons captured by protons into the bound state of quantum number n per cubic centimeter per second is

$$N_k N_e F_{kn} = 0.329 \times 10^{-5} N_k N_e T^{-3/2} \frac{Z^4}{n^3} e^{X_n/kT} \left[-E_i\left(-\frac{X_n}{kT}\right)\right], \quad (1)$$

where N_k and N_e are proton and electron densities, respectively, and E_i is the exponential integral, F_{kn} is a recombination coefficient, and the other symbols have the usual meanings.

2. *Collisional Ionization by Electrons*

Collisional ionization by electrons is important only for ionization from the ground state, since the radiation lifetime of an excited state is much shorter than the collision interval for hydrogen. We use the Smith and Tate data (Mott and Massey 1949). Since these measurements were made on molecular hydrogen, they could well be very much in error in our application, but one really has no better source of information for the true cross-section. As long as these cross-sections are not in error by more than a factor of 2 or 3, they will not change our conclusions materially. A reasonable way to compute the collisional ionization rate, consistent with the unknown accuracy of the given values, is to approximate the Smith and Tate curve with a straight line from the threshold to the maximum cross-section and another straight line thereafter. If the cross-section rises from zero at 13.6 ev to πa_0^2 at 50 ev (a_0 is the Bohr radius), we obtain the ionizations per second per atom, $N_e C_{1k}$, by integrating the electron velocities over a Maxwellian distribution:

$$N_e C_{1k} = 4\pi^2 a_0^2 \left(\frac{m}{2\pi kT}\right)^{3/2} N_e \left\{ \frac{1}{36.4} \int_{(27.2a/m)^{1/2}}^{(100a/m)^{1/2}} \left(\frac{m v^2}{2a} - 13.6\right) v^3 e^{-mv^2/2kT} dv + \int_{(100a/m)^{1/2}}^{\infty} v^3 e^{-mv^2/2kT} dv \right\}. \tag{2}$$

For the relatively low temperatures in prominences, the second integral is essentially zero, and the upper limit on the first integral may be extended to infinity. Then the substitution $x^2 = mv^2/2kT$ leads to the collisional ionization rate with E_1 and kT both in electron volts:

$$N_e C_{1k} = 2.97 \times 10^{-12} N_e T^{1/2} e^{-E_1/kT} \left(\frac{E_1}{2} + kT\right) \text{sec}^{-1}\ \text{atom}^{-1}. \tag{3}$$

3. *Spontaneous Transitions between Levels*

The probabilities for spontaneous transitions between levels, the $A_{n'n}$, are given by Bethe (1933).

4. *Collisional Excitations from Ground State and Other Levels*

For excitation from the ground state we use the values quoted by Giovanelli (1948). He gives the following cross-sections:

$$\sigma_{1s2s} = \sigma_{1s2p} = \frac{4.8 \times 10^{-16}}{E^{1/2}} \text{ (in ev) cm}^2, \tag{4}$$

$$\sigma_{13} = 0.130\sigma_{12}, \tag{5}$$

$$\sigma_{14} = 0.035\sigma_{12}, \tag{6}$$

$$\sigma_{15} = 0.0113\sigma_{12}. \tag{7}$$

These values are based on the work of Ornstein and Lindemann and are supported by results quoted by Bates, Fundaminsky, Leach, and Massey (1950). The collision rate per atom per second is

$$N_e C_{1n} = N_e \int v \sigma_{1n}(v)\, f(v)\, dv; \tag{8}$$

in particular, the number of collisional excitations from the ground to the second state per atom per second is

$$N_e C_{12} = N_e 9.6 \times 10^{-16} \times 1.26\sigma \times 10^{-6} \sqrt{2} \cdot m^{-1/2} 4\pi \left(\frac{m}{2\pi kT}\right)^{3/2} \int_{(2E_2/m)^{1/2}}^{\infty} \frac{v^3}{v} e^{-mv^2/2kT} dv, \tag{9}$$

$$N_e C_{12} = N_e \cdot 5.69 \times 10^{-8} \frac{2}{\pi^{1/2}} \left(\frac{E_n}{kT}\right)^{1/2} e^{-E_2/kT} + 1 - \Phi\left(\frac{E_2}{kT}\right), \tag{10}$$

where $\Phi(x)$ is the probability integral. For the other levels one simply substitutes for E_2 in equation (10) and multiplies by the factor given in equations (4)–(7).

5. *Photoionization and Excitation*

The estimate of the Lyman continuum radiation of the chromosphere given by Woolley and Allen (1950) shows the photoionization by this source to be unimportant. Photoionization from excited levels by the photospheric continuum is, however, quite important when the population of these levels is large.

Let us assume that the black-body temperature of the sun in the Balmer continuum is 5500° and that in the Paschen and higher continua is 6000°. The continuous absorption coefficient for hydrogen is

$$a_n = \frac{1}{n^2} \frac{16\pi^2 Z^2 e^6}{3\sqrt{3} h^3} \frac{1}{\nu^3} \frac{Z^2}{n^3} 2R = 0.280 \times 10^{30} \frac{Z^4}{n^5} \frac{1}{\nu^3}. \tag{11}$$

The rate of photoionization per atom in level n per second, then, is (with a dilution factor of $\frac{1}{2}$)

$$F_{nk} = \tfrac{1}{2} \int_{\nu_n}^{\infty} \frac{cu_\nu}{h\nu} \times 0.285 \times 10^{30} \frac{Z^4}{n^5} \frac{1}{\nu^3} d\nu = 0.1425 \times 10^{30} \frac{8\pi}{c^2} \frac{Z^4}{n^5} \int_{\nu_n}^{\infty} \frac{1}{\nu} \frac{1}{e^{h\nu/kT} - 1} d\nu. \tag{12}$$

If $h\nu_n/kT \gg 1$ (as is the case for the important lower excited levels), the integral is closely approximated by $-E_i(-h\nu_n/kT)$. For higher levels, a series expansion (Peirce 1929) with Bernoulli's numbers and term-by-term integration is necessary.

For the models optically thin in the Balmer lines, it is necessary to include photoexcitation from the second level by the photospheric radiation field. We approximate the frequency distribution of energy in the photospheric field at a frequency removed by $\Delta\nu$ from the center of Hα by

$$u_\nu d\nu = \tfrac{1}{2} u_\nu^0 (6000) \times 0.9 \left[1 - 0.80 \exp - \left(\frac{\Delta\nu}{\gamma}\right)^2\right] d\nu. \tag{13}$$

The form of equation (13) roughly approximates the Balmer absorption lines near their center. The factor $\frac{1}{2}$ is a dilution factor (with no limb darkening); u_ν^0 is the Planck inten-

sity; and $\gamma = 0.928 \times 10^{11}$. Then the rate of transitions $2 \rightarrow n'$ per atom in the second state per second is

$$F_{2n'} = 0.45 u_{\nu}^{0}(6000) B_{2n'} \frac{1}{\sqrt{\pi}\,\Delta\nu_D} \int_{-\infty}^{\infty} \left[1 - 0.8 \exp -\left(\frac{\Delta\nu}{\gamma}\right)^2\right] \exp -\left(\frac{\Delta\nu}{\Delta\nu_D}\right)^2 d\nu \quad (14)$$

$$= 0.1125 n'^2 A_{n'2} e^{-h\nu_n/kT}\left[1 - \frac{0.8\gamma}{(\gamma^2 + \Delta\gamma_D^2)^{1/2}}\right], \quad (15)$$

where $A_{n'2}$ is the spontaneous transition probability, ν_n is the frequency of that transition, and $\Delta\nu_D$ is the Doppler displacement due to the thermal motion of the excited atom. At 50000°, for instance, the rate of absorption of Hα per atom in $n = 2$ per second is 3.09×10^5 photons per second.

6. *Self-absorption*

In the models computed, self-absorption turns out to be important principally in Lyman-α, Lyman-β, and Hα. We can look at this in two equivalent ways: suppose that the prominence knot is entirely uniform and edge effects are negligible. Then we can compute the number of upward transitions per cubic centimeter produced by the radiation of the entire sphere of prominence material in the line in question. Or, alternatively, we may assume that each photon emitted in the prominence traverses, on the average, the radius of the prominence and then compute the total absorption along the path length. In either case we get the same result. The self-absorption per cubic centimeter per second per atom in state n is

$$F_{nn'}^{(SA)} = N_{n'} A_{n'n} l_{nn'}, \quad (16)$$

where

$$l_{nn'} = \frac{l}{2} \frac{h\nu}{c} B_{nn'} \int_{-\infty}^{\infty} \frac{1}{\pi} \frac{\exp - 2\,(\Delta\nu/\Delta\nu_D)^2}{(\Delta\nu_D)^2} = \frac{n'^2}{n^2} \frac{\lambda_{nn'}^3 A_{n'n} l}{16\pi^{3/2}} (m/kT)^{1/2}, \quad (17)$$

where we have taken into account the Doppler emission and absorption profiles. When the self-absorption $N_n F_{nn'}^{(SA)}$ from a level equals the rate of spontaneous emission in the opposite direction, the radiation processes disappear from the equations (see eq. [18]), and the equilibrium is governed by collisions only. Neglect of the photons escaping at the edge exaggerates the self-absorption, but not significantly.

7. *Triple Collisions*

The process of triple collisions, the inverse of collisional ionizations, is slow and is therefore ignored here.

The equations of statistical equilibrium for $n > 1$ have the following form:

$$\sum_{n'=1}^{n-1} N_{n'} F_{n'n} + N_1 N_e C_{1n} + N_e^2 F_{kn} + \sum_{n''=n+1}^{\infty} N_{n''} A_{n''n} = N_n \sum_{n''=n+1}^{\infty} F_{nn''} + \sum_{n'=1}^{n-1} N_n A_{nn'} - N_{n'} F_{n'n}^{(SA)} + N_n F_{nk}, \quad (18)$$

where $F_{n'n}$ is the rate of radiative absorptions of photospheric radiation per atom causing transitions from n' to n, and the A's are Einstein coefficients. All the sums in equa-

tion (18) simplify considerably for each particular level. The first sum on the left is the absorption of photospheric radiation and is significant only for $n' = 2$. Similarly, the first term on the right is important only for $n = 2$, since that is the only level absorbing in the range of maximum photospheric radiation; and $F_{n'n}^{(SA)}$ is significant only for $n = 1$ and $n = 2$. When the prominence becomes optically thick for the transition $n \rightarrow n'$, the term in brackets on the right vanishes, and the equilibrium is determined essentially by collisions. The term $N_n F_{nk}$ is important only for the ionization equilibrium. The equation for statistical equilibrium between the continuum and the bound states will balance collisional ionization from the ground state plus photoionization from upper states against all recombination. It is

$$N_e^2 \sum_{n=1}^{\infty} F_k = N_1 N_e C_{1k} + \Sigma N_n F_{nk} , \tag{19}$$

where we have let $N_k = N_e$. In the sum on the left it turns out fairly accurate to sum to $n = 10$ and approximate roughly the remaining terms.

We can now calculate the occupation numbers of the various states by means of equations (18) and (19). Table 2 gives the occupation numbers per cubic centimeter for each level for a series of temperatures and densities. The hottest models are optically thin in all lines; in these cases the upper levels are excited principally by collisional excitation from the ground state. The somewhat cooler and denser models are optically thick in Lyman-α; therefore, they have a large population in $n = 2$, and the principal source of atoms for higher levels is excitation by the photospheric radiation from $n = 2$. These models radiate quite strongly in Hα. Finally, the coolest and densest models are optically deep in Hα. This makes the computation of occupation numbers, intensities, etc., very complicated, and we have not presented any values for these cases. It must be noted that our use of the term "optically deep" applies to the self-absorption integrated over the entire line. Thus, if the optical depth at the line center were unity, the averaged, or integrated, optical depth would be $1/\sqrt{2\pi}$.

Table 2 also gives the brightness in Hα emission (ergs per square centimeter per second) from a sphere of gas 5000 km in diameter. We may compare this with 2.2×10^5 ergs/cm/sec, estimated by Ellison (1952) for a large, bright, quiescent prominence of area 0.002 of the solar disk—much larger than the sphere that we have assumed.

Although there is no precise photometry available, the prominences in the active regions we have discussed are generally fainter than the bright, quiescent prominences by a factor of 10–100. Thus it appears from Table 2 that hydrogen at 10^5 degrees or higher will radiate quite satisfactorily at no excessive densities. In the case of "coronal rain" and looped prominences, it appears that the material condenses from the corona, and first becomes visible at about 10^5 degrees. Thereafter it cools even more rapidly by radiation.

In this work we have purposely neglected the effects of back-radiation from the corona for two reasons: first, our lack of knowledge of the exact physics of the corona makes it extremely difficult to estimate accurately the ultraviolet flux involved; and, second, the prominences occur under widely varying coronal conditions. The effect of the coronal flux would, of course, be to increase the degree of ionization.

Finally, it should be noted that the physical model used here is highly idealized. A prominence fiber may easily be twice or half as thick as the value chosen (5000 km). Furthermore, the threadlike character will make the prominence optically thick along the long axis, thereby increasing the occupation numbers (and the radiation) by 50 per cent over the values of Table 2. We have purposely not gone into these specifics, for we simply want to outline the important physical processes and, roughly, the amount of radiation that might be expected.

IV. CONCLUSIONS

The results obtained show that it is quite possible, by careful analysis of the emission lines of two or more elements, to measure the kinetic and "turbulent" temperatures of solar prominences. Most prominences, particularly quiescent ones, are in the range 5000°–20000° K. In very active regions the temperatures range up to at least 50000°. Analysis of the statistical equilibrium of hydrogen at these temperatures shows that densities of around 10^{10} protons/cm^3 are sufficient to produce the observed Hα radiation. It would be very useful to obtain data on more lines, particularly the Hα/Hβ ratio, to check our picture of the statistical equilibrium.

TABLE 2

OCCUPATION NUMBERS OF HYDROGEN LEVELS AT VARIOUS TEMPERATURES AND PRESSURES

	2.5×10^9	5×10^9	10^{10}	2×10^{10}	4×10^{10}
	$T=25000°$				
N_1	3.03×10^6	6.06×10^6	12.1×10^6	24.2×10^6	*
N_2	56.8	227	908	3630	*
N_3	0.37	1.48	5.9	23.6	*
N_4	0.061	0.245	0.98	3.92	*
N_5	0.043	0.173	0.69	2.76	*
Hα	0.40×10^4	1.60×10^4	6.37×10^4	25.5×10^4	*
	$T=50000°$				
N_1	0.256×10^6	0.464×10^6	0.928×10^6	1.86×10^6	3.72×10^6
N_2	27	112	448	1792	7170
N_3	0.095	0.385	1.54	6.16	24.6
N_4	0.039	0.156	0.623	2.49	9.96
N_5	0.022	0.086	0.345	1.38	5.52
Hα	0.103×10^4	0.416×10^4	1.66×10^4	6.65×10^4	26.6×10^4
	$T=100000°$				
N_1	0.0575×10^6	0.116×10^6	0.231×10^6	0.362×10^6	0.364×10^6
N_2	.0174	.0118	.895	252	2830
N_3	.015	.059	.236	1.74	12.74
N_4	.012	.052	.209	1.06	5.85
N_5	.010	.040	.162	0.75	5.14
Hα	0.0167×10^4	0.0637×10^4	0.255×10^4	1.88×10^4	13.8×10^4
	$T=200000°$				
N_1	0.66×10^4	1.31×10^4	2.62×10^4	5.24×10^4	10.48×10^4
N_2	0.0021	0.0083	0.0332	0.133	0.531
N_3	0.0014	0.0058	0.023	0.092	0.368
N_4	0.0014	0.0055	0.022	0.088	0.352
N_5	0.0014	0.0052	0.021	0.084	0.331
Hα	15	63	248	994	4000

I should like to express my appreciation for the help, encouragement, and advice of Dr. John W. Evans, of the Upper Air Research Observatory; Dr. Walter O. Roberts and Dr. Donald E. Billings, of the High Altitude Observatory; and Dr. Richard N. Thomas, of Harvard College Observatory. This work was commenced and a large part of it completed while the author was at Harvard College Observatory.

REFERENCES

Bates, D. R., Fundaminsky, A., Leach, J. W., and Massey, H. S. W. 1950, *Phil. Trans. R. Soc. London, A*, **243**, 93.
Bethe, H. 1933, *Handb. d. Phys.*, **24**, 273.
Billings, D. E. 1956, *H.A.O. Solar Research Memorandum*, No. 59.
Brück, H. A., and Moss, W. 1945, *M.N.*, **105**, 16, 282.
Chamberlain, J. W. 1953, *Ap. J.*, **117**, 387.
Cillié, C. G. 1936, *M.N.*, **96**, 771.
Conway, M. T. 1952, *M.N.*, **112**, 55.
Dodson, H. W., and Hedeman, E. R. 1949, *Ap. J.*, **110**, 242.
Dodson, H. W., Hedeman, E. R., and Chamberlain, J. W. 1953, *Ap. J.*, **117**, 66.
Dodson, H. W., and McMath, R. R. 1952, *Ap. J.*, **115**, 78.
Ellison, M. A. 1952, *Pub. R. Obs. Edinburgh*, Vol. **1**, No. 5.
Giovanelli, R. G. 1948, *Australian J. Sci. Res., A*, **1**, 275.
Mott, N. F., and Massey, H. S. W. 1949, *The Theory of Atomic Collisions* (Oxford: Clarendon Press).
Öhman, Y. 1955, *Ark. f. Astr.*, **2**, 1.
Peirce, B. O. 1929, *A Short Table of Integrals* (Boston: Ginn & Co.).
Severny, A. B. 1954, *Izvest. Crimean Ap. Obs.*, **12**, 33.
Unsöld, A. 1955, *Physik der Sternatmosphären* (2d ed.; Berlin: Springer).
Zirin, H. 1956*a*, *Ap. J.*, **123**, 536.
———. 1956*b*, *H.A.O. Solar Research Memorandum*, No. 68.

SHOCK WAVES IN STEADY RADIAL MOTION UNDER GRAVITY*

W. H. McCrea
Berkeley Astronomical Department, University of California†
Received May 7, 1956

ABSTRACT

In the steady radial flow of a polytropic gas toward a center of gravitational attraction, it is shown that a standing shock wave can, in general, exist within a certain distance of the center. This possibility elucidates certain features of Bondi's investigation of such radial motion and, in particular, helps to resolve an indeterminacy which he had noted. Reasons are given for concluding that the phenomenon may have application to accretion by a binary star.

I. INTRODUCTION

The steady spherically symmetric motion of a gas toward a center of gravitational attraction has been studied by Bondi (1952). The main purpose of the present work is to show that a standing spherical shock wave may occur in such motion. If it does, the motion on the supersonic side is given by a particular solution discovered by Bondi, while the motion on the subsonic side is given by one of a set of solutions which he found but which had appeared to be without physical significance. In this and other ways the work assists in the interpretation of Bondi's investigation.

The flow of material toward or away from a star is a process of considerable astrophysical interest. The steady inward motion here considered could not be exactly realized in any actual physical case. However, Bondi has explained how its investigation may indicate the kind of result to be expected in cases of possible practical significance, and we shall briefly mention some other such cases. Corresponding results for outflowing material may be of even more interest. However, they cannot readily be derived along with the present results because the relevant boundary conditions are somewhat different.

All symbols used here that are also used by Bondi play the same part as they do in his work (except for c, as explained below), although one or two of them have a more specialized physical meaning here.

II. SHOCK-WAVE CONDITIONS

The center of gravitational attraction, conveniently called the "star," is a body of mass M at rest at the origin O. It is assumed to act as a sink for any matter falling onto it; but the consequent increase of mass is neglected, this being one of the limitations of the steady-state problem as regards astrophysical applications. The star is supposed to be situated in an infinite gas cloud which is at rest at infinity with uniform density ρ_∞ and pressure p_∞. At any finite distance r from O, the gas must, in general, be in motion in the gravitational field. This motion is assumed to be spherically symmetric and steady. Therefore, it is specified by a radial velocity v, which is a function of r only and, in the present work, is taken to be inward toward O. The self-gravitation of the gas is neglected.

As is usual in the study of compressible flow, we assume the gas to be perfect and to

* Published with the aid of a grant from the American Astronomical Society.

† Normally at Royal Holloway College, Englefield Green, Surrey, England.

have constant specific heats with ratio γ. If p, ρ, and c are the pressure, density, and sound speed at any point, we have

$$c^2 = \frac{\gamma p}{\rho}. \tag{2.1}$$

For the time being we assume $1 < \gamma < \frac{5}{3}$. It should be noted that Bondi's c is our c_∞.

In a region in which the motion is isentropic, we have

$$\frac{p}{p_0} = \left(\frac{\rho}{\rho_0}\right)^\gamma, \tag{2.2}$$

where the subscript denotes values at any particular point in the region. From equations (2.1) and (2.2) we have

$$\frac{c}{c_0} = \left(\frac{\rho}{\rho_0}\right)^{1/2(\gamma-1)} \tag{2.3}$$

and

$$\int \frac{dp}{\rho} = \frac{\gamma}{\gamma-1}\frac{p}{\rho} = \frac{c^2}{\gamma-1}, \tag{2.4}$$

apart from a constant of integration.

We assume the motion to be isentropic except possibly for the presence of a shock wave. In accordance with the assumptions of symmetry and steady motion, if there is such a wave, it can have the form only of a normal standing shock wave at distance $r = r_1$, say. For motion inward, the side toward $r > r_1$ must be the supersonic side. Quantities evaluated on that face of the shock will be denoted by the subscript 1 and on the other face by the subscript 2.

The conditions for conservation of momentum, mass, and energy through the shock are

$$p + \rho_2 v_2^2 = p_1 + \rho_1 v_1^2, \tag{2.5}$$

$$\rho_2 v_2 = \rho_1 v_1, \tag{2.6}$$

$$\tfrac{1}{2} v_2^2 + \frac{\gamma}{\gamma-1}\frac{p_2}{\rho_2} = \tfrac{1}{2} v_1^2 + \frac{\gamma}{\gamma-1}\frac{p_1}{\rho_1}, \tag{2.7}$$

subject to

$$v_2 \neq v_1. \tag{2.8}$$

In dealing with a standing shock wave, it is convenient to use the variable u rather than v, where

$$u = \frac{v}{c}, \tag{2.9}$$

so that u is the Mach number of the flow. Using equations (2.1) and (2.9), the shock conditions then become

$$(1 + \gamma u_2^2)\left(\frac{c_2}{u_2}\right) = (1 + \gamma u_1^2)\left(\frac{c_1}{u_1}\right), \tag{2.10}$$

$$\rho_2 c_2 u_2 = \rho_1 c_1 u_1, \tag{2.11}$$

$$[2 + (\gamma-1) u_2^2]\, c_2^2 = [2 + (\gamma-1) u_1^2]\, c_1^2, \tag{2.12}$$

$$c_2 \neq c_1. \tag{2.13}$$

The last relation follows because any one of the equations $c_2 = c_1$, $u_2 = u_1$, and $v_2 = v_1$ would imply the other two. Eliminating c_2/c_1 between equations (2.10) and (2.12) gives

$$2\gamma u_1^2 u_2^2 - (\gamma - 1)(u_1^2 + u_2^2) - 2 = 0 , \tag{2.14}$$

which is the known relation between the Mach numbers on the two sides of the shock.

III. EQUATIONS OF FLOW

As in Bondi's work, the equations governing the motion may be taken as the continuity equation,

$$4\pi r^2 \rho v = A , \tag{3.1}$$

and Bernoulli's equation,

$$\tfrac{1}{2} v^2 + \int \frac{dp}{\rho} - G\frac{M}{r} = \text{Constant} . \tag{3.2}$$

Here A is the constant flux across any surface inclosing the origin and so is the rate of flow into the sink at O, and G is the gravitational constant. Since $\rho \to \rho_\infty \neq 0$ as $r \to \infty$, it follows from equation (3.1) that

$$v \sim \text{Const.}\ r^{-2} \qquad (r \to \infty) \tag{3.3}$$

Using equation (2.4), we may write equation (3.2) as

$$\tfrac{1}{2} v^2 + \frac{\gamma}{\gamma - 1}\frac{p}{\rho} - G\frac{M}{r} = \text{Constant} \tag{3.4}$$

in a region in which the flow is isentropic. But equation (2.7) shows that the left-hand member is continuous across a shock. Hence the constant in equation (3.4) is the same for all r, whether a shock is present or not. With equation (3.3) the constant is therefore

$$\frac{\gamma}{\gamma - 1}\frac{p_\infty}{\rho_\infty} \qquad (\text{all } r) . \tag{3.5}$$

Writing

$$r = xGM\, c_\infty^{-2} , \tag{3.6}$$

equation (3.5) then becomes

$$c^2 u^2 \left(\frac{1}{2} + \frac{1}{\gamma - 1}\frac{1}{u^2}\right) = c_\infty^2 \left(\frac{1}{x} + \frac{1}{\gamma - 1}\right). \tag{3.7}$$

Thus the motion satisfies equations (3.1) and (3.7) throughout the gas. But if there is a shock at a distance r_1, *the relation between the variables c and ρ is not the same throughout*, i.e., in equation (2.3) a common pair of values c_0 and ρ_0 cannot be used on both sides of r_1. We now derive the equations that hold good if a shock is present; if no shock is present, we have $r_1 = 0$.

If $r > r_1$, we may write equation (2.3) as follows:

$$\frac{\rho}{\rho_\infty} = \left(\frac{c}{c_\infty}\right)^{2/(\gamma-1)} ; \tag{3.8}$$

and so, using equations (2.9) and (3.6), we may write equation (3.1) as follows:

$$x^2 u \left(\frac{c}{c_\infty}\right)^{(\gamma+1)/(\gamma-1)} = \frac{A\, c_\infty^3}{4\pi G^2 M^2 \rho_\infty} \equiv \lambda, \text{ say} . \tag{3.9}$$

Eliminating c/c_∞ between equations (3.7) and (3.9), we obtain

$$u^{-2(\gamma-1)/(\gamma+1)}\left(u^2+\frac{2}{\gamma-1}\right)=\kappa^{-2(\gamma-1)/(\gamma+1)}x^{-(5-3\gamma)/(\gamma+1)}\left(\frac{2x}{\gamma-1}+2\right), \tag{3.10}$$

where

$$\kappa=\lambda \qquad (x>x_1)\,, \tag{3.11}$$

and $x=x_1$ when $r=r_1$.

If $r<r_1$ we may write equation (2.3) as follows:

$$\frac{\rho}{\rho_2}=\left(\frac{c}{c_2}\right)^{2/(\gamma-1)}. \tag{3.12}$$

Proceeding as before, we again obtain equation (3.10), but with

$$\kappa=\nu \qquad (x<x_1)\,, \tag{3.13}$$

where

$$\frac{\nu}{\lambda}=\frac{\rho_\infty}{\rho_2}\left(\frac{c_2}{c_\infty}\right)^{2/(\gamma-1)}=\frac{u_2}{u_1}\left(\frac{c_2}{c_1}\right)^{(\gamma+1)/(\gamma-1)}. \tag{3.14}$$

The second part of equation (3.14) follows from the facts that c_1 and ρ satisfy equation (3.8) and ρ_1 and ρ_2 satisfy equation (2.11). It should be noted that the relation between λ and ν has to take account of the fact that the same relation (3.6) defines x in terms of r *for all* r. Also, using the shock condition, we can show from equation (3.14) that

$$\nu>\lambda \qquad (u_1>1)\,. \tag{3.15}$$

Suppose, now, that for some value $\kappa=\lambda_m$ equation (3.10) yields a solution $u=u_m(x)$ such that $u_m(x)\to 0$ as $x\to\infty$ and $u_m(x_1)\equiv u_1>1$ for some $x_1>0$. Let the corresponding value c_1 of c be got by substituting λ_m, x_1, and u_1 in equation (3.9). Using these values, let u_2 and c_2 be obtained from equations (2.14) and (2.10) or (2.12), and ν from equation (3.14). Setting κ equal to this value of ν, if equation (3.10) then has a solution $u=u(x)$ in $0<x\leq x_1$, it can be verified that this solution must be satisfied by $u=u_2$ when $x=x_1$. *Then the function*

$$u=\begin{cases} u\,(x) & (0<x<x_1)\\ u_m\,(x) & (x_1<x)\end{cases} \tag{3.16}$$

would yield a possible state of motion in which there is a shock wave at $x=x_1$.

IV. EXISTENCE OF SOLUTIONS

Bondi has discussed the solutions of equation (3.10). He showed that there exists a critical value $\kappa=\lambda_m$ given by

$$\lambda_m^{-2}=2^{(\gamma+1)/(\gamma-1)}\left[\tfrac{1}{4}\,(5-3\gamma)\right]^{(5-3\gamma)/(\gamma-1)} \tag{4.1}$$

such that:

a) If $\kappa=\lambda_m$, there is a solution $u=u_m(x)$ that tends to zero as $x\to\infty$, increases monotonically with decreasing x, and tends to infinity as $x\to 0$. In particular, $u_m(x_m)=1$, where

$$x_m=\tfrac{1}{4}\,(5-3\gamma)\,, \tag{4.2}$$

and $u_m(x)>1$ when $x<x_m$.

b) If $\kappa>\lambda_m$, there is a solution in $x\leq x_\kappa$ (say) where $x_\kappa<x_m$ such that the solution gives $u=1$ when $x=x_\kappa$ and gives two values of u, one greater and one less than unity, when $x<x_\kappa$. We shall be concerned with the subsonic values; these decrease monotoni-

cally with decreasing x. (The complete solutions for the stated values of κ have other parts as well, but these and the solutions for $\kappa < \lambda_m$ do not concern us here. Our notation differs from Bondi's by introducing κ, as is necessary because we deal with motions in which κ changes from having Bondi's value λ_c to a different value; our λ_m is Bondi's λ_c.)

Among solutions that start from rest at infinity, u_m is the only one that produces supersonic values for some x and does so for all $x < x_m$. Therefore, if a shock wave occurs at $x = x_1$, the $u_m(x)$ in equation (3.16) can be only this particular solution, and we must also have $x_1 > x_m$. Taking any such x_1, the corresponding value of ν is uniquely determined as described at the end of Section III. Bondi's work then shows that a unique solution of the sort b exists for $\kappa = \nu$, since $\nu > \lambda_m$ from equation (3.15). The verification mentioned shows that this solution is satisfied by the appropriate value of u_2 at $x = x_1$. Therefore, the subsonic part of this solution supplies the function $u(x)$ in equation (3.16). So the existence of motion of the type (3.16) is established, and it follows that *a shock wave can exist at any* $x_1 < x_m$. Also, from b, the Mach number of the flow continues to decrease as x decreases from x_1; therefore, *there cannot be a second shock wave* in the flow.

V. RELATION TO MOTIONS STUDIED BY BONDI

We now see that the two possible motions for $\lambda = \lambda_m$ derived by Bondi are the two extreme cases of the more general motion given by equation (3.16). Bondi's type 2 is the case $x_1 = 0$, i.e., the shock is at the origin (or at the surface of the star). His type 1 is the case $x_1 = x_m$, i.e., the outermost possible position of the shock, in which the discontinuity of u is reduced to zero, although there remains a discontinuity of du/dx.

Bondi gave an interpretation of his solutions for $\lambda < \lambda_m$. But his solutions for $\lambda > \lambda_m$ received no interpretation, although he could use them to show the impossibility of a steady accretion rate exceeding that corresponding to λ_m. However, from the way in which these solutions arise along with the rest, they ought to represent some possible motion. We now see that this is so: they represent the motion on one side of a shock wave in the set of motions intermediate between the extremes of types 1 and 2.

These solutions arise as solutions of the algebraic equation (3.10), and this equation itself does not supply the meaning of κ. We now see, from the rest of the work, that here the immediately relevant parameter is ν, not λ. The solutions under consideration arise for various values of ν but are all associated with motions corresponding to a single value of λ, namely, λ_m. Thus they are all associated with the same rate of accretion. Those parts of Bondi's solutions which are not physically significant in his work or in ours arise for one or more of the following reasons: The equations themselves do not distinguish between inward and outward flow. They do not exclude shocks in which u increases instead of decreasing, these being excluded by the second law of thermodynamics. The condition $v \to 0$ as $r \to \infty$ is sufficient, but not necessary, for the validity of the equations.

VI. PHYSICAL DISCUSSION: THE PARAMETER λ_m

We have to consider the way in which a motion of the sort under consideration could, as nearly as possible, be established in practice. For this purpose it is not most helpful to envisage a star being introduced into an existing gas cloud, because the star's gravitational field must act upon the cloud throughout the process of introduction and so we do not reach the start of the processes under consideration. It is better to think of a stationary star in the presence of a gathering cloud; we suppose the gas to be gradually gathered in from infinity in all directions. As the gas comes under the gravitational attraction of the star, it will tend to fall onto the star, and, according to our treatment of the star as a sink, any gas reaching the star will disappear into it. In general, the speed of the in-falling gas will become supersonic before it reaches the star. Thus the gas entering the star cannot "warn" the gas following behind about its fate. Therefore, there is nothing to check the supersonic flow, and, if a steady motion is attained, *it can be only*

that given by the solution $u_m(x)$ up to the surface of the star. This is Bondi's type 2 motion, and it occurs only for $\lambda = \lambda_m$.

Suppose, however, that the star cannot accept material whose density is below a critical value but can accept any material at or above this density. As will be seen later, this may be a case of astrophysical interest. Then the gas first falling to the star will be stopped but will not disappear. So, for a time, gas will accumulate near the star, forming a growing envelope into which the incoming gas continues to fall. If the critical density at the surface of the star is attained while there is still a region outside the envelope in which the speed is supersonic, then thereafter the star can accept all the incoming material. In that case the boundary of the envelope plays the same part as the surface of the star in the previous case. If a steady state is attained, *it can be only that given by the solution $u_m(x)$ up to the surface of the envelope, which, in fact, forms a standing shock wave of the sort studied above.* Once again the solution occurs only for $\lambda = \lambda_m$.

On the other hand, if the critical density at the surface of the star is not reached until the envelope has extended out into the region in which the incoming material is falling with subsonic speed, then the incoming material becomes "warned" of its presence. So the motion is gradually modified at all distances. A steady state cannot then be attained until such modification has been established out to infinity. The modification is in the direction of checking the flow, and so, if a steady state is established, it must be for a net flux of material less than in the previous cases, i.e., for a value of λ less than λ_m. Also, since the motion is everywhere subsonic, *there cannot be a standing shock wave.*

This discussion supplies a simple physical explanation of the fact that, unless the reaction of the star extends out to infinity, the rate of steady accretion is always the same, namely, that given by $\lambda = \lambda_m$, whether or not there is a shock wave outside the star. Moreover, since the solutions for $\lambda < \lambda_m$ demand such a reaction, the corresponding steady motion could not be established in a finite time. Also we see that the simple explanation of these solutions—that the rate of accretion is less than the maximum possible only if the star cannot accept all the material that falls upon it—is essentially the correct explanation.

Finally, we see that Bondi's type 1 motion for $\lambda = \lambda_m$ is that in which the envelope ceases to grow at precisely its greatest possible size, $x_1 = x_m$. If there is a critical density of the sort contemplated here or any other critical condition for acceptance of the material by the star, it would have no special relationship to x_m. So the occurrence of this particular motion must have zero probability.

VII. ACCRETION ENVELOPE AND ACCRETION BY A BINARY STAR

In astrophysical applications we have to be able to deal with the case when the "star" is a binary system. Here the center of gravitational attraction O may be taken to be the mass-center of the system, but this cannot act as a sink for incoming matter. Accretion can take place only by the component stars in their orbital motion sweeping up material from an accretion envelope that envelops the orbits. A steady state can be attained only when the density of the envelope is sufficiently great for this accretion to equal the primary accretion into the envelope. So here we have effectively the case that was idealized in Section VI in terms of a critical density.

Even in the case of a single star, if it accretes material from a gathering cloud in something like the manner envisaged in Section VI, then in the early stages we should have to regard the portions of cloud material that fall toward the star as having small initial random motions. Consequently, these portions would not fall directly onto the star but would encounter one another in the vicinity of the star. Thus they would tend to establish an accretion envelope rather like the accretion stream in the case of a moving star (Bondi and Hoyle 1944). This would play the part of the envelope mentioned in Section VI, although in this case it would not depend upon a critical density. At any rate, it in-

dicates another simple way in which an actual motion could correspond to one of the theoretical motions in which a shock wave exists.

It was, however, the study of accretion by binary systems that led the writer to notice the possible existence of shock waves in the motions treated by Bondi. The writer believes that this possibility had already been mentioned in a colloquium by Dr. R. Ebert (Göttingen). The argument in Section VI as to the virtual impossibility of the realization of steady motion with $\lambda < \lambda_m$ appears to be equivalent to one first given in conversation by Dr. K. N. Dodd.

VIII. NUMERICAL ILLUSTRATION

In order to illustrate the hydrodynamical theory for a value of γ in the range $1 < \gamma < \frac{5}{3}$, it is convenient to use $\gamma = \frac{7}{5}$. This value was also used by Bondi, and Figure 1 reproduces some features of Bondi's Figure 2, though the present calculations have been done afresh.

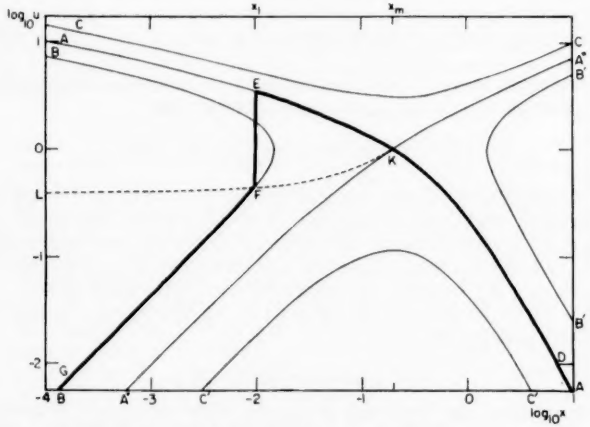

FIG. 1.—Example of motion with shock wave, $\gamma = \frac{7}{5}$. AA, A^*A^*, solution of equation (8.1) for $\kappa = \frac{5}{8}$; BB, $B'B'$, solution for $\kappa \doteq 2.77$; $DEFG$, motion with shock EF; LFK, values of u_2 corresponding to u_1 given by AEK; and CC, $C'C'$, solution for $\kappa = \frac{1}{8}$. Abscissa $\log_{10} x$; ordinate $\log_{10} u$.

Equations (3.10), (4.1), and (4.2) now give

$$u^{-1/3}(u^2+5) = \kappa^{-1/3} x^{-1/3}(5x+2) \tag{8.1}$$

$$\lambda_m = \tfrac{5}{8}, \qquad x_m = \tfrac{1}{5}. \tag{8.2}$$

In Figure 1 the curve AA shows the solution $u = u_m(x)$, and AA and A^*A^* together give the complete solution of equation (8.1) for $\kappa = \frac{5}{8}$.

In order to illustrate the occurrence of a shock wave, suppose it takes place at $x = 10^{-2}$. The solution $u_m(x)$ gives

$$u \doteq 3.43 \equiv u_1 \qquad \text{when} \qquad x = 10^{-2} \equiv x_1.$$

With $\gamma = \frac{7}{5}$, equation (2.14) becomes

$$u_2^2 = \frac{u_1^2+5}{7u_1^2-1}. \tag{8.3}$$

So the value of u_1 gives

$$u_2 \doteqdot 0.454 .$$

From the condition for equation (8.1) to be satisfied by u_2 when $x = x_1$, we find the value of κ that is to be the value of ν in equations (3.13) and (3.14), namely,

$$\nu \doteqdot 2.77 .$$

This can be checked by using the values of u_1 and u_2 in equation (2.10) or equation (2.12) to evaluate c_2/c_1 and substituting directly in equation (3.14). The curves BB and $B'B'$ together give the complete solution of equation (8.1) for $\kappa = \nu$. The thick curve $DEFG$ then represents the motion with the shock wave.

The curve LFK shows the value of u_2 given by equation (8.3) when u_1 has the value given by u_m. The point F is the unique point on the curve BB to which a shock-wave transition is possible for motion from rest at infinity. The curve LFK can be used similarly in determining the flow corresponding to a shock at any other value of x_1 less than x_m.

In order to give an idea of orders of magnitude, without implying that our example has any particular astrophysical significance, we may take

$$M = 1 \text{ solar mass}, \quad c_\infty = 1 \text{ km/sec}.$$

Then, from equation (3.6) in the example the shock occurs at $r \doteqdot 8.9$ astronomical units. Thence, using equation (3.9), we have $c_1 \doteqdot 3.5$ km/sec, and so the quoted value of u_1 gives $v_1 \doteqdot 12$ km/sec. The quoted values of u_1 and u_2 give, from equation (2.12), $(c_1/c_2)^2 \doteqdot 3.2$, and this is equal to the temperature jump at the shock. The resulting value of c_2 gives $v_2 \doteqdot 2.8$ km/sec and, from equation (2.11), $\rho_2/\rho_1 \doteqdot 4.2$.

Finally, in order to illustrate a case where $\kappa < \lambda_m$, the curves CC and $C'C'$ together give the complete solution when $\kappa = \frac{1}{8}$.

IX. EXTREME VALUES OF γ

For various reasons, the foregoing treatment does not apply immediately to the extreme possible values $\gamma = 1$ and $\gamma = \frac{5}{3}$. These cases may be dealt with on their merits. The case $\gamma = 1$ does not yield any essentially new feature. The case $\gamma = \frac{5}{3}$, on the other hand, gives $x_m = 0$, so that no standing shock wave can exist in steady motion from infinity.

The extremes correspond, respectively, to isothermal and to adiabatic behavior of the gas. The behavior of actual interstellar material must be between these extremes. Various cooling mechanisms *tend* to produce isothermal conditions, but the efficiency of these mechanisms would have to be investigated in any particular application of the theory; also the validity of the assumption of constant specific heats would have to be examined.

I am indebted to the Council of Royal Holloway College (University of London) for leave of absence to enable me to hold a visiting professorship at Berkeley and to the Board of Foreign Scholarships for a Fulbright Travel Grant.

REFERENCES

Bondi, H. 1952, *M.N.*, **112**, 195.
Bondi, H., and Hoyle, F. 1944, *M.N.*, **104**, 273.

PRODUCTION OF THE SUN'S NON-THERMAL RADIO EMISSION BY ČERENKOV RADIATION*

L. MARSHALL
Enrico Fermi Institute for Nuclear Studies, University of Chicago
Received August 20, 1956

ABSTRACT

It is proposed that practically all the non-thermal radio emission from the sun, namely, that part correlated with sunspots, can be accounted for as Čerenkov radiation emitted when jets of electrons travel up out of sunspots through regions of progressively lower magnetic field (which determines the cyclotron frequency) and decreasing electron density (which determines the plasma frequency). The behavior of the index of refraction as a function of cyclotron and plasma frequencies, as it regulates the frequency of Čerenkov radiation, is used to explain the main features of the radio spectra, including the sharp cutoff on the low-frequency side. The experimental fact of simultaneous radio emission at two or more discrete frequencies is well accounted for, but the hypothesis of Čerenkov radiation does not seem to provide a satisfactory explanation of the recently observed exact frequency doubling. The magnitude of the intensity is correctly given.

The emission of Čerenkov radiation as a phenomenon which may occur when a particle moves through an electron plasma in a magnetic field has been remarked on by Veksler (1956). A footnote of his paper reads: "This radiation can evidently play a certain part in the radio emission in the upper strata of the atmosphere of hot stars which are characterized by strong magnetic fields." It is the purpose of the present paper to suggest that a great deal, perhaps most, of the non-thermal radio spectrum of the sun may be attributed to this mechanism.

The following discussion depends for experimental knowledge of the sun's radio emission on the compilation "Solar Radio Emission" by J. L. Pawsey and S. F. Smerd (1953). As described therein, the main features of the non-thermal radio spectrum of the sun may be outlined briefly in the following way: (1) The broadcast frequency ranges from about 30000 to 30 Mc/s, limits corresponding to those allowed by the earth's atmosphere. (2) Broadcasts of long duration which may last for days are characterized mainly by relatively high frequencies. (3) Broadcasts of shorter duration—hours, minutes, or seconds—often involve frequencies which initially are high and terminally are low; that is, the broadcast drifts to lower frequencies with time. In addition, such broadcasts show a more or less abrupt cutoff on the low-frequency side. The band widths may be small during more rapid drifts, for example, as small as 10 Mc at a frequency of 200 Mc. (4) The broadcasts are correlated to sunspots, and, in particular, those more striking in intensity and frequency variation are correlated to large sunspots. (5) Perhaps most striking of all is the frequency-doubling characteristic recently observed (see Wild, Murray, and Rowe 1953) in a broadcast consisting of two bands, each decreasing in frequency with time in such a way as to maintain the approximate frequency ratio 2/1 and having roughly equal intensity (see Fig. 1).

To produce these features by radio emission from the Čerenkov effect, we suggest that jets of electrons are created in sunspots, directed at an arbitrary angle to the magnetic field. If the electron jet has a direction such that it spirals up out of the sunspot, the resulting broadcast varies from high frequency to low frequency, corresponding to decreasing magnetic field and decreasing plasma density, and is of short duration because the high-speed electrons soon reach a distance at which the magnetic field is too low to allow emission of Čerenkov radiation. On the other hand, if the electrons move,

* Research supported by a joint program of the U.S. Office of Naval Research and the U.S. Atomic Energy Commission.

for example, at right angles to the magnetic-field direction, they remain circling in a high magnetic field, producing high-frequency radio waves for a long time. Accordingly, one expects broadcasts of frequencies allowed by the magnetic fields and electron densities of the particlar sunspot, varying with time in a way determined by the velocity of the electron jet in the direction of the magnetic field and modified by the geometrical extension of the jet vertically in the sunspot.

The necessary condition for emission of Čerenkov radiation is

$$\left(1-\frac{1}{n^2\beta^2}\right)>0 \qquad \text{or} \qquad n>\frac{1}{\beta}, \tag{1}$$

where β is the velocity of the electron divided by the velocity of light and n is the refractive index of the sunspot's atmosphere for radiation of frequency ω. The value of n

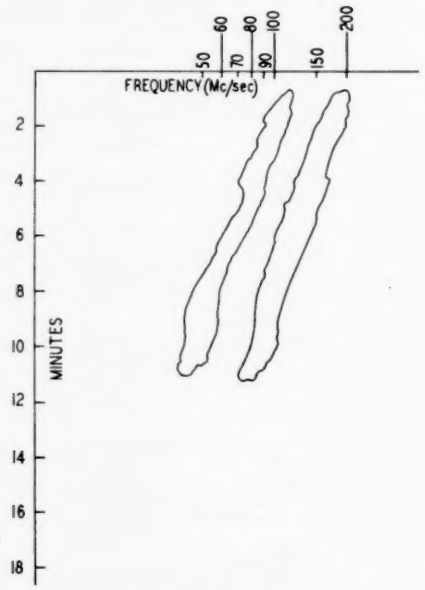

FIG. 1.—A schematic representation of the dynamic radio spectrum of November 21, 1952, observed by Wild, Murray, and Rowe. See, for comparison, Pawsey and Smerd (1953).

for radiation of frequency ω in a dilute electron gas of density N is less than 1 except in the presence of a magnetic field, H, in which case it has the form

$$n^2=1+\frac{4\pi e^2 N}{m\omega^2}\, f(H)\,. \tag{2}$$

The condition for emission of Čerenkov radiation consequently becomes $f(H)>0$.

In addition, n depends on the angle θ between the direction of propagation of the radiation and the direction of the magnetic field H and is given by the expression (cf. Bremmer 1950) which also defines $f(H)$:

$$n^2(\theta)=1-\frac{2x(1-x)}{2(1-x)-y^2\sin^2\theta\pm\{y^4\sin^4\theta+4y^2(1-x)^2\cos^2\theta\}^{1/2}}, \tag{3}$$

the quantities in this expression being defined as

$$x = \frac{\omega_0^2}{\omega^2}; \qquad y = \frac{\omega_H}{\omega}; \qquad \omega_0^2 = \frac{4\pi N e^2}{m}; \qquad \omega_H = \frac{eH}{mc}, \tag{4}$$

where ω_0 is the plasma frequency and ω_H is the cyclotron frequency. It follows that the condition $n > 1$ can be satisfied (cf. Kolominsky 1956, who has also suggested that this kind of radiation may occur in the ionized atmosphere of the sun or stars) for

a) $\omega_0 < \omega < \sqrt{(\omega_H^2 + \omega_0^2)}$ (taking the minus sign);

b) $\omega < \omega_0$ (taking the plus sign).

In the first case, the electric vector rotates in the same direction as the electrons gyrate, and in the second case in the opposite direction (cf. Spitzer 1956).

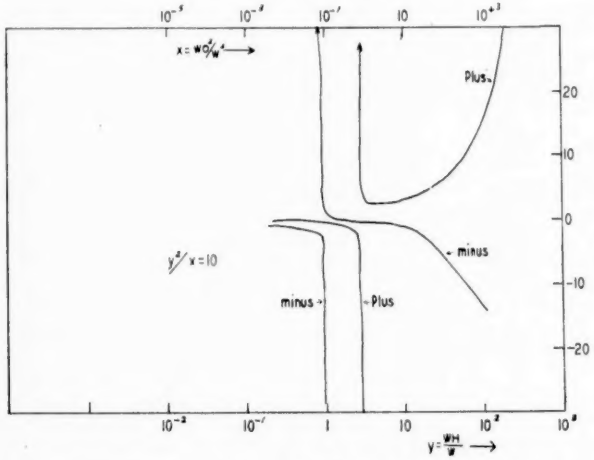

FIG. 2.—$G = n^2 - 1$ versus ω/ω_H for the case $\omega_H^2/\omega_0^2 = 10$. Here n is the index of refraction, ω_H is the cyclotron frequency, and ω_0 is the plasma frequency. The explicit dependence of G on ω_0, ω_H, and ω is given in the text.

The general features of the allowed values of the Čerenkov radiation may be illustrated by consideration, for example, of the case $\omega_H/\omega_0 = \sqrt{10}$. In Figure 2 for this case the quantity G, defined by the relation $n^2 = 1 + G$, is plotted against ω_H/ω. Whenever G is greater than zero, the corresponding value of ω may be emitted. One sees that G goes to infinity in the neighborhood of ω_H and ω_0 and that consequently in these regions all values of β are allowed and that all electrons radiate in these frequency intervals. Between ω_0 and ω_H, G is very small. No Čerenkov radiation is expected in this region if the electrons have β too small to allow radiation. Consequently, one expects from non-relativistic electrons two frequency bands strongly emitted simultaneously and separated by a frequency interval of no intensity. Although, in principle, the widths of the emission bands are determined by the maximum electron velocity, nevertheless the band width is considerably widened by the vertical extension of the electron jet in the sunspot atmosphere.

On this hypothesis the decrease in permissible broadcast frequency with time is di-

rectly caused by the decrease in ω_0 and ω_H as the electron jet travels up out of the sunspot through decreasing electron densities and decreasing magnetic fields.

One sees in Figure 3 that the observed electron densities and large sunspot magnetic fields provide the correct magnitudes of frequencies ω_0 and ω_H to account for the observed radio emission in terms of Čerenkov radiation. In addition, the range also is adequate. The magnitude of the cyclotron frequency for electrons is $\nu_H = eH/2\pi mc = (2.8H)$ Mc/s, where H is the magnetic field in gauss. So, to a field of 5000 gauss in a large sunspot, there corresponds a cyclotron frequency of 14000 Mc/s, and to 50 gauss, 140 Mc/s. The plasma frequency $\nu_0 = \{N_e^2/\pi m\}^{1/2} = 9000\ N^{1/2}$ c/s. The electron density, N_e, ranges (cf. van de Hulst 1953) from 10^{10}/cm^3 at 1.006 sun's radii to 10^6 at 2 sun's radii from the center of the sun, corresponding to a variation in ν_0 from 900 to 9 Mc/s.

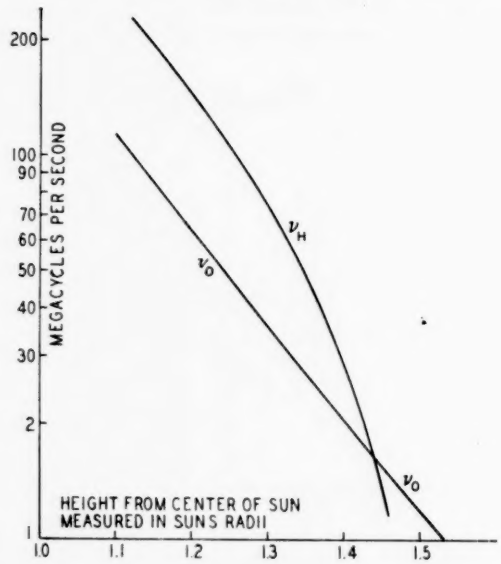

FIG. 3.—Variation of the cyclotron frequency ω_H and the plasma frequency ω_0 in the sun's atmosphere above a large sunspot, these values being acceptable within the present limits of experimental determination (for comparison see Pawsey and Smerd, 1953, p. 478).

Over nearly half a sun's radius ω_0 may be equal to approximately $\omega_H/2$ for a large sunspot, as is shown in our Figure 3 (see for comparison Pawsey and Smerd 1953, p. 478, Fig. 6).

One is tempted to interpret the double-frequency storm of Figure 1 as a direct consequence of such a frequency dependence of ω_0 and ω_H above a large sunspot as is shown in Figure 3. But the observation by Wild, Roberts, and Murray in 1954 of three more such double-banded broadcasts displaying exact frequency doubling so firmly establishes the phenomenon that one must admit that the foregoing hypothesis is unsatisfactory.

An additional feature of time-dependent radio emission spectra noticed by Wild, Roberts, and Murray (1954) is that the rate of drift of frequency with time decreased rapidly at lower frequencies, so that the broadcasts emitted the lowest frequency for perhaps half the time of the entire broadcast. This behavior can be accounted for as

resulting from the constraint of electron trajectories to follow lines of force in a looped prominence above a sunspot. At the top of a looped prominence, the lines of force go parallel to the surface of the sun. Here the magnetic field H stays constant, and one assumes that the plasma density also stays constant. (The latter follows because the plasma is constrained to move along lines of force—hence its flux nv is $\sim H$, which is here constant—and because its velocity v also remains constant at the top of a looped prominence where the lines of force neither diverge nor converge.) Therefore, as long as the particle travels in this region, it emits at roughly constant frequencies. As it starts down the other side, its radiation, which is emitted largely forward, probably cannot escape from the sun.

Observed broadcasts of more than two emission bands may be accounted for as resulting when two or more electron jets follow one another up out of a sunspot.

For smaller sunspots having lower fields, ω_H must become equal to ω_0 at lower altitudes and therefore at higher frequencies. On this hypothesis one may expect to see broadcasts which display initially two frequency bands which finally converge, unless, of course, jets of electrons of sufficient energy are unable to form in the smaller sunspots.

The Čerenkov radiation hypothesis accounts for the abrupt cutoff of broadcasts on the low-frequency side as resulting from the abrupt change of n from large positive values to large negative values, and for the gradual fall-off on the high-frequency side as following from the term $(1 - 1/\beta^2 n^2)$ in the expression for Čerenkov radiation intensity together with the gradual decrease in n.

It is interesting to note an event described by Menzel (1956) which took place in a large flare on the limb of the sun, observed February 10, 1956. In this case a piece of material in a solar flare high above the sun's surface suddenly accelerated from 60 to 700 miles/sec within 2 minutes and then rose at a steady speed until it faded from sight about 200000 miles above the sun. Simultaneously, strong solar radio broadcasts were observed. An explanation of this phenomenon may be that a jet of electrons came up from the sunspot through the material of the solar prominence, emitting Čerenkov radio waves on the way and, during the short time of its passage through the gas, accelerated it perhaps by forces of the kind recently proposed by Veksler (1956). The gas of the solar prominence thus received a sudden acceleration and then continued at constant velocity, being left behind by the fast electron jet.

The band width of a broadcast may be related to the geometrical extension of the jet in the sunspot. Accordingly, the broadcast of Figure 1 shows a band width of about 20 Mc/s at 50–200 Mc/s, from which one estimates a thickness of 0.02 sun's radius or about 15000 km.

The experimentally observed intensity of typical broadcasts, e.g., about 10^{-19} watt/meter^2 per unit frequency interval in the range 100–1000 Mc can be well accounted for by the Čerenkov radiation hypothesis. The Čerenkov radiation intensity in photons per centimeter of path per unit frequency interval per particle is given by

$$\frac{\Delta I}{\Delta \nu} = \frac{4\pi e^2}{h c^2} \times \left(1 - \frac{1}{\beta^2 n^2}\right), \tag{5}$$

or $1.7 \times 10^{-12} \times (1 - 1/\beta^2 n^2)$. The radio energy per square meter per unit frequency interval per second received on the earth is given by

$$\frac{1}{4\pi r^2} \times v \times \left\{\begin{matrix}\text{effective}\\ \text{volume of}\\ \text{flare}\end{matrix}\right\} \times \left\{\begin{matrix}\text{density}\\ \text{of}\\ \text{electrons}\end{matrix}\right\} \times \left\{\frac{\Delta I}{\Delta \nu}\right\} \times \left\{\begin{matrix}\text{energy}\\ \text{per}\\ \text{photon}\end{matrix}\right\},$$

where v = velocity of particle and r is the distance from sun to earth = 1.5×10^{11} meters. The diameter of a large sunspot is approximately 7000 km. Assume that the

electron jet has a diameter of 3000 km and a height of 10000 km, corresponding to a volume of 10^{26} cm^3. The electron density may be taken as 10^8/cm^3, and the average frequency as 100 Mc/s. The intensity is

$$\frac{v}{25\times10^{22}}\times10^{26}\times10^{8}\times1.7\times10^{-12}\left(1-\frac{1}{\beta^2n^2}\right)\times6\times10^{-27}\times10^{8}$$
$$=0.5\times10^{-19}v\left(1-\frac{1}{\beta^2n^2}\right)\text{ ergs/meter}^2\text{/sec per unit frequency interval.}$$

Using 1 watt = 10^7 ergs/sec and assuming $v = 10^8$ cm/sec and $1 - 1/\beta^2n^2 \sim 1$, the intensity is

$$\frac{0.5\times10^{-19}}{10^7}\times10^8=5\times10^{-19}\text{ watt/meter}^2\text{ per unit frequency interval,}$$

in good agreement with experimentally observed intensities (cf. Pawsey and Smerd 1953).

Allowed radiation, once emitted and proceeding away from the surface of the sun, travels from then on in regions of decreasing ω_0 and ω_H. Consequently, its index of refraction remains greater than zero, and it can escape from the sun. It may, however, be turned back by a zero index of refraction in the earth's ionosphere.

One expects that electrons at all altitudes in the sunspot will emit Čerenkov radiation of frequencies ω_0 and ω_H of their immediate surroundings, of band width allowed by the Maxwellian velocity distribution ($\sim10^7$ cm/sec) corresponding to their temperature ($\sim10^6$ degrees). And, indeed, there is apparently considerable background radio signal at all such frequencies but muted by self-absorption in the plasma. Only when there is a jet of electrons of greater-than-average velocity, which can produce radiation of somewhat smaller frequency than average, does one expect a strong broadcast which escapes the electron plasma without large absorption. The average electron velocity corresponding to the temperature of the corona, namely, 10^6 degrees, is 5×10^8 cm/sec or $\beta = 0.02$. For comparison, a lower limit for that component of the electron-jet velocity in the direction of the magnetic field may be estimated from the time duration of those broadcasts whose frequency dependences show changes with time and in which the band width at any instant is relatively narrow. Such estimates vary from 100 to 10^5 km/sec, corresponding to $\beta_\parallel = 0.003$ to $\beta_\parallel = 0.3$. The fact that the observed parallel component remains significantly less than c is taken as tentative evidence that the electron jets are not always relativistic. (But broadcasts have been observed which appear to give suddenly, at onset, a wide range of frequency and to show no variation of that frequency range with time. Such an event could be caused by a jet of relativistic electrons of long geometric extension in the atmosphere, the front of which moves through one sun's radius in a time of the order of 1 second, thus emitting radiation throughout a wide range of frequencies almost instantaneously, and continuing so to emit for as long as the jet endures.) In continuation, the fact that the parallel velocity component is often larger than the average thermal velocity is in good agreement with the requirement that electrons of more-than-average velocity give a strong radio signal.

There remains an interesting situation in the case of simultaneous emission of the two frequency bands near ω_0 and ω_H for the case $\omega_0 < \omega_H$. Namely, one might expect that radiation of the lower frequency, corresponding to ω_0, would move out from the surface of the sun into a region where it became equal to ω_H for a lower electron density and be reabsorbed. But an additional feature prevents this from happening, namely, radiation of frequency ω_H is emitted circularly polarized, rotating in the direction in which electrons gyrate (cf. Spitzer 1956) (corresponding to the minus sign in n), and radiation in the other frequency band $\sim\omega_0$ (corresponding to the plus sign) rotates in the opposite

sense. Consequently, although it passes through a region in which electrons have a cyclotron gyration at the same frequency, they cannot absorb it because they must rotate in the opposite direction.

In addition, there should be allowed strong Čerenkov radio emissions for $\omega \ll \omega_0$ (see Fig. 2), and this probably is part of the broadcast from regions of high electron density; but, because the earth's ionosphere reflects radiation of low frequency, it can be received only if emitted from relatively low altitudes in the sunspot. In this case it may not readily be recognized as belonging to a three-part spectrum because of the large separation of the allowed emission bands.

In general, there can be little contribution from the cyclotron frequencies of nuclear species—e.g., protons, helium ions, carbon ions—because in fields of 5000 gauss or less the corresponding frequencies are no more than 15 Mc and cannot generally penetrate the earth's ionosphere. Likewise, plasma frequencies corresponding to oscillations of nuclear species—for example, of helium ions and carbon ions—can contribute very little because the abundances of nuclei heavier than hydrogen are so low (cf. Suess and Urey 1951).

REFERENCES

Bremmer, H. 1949, *Terrestrial Radio Waves* (New York: Elsevier Publishing Co., Inc.), p. 282.
Hulst, H. C. van de. 1953, "The Chromosphere and the Corona," in *The Sun*, ed. G. P. Kuiper (Chicago: University of Chicago Press).
Kolominsky, A. A. 1956, *Doklady U.S.S.R. Academy of Sciences*, **106**, 982.
Menzel, D. H., 1956, *Sky and Telescope*, **15**, 398.
Pawsey, J. L., and Smerd, S. F. 1953, "Solar Radio Emissions," in *The Sun*, ed. G. P. Kuiper (Chicago: University of Chicago Press).
Spitzer, Lyman, Jr. 1956, *Physics of Fully Ionized Gases* (New York: Interscience Publishers).
Suess, H. E., and Urey, H. C. 1956, *Rev. Mod. Phys.*, **28**, 60.
Veksler, V. I. 1956, paper No. A30 presented at the Cern Symposium in Geneva, entitled "Coherent Method of Acceleration of Particle Bunches."
Wild, J. P., Murray, J. D., and Rowe, W. C. 1953, *Nature*, **172**, 533.
Wild, J. P., Roberts, J. A., and Murray, J. D. 1954, *Nature*, **173**, 532.

NOTES

PHOTOMETRIC ANALYSIS OF A SPECTROGRAM OF A PERSEID METEOR

In a recent paper (Cook and Millman 1955) published by the writers the light-curve of a Perseid meteor was determined by making a microdensitometer trace along the zero-order image of the meteor. The magnitudes obtained are erroneously stated (*ibid.*, p. 259) to be photographic. The blaze of the grating operates to redden the image strongly, and, to avoid confusion, these magnitudes should be called "panchromatic." It is the purpose of this note to describe the determination of the correction in magnitudes to reduce the panchromatic magnitudes previously given (*ibid.*, Table 3 and Fig. 5) to photographic magnitudes.

It is fortunate that the pass band of the equipment in the second order corresponds essentially to a photographic sensitivity range. As can be seen from Figure 4 (*ibid.*) this runs from 3700 to 4900 A, with slight extra extensions of 200 A or so beyond this range. The maximum intensity occurs on α Lyrae at 4130 A. The effective wave length may then be taken as falling between this and the middle of the pass band at 4300 A and must, therefore, lie very close to the standard effective wave length for photographic magnitudes, 4250 A.

In principle, then, the apparent photographic magnitude of the meteor can be derived from a comparison of the total areas under the rectified intensity-curves of the second orders for the meteor and for α Coronae Borealis. Field correction and reciprocity failure must, of course, be taken into account. However, α Coronae Borealis is too faint to allow an accurate planimetering of the relative intensity curve. Instead, six standard wave lengths were adopted: 4130 A in the second order and 4530, 5066, 5730, 5980, and 6390 A in the first order. The sums of these intensities, corrected for differential field correction, were formed both for α Coronae Borealis and for α Lyrae. The latter star was photographed on another frame of the same film on the same night with the camera pointed at the same elevation and azimuth. Since these two stars are of the same spectral type, the ratio of the area under the second-order spectrum to the sum of the six intensities measured should be the same for both objects. Hence the area under the second-order spectrum for α Coronae Borealis can be computed through planimetering the spectrum of α Lyrae.

The effective exposure time to be used on the star is that for a continuum (*ibid.*, eq. [2], p. 257). For the meteor the proper value will lie somewhere between that for a continuum and that for a spectral line (*ibid.*, eq. [4], p. 258). The resulting absolute photographic magnitude found at position 4 was -8.8 mag. using the exposure time for a continuum, and -9.1 mag. using the time for lines. The best compromise seems to be to adopt -8.9 mag. as the photographic absolute magnitude. The panchromatic absolute magnitude (*ibid.*, Table 3, p. 257) was -9.3, whence the reduction from panchromatic to photographic magnitude is $+0.4$ mag.

A comment on the rectification of the tracings is in order. Recent calibrations on some Eastman Aero Super XX film at many wave lengths have been made with a spectral step-wedge and show noticeable deviations in behavior, the shorter wave lengths exhibiting less steep calibration-curves and the longer wave lengths steeper curves (Millman, Locke, and Kennedy 1955). Thus the hope expressed (Cook and Millman 1955, p. 251)

that a calibration in integrated light would prove satisfactory has not been fulfilled. An investigation of the effects of this dependence of calibration-curve on wave length showed that an accuracy of better than 8 per cent may be achieved by treating the conversion from one curve to another as a change in contrast, γ. The range in γ appears to be a factor of nearly 2; but, as a consequence of the corresponding change in the "intensity" of the sky fog and scattered light, the effects upon the deduced intensities in the range of microphotometer deflection used were rather small, being less than a 15 per cent change everywhere. Therefore, in this particular case the use of a calibration in integrated light appears to have been a successful calculated risk.

ALLAN F. COOK
PETER M. MILLMAN

HARVARD COLLEGE OBSERVATORY
AND
NATIONAL RESEARCH COUNCIL OF CANADA

REFERENCES

Cook, A. F., and Millman, P. M. 1955, *Ap. J.*, **121**, 250.
Millman, P. M., Locke, J. L., and Kennedy, J. E. 1955, private communication.

A NEW COLOR-MAGNITUDE DIAGRAM FOR THE HYADES CLUSTER

In an earlier paper (Johnson and Knuckles 1955) one of us, together with C. F. Knuckles, published new photoelectric magnitudes and colors for the Hyades cluster. It was not possible to correct the magnitudes for differences in the individual distances, since no proper motions of sufficient accuracy were available. The published color-magnitude diagram therefore did not reveal a fine structure. Independently, O. Heckmann and K. Lübeck (unpublished) derived photographic magnitudes and proper motions in an area containing 97 members of the cluster. This work indicated that the application of individual distance moduli computed from the new proper motions would improve the color-magnitude diagram. The use of the more accurate photoelectric data promised to give a further gain in resolving the fine structure of the color-magnitude diagram. Details concerning the various sources of the proper motions and their combination with additional observations will be published in a forthcoming issue of the *Zeitschrift für Astrophysik*. Table 1 gives the new distance moduli. The assumption of a space motion $V = 45.3$ km/sec in the direction $A = 94\overset{\circ}{.}0$, $D = +7\overset{\circ}{.}6$ was made. The formula used was

$$m - M = -5 - 5 \log \frac{4.738\mu}{V \sin \lambda},$$

where λ is the angular distance of an individual star from the convergent point. For m the photoelectric visual magnitude of Johnson and Knuckles (1955) was used. Figure 1 shows the new color-magnitude diagram.

The distance moduli $m - M$ range from 2.56 to 3.69 mag. For $M < 3.5$ the average mean error of $m - M$ is ± 0.03 mag., while for $M > 3.5$ it is ± 0.09. It would be desir-

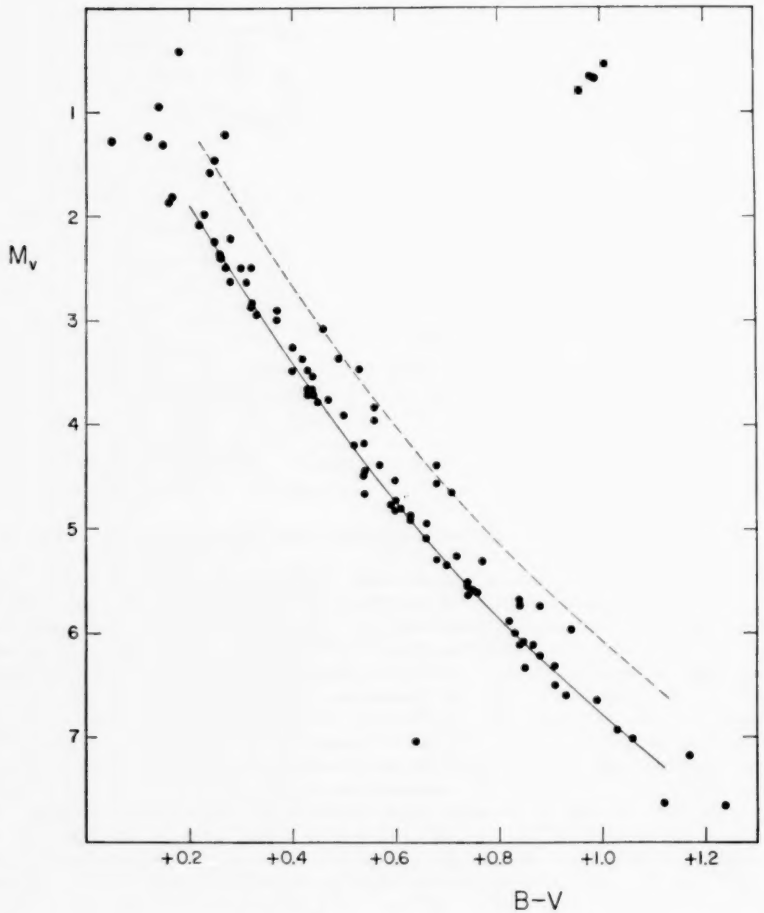

FIG. 1.—The color-magnitude diagram of the Hyades, with individual distance moduli from Bergedorf proper motions. The broken line corresponds to the maximum by which a binary could lie above the main-sequence line.

able to improve the latter value. The accuracy is sufficient to show, however, a clear concentration of stars near a ridge line at the lower boundary of the main sequence and a certain percentage of stars, probably double, above the ridge line. The vertical distance of $0^{M}.75$ between the full and the broken line corresponds to the maximum by

TABLE 1

DISTANCE MODULI OF MEMBERS OF THE HYADES CLUSTER, DETERMINED FROM BERGEDORF PROPER MOTIONS

No.*	$m-M$	No.*	$m-M$	No.*	$m-M$
11+12	2.91	49	3.46	84	3.00
15	2.99	50	2.89	85	3.03
16	3.69	51	3.25	87	3.06
17	3.10	52	2.96	88	3.11
20	3.05	53	3.07	89	3.07
21	3.26	54	3.27	91	3.20
22	3.03	55	3.04	92	3.11
23	3.15	56	3.02	93	3.18
24	3.43	57	3.09	94	2.90
25	2.95	58	2.96	95	3.08
26	2.99	59	3.01	96	2.83
27	3.20	60	3.07	97	3.06
28	2.98	62	3.20	99	3.04
29	3.04	63	3.14	101	2.99
30	2.96	64	3.17	102	3.00
31	3.08	65	2.96	103	3.15
32	3.11	67	3.22	104	3.03
33	3.18	68	3.03	108	3.37
34	3.09	69	3.05	141	3.02
35	3.26	70	2.98	162	3.18
36	3.13	71	3.05	172	3.16
37	3.12	72	2.99	173	2.83
38	2.89	73	3.03	174	2.98
39	2.56	74	3.06	175	3.37
40	3.03	75	3.12	176	3.05
41	3.11	77	3.14	177	2.93
42	3.24	78	3.13	178	2.89
43	3.09	79	2.96	179	2.92
45	3.14	80	3.08	180	3.02
46	3.00	81	3.33	181	3.14
47	2.94	82	2.98	182	3.22
48	2.94	83	3.11	183	3.19
				184	3.32

* The numbers are those of Johnson and Knuckles (1955).

which a binary could lie above the ridge line in the absence of accidental errors. The striking similarity between the Hyades and Praesepe clusters, which has often been stated, is now more firmly established.

O. HECKMANN
H. L. JOHNSON

HAMBURGER STERNWARTE
HAMBURG-BERGEDORF, GERMANY
AND
LOWELL OBSERVATORY
FLAGSTAFF, ARIZONA

REFERENCES

Johnson, H. L., and Knuckles, C. F. 1955, *Ap. J.*, **122**, 209.

OBSERVATIONS OF THE INTENSITY OF SOLAR LYMAN-ALPHA EMISSION

Over the last seven years, rocket experiments have yielded a number of measurements of the intensity of hydrogen Lyman-α radiation from the sun. The results are given in Table 1. All measurements were made at White Sands Proving Ground, New Mexico. No evidence of flare activity or SID was reported by solar observatories or ionosphere stations during the times of any of the flights. The results may therefore be taken to represent "quiet" sun conditions.

In the solar spectrum between 1050 and 1350 A the Lyman-α line is by far the most prominent feature. It has been estimated (Byram, Chubb, Friedman, and Gailar 1953) that at least 90 per cent of the total intensity in this band of wave lengths is contained in this one line. Even though the detector sensitivities may span a range of wave lengths 200 A wide, a straight-line relationship characteristic of monochromatic radiation is observed when the logarithm of photon-counter or ion-chamber response is plotted

TABLE 1

TABLE OF LYMAN-α MEASUREMENTS

Reference	Launching Time (M.S.T.)	Intensity outside Earth's Atmosphere (ergs/cm²/sec)	Instrumentation	Band Width (angstroms)
FLB	1000, 9/29/49	1–10	Photon counter	1100–1350
TWP	1101, 2/17/50	0.4	Thermoluminescent phosphor	1050–1240
BCFG	0659, 4/30/52	0.15	Photon counter	1180–1300
BCFG	0644, 5/5/52	0.10	Photon counter	1180–1300
R	1238, 12/12/52	0.5	Spectrograph	.....
JMPT	0830, 2/2/54	1.0	Spectrograph	.....
JMPT	0830, 2/21/55	0.4	Spectrograph	.....
BCFK	1550, 10/18/55	5.7 (−1, +3)	Ion chamber	1100–1345
BCFK	1715, 10/21/55	4.0 (±0.8)	Ion chamber	1100–1345
BCFK	0830, 11/4/55	9.2 (±3)	Ion chamber	1100–1345

against residual air mass. This is illustrated by Figure 1, which is typical of data obtained with the ion-chamber detectors last fall and with the photon counters of 1952.

In the first photon-counter experiment flown in 1949, there was evidence of a weak tail of longer-wave-length sensitivity, and the calibration technique was comparatively crude, so that the intensity could be estimated only within limits differing by an order of magnitude. Subsequently, the thermoluminescent-phosphor measurement, the 1952 photon-counter data, and the intensities obtained from densitometry of the photographed spectra, all indicated intensities of about a few tenths of an erg per square centimeter per second. The photographic measurements were intended primarily to produce well-resolved spectral details, and no estimate is given of the accuracy of the estimated line intensities. The best photon-counter experiment yielded the lowest observed flux of the Lyman-α radiation. Until the ion-chamber measurements of last fall were made, the large scattering of results was attributed as much to experimental uncertainties as to real variations in solar emission.

The ion-chamber technique, which we used in the last three experiments, is simple and reliable. The chambers were filled with nitric oxide gas, which was photoionized by Lyman-α quanta transmitted through a lithium fluoride window. Only the window transmission and the ionization cross-section of nitric oxide entered into the computation

of the quantum efficiency of the chamber. The window effect is readily measured, and the cross-section of nitric oxide has been accurately determined by Watanabe, Marmo, and Inn (1953). The ion chambers used in the rockets were calibrated by direct comparison with a standard nitric oxide chamber. The limits of error indicated for the rocket measurements are based on factors associated with the specific characteristics of each flight and will be discussed in detail in a separate paper.

The Lyman-α intensities observed in the last three experiments are surprisingly high compared to earlier measurements. In contrast, the X-ray emission from the corona at wave lengths in the neighborhood of 40–100 A was found to be comparatively constant in several experiments performed by us in 1953 and 1955. Although the tail of the X-ray emission spectrum at wave lengths shorter than 20 A has been observed to fluctuate markedly, it is probably always a minor portion of the intensity in the total X-ray spec-

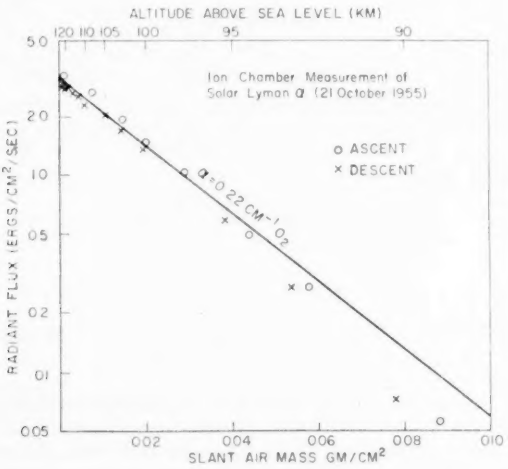

FIG. 1.—Variation of Lyman-α intensity with residual air mass and altitude. Solid line is drawn with slope equal to laboratory value of absorption coefficient of molecular oxygen.

trum. It might be expected that, since the Lyman-α radiation originates in the turbulent fringes of the chromosphere, it would vary much more widely and rapidly than X-ray emission from the corona. If the ionospheric electron density is used as a gauge of solar ionizing radiations, the X-ray spectrum which is absorbed in the E and F regions must vary by a factor of about 2.5 in intensity from minimum to maximum of a sunspot cycle. No similar data on electron density from critical reflection frequencies are available for the D region, which is believed to be produced by the Lyman-α radiation. However, the absorption of frequencies of 2–4 megacycles/sec in the D region has been regularly observed. To a first approximation, the absorption is proportional to the electron density or the square root of the ionizing radiation. According to Appleton and Piggot (1954), a characteristic dependence on sunspot number is observed, with the absorption varying by a factor of 2 or 3 from minimum to maximum of an 11-year cycle. On the other hand, the absorption may fluctuate as much as by a factor of 4 from day to day for constant solar zenith angle (Beynon and Davies 1954).

The tabulated measurements are hardly adequate to give a clear picture of day-to-day variations or of any dependence of solar Lyman-α intensity on sunspot number over a

complete sunspot cycle. The high intensities observed late in 1955 may be associated with the rapidly rising phase of the present cycle. Fortunately, the observation of Lyman-α can be accomplished with small-rocket techniques, and about fifty separate measurements will be attempted, beginning during the current year and extending through the IGY period of 1957–1958. These experiments will be grouped so as to provide a picture of short-period as well as long-period variations.

E. T. Byram
T. A. Chubb
H. Friedman
J. E. Kupperian, Jr.

Naval Research Laboratory
Washington 25, D.C.

REFERENCES

Appleton, E., and Piggot, W. R. 1954, *J. Atm. and Terr. Phys.*, **5**, 141.
Beynon, W. J. G., and Davies, K. 1954, *Report of the Physical Society Conference on the Physics of the Ionosphere* (London: The Society), p. 40.
Byram, E. T., Chubb, T. A., Friedman, H., and Gailar, N. 1953, *Phys. Rev.*, **91**, 1278.
Friedman, H., Lichtman, S. W., and Byram, E. T. 1952, *Phys. Rev.*, **83**, 1025.
Johnson, F. S., Purcell, J. D., Malitson, H. H., and Tousey, R. 1955, *A.J.*, **60**, 165 (private communication of L-α intensities).
Rense, W. A. 1953, *Phys. Rev.*, **91**, 299.
Tousey, R., Watanabe, K., and Purcell, J. D. 1951, *Phys. Rev.*, **83**, 165.
Watanabe, K., Marmo, F. F., and Inn, C. Y. 1953, *Phys. Rev.*, **90**, 155.

A POSSIBLE CAUSE OF THE EJECTION OF MATERIAL BY LATE-TYPE GIANTS

The possibility that an ejection of mass into the interstellar medium occurs at the surface of late-type giants has considerable importance in the theory of stellar evolution. In a recent important paper Deutsch (1956) has presented strong observational evidence for the ejection of material by the M supergiant component of α Herculis. It is the purpose of the present note to suggest a physical reason why such a loss of mass should take place.

According to a recent discussion of giant stars (Hoyle and Schwarzschild 1955), it has become clear that the hydrogen convection zone lying immediately below the photosphere plays an important role in controlling the internal structure of these stars. Material in the ionization zone possesses two contributions to its internal energy: the energy of ionization and the energy of thermal motion. Of these, only the latter contributes directly to the gas pressure. This means that a stellar model can be obtained which satisfies the usual condition of hydrostatic equilibrium but which is nevertheless unstable in the sense that ionized hydrogen immediately below the photosphere can possess sufficient *total* energy to escape entirely from the gravitational field of the star. It is reasonable to suppose that in such a case perturbations of the equilibrium model will lead to material being ejected to infinity from the surface of the star.

A consideration of numerical values will be of interest. Ionized hydrogen at a thermal temperature of 20000° K possesses a total energy of 1.795×10^{13} ergs/gm, of which 1.300×10^{13} ergs are contributed by the ionization energy. If this total energy were converted entirely into a kinetic energy of mass motion, the resulting velocity would be 60 km/sec, very closely. This value may be compared with the estimate of 100 km/sec given by Deutsch for the velocity of escape from the M supergiant component of α

Herculis. The discrepancy is probably not serious, since the value of 100 km/sec depends on the square root of the mass adopted for the M supergiant, and this is uncertain. Thus Deutsch adopts the values shown in the accompanying tabulation. The mass was ob-

Mass ($\odot = 1$)	Bolometric Magnitude	Effective Temperature	Radius ($\odot = 1$)
15	−5.9	2700° K	580

tained from the empirical mass-luminosity relation of Russell and Moore (1940). But this relation is unreliable precisely for giant stars, yielding masses that are systematically too large. The relation would, for example, give about $6\odot$ for the mass of type II giants, whereas evolutionary theory yields about $1.25\odot$, as does the pulsation theory of RR Lyrae stars (Sandage 1956).

The situation for ordinary giants is also of interest. A type I giant of mass $1.25\odot$ and bolometric magnitude −3.0 will have a velocity of escape less than our 60 km/sec if, in the course of evolution, its effective temperature falls below about 2870° K (at this surface temperature the bolometric correction is about 3 mag., so that the present bolometric magnitude corresponds to a visual magnitude of about 0.0). Thus we may expect loss of material to occur from very late type I giants. Whether loss of material should occur from type II giants is uncertain. The latest type II giants also have mass about $1.25\odot$ and bolometric magnitude about −3.0, but it is uncertain whether or not their surface temperatures fall as low as 2870° K.

It remains to estimate the rate at which loss of mass can take place in accordance with the present suggestion. At first sight, it is tempting to argue that the rate should be calculated to give an approximate equipartition between the radiant energy emitted by the star and the kinetic energy of the outward-streaming material, but this takes no account of the source of the momentum of the material. If we had only to account for the momentum possessed by a single outburst of material, it could be argued that the outward momentum was balanced by an inward mechanical reaction on the star. In the case of continuous emission this argument cannot be invoked, however, because the material cannot gain systematic outward momentum by reacting on itself. Rather, it seems as if the outward flow of radiation from the deep interior of the star supplies the only systematic source of outward momentum. It is plausible, therefore, to set the rate at which momentum is carried by the outward-moving material equal to the rate at which momentum is carried outward by the radiation. On this basis the rate of escape of material from a star of specified bolometric magnitude can readily be calculated. In particular, for the case of the M-supergiant component of α Herculis the rate of mass loss comes out at about $5.8 \times 10^{-6}\odot$ per year. This estimate is about a hundred times greater than that given by Deutsch; so that the present method of estimating the rate of mass loss may possibly yield values that are too high. If the present rate is accepted in order of magnitude, however, a significant feature is that mass loss can have a profound effect on the evolution of very late-type stars. Thus, if a star loses mass by the present process, the rate of loss, calculated on the above basis, will always be large enough to remove an appreciable fraction of the whole star in a time less than would otherwise be required for significant evolution to take place through the operation of nuclear processes.

Let the number of grams undergoing nuclear processes in a star be m per second, and let the energy released be q ergs/gm. Writing mq for the luminosity, the amount of material ejected per second is $mq\ (6 \times 10^6 c)^{-1}$, when calculated on the above basis, where a velocity of ejection of 6×10^6 cm/sec is used and c is the velocity of light in centi-

meters per second. The time required for important mass loss to occur is obtained by dividing the total mass of the star, M, by this rate:

$$\frac{6 \times 10^6 M c}{m q}.$$

This estimate may be compared with the time required for an appreciable fraction of the star to undergo the nuclear processes, this being simply M/m. The ratio of the time scale for loss of mass to that for evolution by nuclear processes is accordingly $6 \times 10^6 c/q$. The value of q corresponding to the conversion of hydrogen to helium is about 6×10^{18}, and the value corresponding to the conversion of helium to carbon, oxygen, and neon is about 10^{18}. Hence for either of these nuclear processes the rate of mass loss has the more important effect on evolution. This result is independent of the star under consideration, provided only that the star has sufficiently low surface gravity for the velocity of escape to be less than about 60 km/sec.

F. HOYLE

ST. JOHN'S COLLEGE
CAMBRIDGE, ENGLAND

REFERENCES

Deutsch, A. J. 1956, *Ap. J.*, **123**, 210.
Hoyle, F., and Schwarzschild, M. 1955, *Ap. J. Suppl.*, **2**, 1.
Russell, H. N., and Moore, C. E. 1940, *The Masses of the Stars* (Chicago: University of Chicago Press), p. 112.
Sandage, A. R. 1956, *Ap. J.*, **123**, 278.

ACCRETION HEATING IN THE HERBIG-HARO OBJECTS

In a recent paper of great interest, Böhm (1956) discusses the brightest of the Herbig-Haro objects and reaches the conclusion that the emission cannot be a consequence of accretion heating. This conclusion would seem to merit further argument. To demonstrate that accretion heating is incapable of sustaining the line emission of the brightest Herbig-Haro object, it would be necessary to prove that the kinetic energy supplied to a central star by the infall of accreted material is always less, even under the most favorable conditions, than the energy required to maintain the emission. The energy required to sustain the line emission is $\sim 10^{33}$ ergs/sec, while the kinetic energy of material falling into a star of solar mass and dimensions amounts to $\sim 10^{15}$ ergs/gm. Hence, given an efficient process for converting kinetic energy into ultraviolet light, the kinetic energy of accreted material would be capable of maintaining the emission if the accretion rate were as large as 10^{18} gm/sec. This rate agrees closely with the mean rate of star formation, given by dividing the mass of the star by the time scale for its formation (mass $\sim 2 \times 10^{33}$ gm; time-scale $\sim 10^{15}$ sec). Since, moreover, the Herbig-Haro objects are very likely stars at an early stage of their history, it is to be expected, on quite general grounds, that maximum accretion rates of this order are attained in these objects.

The discrepancy between the present considerations and Böhm's estimate of accretion rates is worthy of notice. For a cloud density of 10^4 hydrogen atoms/cm^3, an accretion rate of 10^{18} gm/sec demands a cloud temperature of no more than $\sim 100°$ K. Although this represents a very reasonable value for an H I region, it is much less than the electron temperature of 7500° K derived by Böhm. A reconciliation between Böhm's high temperature and the $\sim 100°$ K required for accretion heating would be forthcoming if the material surrounding the central star does not possess uniform temperature, if intermixed within it are both localized H I and H II regions. The rapid fluctuations sometimes observed in this class of objects would indeed seem to be consistent with the view that the

structures of the gaseous masses surrounding their central stars do not possess any very simple symmetry.

It may be added that the possibility favored by Böhm, of a central star radiating beyond the Lyman limit at a temperature of some 29000° K, would surely lead to difficulties if the star possessed normal dimensions; for then the emission would be substantially too large, of order 10^{35} ergs/sec or more.

F. HOYLE

ST. JOHN'S COLLEGE
CAMBRIDGE, ENGLAND

REFERENCES

Böhm, K. 1956, *Ap. J.*, **123**, 379.

THE ENERGY OF INTERACTION OF He^+ AND H^-

The potential of intermolecular force plays a dominant role in statistical-mechanical theories, the task of which it is to predict the macroscopic properties of a system in terms of molecular variables. There exists a number of methods of determining intermolecular forces (Hirschfelder, Curtiss, and Bird 1954), one of which is a priori calculations based on quantum mechanics. In this note we report an estimate, derived from a quantum-mechanical perturbation calculation, of the energy of interaction of a positive helium ion and a negative hydrogen ion (He^+-H^-), a system not of chemical, but possibly of astrophysical, interest. We were led to this problem during the theoretical evaluation of the intermolecular potential of the system consisting of a helium atom and a hydrogen atom (Mason, Ross, and Schatz 1956), a case for which experimental corroboration can be obtained from measurements of the scattering of high-velocity beams of hydrogen atoms in room-temperature helium gas (Amdur and Mason 1956).

The present treatment considers only the repulsive and coulombic forces of the system He^+-H^-; thus ion-induced dipole and London dispersion forces are neglected. We construct an approximate wave function for the system from 1s hydrogen-like atomic orbitals:

$$u_{\mathrm{He}}(1) = \left(\frac{z'^3}{\pi}\right)^{1/2} \exp\left(-z' r_{1\mathrm{He}}\right), \qquad u_{\mathrm{H}}(1) = \left(\frac{z^3}{\pi}\right)^{1/2} \exp\left(-z r_{1\mathrm{H}}\right), \tag{1}$$

together with the orthonormal spin functions $\alpha(1)$ and $\beta(1)$. Here "1" refers to electron 1, z and z' are effective nuclear charges, and $r_{1\mathrm{He}}$ and $r_{1\mathrm{H}}$ denote the distances from electron 1 to the helium and hydrogen nuclei, respectively. The customary atomic units are used, in which the unit of length is $a_0 = 0.5292$ A, and the unit of energy is $e^2/a_0 = 27.21$ ev $= 627.2$ kcal/mole. In terms of these functions, we can write, for the completely antisymmetric wave function of the system, the Slater determinant,

$$\Psi = \begin{vmatrix} u_{\mathrm{He}}\alpha & u_{\mathrm{H}}\beta & u_{\mathrm{H}}\alpha \end{vmatrix}. \tag{2}$$

If Ψ, as in the present case, is an approximation to the true wave function, then the first-order perturbation approximation to the energy is given by

$$E = \frac{\int \Psi^* H \Psi \, d\tau}{\int \Psi^* \Psi \, d\tau}, \tag{3}$$

where H is the Hamiltonian operator for the system, assumed to be a function of the configuration co-ordinates only, and the integration extends over all co-ordinates, including those of spin. Substitution of equation (2) in equation (3) and evaluation of the integrals lead to a complicated expression for E as a function of z', z, and the internuclear separation R, referred to the separated nuclei and electrons as the zero of energy. The explicit expression for E can be obtained from Mason, Ross, and Schatz (1956), where it is given as H_{22}/Δ_{22}.

TABLE 1

CALCULATED POTENTIAL ENERGY OF INTERACTION FOR THE SYSTEM He^+-H^-

R (a_0)	$V(R)$ (e^2/a_0)	R (a_0)	$V(R)$ (e^2/a_0)
1	+0.2689	4	−0.2308
2	− .2212	5	−0.1949
3	−0.2617		

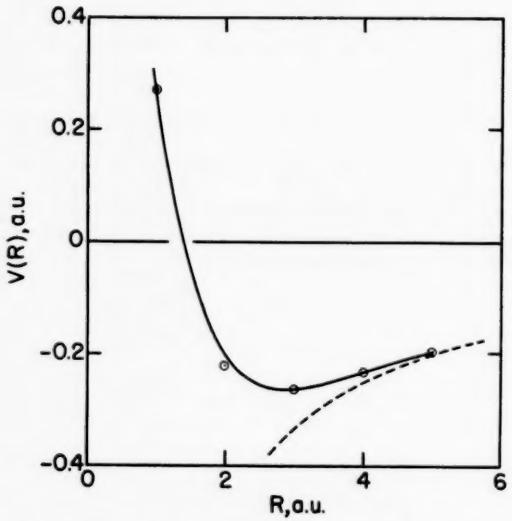

FIG. 1.—The energy of interaction for the system He^+-H^-, in atomic units. The circles represent the calculated energies; the solid line represents the energies as given by equation (4); and the broken line represents the coulombic energy of attraction between the ions.

The potential energy of interaction of the system at a given internuclear separation is the difference between the energy E at that separation and the energy at infinite separation; i.e., $V(R) = E(R) - E(\infty)$, where $E(R)$ and $E(\infty)$ are evaluated from equation (3) with the *same* approximate wave functions (Margenau and Rosen 1953). We have determined $V(R)$ at five internuclear distances for the case $z' = 2$, $z = 11/16$, with results as shown in Table 1. The values of the effective nuclear charges are those which

give the best energy values for the isolated ions, as determined by a variational procedure (Pauling and Wilson 1935).

The values of the intermolecular potential given in Table 1 can be represented with fair accuracy by the equation

$$V(R) = 5.202 \exp(-1.437R) - \frac{1}{R}, \tag{4}$$

where $V(R)$ is in units of e^2/a_0 and R is in units of a_0. This equation is shown in Figure 1, together with the calculated points; for large values of R, $V(R)$ approaches the coulomb attraction between two singly charged ions, $-1/R$. The minimum of equation (4) is located at approximately $R = 2.86\ a_0$, with a depth of $0.264\ e^2/a_0$, and the fundamental vibration frequency as calculated from the curvature at the minimum is 1720 cm^{-1}.

It is difficult to estimate the reliability of the present calculations; however, the same approximation method as used here leads in the related system He-H to an intermolecular potential which appears to be accurate within about 25 per cent, at least for $R > 2$ (Amdur and Mason 1956; Mason, Ross, and Schatz 1956). It is possible that the potential energy-curves of excited states of the system He-H lie close to, or cross, the potential energy-curve of the system treated here. The existence of such interactions, not considered in this note, would alter the present results. The interaction with the ground state of He-H is negligible.

JOHN ROSS
EDWARD A. MASON

BROWN UNIVERSITY
AND
UNIVERSITY OF MARYLAND

REFERENCES

Amdur, I., and Mason, E. A. 1956, *J. Chem. Phys.*, in press.
Hirschfelder, J. O., Curtiss, C. F., and Bird, R. B. 1954, *Molecular Theory of Gases and Liquids* (New York: John Wiley & Sons).
Margenau, H., and Rosen, P. 1953, *J. Chem. Phys.*, **21**, 394.
Mason, E. A., Ross, J., and Schatz, P. N. 1956, *J. Chem. Phys.*, in press.
Pauling, L., and Wilson, E. B., Jr. 1935, *Introduction to Quantum Mechanics* (New York: McGraw-Hill Book Co., Inc.), pp. 184–185.

ABSTRACTS OF ASTROPHYSICAL JOURNAL SUPPLEMENT SERIES

Supplement No. 22, Volume II

CATALOGUES OF Hα-EMISSION STARS AND NEBULAE IN THE MAGELLANIC CLOUDS

KARL G. HENIZE

University of Michigan Observatory

The first of the two papers which constitute this supplement presents a catalogue, identification charts, and brief discussion of 236 Hα-emission stars and 532 emission nebulae in the Magellanic Clouds, discovered on objective-prism photographs. The plates were taken with the Mount Wilson 10-inch camera at the Lamont-Hussey Observatory of the University of Michigan.

For each emission-line star, the catalogue includes accurate co-ordinates, qualitative estimates of the intensity of emission and continuum, the sharpness of Hα, and the photographic magnitude. For nebulae, the dimensions, form, and probable exciting stars are also tabulated.

An earlier discussion of the material (Henize and Miller 1951) is supplemented by comments on classification systems for nebulae and absolute luminosities of the Be stars.

REFERENCES

Henize, Karl G., and Miller, Freeman D. 1951, *Pub. Obs. U. Michigan*, **10**, 75.

A PHOTOMETRIC CATALOGUE OF EMISSION NEBULOSITIES IN THE LARGE MAGELLANIC CLOUD

LOWELL DOHERTY, KARL G. HENIZE, AND LAWRENCE ALLER

University of Michigan Observatory

This paper gives photometric data for 285 regions selected in 115 nebulosities in the Large Magellanic Cloud. For each of these Hα-emission regions the cross-sectional profile obtained from microphotometer tracings is represented by simple geometrical figures, which, in turn, have been described by a system of letters and numerals. Data from photometrically calibrated widened and unwidened spectra permit the reduction of these cross-sectional profiles to approximate surface brightnesses in units of ergs per square centimeter per second per steradian by the method of Ambarzumian. Each tracing is described in the catalogue by its angular size in seconds of arc, profile, and intensity, while its position is shown on an appropriate chart. Equivalent Hα stellar magnitudes are given for six Hα-emission stars.

from Chicago

BOOKS IN PHYSICS

ANALYTICAL EXPERIMENTAL PHYSICS

Second Revised Edition

By Michael Ference, Jr., Harvey B. Lemon, and Reginald J. Stephenson

Significant features of this new edition are use of the meter-kilogram-second, or mks, system of units throughout—but retaining the cgs and British Engineering systems; a gradual increase of calculus during the course of the book; a discussion of modern rockets; an account of the Coriolis force; increased emphasis on the fundamental aspects of wave motion in the sections on light and sound; and up-to-date material in the discussions of quantum, atomic, and nuclear physics, electricity, heat, and thermodynamics. *$8.00*

ELECTRONS (+ and −), PROTONS, PHOTONS, NEUTRONS, MESOTRONS, AND COSMIC RAYS

Second Edition

By Robert A. Millikan

A veritable education in modern atomic progress. A brilliant survey of the advances made in physics in the last half century. *$9.00*

FROM GALILEO TO THE NUCLEAR AGE

By Harvey Bruce Lemon

Text edition, $5.00; Regular edition, $7.00

THE UNIVERSITY OF CHICAGO PRESS

5750 ELLIS AVENUE · CHICAGO 37 · ILLINOIS

BOOKS FROM CHICAGO

THE SOLAR SYSTEM

Edited by GERARD P. KUIPER

Vol. I. *The Sun.* $12.50
Vol. II. *The Earth as a Planet.* $12.50

FOR LATER PUBLICATION:

Vol. III. *Planets and Comets*, Part I: Planets and Satellites.
Vol. IV. *Planets and Comets*, Part II: Minor Planets, Meteorites, Comets, Origin of the Solar System.

The most authoritative and comprehensive treatment of our knowledge of the solar system. A monumental series that will give the solar physicist all he can reasonably expect in the way of an advanced text for many years to come.

THE ATMOSPHERES OF THE EARTH AND PLANETS

Edited by GERARD P. KUIPER $8.50

THE FACE OF THE MOON

By RALPH B. BALDWIN $5.00

PRINCIPLES OF METEOROLOGICAL ANALYSIS

By WALTER J. SAUCIER $10.00

THE UNIVERSITY OF CHICAGO PRESS
5750 ELLIS AVENUE CHICAGO 37, ILLINOIS